UCID-20154

Feasibility Study of a Fission-Suppressed Tokamak Fusion Breeder

R. W. Moir, J. D. Lee, W. S. Neef, D. L. Jassby,
D. H. Berwald, J. K. Garner, R. H. Whitley,
N. Ghoniem, C. P. C. Wong, I. Maya, K. R. Schultz,
J. S. Karbowski

December 1984

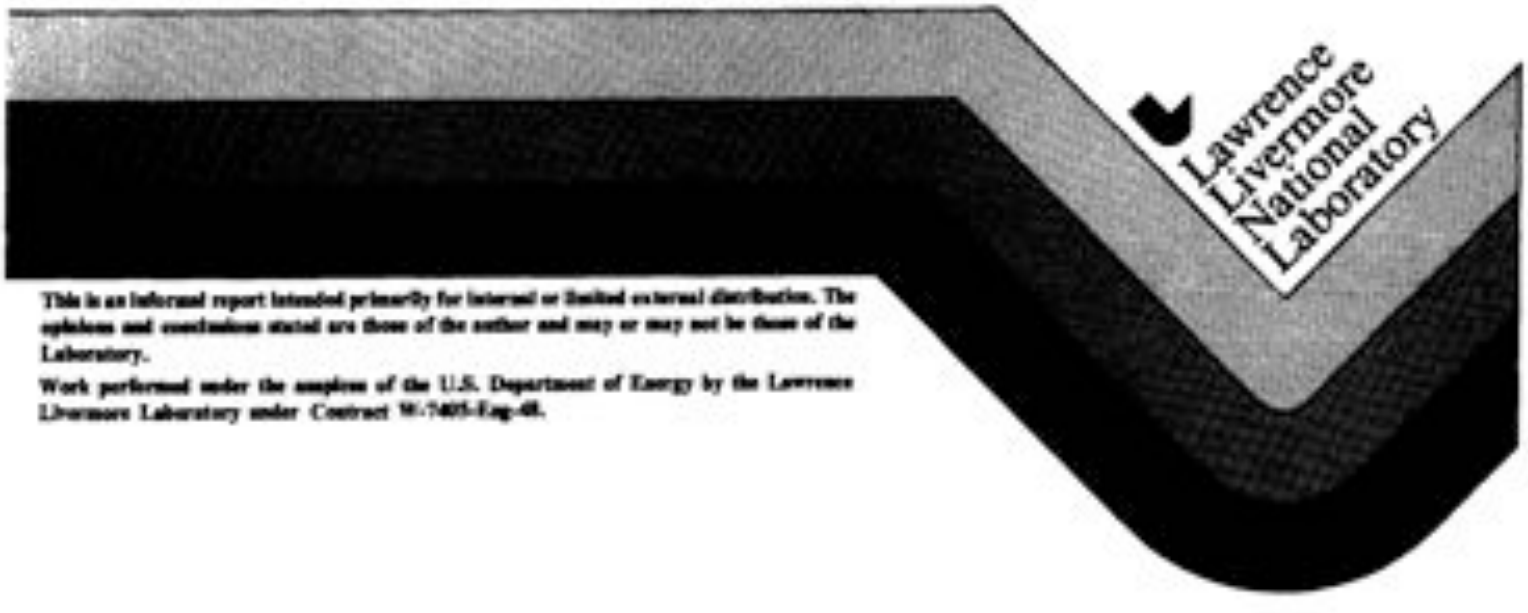

Printed in the United States of America
Available from
National Technical Information Service
U.S. Department of Commerce
5285 Port Royal Road
Springfield, VA 22161
Price: Printed Copy $; Microfiche $4.50

Page Range	Domestic Price	Page Range	Domestic Price
001-025	$ 7.00	326-350	$ 26.50
026-050	8.50	351-375	28.00
051-075	10.00	376-400	29.50
076-100	11.50	401-426	31.00
101-125	13.00	427-450	32.50
126-150	14.50	451-475	34.00
151-175	16.00	476-500	35.50
176-200	17.50	501-525	37.00
201-225	19.00	526-550	38.50
226-250	20.50	551-575	40.00
251-275	22.00	576-600	41.50
276-300	23.50	601-up[1]	
301-325	25.00		

[1]Add 1.50 for each additional 25 page increment, or portion thereof from 601 pages up.

Feasibility Study of a Fission-Suppressed Tokamak Fusion Breeder

R.W. Moir, J.D. Lee, W.S. Neef
Lawrence Livermore National Laboratory
Livermore, CA 94550

D.H. Berwald, J.K. Garner, R.H. Whitley, N. Ghoniem
TRW Energy Development Group
Redondo Beach, CA 90278

C.P.C. Wong, I. Maya, K.R. Schultz
GA Technologies, Inc.
San Diego, CA 92138

D.L. Jassby
Princeton Plasma Physics Laboratory
Princeton, NJ 08544

J.S. Karbowski*
Westinghouse Electric Corporation
Madison, PA 15663

December 1984

*Present address: Princeton Plasma Physics Laboratory

ABSTRACT

The preliminary conceptual design of a tokamak fissile fuel producer is described. The blanket technology is based on the fission suppressed breeding concept where neutron multiplication occurs in a bed of 2 cm diameter beryllium pebbles which are cooled by helium at 50 atmospheres presssure. Uranium-233 is bred in thorium metal fuel elements which are in the form of snap rings attached to each beryllium pebble. Tritium is bred in lithium bearing material contained in tubes immersed in the pebble bed and is recovered by a purge flow of helium. The neutron wall load is 3 MW/m^2 and the blanket material is ferritic steel. The net fissile breeding ratio is 0.54 ±30% per fusion reaction. This results in the production of 4900 kg of ^{233}U per year from 3000 MW of fusion power. This quantity of fuel will provide makeup fuel for about 12 LWRs of equal thermal power or about 18 1 GW_e LWRs. The calculated cost of the produced Uranium-233 is between $23/g and $53/g or equivalent to $10/kg to $90/kg of U_3O_8 depending on government financing or utility financing assumptions

Additional topics discussed in the report include the tokamak operating mode (both steady state and long pulse considered), the design and breeding implications of using a poloidal divertor for impurity control, reactor safety, the choice of a tritium breeder, and fuel management.

TABLE OF CONTENTS

TABLE OF CONTENTS (Cont'd)

CHAPTER II TOKAMAK DRIVER DEFINITION

TABLE OF CONTENTS (Cont'd)

CHAPTER III HELIUM COOLED BLANKET

TABLE OF CONTENTS (Cont'd)

TABLE OF CONTENTS (Cont'd)

CHAPTER IV LITHIUM COOLED TOKAMAK HYBRID BLANKET CONCEPT

CHAPTER I

INTRODUCTION AND EXECUTIVE SUMMARY

I.A BACKGROUND AND MOTIVATION

Only a few energy sources can be considered inexhaustible in a practical sense. These include solar energy, nuclear fusion energy, and nuclear fission energy with a technology to convert abundant resources of naturally occurring fertile isotopes (i.e., ^{232}Th or ^{238}U) to fissile isotopes (i.e., ^{233}U or ^{239}Pu). The fast-fission breeder (e.g., LMFBR) represents one such breeding technology. The fusion breeder, a higher performance, but higher risk, long range option, would use the excess neutrons which might be produced in nuclear fusion reactors to produce fissile fuel for use in conventional fission convertor reactors such as the light water reactor (LWR) or for use in higher performance fission converter reactors such as the high temperature gas cooled reactor (HTGR).

Results show that fusion breeders* have potential to breed unprecedented quantities of fissile fuel (1,2)** and several studies affirm the general conclusion that the fusion breeder can be potentially superior to other breeding options when viewed from the joint perspectives of cost of electricity, (3,4) and ability to displace expected fossil fuel shortfalls and provide real energy growth during the first half of the next century (5,6). Because each fusion breeder can produce enough fissile fuel to support about 10-15 relatively inexpensive LWRs of equivalent thermal power, this application can provide nuclear fission with an economically superior breeder candidate - even if the cost of the fusion breeder is several (e.g., three) times that of a fission plant of comparable power (1).

---

* Fusion breeders are a subset of a larger nuclear reactor family, fusion-fission hybrid reactors, or hybrids. A hybrid may be defined as any fusion reactor containing heavy metal in its nuclear blanket. Fusion breeders are hybrids that are optimized for fissile fuel production.

** Executive Summary references provided only for background information which is not cited in the main report.

Research in the area of fusion-fission hybrid reactor concepts began about 30 years ago, (7) but was not actively pursued from the mid-50's to the early 70's. Since then, research activities have progressed through several conceptual design studies (1,2,3,5,6,8,9). The most recent design studies address the fission-suppressed mode of operation. In this mode, neutron multiplication for fissile breeding would be accomplished via non-fissioning neutron multipliers (e.g., beryllium, lithium-7, lead) rather than as a result of fast and/or thermal fissioning in the blanket. In comparison with the older fast-fission blanket designs, fission-suppressed blanket designs emphasize improved safety (i.e., lower fission product after-heat and hazard) and a much higher net fissile output per unit of installed thermal capacity. Although they are slightly more demanding in the area of fusion driver performance, it appears that the fusion scientific feasibility demonstrations of the 1980's will provide confidence that the minimum level of fusion performance and technology required for an economical fission-suppressed fusion breeder (i.e., plasma gains $\geq$ 5 and availability $\geq$ 50%) can be achieved in the 2020 timeframe. However, such an achievement will require that the fusion program continues to proceed towards an aggressive engineering development phase (10,11).

Clearly, the need for a fusion breeder is predicated upon the assumption that the nuclear power industry will regain its former vitality to the extent that the fission fuel cycle is closed and future plant capacity (and/or the expectation of such capacity) exerts an upward pressure on the cost of mined uranium. Although the outlook for such a scenario appears bleak from today's perspective, one or more of the following circumstances could motivate a resurgence of fission power and/or enable the fusion breeder to become economically attractive in the 2020 timeframe:

- An improved framework for the licensing, financing, and operation of fission plants in the U.S.
- Higher economic and electricity demand growth than experienced during recent years.
- Economic advantages in Europe (e.g., France) and Japan which can be attributed to inexpensive nuclear power plants built during the 80's and 90's combined with a successful operating experience with the existing LWRs.
- A new shortage of fossil fuels.

- The introduction of an intrinsically safer fission plant (e.g., the modular HTGR and/or novel new LWR designs).
- Continued concern relative to CO_2, acid rain, and other adverse environmental conditions resulting from fossil electricity generation.
- Lower than projected uranium resources.
- Inelasticities in the price of uranium as the price of oil, coal and other fuels rise (e.g., the 1973 Arab Oil Embargo experience).

Stated more concisely, a fusion breeder advantage relative to mined uranium requires a healthy enough nuclear industry to roughly double the price of uranium during the early decades of the next century.

By producing fuel for fission convertor reactors, the fusion breeder can also provide important institutional advantages. These result from its primary role as a fissile fuel (rather than power) producer. Fusion breeders and their associated fuel reprocessing facilities could be located together in remote, safeguarded fuel cycle centers and could be functionally equivalent to the existing combination of uranium mines (mills, etc.) and enrichment plants. Therefore, the current institutional framework, consisting of government ownership and/or operation of enrichment and reprocessing plants, could be maintained with the utilities continuing to operate LWRs or improved fission convertors far into the next century. This arrangement could lead to a long term, stable fuel source which would provide long range stability to the fission power reactor industry. Because each fusion breeder would support many LWRs (18 1 GW_e in this study) and because a new power reactor would not be introduced to the utilities and reactor vendors, a capability to meet a rapid growth in electrical demand might be provided more easily than with fast fission (e.g., LMFBR) breeders (6,12).

The fusion breeder could also accelerate the commercial development of fusion power plants because lower fusion performance and higher fusion component costs than would be acceptable for fusion-electric power plants do not cause the fusion breeder option to become unattractive (1,4). The early commercialization of fusion breeders could give the industrial sector experience relevant to the development, operation, and improvement of nearly all fusion component technologies.

References, Section I.A.

1) D. H. Berwald, et al., "Fission-Suppressed Hybrid Reactors - The Fusion Breeder," Lawrence Livermore National Laboratory Report UCID-19638 (1982).

2) R. W. Moir, et al., "Helium Cooled Molten Salt Fusion Breeder," Lawrence Livermore National Laboratory Report UCID-20153 (1984).

3) Proc. Second Fusion-Fission Energy Systems Review Meeting, CONF-771155, U.S. DOE (July, 1978).

4) D. L. Chapin, et al., "Preliminary Feasibility Assessment of Fusion-Fission Hybrids," Westinghouse Fusion Power Systems Department, WFPS TME-81-003 (1980), summarized in proc. Fourth Topical Meeting on the Technology of Controlled Nuclear Fusion (October 1980), CONF-801011, U.S. DOE (1981).

5) J. A. Maniscalco, et al., "Recent Progress in Fusion-Fission Hybrid Reactor Design Studies," Nuclear Technology/Fusion Vol. 1, p. 419 (1981).

6) J. D. Lee, et al., "Feasibility Study of the Fission-Suppressed Tandem Mirror Hybrid Reactor," Lawrence Livermore National Laboratory Report UCID-19327 (1982).

7) D. H. Imhoff, et al., "A Driven Thermonuclear Power Breeder," California Research and Development Corporation, CR-6 (1954).

8) B. R. Leonard, Jr., "A Review of Fusion-Fission (Hybrid) Concepts," Nucl. Tech. 20 161 (1973).

9) D. L. Jassby, Ed., Proc. 3rd US/USSR Symp. Fusion-Fission Reactors, Princeton, NJ (1979).

10) D. H. Berwald, et al., "Alternative Technological Pathways for Fusion," TRW-FRE-003, TRW Energy Development Group (1983).

11) G. Gibson, et al., "Alternative Technological Pathways for Tokamak Fusion Systems," Nuclear Technology/Fusion Vol. 4 1037 (1983).

12) S. I. Abdel-Khalik, "On the Role of Fusion-Fission Hybrids in The Nuclear Future of The United States and The Western World," Nuclear Technology/Fusion, 3, 1, 53 (1983).

I.B. PROGRAM ORGANIZATION

Fusion reactor design is best addressed by use of a multi-disciplinary team approach. The nine organizations which were involved in the Fusion Breeder Program during 1983 have been assigned complementary roles, by discipline. A list of organizations and their principal activities is provided below:

Organization	Principal Activities
Lawence Livermore National Laboratory	Program Manager, Tandem Mirror Physics and Technology, Nuclear Data and Design, Molten Salt Blanket Design
TRW Inc.	Design Integration, Tokamak and Tandem Mirror Reactor Systems Modeling, Blanket Design Support, Fuel Cycle Economics
GA Technologies, Inc.	Fluid Mechanics and Heat Transfer, Helium Blanket Sub-Module Configuration, Solid Breeders, Reactor Safety Systems
Westinghouse Electric Company	Reactor Mechanical Configuration, Operation and Maintenance
Oak Ridge National Laboratory	Molten Salt Chemical Engineering, Liquid Metal Compatibility
Princeton Plasma Physics Laboratory	Tokamak Plasma Engineering and Technology
Idaho National Engineering Laboratory	Fission Reactor Testing, Beryllium Irradiation Damage
University of California, Los Angeles	Blanket Stress Modeling, Structural Irradiation Damage
Energy Technology Engineering Center	Materials

The above activities were performed during 1983 on a variety of Fusion Breeder Program projects including the fission-suppressed tokamak fusion breeder feasibility assessment.

I.C PROGRAM GOALS AND APPROACH

A reference fission-suppressed fusion breeder conceptual design, based upon the tandem mirror fusion confinement concept, was developed during 1981 (1) and 1982 (2). This design, featuring a liquid lithium cooled, beryllium multiplier, thorium breeder blanket was investigated with respect to key issues during 1983 and 1984 (3). A higher performance helium cooled, molten salt blanket was also studied during this period (4).

In assessing the reference blanket design, it became clear that the liquid metal blanket concept could not be directly translated to a tokamak fusion driver. Specifically, issues associated with flowing the liquid metal coolant over longer pathlengths in the higher magnetic fields and surface heat loads of a tokamak caused a concern regarding the expectation of prohibitively high MHD pressure drops and/or structural temperatures. Consequently, a principal program goal during 1983 and 1984 was the development of a feasible blanket design concept for tokamak applications.

During this activity, helium, liquid lithium, and molten salt (FLIBE) coolants were considered. The molten salt coolant option was eliminated early in the study because of its detrimental effects on nuclear performance, its high melting point, and its poor heat transfer properties as a coolant.* A liquid lithium coolant option with a fissile breeding blanket only on the outboard side was considered during the study and may be feasible. However, the latter design was eliminated from final consideration because the fuel breeding performance of such a configuration is expected to be substantially lower than that of the selected helium cooled blanket concept and because of uncertainties in our ability to model the MHD pressure drop.

Although helium appears to be the most attractive coolant for tokamak applications, several generic issues have been identified during the past several years (5). These include the following:

- the coupling of large first wall surface heat fluxes to a relatively poor heat transfer medium.

---

* A more promising molten salt blanket concept, being pursued, features a helium coolant and a molten salt breeder (see reference 4).

- the accommodation of uncertainties in the first wall erosion/redeposition rates.
- the complexity of helium cooled blankets as related to tritium control, helium flow control, heat transfer, and reliability.
- the diffusion and/or leakage of tritium to the primary loop and the control of tritium in the primary loop to prevent environmental releases.

These issues are common to all helium cooled blanket concepts for fusion applications and are not unique to hybrid blankets. As the first three are aggravated by increased wall loadings, the lower neutron wall requirements for hybrid applications (2-3 MW/m^2) relative to fusion-electric applications (4-5 MW/m^2) can be a significant developmental advantage (5,6).

Several "hybrid-unique" program goals which specifically relate to this first assessment of a helium cooled fission-suppressed tokamak breeder include the following:

- the modification of previously proposed tokamak configurations and maintenance schemes to accommodate the mobile fuel and passive dump requirements of fission-suppressed fusion breeders (Section III.A of this report).
- a comparative assessment of several tritium breeder choices (e.g., Li_2O, FLIBE) in conjunction with helium cooling and beryllium neutron multiplication (Section III.B).
- an assessment of the relative breeding efficiency of tokamaks versus tandem mirrors (Section III.C).
- the development of a reactor systems engineering (i.e., systems costing code) capability for tokamak fusion breeders (Section III.F).
- the identification of tokamak current drive candidates and operating modes which provide a low physics risk consistent with the capital cost and power flow requirements for fusion breeder applications (Sections II).

In summary, goals for development of the fusion breeder design discussed in this report are to address the design feasibility issues associated with a helium cooled, fission-suppressed, tokamak fusion breeder. Such a design concept has not been considered in the past, and several new issues have been addressed during the course of the study. The approach towards an assessment

of concept feasibility has been to conduct a preliminary conceptual design study focusing upon the key nuclear subsystems. In our judgement, the overall design concept can be feasible and attractive subject to the resolution of several concerns which are generic to helium cooled fusion blankets.

The resulting design is preliminary and does not reflect the level of study relative to key issues, design trades, and optimization which has been incorporated into our liquid metal cooled blanket design for the tandem mirror (2,3). An equivalent level of design maturity will require additional study.

References, Section I.C

1) J. D. Lee, et al., "Feasibility Study of the Fission-Suppressed Tandem Mirror Hybrid Reactor," Lawrence Livermore National Laboratory Report UCID-19327 (1982).

2) D. H. Berwald, et al., "Fission-Suppressed Hybrid Reactor - The Fusion Breeder," Lawrence Livermore National Laboratory Report UCID-19638 (1982).

3) Lawrence Livermore National Laboratory Report UCID-20166 (1984)

   Vol. 1: Liquid Metal MHD Pressure Drop Effects In The Packed Bed Blanket by T. McCarville, D. Berwald, and C. P. C. Wong.

   Vol. 2: Reactor Safety Assessment by I. Maya, C. G. Hoot, C. P. C. Wong, K. R. Schultz, J. K. Garner, S. J. Bradbury, W. G. Steele, and D. H. Berwald.

   Vol. 3: Beryllium Lifetime Assessment by L. G. Miller, J. M. Beeston, B. L. Harris, and C. P. C. Wong.

   Vol. 4: Structural Analysis by R. Orient, R. A. Westman, and N. Ghoneim.

   Vol. 5: Neutronics Issues and Optimization by J. D. Lee.

   Vol. 6: Materials Compatibility Issues and Experimental Results by J. H. DeVan and P. Torterelli.

4) R. W. Moir, et al., "Helium Cooled Molten Salt Fusion Breeder," Lawrence Livermore National Laboratory Report UCID-20153 (1984).

5) M. Abdou, et al., "Blanket Comparison and Selection Study," Interm Report, ANL/FPP-83-1, Argonne National Laboratory (1983).

6) D. H. Berwald, et al., "Alternative Technological Pathways for Fusion," TRW-FRE-003, TRW Energy Development Group (1983).

I.0 TOKAMAK DRIVER OVERVIEW

I.0.1 Tokamak Technology Options For The Fusion Breeder

The specification of a tokamak driver for the fusion breeder reactor can be similar to the driver specification for a fusion-electric reactor. However, fusion breeder reactors can tolerate the impact of more expensive and/or more power consuming design options which provide a lower technological risk than those which can be tolerated for the fusion-electric application. In this context, we initially investigated a fusion breeder tokamak driver which utilizes steady state negative ion neutral beam current drive, a single null poloidal divertor, and a 3 MW/m^2 neutron wall loading limit. A higher performance and lower cost, inductively driven, long pulse mode with lower hybrid RF current startup was also considered.

In comparison with lower hybrid RF current drive option, neutral beams have an experimental basis for plasma heating and are expected to provide greater confidence for bulk heating, steady state current drive, and stability control at reactor relevant densities and temperatures. However, negative ion neutral beams are both inefficient and expensive. About 310 MW of injected power are required to drive the plasma current for an otherwise ignited 3000 MW_f tokamak with a plasma current of ~ 10 MA (i.e., fusion gain = 9.7). For 65% efficient neutral beam lines (LBL self-extracting source, quadrupole acceleration, laser photo-detachment neutralization), the beam recirculating power requirement is about 475 MWe - a prohibitive power drain for fusion-electric applications. The cost is also high. With a unit cost of ~ 4 \$/W, the neutral beamlines alone would cost ~ 1250 \$M (direct). The negative ion beam current drive mode is marginally tolerable for the fusion breeder and provides a lower risk driver option for this study.

The long pulse inductive current drive mode, recently proposed for reactor applications, utilizes lower hybrid RF current drive to start the current at low density prior to ion cyclotron RF heating and inductive current drive. The latter option is more efficient and less costly than neutral beam current drive, but does introduce mechanical and thermal cycling of reactor components (~ $7 \cdot 10^3$ cycles/yr for ~ 3000 second pulses). The inductive current drive option has potential to substantially improved economics (i.e., lower cost of fissile product) and was selected as the preferred operating mode later in the study (see Section I.J).

A single null poloidal divertor, similar to the INTOR design, was selected over a pumped limiter for the fusion breeder despite known disadvantages with respect to breeding losses, cost, and complexity. The divertor presently has a superior experimental basis for ash removal and impurity control, avoids the leading edge thermal/erosion problem encountered in pumped limiter design, and offers the possibility of a low plasma sheath potential with the prospect for low erosion of a high-Z plasma side material. In the fusion breeder design, shown schematically in Figure I.D.1,* a top-mounted divertor was selected to better accommodate blanket safety requirements for a rapid gravity assisted fuel dump (see Sections III.E and III.I).

The 3 MW/m^2 neutron wall loading limit is lower than the 5 MW/m^2 goal often specified for fusion-electric blankets. The lower limit provides an additional safety factor with respect to the first wall heat flux, erosion rate, and irradiation lifetime which is believed to be required for fusion-electric applications, but increases the required first wall/blanket/shield area by over 60% and results in cost increases.

I.D.2 Tokamak Driver Overview

Figure I.D.2 shows the radial buildup of the neutral beam driven, steady state tokamak and Table I.D.1 gives the major parameters for optimal tokamaks for both steady state and long pulse operation. In both cases, the geometric parameters are determined from the required fusion power (3000 MW_f), the desired neutron wall loading (3 MW/m^2), the maximum beta allowed in dee-shaped plasmas, the maximum plasma current that can be established for a specified maximum field at the TF coil (11 T), and the maximum inboard/shield thickness (1.5 m from first wall to magnet conductor).

The plasma is doped with xenon ($Z_{eff} \sim 2.7$) such that the fraction of plasma thermal efflux (600 + 170 = 870 MW) removed by radiation to the first wall is 50%. Enhanced radiation also reduces $n\tau_E$ to its equilibrium value for

---

* Dimensions shown in this figure relate to the steady-state, neutral beam driven, design option. The smaller, long pulse tokamak dimensions are provided in Section I.E.

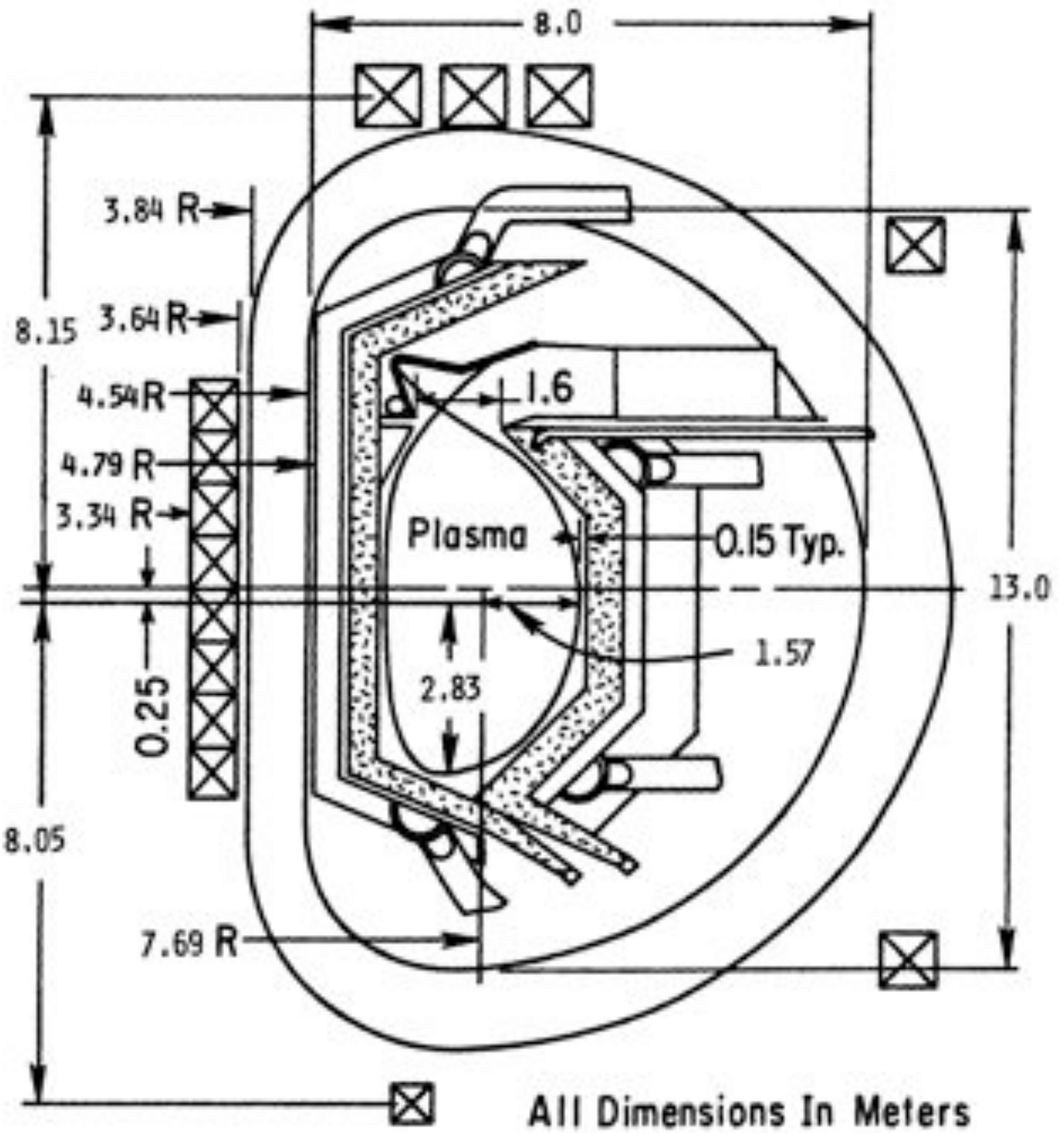

Figure I.D.1. Elevation View of the Steady State, Neutral Beam Driven Tokamak Driver.

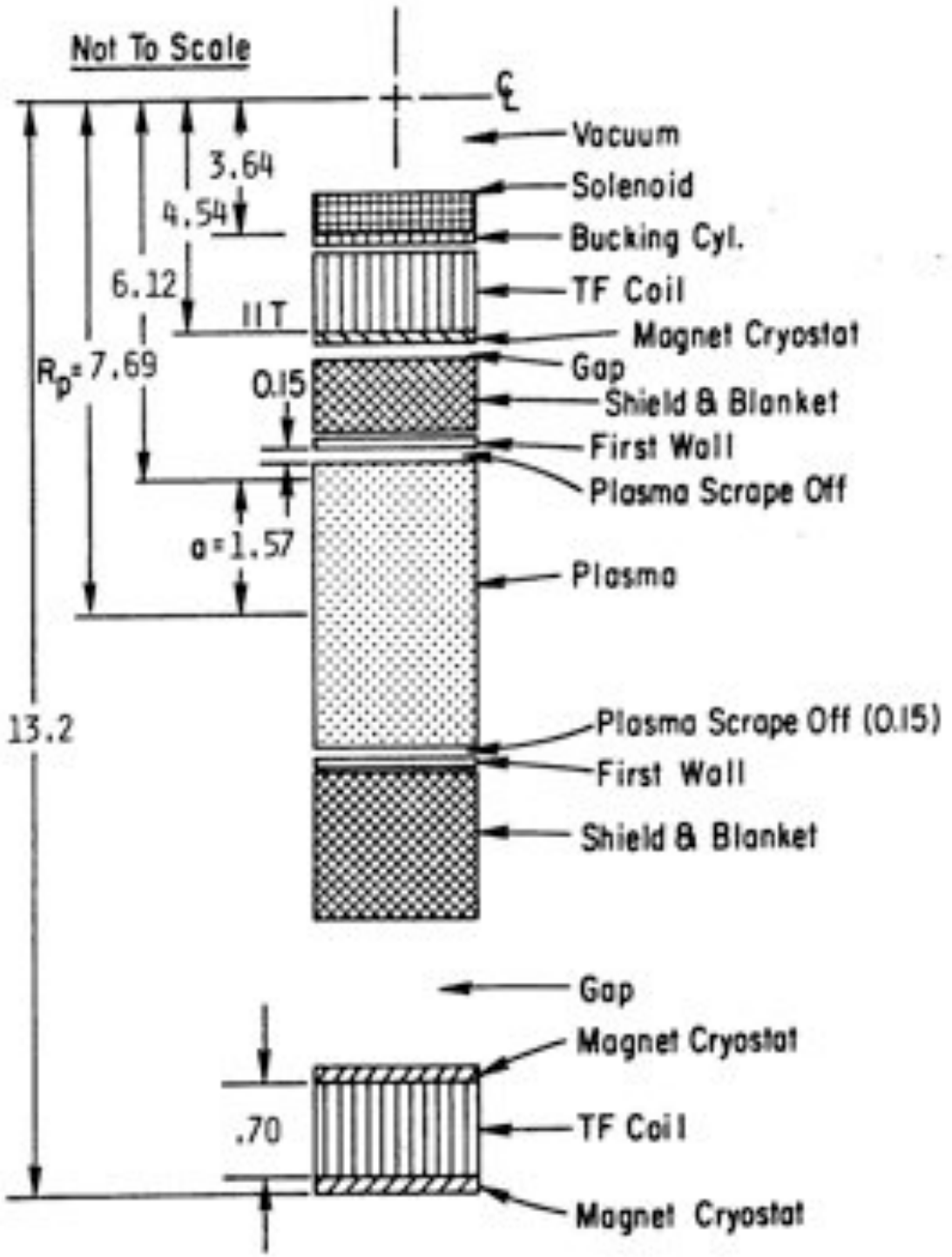

Figure I.D.2. Radial Build-up of the Steady State, Neutral Beam Driven Tokamak Fusion Driver. (Dimensions in Meters)

TABLE II.0.1. PRINCIPAL PARAMETERS OF THE TOKAMAK DRIVERS.

PARAMETER	UNIT	STEADY STATE MODE	LONG PULSE MODE
GEOMETRY			
Major Radius	m	7.69	6.75
Minor Radius	m	1.57	1.80
Aspect Ratio		4.90	3.75
Elongation		1.80	1.80
TF Coil Inboard Radius	m	4.54	3.37
Inboard B/S Thickness	m	1.2	1.2
Max B - TF Coils	T	11.00	11.00
PLASMA			
B at Plasma Center	T	6.49	5.50
Inverse Rotational Transform		2.25	2.25
Plasma Current	MA	9.81	12.4
<Beta>		.045	.059
<Density>	$10^{14}/cm^3$	1.34	1.25
<Temp>	keV	15.00	15.00
OH Bore Radius	m	3.34	2.14
OH Coil Delta B	T	18	18
Solenoid Flux	V-S	732	300
Z_{eff}[a]		2.7	2.7
Loop Volt	V	.12	.10
Max Pulse Length	s	55[b]	3000
Curr. Drive Mechanism		NB	Inductive
Curr. Drive Power	MW	310	92[c]
NTAU (for Z_{eff} = 1	$10^{14}s/cm^3$	19	17
Radiation Fraction[a]		.52	.52
NTAU Reduction Factor Due to Radiation[a]		2.1	2.1

TABLE II.D.1. PRINCIPAL PARAMETERS OF THE TOKAMAK DRIVERS (Continued)

PARAMETER	UNIT	STEADY STATE MODE	LONG PULSE MODE
MAGNETS			
TF Horiz Bore	m	8	8
TF Vert Bore	m	13	13
Max B-TF Coils	T	11	11
TF Coil Material		Nb_3Sn	Nb_3Sn
Max B-PF Coils	T	8	8
PF Coil Material	T	NbTi	NbTi
POWER PRODUCTION			
Fusion Power	MW	3000	3000
Fusion Gain, Q_p		9.7	Ignited
First Wall Area[d]	m^2	744	744
Surface Heat Flux[e]	W/cm^2	67	44
Neutron Wall Load	MW/m^2	3.0	3.0

a) produced by Xenon injection.

b) possibly limited to several hours.

c) ICRH plus LHRF during startup only.

d) assumes divertor throat subtends 7% of the solid angle from the plasma center to the minor radius.

e) assumes divertor removes 75 of 80 parts of non-radiated plasma thermal efflux.

ignition. A reasonable first wall erosion rate of about 2.25 mm/yr, providing a four calendar year blanket lifetime for a sacrificial first wall thickness of 9 mm (8.4 MW-yr/m^2 at 70% capacity factor) was selected as a design basis.

As mentioned earlier, impurity control is accomplished using an INTOR-type single null poloidal divertor. As in the INTOR study, the divertor collector plates would be covered with beryllium tiles which will limit high-Z reflux during the erosion process while providing some neutron multiplication and adequate heat transfer for the large divertor heat flux (~ 365 W/cm^2 in the long pulse mode and 1.5 times higher in the steady state mode). A detailed design was not performed, but it was assumed that the divertor coolant is low temperature water in copper tubes (no thermal recovery). Attention was given to neutron losses through the divertor and providing a maintainable configuration for the top-mounted divertor. The design concept anticipates periodic replacement of the divertor collector tiles by horizontal translation at an interval more frequent than replacement of the blanket/divertor sectors.

With the exception of one set of trapped divertor field coils (not shown in Figure I.D.1), all of the major coil systems in the fusion breeder tokamak are superconducting. The TF and OH coil superconductors are specified to be Nb_3Sn (~ 11 T) while the PF coils are assumed to be constructed of NbTi superconductor (~ 8 T). All of the PF coils, with the exception of the trapped divertor coils, are located outside of the TF coil bore and outside of the EF coils. In all, there are 10 TF coils and a corresponding number of blanket sectors.

The OH solenoid has a flux swing that is large enough to provide startup of the full plasma current (in the neutral beam driven steady state operation mode) or to drive a 3000 s pulse (in the long pulse mode). In the steady state mode, the startup sequence requires about 25 s and utilizes electron cyclotron resonance heating to pre-ionize the filling gas and provide some electron heating. Next, the full current (~ 10 MA) and higher densities and temperatures are generated using the solenoid flux linkage and ohmic heating. When the density becomes high enough to trap the 1.5 MeV neutral beams, they are activated one-by-one to provide the additional required heating and to sustain the current drive. Once heated to a 15 KeV equilibrium operating temperature, the 3000 MW_f plasma is much larger than required to sustain ignition conditions. Nevertheless, since about 310 MW of negative ion

neutral beam power are required to drive the 10 MA plasma current in steady state, the tokamak operating regime is effectively subignition (Q_p = 9.7) with the neutral beams also providing an effective means of thermal and stability control by appropriate variation of the beam power. The plasma is fueled by injection of frozen deuterium and tritium pellets. The rate of injection is another plasma control mechanism.

The long pulse mode would reserve the OH coil flux swing for current drive. In this case, the neutral beams would be replaced by lower hybrid and ion cyclotron RF systems. Sequentially, the plasma would be ionized using electron cyclotron resonance heating, the current startup would be provided at low density by ~ 25 MW of lower hybrid RF, the plasma would be heated using ~ 80 MW of ion cyclotron heating, and the pulse would be maintained for several thousand seconds. The long pulse operating mode will save cost and recirculating power (i.e., no RF during the long pulse), but will introduce a possibly excessive level of mechanical and thermal cycles (~ $7 \cdot 10^3$ yr^{-1}).

I.E MECHANICAL DESIGN AND CONFIGURATION

I.E.1 Reactor Configuration

A key design requirement, unique to hybrid applications, is to provide a mechanical design which will enable the use of a mobile fuel form for fuel replacement/reprocessing. Other key considerations are the design of a first wall thin enough to provide attractive neutronic performance, the specification of a structural material and configuration which can be tolerant of irradiation induced swelling, and considerations relating to remote maintenance and the removal of blanket sectors. The remote maintenance guidelines require that the blanket sectors and the divertor internals be removable within the fixed space between the toroidal magnets. Safety considerations require that the reactor fuel inventory can be dumped by gravity.

The resulting helium cooled Fusion Breeder Reactor configuration is shown schematically in Figure I.E.1. Its key design specifications address a set of tokamak dimensions (shown in Table I.E.1) which are consistent with the smaller, long pulse mode driver.* The plasma is surrounded by poloidally oriented lobe shaped modules with cylindrical noses which face the plasma. Figure I.E.2, a plan cross section through the horizontal centerline of the reactor, shows the lobes and their orientation with respect to the plasma for one of the ten blanket sectors. The poloidal lobe arrangement allows the mobile fuel, in the form of pebbles (spheres), to be loaded at the top of the reactor, flow through the modules, and be discharged at the bottom of the reactor when it is desired to dump the fuel for reshuffling/reprocessing or safety reasons. As shown in Figure I.E.3, the pebbles are a composite of beryllium/thorium, constructed of 2 cm dia. Be spheres, each with a circumferential groove to accept a thorium snap-ring. As indicated in Figure I.E.1, each sector of the blanket is cooled by helium which enters the coolant inlet manifolds at the top of the blanket and exits the coolant outlet manifolds at the bottom of the blanket. The fuel sphere inlets (top) and outlets (bottom) are also indicated.

---

* The original design guideline addressed a major radius of 6.75 m.

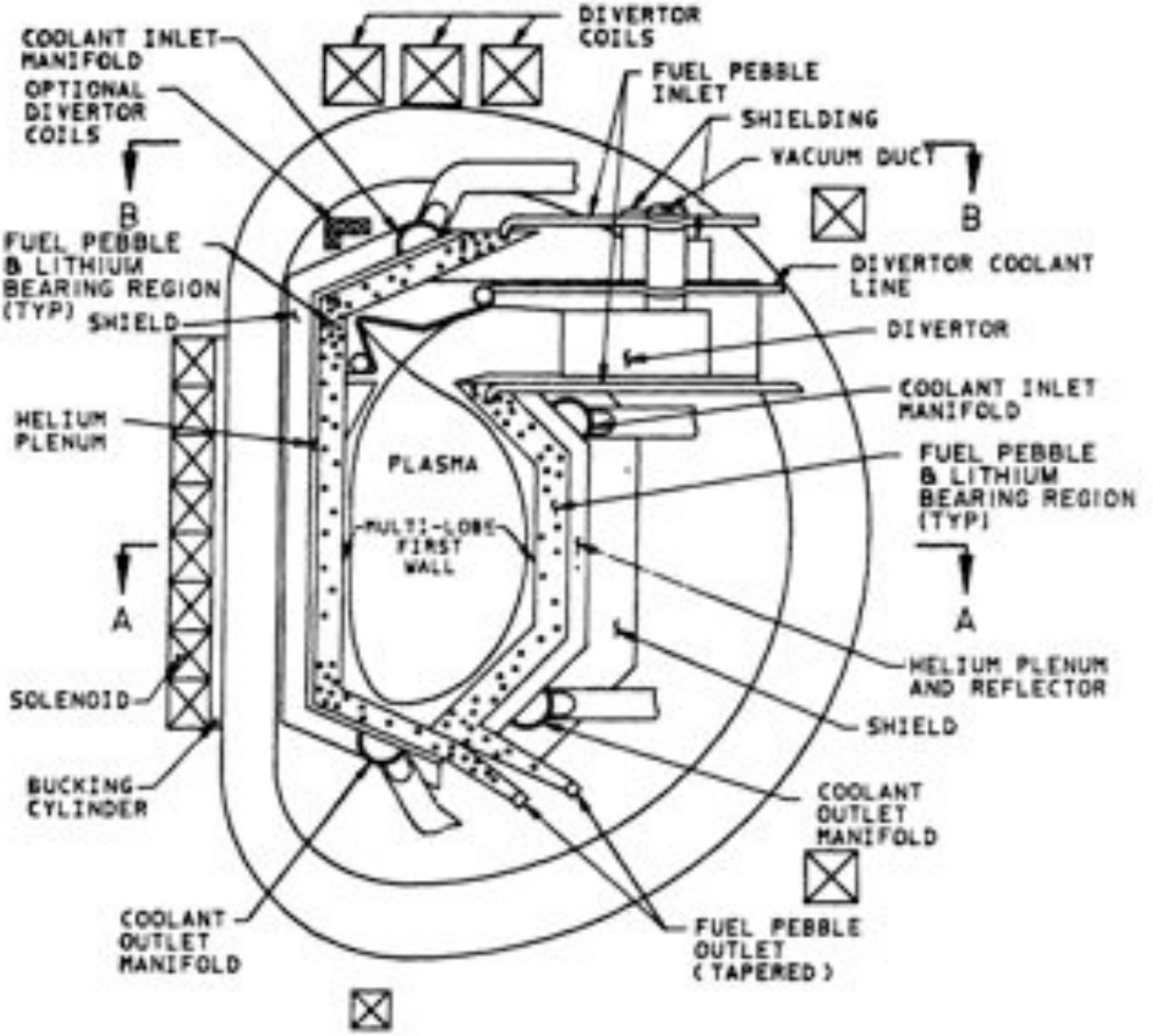

Figure I.E.1. Cross Section Elevation View Of The Helium Cooled Fusion Breeder Reactor Concept With a Top Mounted Divertor.

TABLE I.E.1. Design Parameters For the Helium Cooled Fission-Suppressed Tokamak Fusion Breeder Concept.

Fusion Power	3000 MW
First Wall Neutron Loading	3.0 MW/m^2
First Wall Surface Heat Load	0.43 MW/m^2
Plasma Size and Radius:	
Major Radius	6.75 m
Minor Radius	1.8 m
Elongation	1.8
Number of TF Coils	10
TF Coil Clear Bore (Modified "D"):	
Horizontal	10.4 m
Vertical	14.4 m
Radius From Reactor Centerline to Maximum Field	3.3 m
Field on Axis	5.4 tesla
Distance From Plasma Centerline to Divertor Coils[a]	9.6 m
Coolant	Helium
Pressure	5.1 MPa (740 psi)
Fuel Form	Composite Be/Th Pebbles (spherical)
Pebble Diameter	2 cm
Fuel Processing	Batch
Blanket Structure	Ferritic Steel (2-1/4 Cr-1 Mo)
Maximum Structural Temperature	<475°C
Blanket Lifetime	3-4 years

[a] For other PF coil locations see Section II.

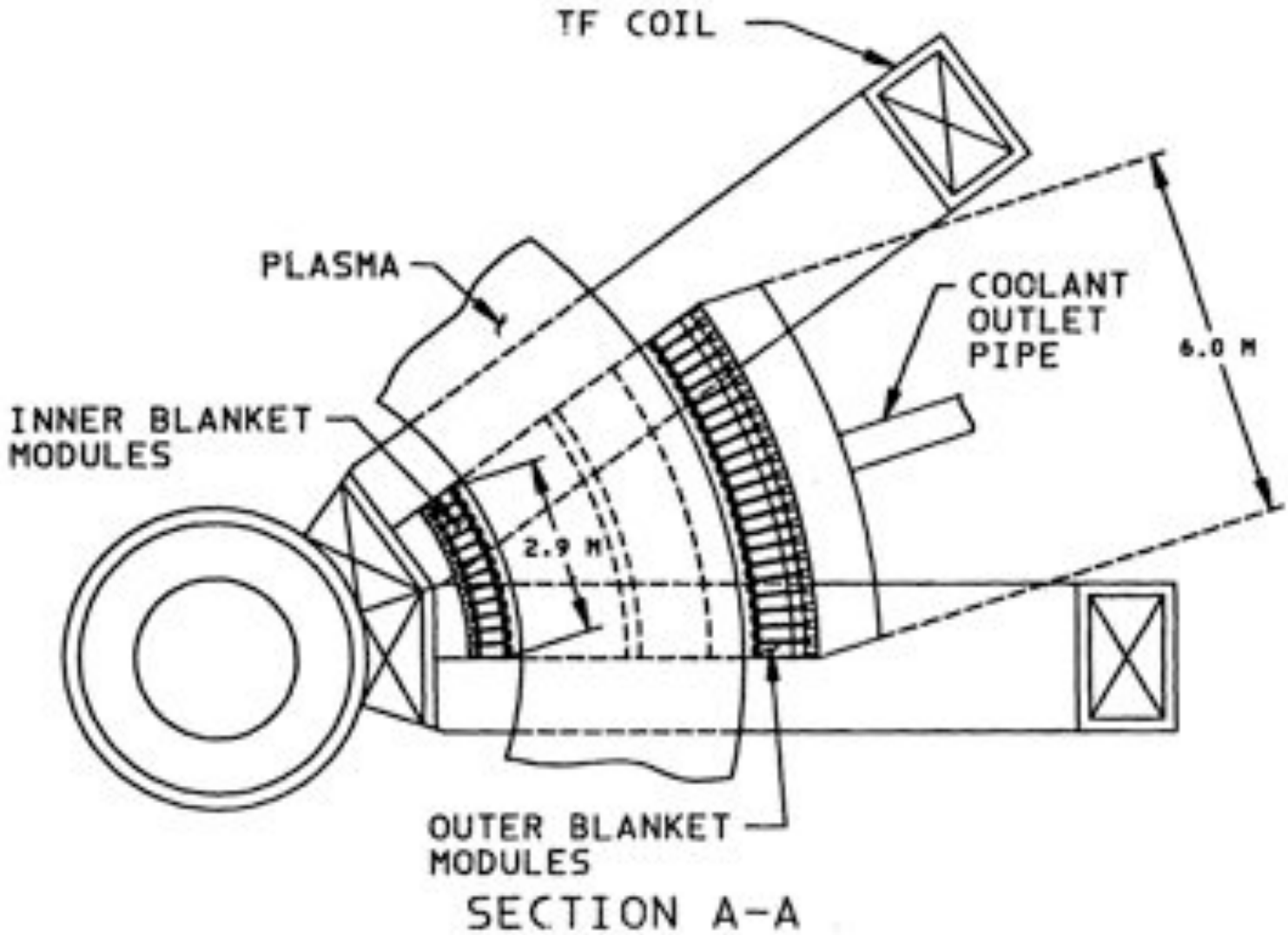

Figure I.E.2. Top View of a Fusion Breeder Reactor Sector Showing Section Through Horizontal Centerline and Lobe Module Arrangement.

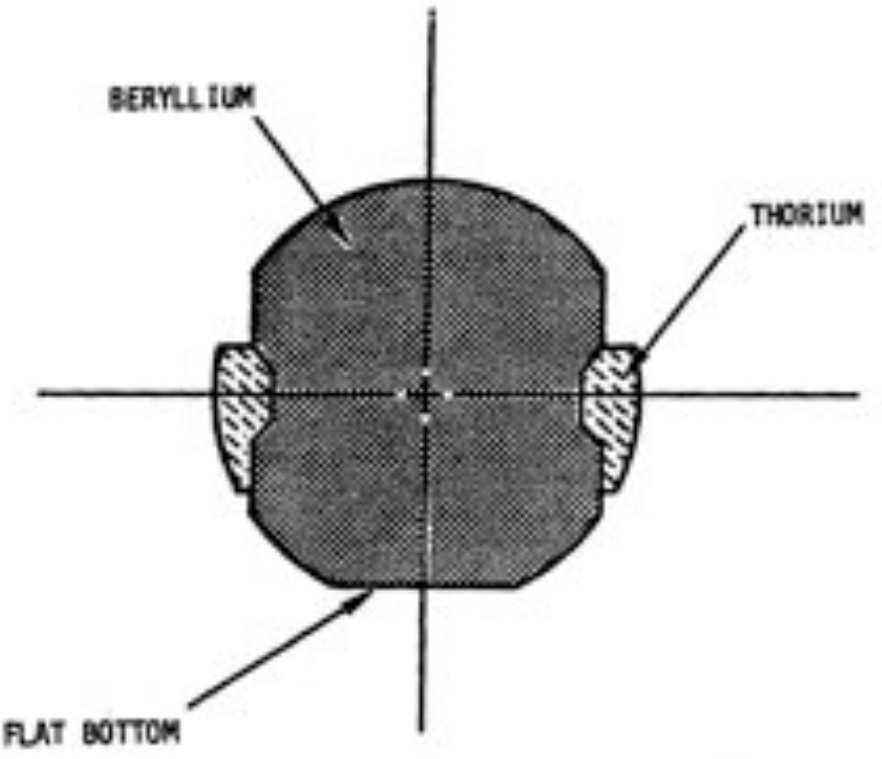

Figure I.E.3. Beryllium Pebble/Thorium Snap-Ring Composite Fuel Form.

The choice of a ferritic rather than an austenitic steel structural material for the reactor was based upon the current perception that volumetric swelling will be much lower for the ferritics. In addition, the ferritics offer higher thermal conductivity and their use is expected to result in a lower thermal stress in the first wall. Among the ferritics, HT-9 and 2-1/4 Cr-1 Mo are often selected as "typical" alloys. HT-9 features higher strength at elevated temperatures, but is expected to swell more (due to its higher chromium content). The 2-1/4 Cr-1 Mo alloy has been widely used in industrial applications, has adequate strength to ~ 475°C, and was selected for this study with HT-9 as a backup.

I.E.2 Blanket Sub-Module Configuration

An enlarged view of a typical sub-module is provided in Figure I.E.4. The module consists of a double walled 2-1/4 Cr-1 Mo ferritic steel construction with straight side walls and a semicircular nose. The outer wall serves as the primary pressure carrying structure. The inner portion between the double wall forms the coolant channel. The helium coolant enters at the rear of the module and passes along both sides of the module to the nose. At the center of the nose an opening is provided to permit the coolant to enter the near semicircular inlet plenum. The helium then passes through a perforated plate into the fueled region of the modules which contains the Be/Th pebbles and rows of steel tubes containing the tritium breeding material. The tubes are 2 cm in diameter and arranged in an array with a triangular pitch of 8 cm. An additional set of plena are provided on each side of the module to permit a small amount of helium purge flow to be supplied to the horizontally oriented tritium breeder tubes to remove the generated tritium.*

The semicircular nose of the toroidal lobe type sub-module, Figure I.E.5, is corrugated circumferentially around the nose. The corrugations were adopted for the 1983 Blanket Comparison Study and this study. This optional feature requires further evaluation, but is expected to permit the corrugations to deflect poloidally around the blanket sector to better

---

* Although lithium oxide was considered as the tritium breeding material in this study, other materials (e.g., lithium aluminate, FLIBE, liquid lithium) might, ultimately, be preferred.

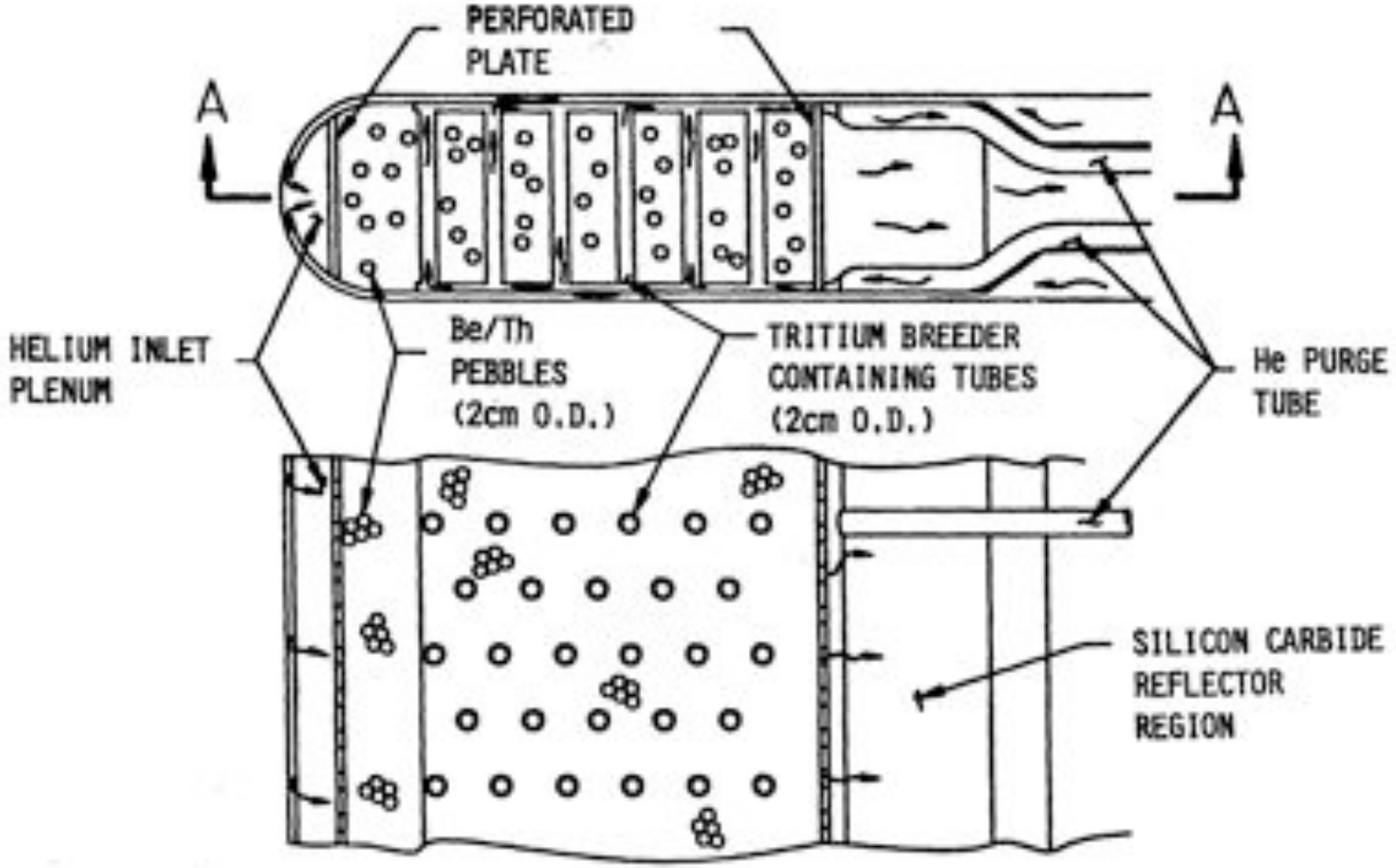

Figure I.E.4 Enlarged Cross Section Of The Outer Blanket Module Showing The Fertile Fueled and Li_2O-Containing Tube Arrangement.

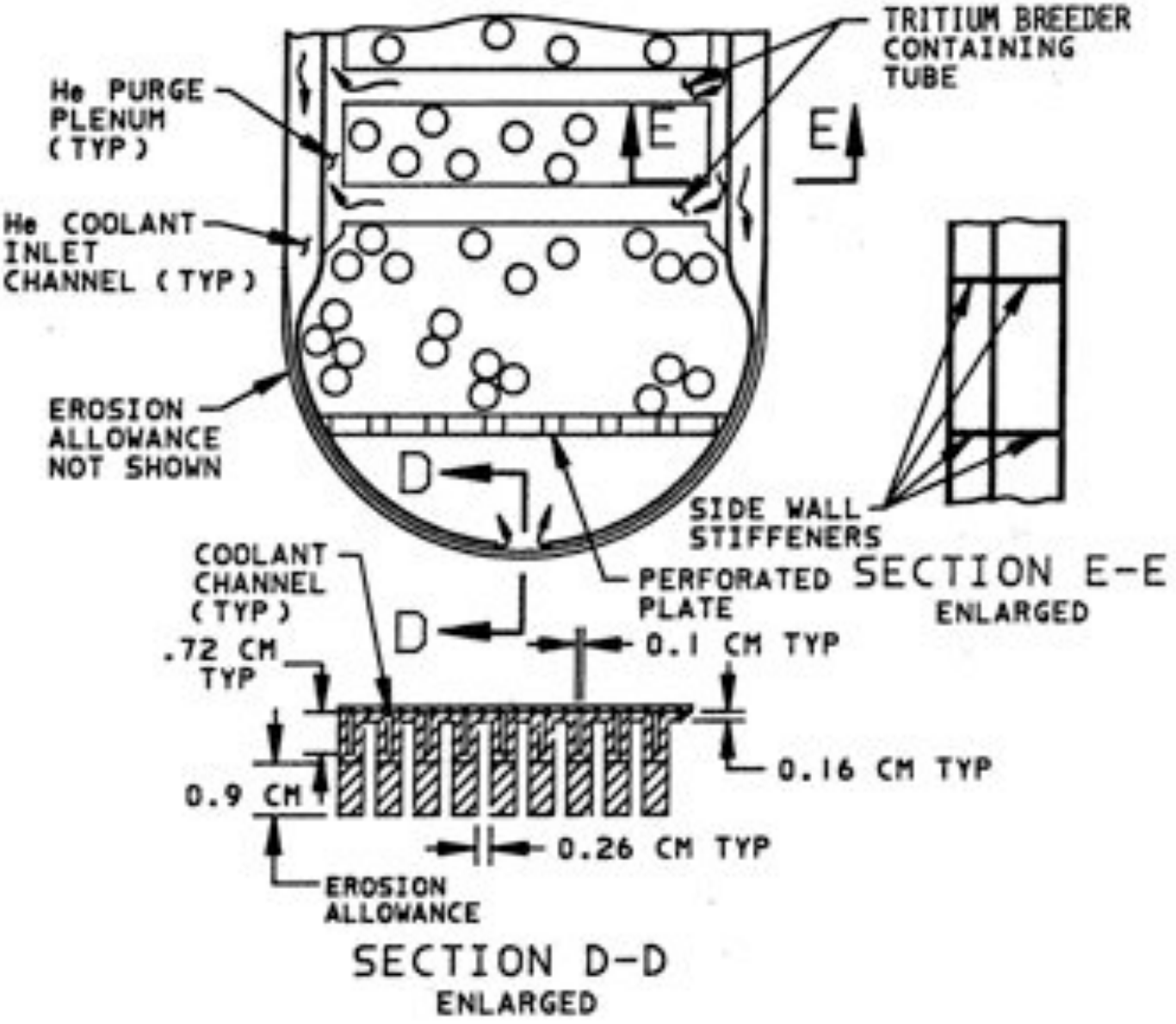

Figure I.E.5. Enlarged View Of The Front Of a Module Showing Corrugated First Wall, Side Wall Stiffeners and Tritium Breeder Containing Tubes (not to scale).

accommodate irradiation induced swelling and thermal expansion. The corrugated nose would also deflect by flexing along the circular arc formed by its semicircular shape. The nose blends into the side walls of the modules where contact with the adjacent modules prevents any deflection. Each 0.4 cm thick side wall acts as a tension tie to carry the coolant pressure load from the corrugated nose of the module to the back module support structure. The corrugation has a 9 mm erosion allowance to accommodate sputtering of the material from the first wall during a four calendar year operating lifetime.

I.E.3 Fuel Region Design and Inlet/Outlet Piping Considerations

Both the sphere inlet and outlet piping are sized to prevent the spherical pebbles from binding or jamming and to provide free flow of the pebbles when necessary for loading and unloading the fueled region. In addition, the fuel zone of the blanket is free of unnecessary restrictions which could impede the motion of the pebbles. Small scale experiments performed at LLNL have demonstrated that the spacing of the breeder tubes in the fueled region of the module (Figure I.E.4) will allow the pebbles to move and to achieve an adequate packing fraction of 50-60%. In order to minimize the thickness of the tritium breeder containing tubes, the helium purge flow in the tubes is maintained at approximately the same pressure as the module coolant pressure. To substain the full (100 MPa) buckling pressure, some support due to breeder packing in the tubes is assumed.

Each of the lobe sub-modules shown in Figure I.E.2 must be serviced by an individual pebble feed tube as indicated in Figure I.E.1. The feed tubes would be operated pneumatically, transporting single pebbles from a batch tank to the blanket. To avoid cutting and welding 34 pipes per sector changeout, an arrangement such that the fuel feed system would be integral to the blanket/shield/divertor assembly is postulated (but not yet designed). Fuel pebbles discharged through the blanket by gravity enter a flattened funnel shaped duct which provides a single common exit from all of the sub-modules in each blanket sector.

The proposed concept requires only a single inlet coolant pipe and exit coolant pipe per sector for each (inner and outer) blanket. The inlet plenum is wide at the top and narrows towards the bottom while the outlet manifold has the opposite orientation.

I.E.4 Design Issues

A helium cooled reactor/blanket concept with a mobile fuel form appears to be a viable concept based on the scoping design and analysis effort to date. A single coolant path for the first wall and the interior of the blanket leads to a relatively simple concept and the use of 2-1/4 Cr-1 Mo represents a state-of-the-art material selection. The first wall concept is directed towards accommodating the effect of irradiation induced swelling, but additional study is required to confirm the four year (8.4 MW-yr/m^2) blanket lifetime which has been postulated.

Because of the limited effort in the study to date, design issues remain which will require further study. Some of these items/issues are the following:

- The lifetime of the blanket module, as affected by irradiation damage (i.e., swelling, creep, embrittlement) should be investigated in the context of identifying the key failure modes.

- Concepts are needed for preventing the lobe side wall deformations at the interface between blanket sectors.

- The need for corrugations and the tolerance to which the narrow flow channels (1 mm) on the inner side of the corrugation can be manufactured needs to be assessed.

- The relative merits and disadvantages of the horizontally (toroidally) aligned tritium breeder containing tubes in comparison with an alternative vertical (poloidal) arrangement with periodic tube sheets should be investigated more completely.

- The proposed loading of beryllium/thorium pebbles into the top of the blanket lobes through small, individual tubes should be investigated via the design of a fueling machine.

- Configuration and mechanical support arrangement for the silicon carbide reflector needs further study.

- The shield design should be pursued further to understand the shield/blanket interfacing and provide a concept for an integrated shield and blanket design.

- The consequences of having the vacuum pumps and additional shielding above the reactor with the top mounted divertor needs further investigation.

- Procedures and equipment to replace the sector modules (including the divertor) require further study.

Further efforts should also include the interfacing of the additional system components (i.e., heat exchangers, vacuum pumps, helium pumps, etc.) and interconnecting piping. The vacuum sealing boundary should be better defined and seal concepts pursued.

I.F CHOICE OF A TRITIUM BREEDER

A principal goal of fusion breeder blanket design is to maximize fissile fuel production via the use of an efficient neutron multiplier (see Section I.G). A consequence of the use of a separate neutron multiplier (in this case beryllium) is that the tritium breeding material is not required to provide a capability for insitu neutron multiplication. Rather, the preferred tritium breeder is required to result in a practical engineering design which minimizes both the tritium breeder volume fraction and any parasitic absorption of neutrons. As a result of this design orientation, a number of tritium breeding materials which cannot provide adequate tritium breeding in the absence of an effective neutron multiplier for fusion-electric blanket (e.g., lithium aluminate, FLIBE) can be considered for use in the fusion breeder.

Key properties of several candidate tritium breeders are summarized in Table I.F.1. These candidates were selected because they represent distinct classes of breeders: liquid versus solid, insitu neutron multiplication versus none, and tritium release as T_2 versus T_2O. As shown in the table, the characteristic dimensions and structure (clad) fractions associated with all of the breeders are reasonable.

Li_2O has the highest lithium atomic density among all tritium breeders. The bred tritium is expected to be released as T_2O, a chemical form which is markedly less apt to leak through the steel tube into the helium coolant than the atomic form, T_2. Thus, a purge flow tritium extraction design is usually adopted. However, recent $LiAlO_2$ insitu tritium extraction experiments indicate that a large fraction of the tritium may be released in noncondensable form. Similar behavior can be expected for Li_2O. Since the results of this experiment are not fully understood, further investigations are needed. Li_2O has the disadvantage of being very hygroscopic, which implies the need for special attention during manufacturing and fabrication. Temperature control and irradiation damage effects (e.g., reductions in thermal conductivity) which influence the steady-state tritium inventory in Li_2O and irradiation growth (i.e., swelling) are key issues for this breeder. A final issue involves the activation of impurities the solid breeder and the radiological consequences associated with recycle of the breeder material and personnel exposure during the refabrication process.

Table I.F.1. Tritium Breeder Properties and Thermal/Mechanical Aspects.

	Li_2O	$LiAlO_2$	17Li83Pb	Li	FLIBE (66-34)	FLIBE (47-53)
k(W/m-K)	3	1.73	16	56	1	0.8
ρ (kg/m^3)	2010	2520	9400	450	2000	2000
C_p (J/kg-K)	2600	1464	1600	4200	2380	2350
MP (°C)	1430	1610	235	180	460	363
Preferred Fuel Form	Plate	Plate	Tube	Tube	Tube	Tube
h (W/m^2-K)	3000	3000	2000	2000	2000	2000
Interface T_{max}, (°C) PCA/HT-9	550/550	550/550	430/475	495/550	550/550	550/550
Breeder Temperature Window (°C), min/max	420/800	420/1200	235/1370[b]	180/1370	460/1370	363/1370
Breeder ΔT (°C)	$q'''x^2/2k$	$q'''x^2/2k$	$q'''r^2/4k$	$q'''r^2/4k$	$q'''r^2/4k$	$q'''r^2/4k$
Characteristic x or r (cm), (9 W/cc)/ (18 W/cc)[c]	1.4/1.0[c]	1.6/1.13[d]	3.6/1.3[e]	5.8/2.9[c]	2.4/1.7[d]	1.9/1.4[d]
Clad/breeder fraction (%)[f]	1.8/2.5	1.6/2.2	1.4/2.8	0.8/1.7	2.1/2.9	2.6/3.6

[a]Max. temp.less than 550°C (structural stress limit) defined by max. corrosion rate of 20 μm/yr.

[b]Boiling point of Li = 1370°C at one atms.

[c]x-plate 1/2 width, r-tube radius. Helium coolant characteristics: P = 50 atm, T_{in} = 275°C: T_{out} = 500°C, $T_{coolant}$ = 420°C; q''' = 9 W/cc at Γ = 1.5 MW/m^2.

[d]Breeder element dimension limited by T_{window} and interface T_{max}.

[e]Breeder element dimension limited by interface T_{max}.

[f]Clad thickness = 0.25 mm.

$LiAlO_2$ is the solid breeder that has the most available and most favorable material property data. It is very stable and has a large temperature window for tritium recovery (see above paragraph). The activation of $LiAlO_2$ is an issue.

Among the Li-Pb eutectics, 17Li83Pb is favored because a low chemical reactivity results due to its high content of lead (which is also a good neutron multiplier). It has a low melting point of 235°C and a very low solubility for tritium. Thus, the tritium inventory will be low, but the problem of handling T_2 in the blanket without excessive leakage appears to be very difficult. As shown in Table I.F.1, the weight and corrosiveness of 17Li83Pb are additional concerns.

Lithium is the best known liquid tritium breeder. It can breed adequate tritium without a neutron multiplier, but its high chemical reactivity leads to potential safety concerns. Since the bred tritium is held in lithium in the form of LiT, normal releases of tritium will be minimized, but lithium will need to be circulated outside of the blanket for tritium extraction.

Because of its low lithium density, FLIBE, or lithium-beryllium fluoride molten salt, requires isotopic enrichment in ^6Li for adequate breeding. It is known to have the advantages of excellent irradiation stability, low pressure operation, and chemical compatibility. These features imply safety advantages when compared to lithium and operational advantages when compared to the solid breeders and Li-Pb. The potential problem of TF (hydrofluoric acid) formation can be resolved by the addition of a reducing agent (e.g., excess beryllium) in the salt, but the issue of tritium release in the form of T_2 becomes the same as for 17Li83Pb.

Based upon our survey of the potential breeders discussed above, the following observations can be made:

- Among the solid breeders, Li_2O and $LiAlO_2$ are both credible and are similar in engineering application. Li_2O was selected over $LiAlO_2$ due to existing emphasis in the fusion-electric program. $LiAlO_2$ could ultimately be preferred for this application due to its chemical stability, resistance to irradiation damage, and larger temperature window. The higher lithium density of Li_2O is an advantage, but not a high priority issue because of the separate neutron multiplier. Tritium control may be an important issue in either case.

- Among the liquids, lithium is rejected due to safety concerns (an unnecessary burden).
- FLIBE and 17Li83Pb are both credible liquid breeders and are similar in engineering application. FLIBE is non-corrosive at the design operating temperature and is favored in this respect. 17Li83Pb has a lower melting temperature and is preferred if corrosion is not limiting.

I.G NUCLEAR ANALYSIS

I.G.1 General Considerations

The most important objective of any fusion breeder blanket design is the achievement of the highest possible fissile breeding within the constraints posed by a specified engineering design configuration. The requirement that the reactor breed enough tritium for self-sufficiency must also be satisfied. For fission-suppressed blankets, a third objective is to limit the fission rate in the blanket such that the blanket operating power density, the blanket after-heat power density, and the generation of radioactive fission products are limited to provide superior blanket safety characteristics as well as the maximum amount of fissile fuel per unit of thermal power generation.

As ^{233}U fuel (bred from ^{232}Th) is more efficiently used in fission reactors than ^{239}Pu fuel (bred from ^{238}U), our blanket studies have emphasized ^{233}U breeding for use in LWRs and more advanced convertor reactors. The combination of ^{233}U breeding and fission suppression leads to a level of breeding performance such that a 3000 MW_f tokamak fusion breeder could provide makeup fissile material to support 19, 1 GW_e LWRs on the denatured thorium fuel cycle. The fusion breeder also produces an average net electrical output of 1200 MW_e.

The focus of our nuclear design work has been directed towards estimating the performance of a tokamak fusion breeder using a variation of the reference tandem mirror blanket design developed during 1982. Some of the differences in the blanket materials and geometries are given in Table I.G.1. Although both designs utilize packed beds of beryllium pebbles with thorium snap-rings, the tandem mirror blanket uses a liquid lithium coolant and tritium breeder, while the tokamak blanket uses a helium coolant with the tritium breeder located in discrete tubes which run through the bed. Since the use of a beryllium moderator introduces significant neutron moderation, heterogeneous effects can be important and differences in performance due to the design of blanket internals can be significant.

TABLE I.G.1. Fusion Breeder Blanket Compositions.

	Tokamak Inner Blanket	Tokamak Outer Blanket	Tandem Mirror Blanket
FIRST WALL ZONE			
Thickness (cm)	7.5	7.5	6.3
Structure material	Fe	Fe	Fe
Structure Vol. Fraction	0.14	0.14	0.18
Coolant	He	He	Li
Coolant Vol. Fraction	0.86	0.86	0.82
PACKED BED ZONE			
Thickness (cm)	44	77	42
Structure	Fe	Fe	Fe
Structure Vol. Fraction	0.058	0.058	0.074
Coolant Vol. Fraction	0.38	0.38	0.38
Multiplier Material	Be	Be	Be
Multiplier Vol. Fraction	0.45	0.45	0.54
Tritium Breeder	Li_2O	Li_2O	Li (Also coolant)
Tritium Breeder Vol. Fraction	0.09	0.09	0.38
Fertile Fuel	Th	Th	Th
Fertile Fuel Vol. Fraction	0.024	0.024	0.029
BACK ZONE			
Thickness (cm)	5	5	42
Structure Vol. Fraction	0.08	0.08	0.065
Coolant Vol. Fraction	0.12	0.12	0.696
Moderator Material	SiC	SiC	C
Moderator Vol. Fraction	0.80	0.80	0.238

From a nuclear performance point of view the principal differences which relate to the use of a tokamak rather than a tandem mirror are that the tokamak:

1) does not have end cells (that consume but do not produce tritium)
2) has severe space limitations for the inboard blanket and shield
3) requires thicker and more complex first walls due to higher erosion and surface heat fluxes
4) has a poloidal divertor that can cause significant neutron loss
5) has a more complicated geometry that, when coupled with the desire to use gravity for pebble fueling, can impact performance.

I.G.2 Nuclear Analysis

The procedure used to perform the nuclear analysis consisted of developing geometric models to address various nuclear effects within the blanket. These effects were then analyzed with two Monte Carlo transport codes: TART, a coupled neutron-photon, 3-D Monte Carlo transport code using a 175 group nuclear data set generated from ENDL, the Livermore-evaluated nuclear data library; and ALICE, a variant of TART that treats resonance effects by using the probability table method. Most cases were run with 5000 source neutrons resulting in less than 2% standard deviation. The models developed for the Monte Carlo analysis are simplications of the actual geometry and are intended to reasonably approximate its important aspects.

Three models were developed and employed for this analysis. The first is a toroidal 2-D model (i.e., a figure of revolution) with no penetrations, approximating the overall aspects of the toroidal geometry. The second, shown in Figure I.G.1, is a unit cell consisting of a tube-containing Li surrounded by homogenized Be + Th. This model was developed to examine heterogeneous and resonance self-shielding effects. The third, shown in Figure I.G.2, is a toroidal 2-D model with a poloidal divertor. It was used to estimate the effects of a major penetration.

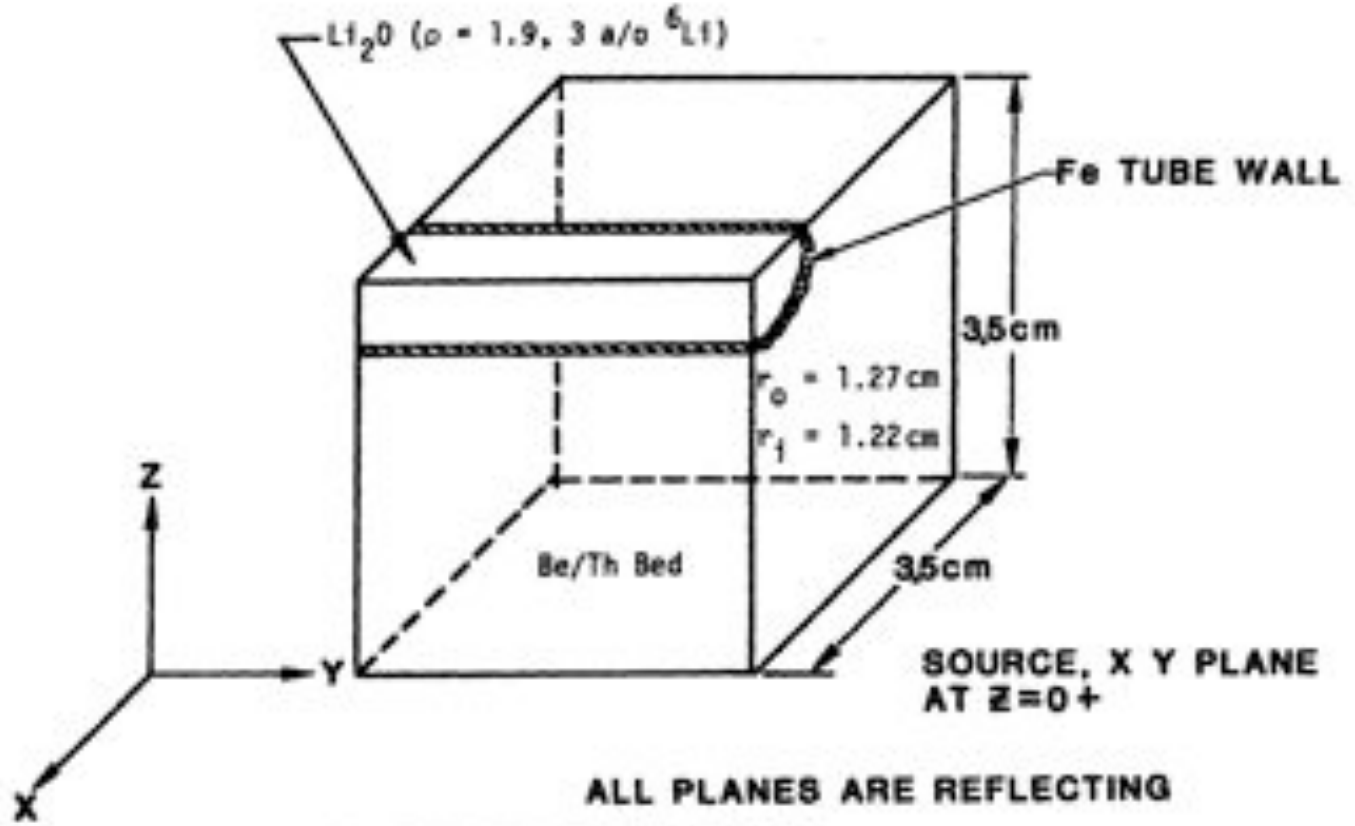

Be/ Th BED COMPOSITION

Be* = 47.5 v/o

Th** = 2.5 v/o

He = 50.0 v/o

*(Fe - 0.1 a/o in Be)

**(U - 0.5 a/o in Th)

**(Pa - 0.5 a/o in Th)

Figure I.G.1. Unit Cell Model.

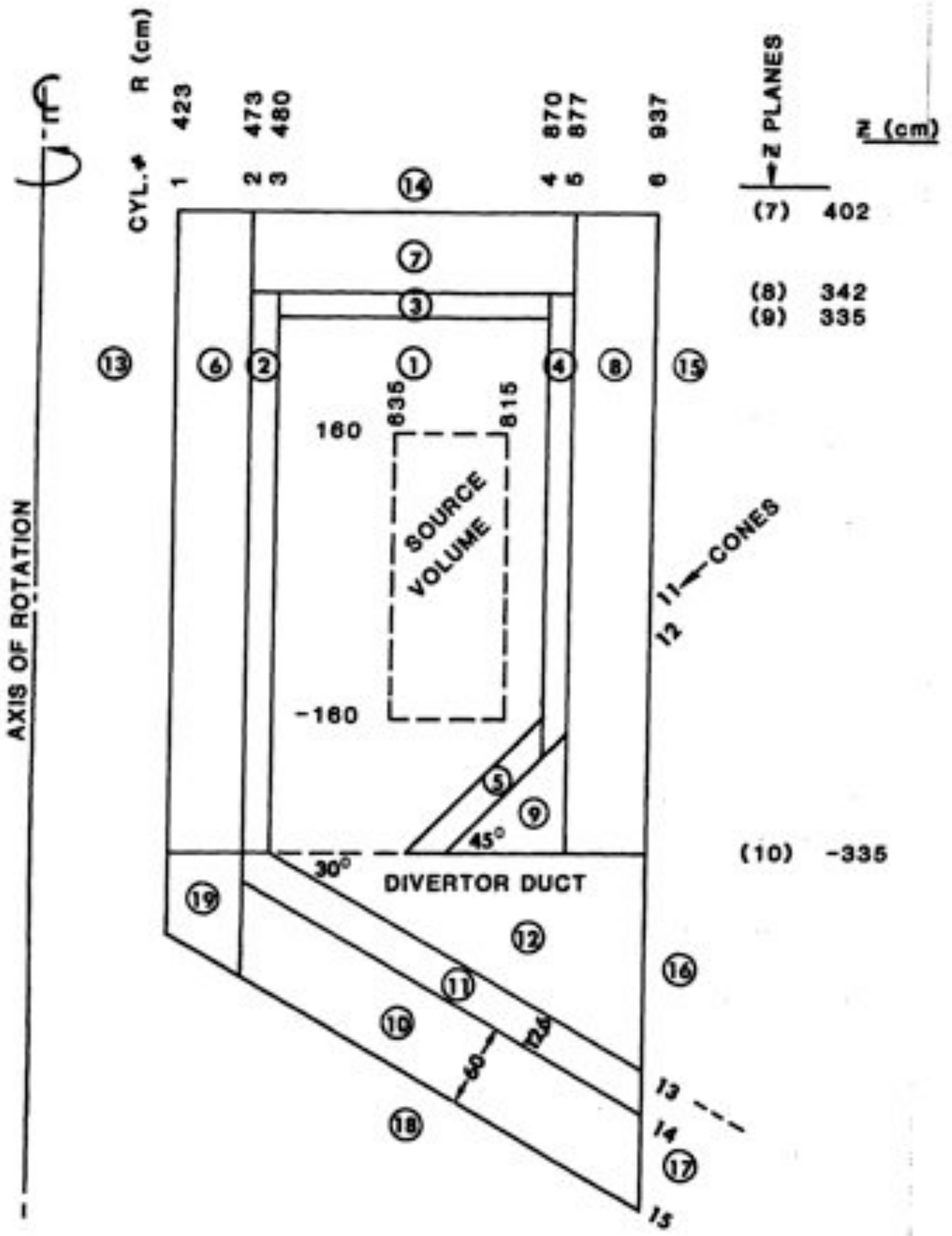

Figure I.G.2. 2-D Tokamak Neutronics Model With Poloidal Divertor.

Results from these three models were then combined giving the following estimate of overall performance:

Total net breeding	1.55 (±10%)
Tritium breeding	1.01
Net ^{233}U breeding	0.54 (±30%)
Energy (@ U/Th = 1.0%)	26 MeV (-20%, +40%)

These results are normalized to one D-T fusion neutron. The uncertainties listed are estimates that include data and modeling-caused uncertainties in addition to the 2% statistical uncertainty. The total energy deposited per fusion is expected to have a larger uncertainty in the upwards direction than the downwards direction due to remaining uncertainties in the details of the resonance self-shielding treatment.

The tritium breeding can be increased as required, but any additional bred tritium must be subtracted from the net fissile fuel production. It is important to note that even a 1% loss of tritium from a 3000 MW_f plant would represent a release of $4.5 \cdot 10^5$ curies per day! Similarly, the allowed recovery cost at 10,000 $/g would be ~ 12 $M/yr per percent tritium.

Future nuclear modeling work should be focused upon quantifying and reducing the uncertainties, optimizing the design to maximize specific breeding (i.e., breeding per unit of thermal energy deposited in the blanket) and exploring other promising design concepts. For example, significantly higher specific fissile breeding appears to be achievable by increasing the Th content above the 2 v/o used here.

Based on this work, the net fissile breeding ratio of the tokamak fusion breeder was found to be 13% less than the reference tandem mirror fusion breeder. While there is significant uncertainty, these initial results indicate that a tokamak with this general configuration can be used as the driver of a fission-suppressed fusion breeder, but that its fissile breeding ratio will be somewhat less than its tandem mirror counterpart.

I.H FLUID DYNAMICS AND HEAT TRANSFER

I.H.1 General Considerations and Design Limits

The requirement for the helium cooled first wall to accommodate high surface heat fluxes and high erosion rates leads to a difficult heat transfer problem for the tokamak reactor first wall. The bellows first wall design was conceived to accommodate these problems and to also accommodate the effects of irradiation-induced swelling. Two-dimensional thermal-mechanical analyses of the bellows first wall were performed to identify the temperature and stress distributions and to guide the design.

The helium-cooled, fission-suppressed, hybrid reactor blanket features a unique configuration consisting of a packed bed of beryllium/thorium pebbles surrounding purged tubes which contain the tritium breeder and are distributed throughout the bed. Heat transfer calculations were performed to show that the selected pebble and tube sizes can satisfy the respective material temperature limits. After the blanket configuration was defined, the blanket loop pressure drops and the pumping power were calculated to assure that they are acceptable.

The temperature limits of key materials were first established. In the blanket region, the key materials are the structural material, the neutron multiplier and the tritium breeding material. As discussed in Section I.E, 2-1/4 Cr-1 Mo was recommended to be the structural material. This easily manufactured ferritic steel alloy has a maximum allowable temperature of 475°C for high stress applications. For the nominal choice of Li_2O as the tritium breeder, the temperature limits are T_{min} = 410°C and T_{max} = 800°C.

A helium pressure of 40 to 80 atm will be needed for an efficient primary loop design. Steam-generator design conditions dictate a minimum coolant inlet temperature of about 275°C and a minimum coolant temperature rise of above 100°C. An outlet temperature of 500°C was selected td give a gross thermal cycle efficiency of 39%. Structure temperatures above 475°C occur only towards the rear of the blanket where the stress and neutron flux are lowest.

I.H.2 Bellows First Wall Design and Analysis

The primary purpose of the first wall is to provide a boundary between the pressurized coolant and the vacuum of the plasma chamber. At the same time, it has to handle the transmission of thermal power through the wall to the high pressure helium coolant. There are two contributions to the heating of the wall: volumetric power generation due to the neutron wall loading (3 MW/m^2) and the plasma-side surface heat flux (0.25-0.50 MW/m^2). In addition to these effects, the selected structural configuration has to accommodate high fluence neutron-induced swelling while being eroded away at an assumed rate of 2.25 mm/year.

Two dimensional, steady-state, temperature distributions were calculated for the bellows first wall using TACO2D, a finite element heat transfer code. The temperature profile calculated by TACO2D was then coupled along with the hydrostatic helium pressure boundary condition into NIKE2D, an implicit, finite deformation, finite element stress code. The neutron swelling effects were not included in the stress analysis. Figure I.H.1 presents the two-dimensional bellows first wall configuration which was modeled using the above codes. This basic configuration was analyzed for two conditions: the beginning-of-life (BOL) in which the 9 mm sacrificial layer on the plasma side of the wall has not eroded, and the end-of-life (EOL) in which the sacrificial layer has completely eroded.

Figures I.H.2 and I.H.3 graphically display the bellows first wall temperature profiles calculated by TACO2D at the beginning and end of life. Figures I.H.4 and I.H.5 present the beginning and end of life principal stresses calculated by NIKE2D. The results of these figures are summarized in Table I.H.1. This table shows that, with the present bellows first wall design, the design guideline maximum temperature (475°C) is slightly exceeded at the beginning of life. However, it is important to note that the hot spot areas, which occur in the sacrificial layer closest to the plasma, are required to provide only minimal structural support. The design guideline maximum stresses (~ 210 MPa) are met for both the BOL and the EOL conditions.

The above calculations were performed at a neutron and surface loading of 3 and 0.25 MW/m^2, respectively. Figure I.H.6 shows the estimate T_{max} at the beginning of life as a function of surface loading. Assuming a maximum

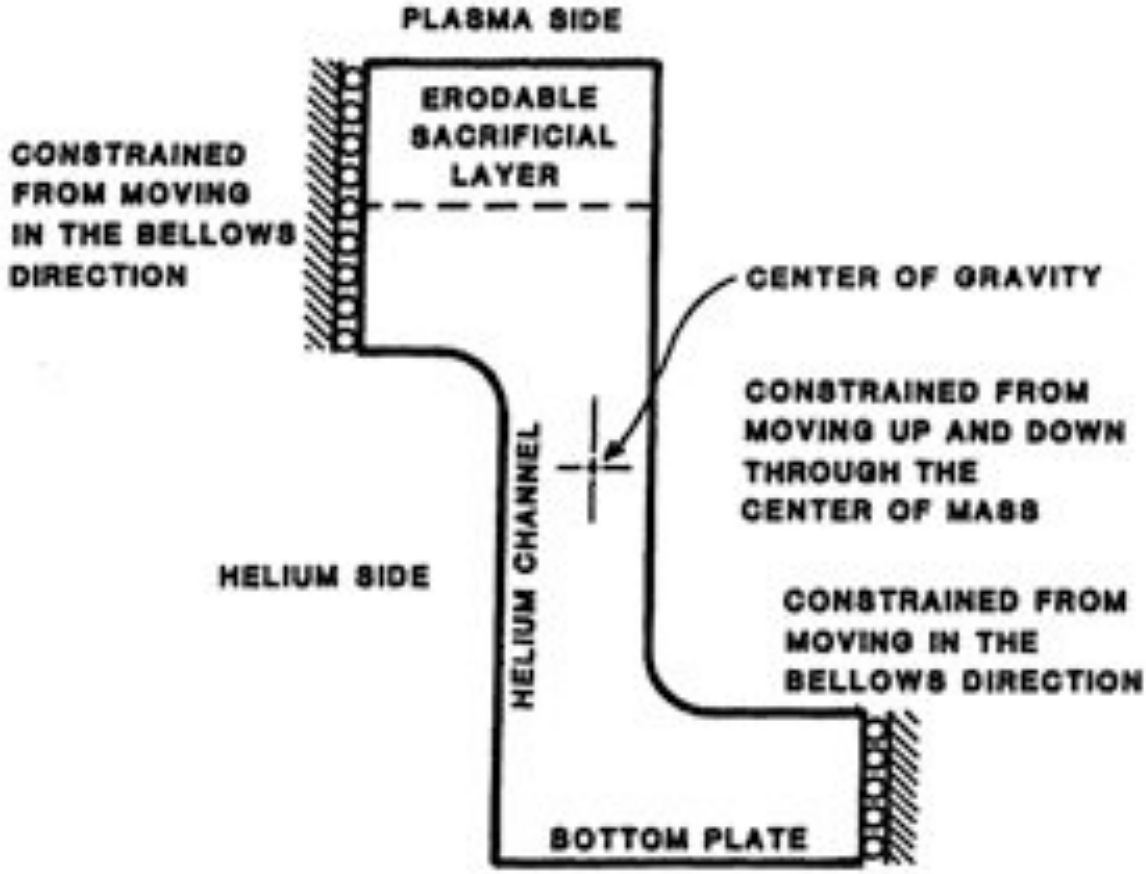

Figure I.H.1. Two-dimensional Bellows First Wall Configurations (Representation of a Unit Element)

Table I.H.1. Bellows First Wall Thermal And Structural Analysis Summary

2-1/4 Cr-1 Mo	
Maximum temperature, (°C)	
Beginning of life	542
End of life	342
Maximum stress, (MPa)	
Beginning of life	201
End of life	176

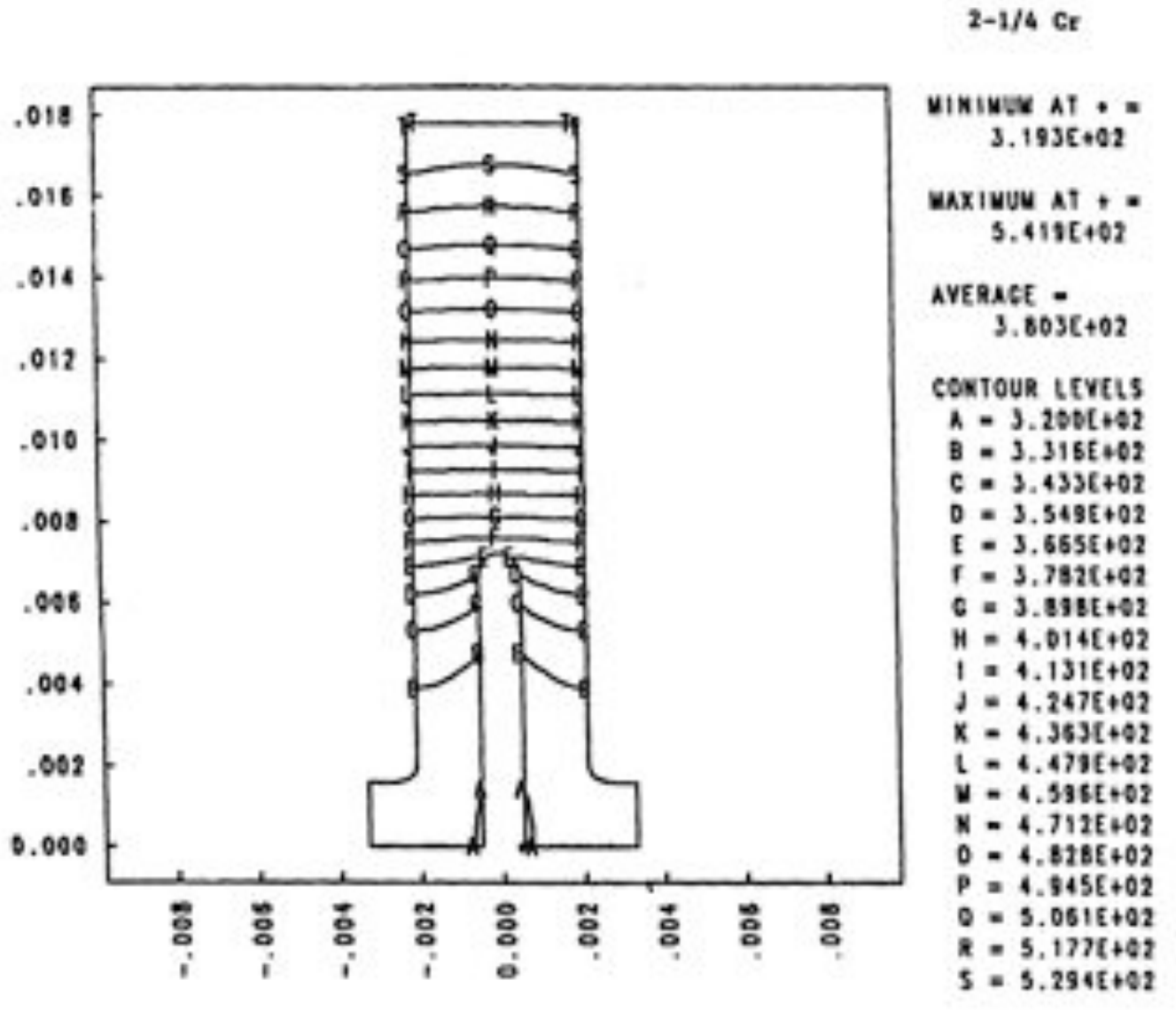

Figure I.H.2. Bellows First Wall Temperature Contours (°C) at Beginning-Of-Life.

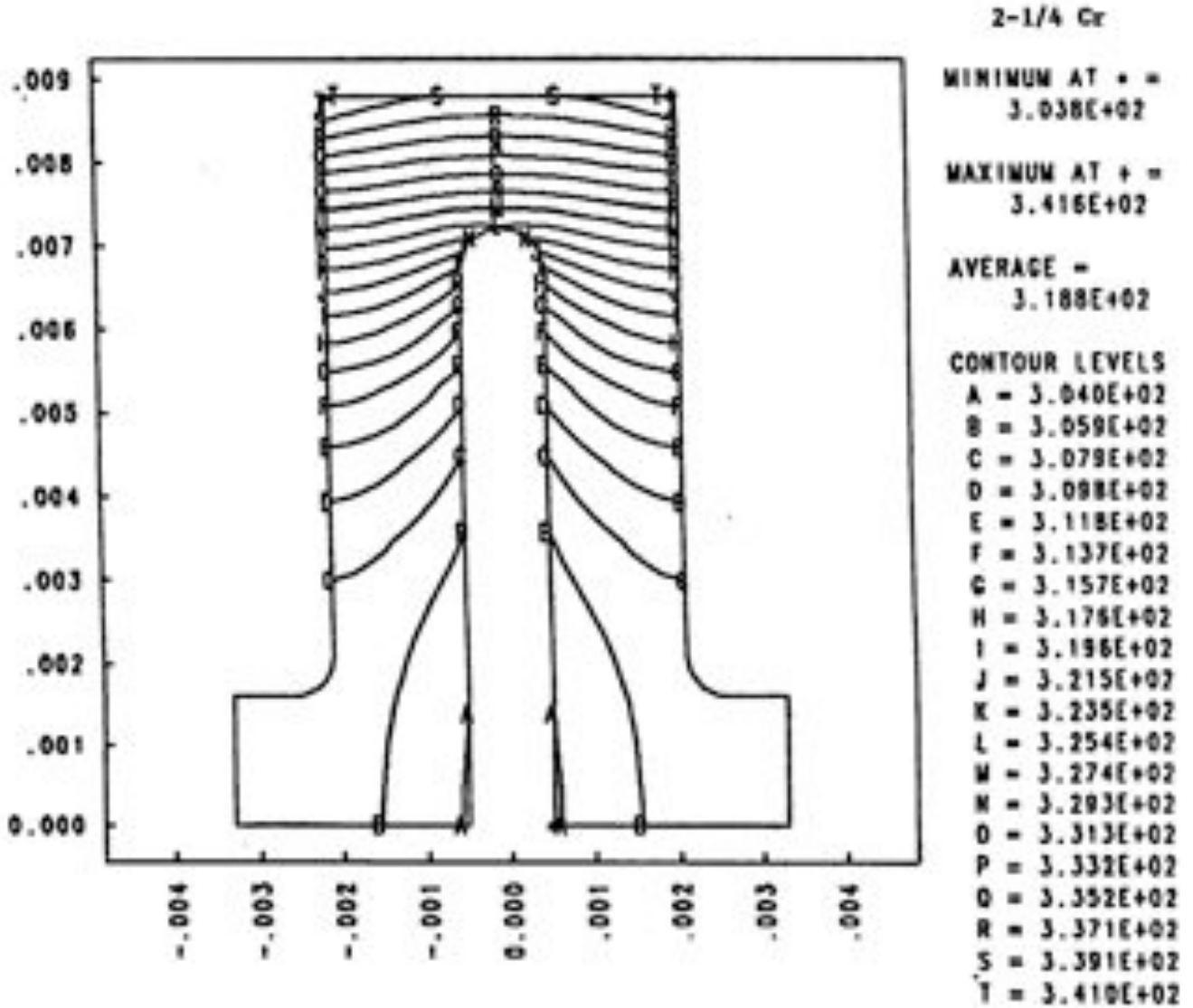

Figure I.H.3. Bellows First Wall Temperature Contours (^{0}C) at End-Of-Life.

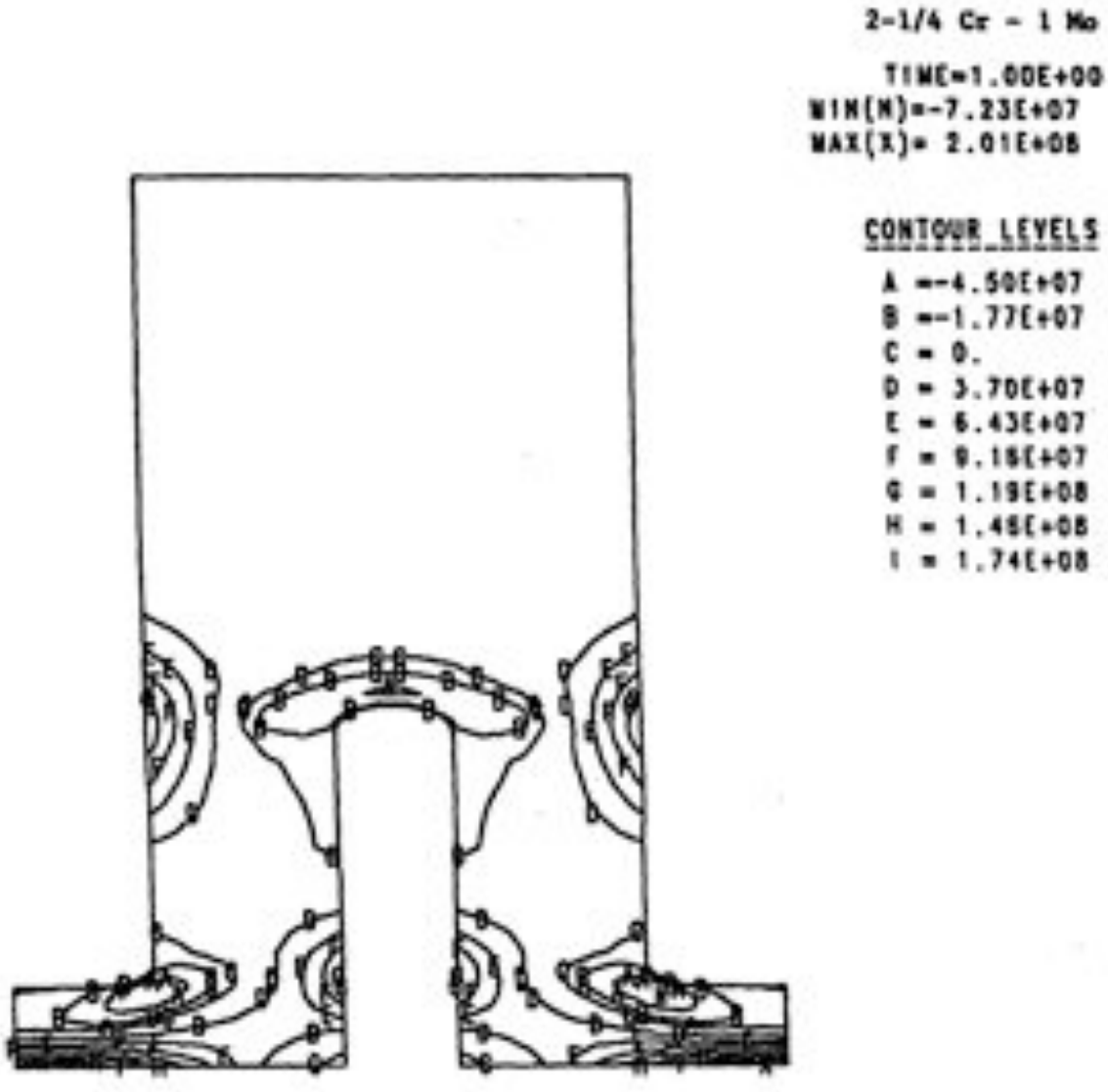

Figure I.H.4. Uneroded Bellows First Wall Thermal and Pressure Stress Contours at Beginning-Of-Life (not to scale).

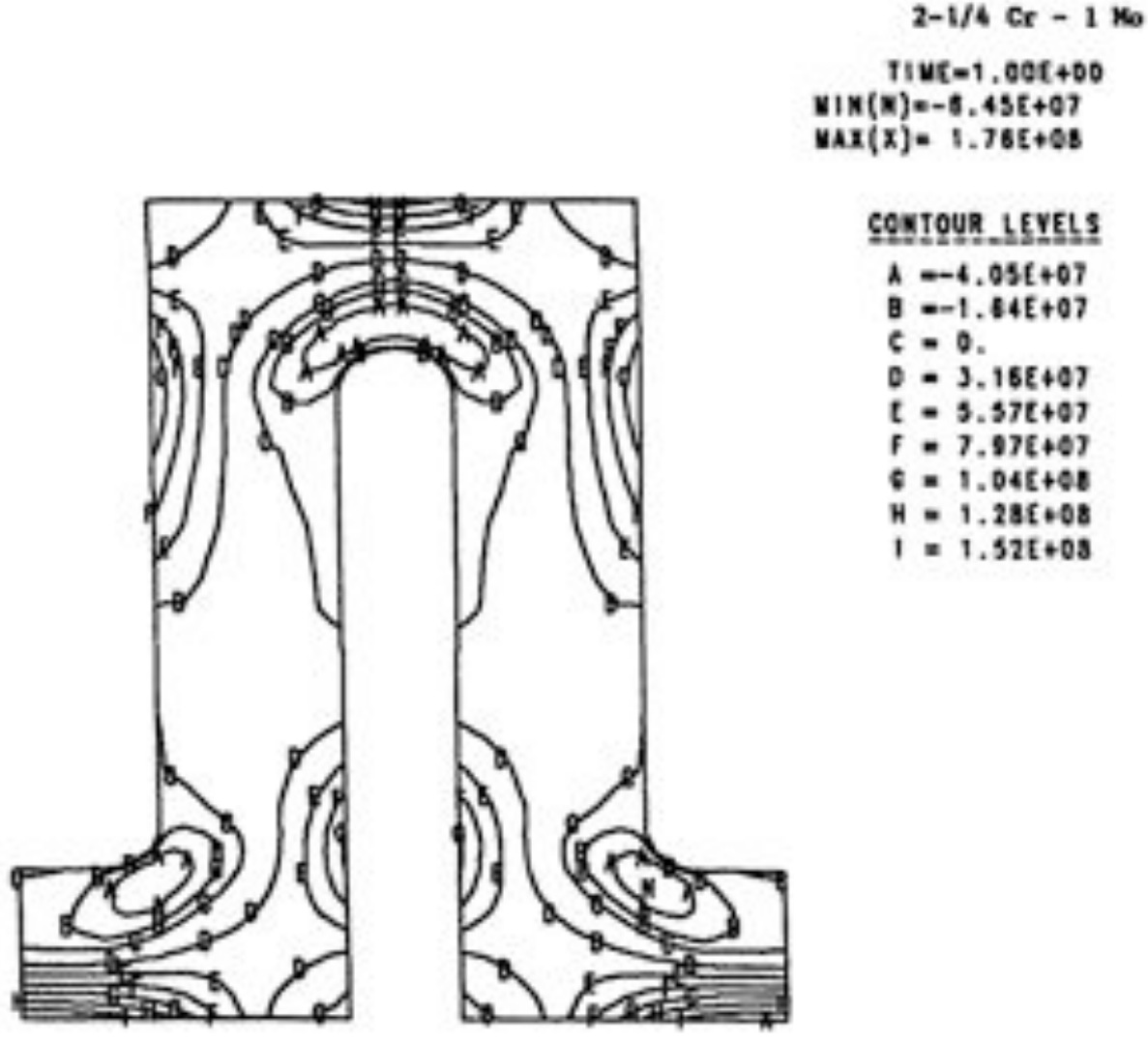

Figure I.H.5. Uneroded Bellows First Wall Thermal and Pressure Stress Contours at End-Of-Life (not to scale).

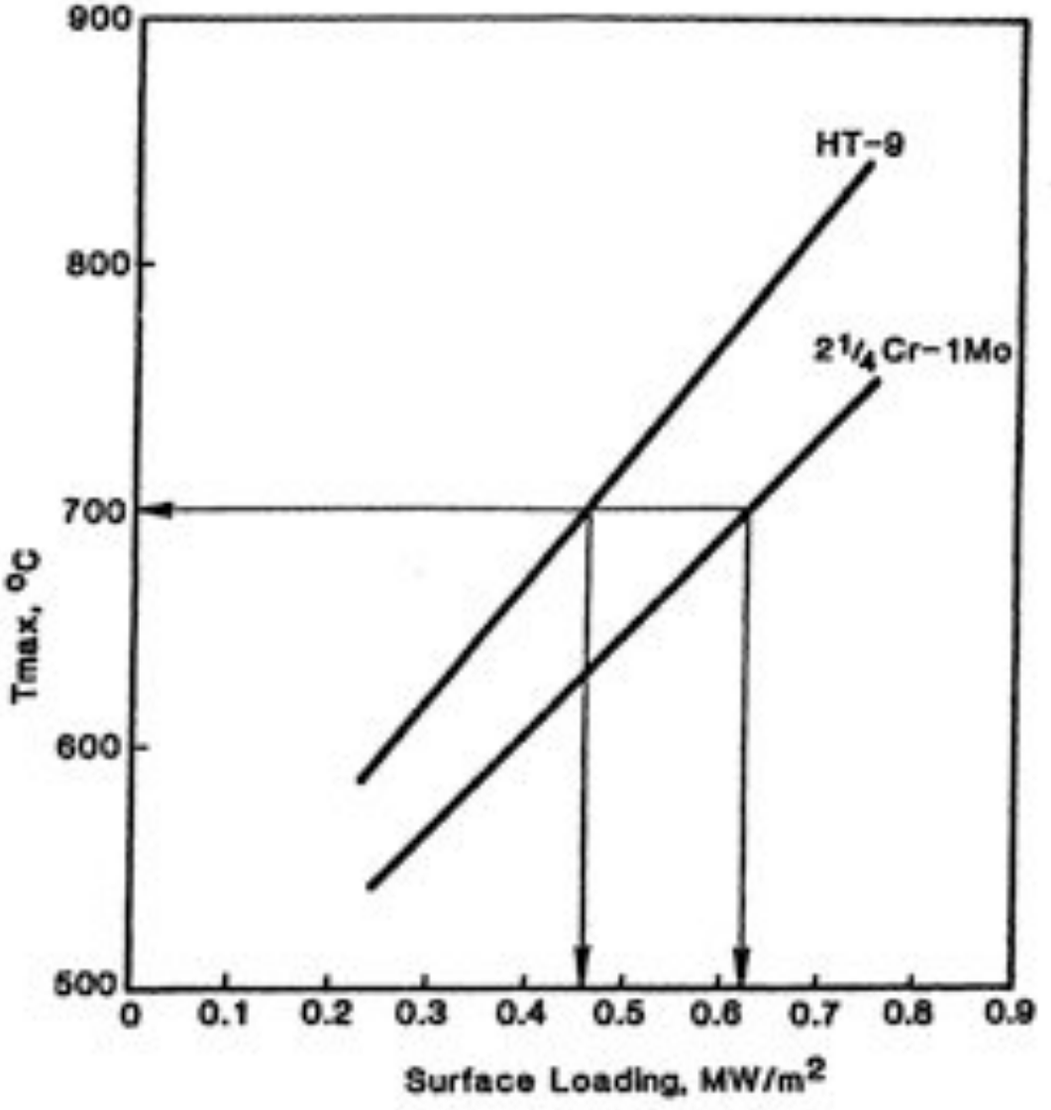

Figure I.H.6. Maximum First Wall Temperature as a Function of Surface Loading

allowable temperature of 700°C on the eroded layer where the stress capability requirement is minimum, the 2-1/4 Cr-1 Mo can withstand surface loadings higher than 0.6 MW/m^2. This observation provided a basis for our decision to increase the plasma radiation fraction to 52% (0.44 MW/m^2) to minimize first wall erosion and the divertor heat flux.

I.H.3 Blanket Fuel Element Design

Calculations were performed for the packed bed of beryllium pebbles and breeder tubes. An applicable heat transfer coefficient for a tube bank embedded in a packed bed of spherical pebbles was not available, but was estimated. Based on this estimate, the breeder temperature distribution as a function of radial position is given in Figure I.H.7. As shown, the design temperature limits for a lithium oxide breeder are satisfied. The 2-1/4 Cr-1 Mo tube temperature is higher than the design limit of 475°C at the back of the blanket, but the tube wall thickness can be increased in that location to reduce the stress without excessive penalty.

Calculations were performed to estimate the total pressure drop of the whole blanket cooling circuit including the steam generators for a 5000 MW_{th} reactor with a maximum blanket energy multiplication of 2. The pressure losses due to friction, acceleration of flow from density change as a function of temperature, joints, turns, expansions, and contractions were all taken into consideration. The resulting $\Delta P/P$ = 3.22% and pumping power fraction of 4% are within the respective design limits of 4.3% and 5%. For the selected coolant inlet/ outlet temperatures of 275°C/500°C, the gross power conversion efficiency is expected to be 39% while the net power conversion efficiency is expected to be 36.5% (including pump power losses).

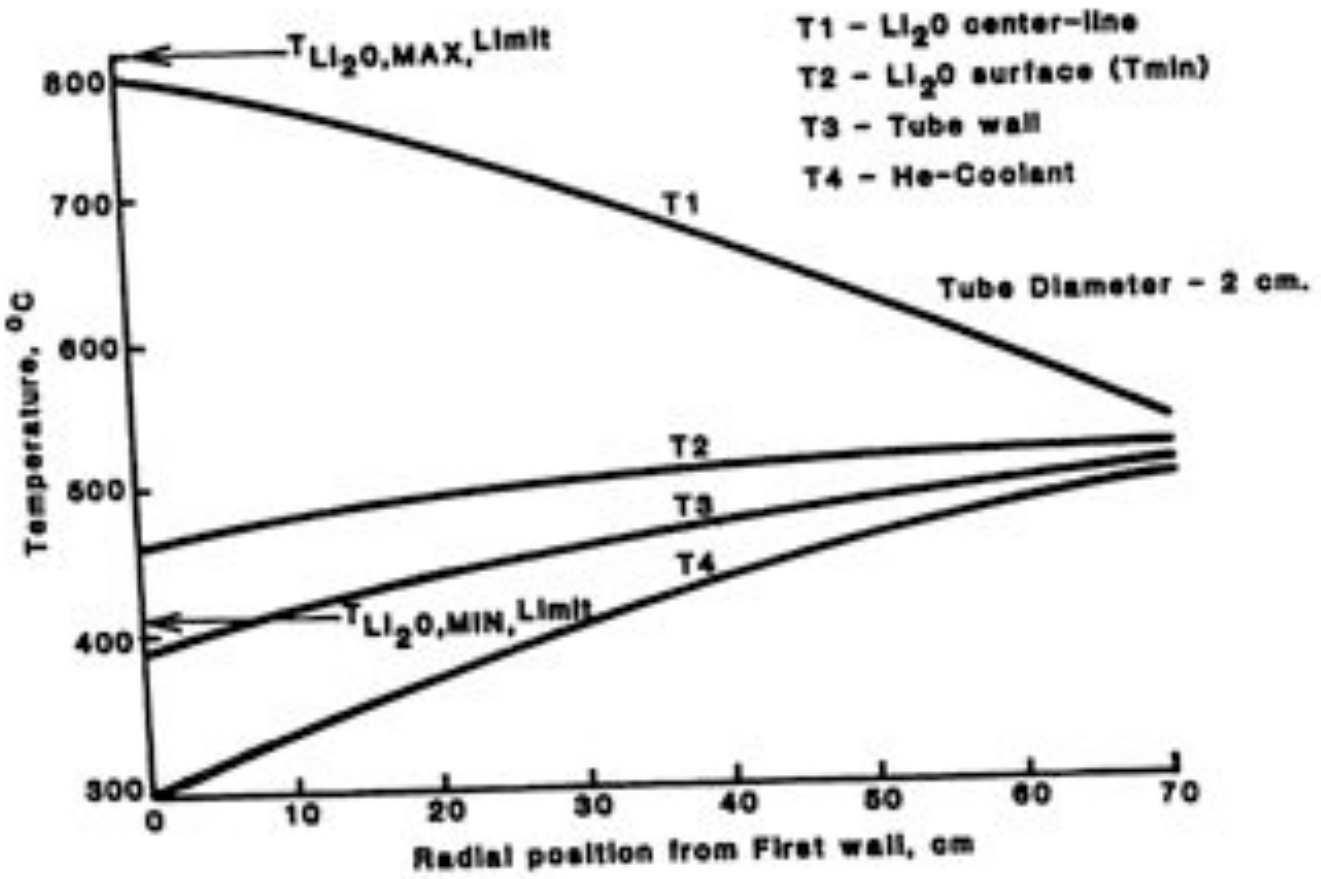

Figure I.H.7. Li_2O Tube Temperature Distribution.

I.I REACTOR SAFETY ISSUES

The primary safety concern related to the design of fissile fuel-producing blankets is the potential hazard associated with the release of the actinide, fission product, and activation product radioactivity. This radioactivity, produced by fissioning and parasitic captures of neutrons in the fertile and fissile materials and metallic structures, could be mobilized during postulated accidents. The issues of tritium safety, though requiring appropriate design attention, pose a relatively lower level of risk during major events.

The major source of stored energy for radioactivity mobilization is the heat generated by the decay of radio nuclides in the blanket (primarily ^{233}Th, ^{233}Pa, and fission products). The initiating events of major consequence are those that lead to a loss of cooling capability. The major differences between the reference liquid lithium cooled tandem mirror fusion breeder and the tokamak fusion breeder design are the absence of stored chemical energy from lithium reactivity, the much higher wall loading (~ 3 vs 1.3 MW/m^2 in the reference blanket), and effects due to using a helium rather than lithium coolant (e.g., a lower conductive heat removal capability in a loss of coolant flow event, easier fuel dump, different accident initiators). Importantly, the decay heat removal load per unit wall area will increase due to the higher wall loading, but it is expected that coolant flow can be maintained at reduced pressure in all cases with redundant helium circulators.

The maximum radio-nuclide hazard inventory (at time of fuel discharge) is not expected to differ substantially between the tokamak and reference tandem mirror reactors - a result of the opposing effects of higher wall loading versus the compactness of the tokamak design. Specifically, the major contributions to the radioactive inventory per unit volume are the actinides. These reach equilibrium in roughly 60 days and their respective concentrations are proportional to the wall loading. The volume of actinides is roughly inversely proportional to the wall loading.

The factor of four to five lower number of modules (or sectors) in a tokamak results in a higher radioactive inventory per module. Thus, individual module failures could have correspondingly higher consequences, and heat removal sytems would face higher heat loads. Other factors are the higher

complexity of the tokamak and the decrease in the fuel ball adiabatic melt time and, thus, the shortened time for corrective action due to the higher afterheat level.

Due to the compactness of the tokamak and the absence of liquid metal MHD effects, gravity dump of the mobile fuel to a dump tank beneath the reactor is possible at a reasonable distance (~ 7 m) without forced flow. Freeze valves in conjunction with a purely gravitational dump would provide a totally passive dump system. If a suitable nonreactive thermal contact medium within the dump tank could be identified, passive cooling may be possible in conjunction with heat pipes and convective air heat exchangers, but thermal shock to the dumped fuel could be a concern.

I.J SUMMARY OF FUEL CYCLE AND ECONOMICS ANALYSIS

In this section, the overall performance and cost of a helium cooled, beryllium blanket tokamak fusion breeder reactor are estimated and are combined with similar data for ^{233}U burning LWR fission reactors to obtain an estimate of the costs of electricity and bred fuel for a symbiotic electricity generation system consisting of the fusion breeder, its LWR clients, and the associated fuel cycle facilities. The results are compared with those for a reference case, the liquid lithium cooled fusion breeder tandem mirror design of 1982.

Table I.J.1 compares the key tokamak breeder fuel cycle parameters with those for the reference tandem mirror breeder. Figure I.J.1 shows the corresponding fuel cycle availability budget. The calculation of the actinide concentrations and the development of the availability budget assume a 90% operational availability during scheduled operation. In the case of the tokamak breeder, this allows as many as 12 unscheduled and 34 scheduled outage days during the 155-day fuel cycle period. The total yearly fissile breeding is 13% lower for the tokamak breeder.

The performance and cost of the helium cooled, beryllium blanket tokamak was analyzed using TRW's Tokamak Reactor Systems Code (TSC). These results are shown in Tables I.J.2, I.J.3, and I.J.4. The tokamak cases are for current drive by induction and neutral beams. The tandem mirror breeder was modeled using the TRW's Tandem Mirror Reactor Systems Code. Comparisons between the tandem mirror and tokamak results should be made with some reservations because, 1) the two designs represent different levels of effort, and 2) the models in TSC and TMRSC are somewhat different.

As shown in Table I.J.2, the reference tandem mirror produces the most electricity, 24% higher than the inductive current drive tokamaks and 82% higher than the neutral beam driven tokamak. The inductively driven tokamak has a 47% higher (442 MW_e) net electricity production compared to the neutral beam current drive case. These results are also reflected in the net plant efficiency figures (34%, 30%, and 20%). It is clear that neutral beam driven systems will result in substantial power flow penalties.

Table I.J.1. Summary of Breeder Fuel Cycle Characteristics.

	TOKAMAK	TANDEM MIRROR
Net Fissile Production (Kg/yr)[a]	4905	5635
Fissile Inventory (Kg)		
In-Core[a]	1535	1180
Post Discharge	2419	2815
Plant Capacity Factor (%)	70	70
Enrichment (%)[b]		
^{233}Pa	0.43	0.4
^{233}U	1.00	0.7
Total	1.43	1.1
Energy Multiplication		
BOC	1.30	1.25
EOC	2.10	2.50
AVE[a]	1.70	1.89
Full Cycle Period (days)	155	321[c]

a) average over cycle.
b) atoms per ^{232}Th atom (%).
c) 1.5 batches of fuel during this period assuming a two-zone blanket with fuel replaced twice as often in the first zone.

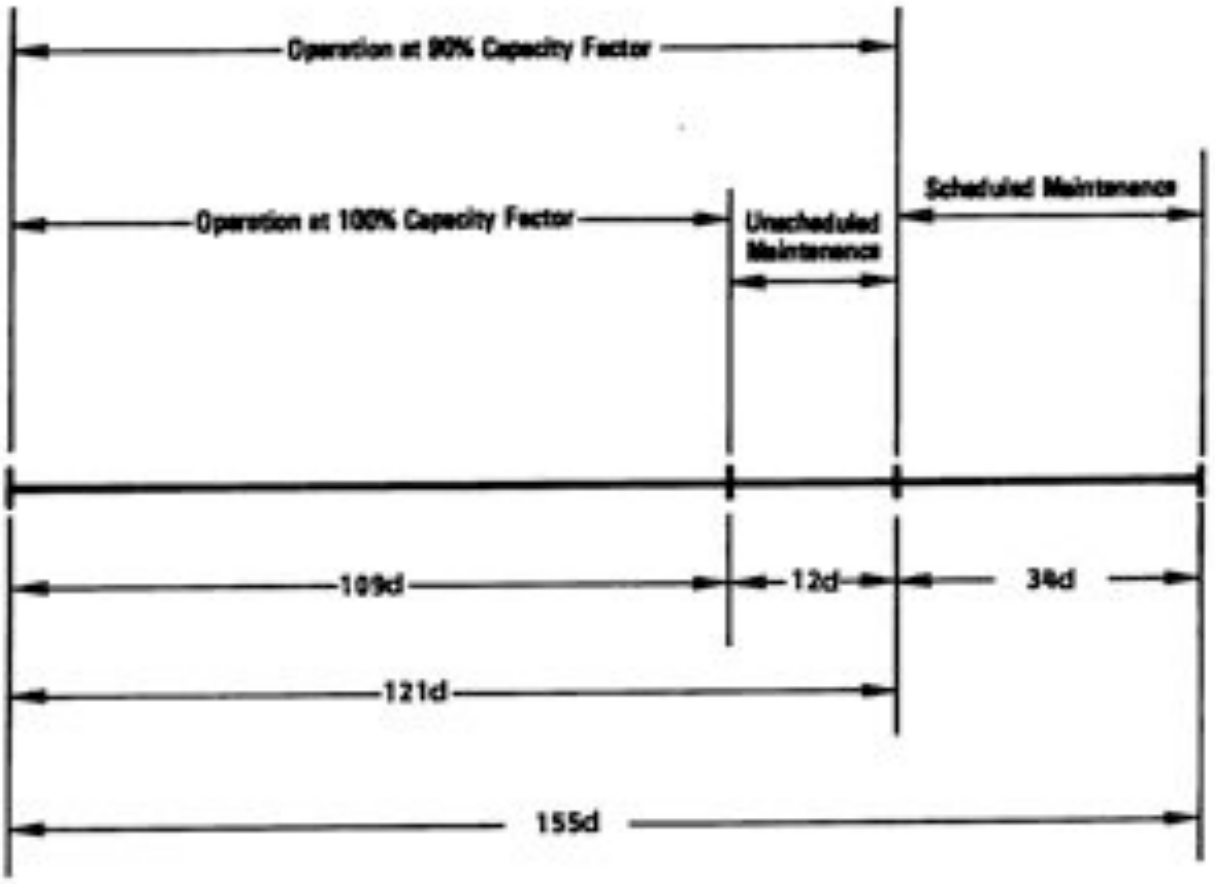

Overall Availability = 109/155 = 0.70

Figure I.J.1. Tokamak Breeder Availability Budget.

Table I.J.2. Fusion Breeder Performance Comparison.

	Fusion Breeder Type		
	Reference Lithium (Tandem Mirror)	Tokamak (Inductive CD)[b]	Tokamak Neutral Beam (CD)[c]
Major radius (m)	193 (length)	6.75	7.69
Minor radius (m)	1.5 (cc radius)	1.80	1.57
Fusion power (MW)	3000	3000	3000
Pulse length (s)	ss	2700	ss
Blanket energy multiplication:			
Minimum	1.25	1.30	1.30
Maximum	2.50	2.10	2.10
Average	1.88	1.70	1.70
Gross nuclear power (MW)[a]	5100	4680	4680
Gross electric power (MW)[a]	2226	1667[f]	1850[g]
Driver recirculating power (MW)	325	6.7[f]	621
Additional recirculating power (MW)	180	275	286
Net electric power (MW)[a]	1720	1385[f]	943
Net fissile production (Kg/yr)[d]	5635	4905	4905
Fissile inventory (Kg)[d]	3995	3954	3954
In-core[a]	1180	1535	1535
Post discharge[e]	2815	2419	2419
Plant capacity factor (%)[a]	70.0	70.0	70.0
Plant efficiency	.34	.30[f]	.20

a) average over fuel cycle period.
b) inductive current drive.
c) neutral beam current drive.
d) includes average plant capacity factor.
e) assumed to be half-year's average production.
f) averaged over reactor operational period.
g) includes NB thermal energy deposited on FW and converted in the T/G.

Table I.J.3. Fusion Breeder Cost Comparison ($ Million, 1983).

	Fusion Breeder Type		
	Reference Lithium (Tandem Mirror)	Tokamak (Inductive CD)	Tokamak Neutral Beam (CD)
Land and land rights	6.3	6.3	6.3
Structures and site facilities	563	531	531
Fusion driver components[a]	863	458	1638
First wall/blanket shield[b]	499	395	423
Heat transport components[c]	502	245	258
Misc. reactor equipment	299	288	274
Turbine plant equipment	370	401	432
Electrical plant equipment	158	164	167
Misc. plant equipment	19	53	53
Fuel cycle facilities[d]	382	330	330
Direct Cost	3660	2871	4112
Contingency (20%)	732	574	822
Total Direct Cost	4392	3445	4934
Indirect Cost (34%)	1485	1163	1665
Total Overnight Cost	5877	4608	6599
Cost of Interest and Escalation During Construction (17.5%)	1028	806	1155
Total Plant Cost	6905	5414	7754
Fusion Breeder Cost/LWR Cost[e]	2.76	2.36	3.38

a) includes magnets, heating systems, direct convertor.

b) includes beryllium and lithium.

c) includes circulators for helium loops.

d) includes reprocessing, beryllium fabrication, thorium fab.

e) basis: $\$/KW_t$

Table I.J.4. Fusion Driver Component Costs ($ Million, 1983).

	Fusion Breeder Type		
	Reference Lithium (Tandem Mirror)	Tokamak (Inductive CD)	Tokamak (Neutral Beam CD)
Tokamak Magnets	--	355	328
TF coils	--	230	289
PF coils	--	50	37
Solenoidal coil	--	75	2
Tandem Mirror Magnets	601	--	--
Central cell	460	--	--
Barrier coil 1	40	--	--
Barrier coil 2	37	--	--
Transition coil	21	--	--
Yin-yang pair	43	--	--
RF Systems	75	103	6.3
ICRF	19	71	--
ECRF	56	6.3	6.3
LHRF	--	26	--
Neutral Beam Systems	150	--	1304
Direct Converter	36	--	--
Total Fusion Driver Components	863	458	1638

As shown in Tables I.J.3 and I.J.4, the cost difference between the two tokamaks is primarily caused by the high cost of the neutral beam system. The neutral beam driven tokamak is also slightly more expensive in other areas because it optimizes at a slightly larger physical size (7.7 m). The size optimization is driven by plasma scaling laws which predict both a decreasing plasma current requirement and a decreasing neutral beam absorption efficiency as the reactor major radius increases.

The optimal major radius of the 3000 MW_f inductively driven tokamak (6.75 m) is also larger than the smallest possible major radius (6.29 m). It is determined by trading longer pulse lengths and a higher duty factor (at larger major radii) against lower capital costs (at smaller major radii). In the case of the miscellaneous reactor equipment account, the inductively driven tokamak is slightly more expensive due to various costs associated with pulsing. These include the increased costs of the magnet support structure, the vacuum system, and the magnet power supplies.*

Cost differences between the tokamaks and the tandem mirror reflect the different nature of the two plasma confinement schemes as well as modeling differences. The major difference is the cost of fusion driver components. The large cost of the tandem mirror central cell magnets, first wall, blanket, and shield can be attributed to its low wall loading (1.3 MW/m^2 versus 3 MW/m^2 for the tokamak). The inductively driven tokamak is about 22% less expensive than the tandem mirror but about 30% less expensive than the neutral beam driven tokamak.

A summary of economics results for symbiotic electricity generation systems consisting of fusion breeders and their supported LWR client reactors is shown in Table I.J.5. This table includes cases for the utility and government ownership of the reference tandem mirror breeder (cases 1 and 2), cases for the inductively driven tokamaks (cases 3 and 4), and two cases for the neutral beam driven tokamak breeder (cases 5 and 6). The first column of the table indicates the 30 year average present value of the cost of electricity produced by the symbiotic system in 1984 dollars. This value is obtained by discounting the cost of electricity in a given year back to the

---

* Energy storage system cost not yet included.

first year of operation and averaging the results of the 30 values. The second colum represents the average present values of bred fissile fuel calculated in the same manner.

The third and fourth columns relate to a comparison of the symbiotic system of fusion breeders and their client LWRs with an LWR which uses conventional, mined uranium and a full fissile recycle (i.e., reprocessing) fuel cycle. The cost of mined uranium is assumed to be 55 $/kg (1984 dollars) in the first year of operation and is assumed to escalate at a rate of 2%/yr above general inflation over the 30 year operating lifetime of the LWR. The "breakeven year" is the year in which the cost of electricity for the U_3O_8 fueled LWR exceeds that of a symbiotic system which begins operation in the same year.

Table I.J.5. Summary of Economic Analysis.

	Description	Average Present Value Elect. Cost (mil/KWeH)	Average Present Value ^{233}U Cost ($/g)	Breakeven Year[a]	Benefit[a] ($ B)	Breakeven U_3O_8 Price[b] ($/Kg)
1)	Mirror/Gov't	31.7	31.5	8	3.7	42
2)	Mirror/Utility	34.7	64.7	24	-8.9	116
3)	Tokamak/Gov't/Ind CD[c]	30.6	22.9	1	5.6	13
4)	Tok/Utility/Ind CD	33.4	53.4	21	-4.6	91
5)	Tok/Gov't/NB CD[d]	34.8	69.1	29	-9.5	132
6)	Tok/Utility/NB CD[d]	38.9	115	--	-24.2	250

a) nominal results assumed $55/kg ^{233}U starting price of U_3O_8 with 2%/yr escalation above inflation.

b) U_3O_8 starting price required to produce a zero net benefit over the 30 year breeder life cycle.

c) Gov't owned tokamak breeder with inductive current drive.

d) Utility owned tokamak breeder with neutral beam current drive.

The "benefit" is the present value of the annual cost difference of operating the number of LWRs in the symbiotic system using mined U_3O_8 versus fuel bred in the fusion breeder summed over 30 year. More consisely, it describes the overall cost savings per fusion breeder if the fusion breeder were introduced at a 55 \$/kg U_3O_8 price. Negative values for the benefit represent uneconomical cases. The cost of U_3O_8 which is sufficient to provide a zero 30 year benefit is the "breakeven U_3O_8 price" shown in the last column of Table I.J.5.

Results for the inductively driven tokamak cases are very similar to those for the tandem mirror cases. In both utility owned cases, breakeven occurs after more than twenty years of operation and results in a net loss (over 30 years) of several billion dollars. In both cases, the price of uranium must approximately double to achieve a 30 year breakeven. For government ownership of either the tokamak or the tandem mirror breeder, substantial net benefits (5.6 and 3.7 \$billion respectively) accrue over the 30 year lifetime. The government owned tokamak breeder breaks even at a U_3O_8 price as low as \$13/kg. Conversely, the neutral beam driven tokamak is not likely to achieve economic breakeven regardless of ownership until U_3O_8 prices increase substantially.

The following conclusions result from the above modeling of the potential economic performance of the tokamak breeder:

- The tokamak breeder economics results are similar to previous results for the reference tandem mirror fusion breeder.

- Government ownership of the fusion breeders presents substantial economic advantages and fits well into the institutional framework of a government sponsored fuel cycle center (similar to the current fissile enrichment plants).

- The government owned, inductively driven, tokamak breeder could be economical at less than current U_3O_8 prices given a long term U_3O_8 price escalation rate which is 2% above general inflation and a full fissile recycle nuclear economy.

- NB current drive carries a substantial economic penalty but could breakeven in a government ownership case at a market price for U_3O_8 of 132 $/kg.

- Economic issues yet to be addressed include the potential impacts of lower LWR SWU costs, higher LWR fuel reprocessing costs, etc.

CHAPTER II

TOKAMAK DRIVER DEFINITION

II.A INTRODUCTION AND DESIGN SUMMARY

II.A.1 Design Guidelines

The major design guidelines for the tokamak driver, summarized below, were derived at the beginning of the project from objectives discussed in Chapter I and elsewhere in this report. Further background information can be found in an FY 1982 report (1).

1) Fusion power to be about 3000 MW.
2) Neutron wall loading to be less than 3.0 MW/m^2.
3) Operation to be steady-state with neutral beam current drive or very long pulse with RF current startup (both considered).
4) The ratio of circulating power to gross electric power should be minimized by operating the plasma at ignition in the long pulse mode, or at $Q \sim 10$ if the steady-state current drive option is selected. In the latter case, it is desirable that the method used for bulk plasma heating also be capable of driving the plasma current.
5) The TF (toroidal-field) coils must be superconducting. All PF (poloidal-field) coils (with the possible exception of one or more divertor coils) should be be superconducting and located outside the TF coils.
6) The erosion rate of the first wall should be minimized. A magnetic divertor is used to control impurity levels in the plasma. The plasma is doped with a small, controlled level of a high-Z material to enhance the radiation fraction of the energy deposited within the plasma.
7) All particle pumping is to be accomplished by the divertor, with pellet injection used to maintain steady-state plasma density.

8) The dimensions and materials of in-vessel components should be selected to minimize neutron losses.

9) The central solenoid should have sufficient diameter and field range to provide complete plasma current startup for the steady-state option, or to maintain the current for several thousand seconds if the long pulse option is selected.

10) There must be sufficient space for a full-sized breeding blanket on the inboard side of the tokamak.

11) Plasma vessel and divertor sectors are to be removable by horizontal (i.e., radial) extraction between TF coils.

The next section gives an overview of the driver design that was conceived to satisfy the above requirements.

II.A.2. Design Overview

Figure II.A.1 shows the radial buildup of the neutral beam driver, steady state tokamak* and Table II.A.1 gives the major parameters for optimal tokamaks for both steady state and long pulse operation. In both cases, the requirements for a fixed fusion power and a maximum wall loading can be satisfied by a range of major radii subject to constraints on "beta" for dee-shaped plasmas and constraints on the maximum field at the TF coil (limited to 11 T). The quantity "beta" is defined as the ratio of spatially averaged plasma pressure to the magnetic field pressure and is a function of the aspect ratio. The inboard blanket/shield thickness is specified to be 1.5 m to allow sufficient room for an efficient breeding blanket at a reasonable major radius. Note that the neutral beam driven tokamak optimizes at a considerably larger size for the same fusion power. This results because, at fixed fusion power, the plasma current and, therefore, neutral beam power, decreases with increasing major radius.

In the steady state operating mode, the plasma current is started up by the central OH solenoid, which has a flux swing of 732 Webers. The current is

* The geometry of the long pulse option is shown throughout Chapter III and is not shown in Chapter II.

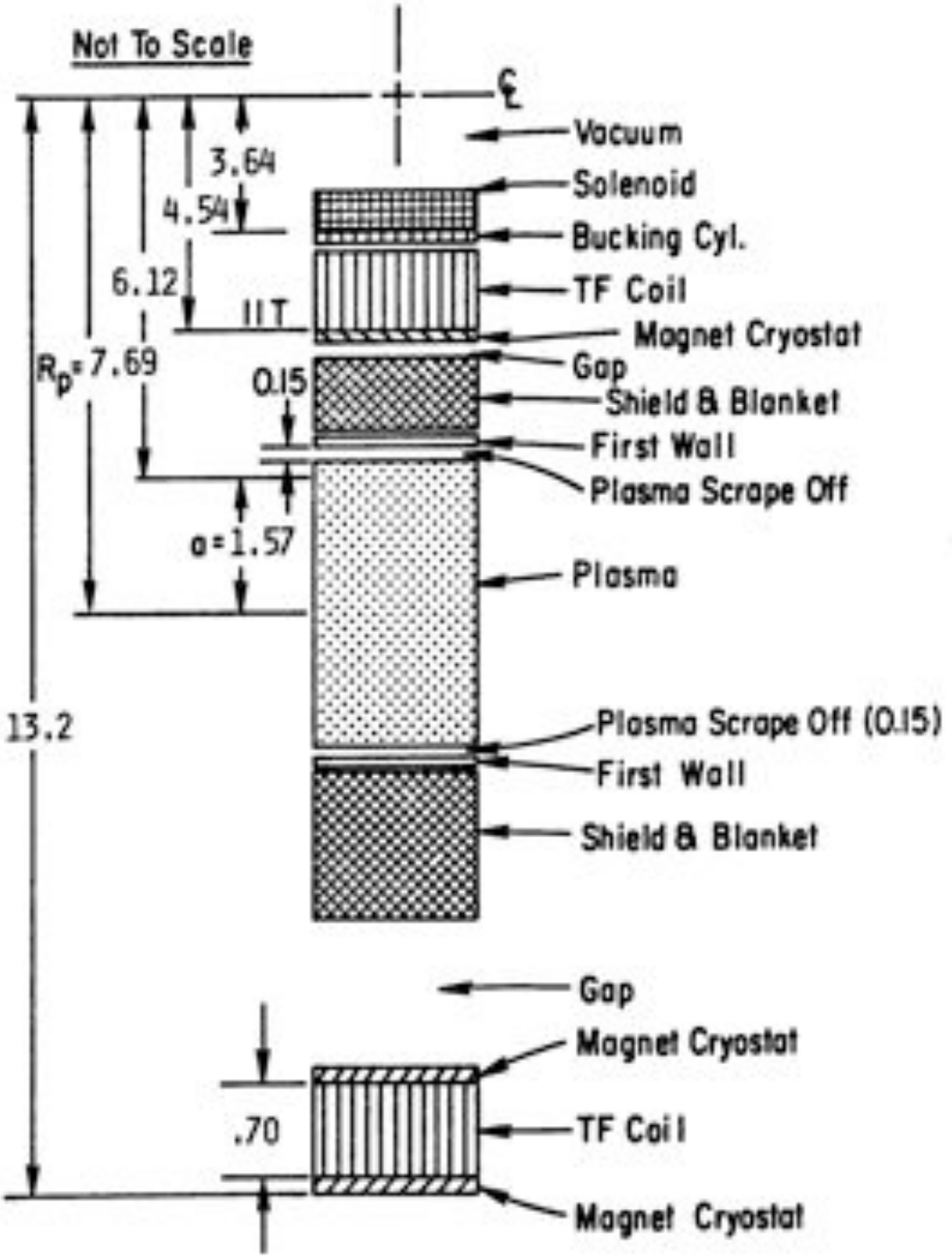

Figure II.A.1. Radial Buildup of Steady State, Neutral Beam Driven Tokamak Fusion Breeder.

sustained by the injection of 310 MW of 1.5 MeV negative-ion based neutral beams. This results in a fusion energy amplification, Q_p, of approximately 9.7.

In the long pulse operating mode, 25 MW of RF radiation (lower hybrid) is used to start up the bulk of the plasma current. The current can be maintained for 3000 seconds by means of the flux swing in the OH solenoid. With a downtime between pulses of 100 s*, the duty factor would be 97%. The plasma would be heated to ignition by 67 MW of ICRF, thereby eliminating neutral beams completely. This mode has the major advantage of eliminating the continuous ~ 475 MW-electric required by the neutral beam supplies in the steady state mode, but has the disadvantage of introducing mechanical and thermal cycling of the reactor components. With a pulse length of 3000 s, cyclic fatigue problems become an important issue, but the economics improvements relative to the neutral beam case appear to be sufficient to merit selection of the long pulse mode as a baseline. If the Z_{eff} were held to about 1.4, the burn time in the long pulse mode would increase to about 5800 s and cyclic fatigue problems would be reduced, but first wall erosion and the heat load on the divertor would be greatly increased. A disadvantage of the divertor is the associated neutron loss - a 15% impact on total breeding (see section III. C).

* Considering the cost of energy storage, a shorter downtime (~ 30 s) may be optimal.

TABLE II.A.1. PRINCIPAL PARAMETERS OF THE TOKAMAK DRIVERS.

PARAMETER	UNIT	STEADY STATE MODE	LONG PULSE MODE
GEOMETRY			
Major Radius	m	7.69	6.75
Minor Radius	m	1.57	1.80
Aspect Ratio		4.90	3.75
Elongation		1.80	1.80
TF Coil Inboard Radius	m	4.54	3.37
Inboard B/S Thickness	m	1.2	1.2
Max B - TF Coils	T	11.00	11.00
PLASMA			
B at Plasma Center	T	6.49	5.50
Inverse Rotational Transform		2.25	2.25
Plasma Current	MA	9.81	12.4
<Beta>		.045	.059
<Density>	$10^{14}/cm^3$	1.34	1.25
<Temp>	keV	15.00	15.00
OH Bore Radius	m	3.34	2.14
OH Coil Delta B	T	18	18
Solenoid Flux	V-S	732	300
Z_{eff}[a]		2.7	2.7
Loop Volt	V	.12	.10
Max Pulse Length	s	SS[b]	3000
Curr. Drive Mechanism		NB	Inductive
Curr. Drive Power	MW	310	92[c]
NTAU (for Z_{eff} = 1)	$10^{14}s/cm^3$	19	17
Radiation Fraction[a]		.52	.52
NTAU Reduction Factor Due to Radiation[a]		2.1	2.1

TABLE II.A.1. PRINCIPAL PARAMETERS OF THE TOKAMAK DRIVERS (Continued)

PARAMETER	UNIT	STEADY STATE MODE	LONG PULSE MODE
MAGNETS			
TF Horiz Bore	m	8	8
TF Vert Bore	m	13	13
Max B-TF Coils	T	11	11
TF Coil Material		Nb_3Sn	Nb_3Sn
Max B-PF Coils	T	8	8
PF Coil Material		NbTi	NbTi
POWER PRODUCTION			
Fusion Power	MW	3000	3000
Fusion Gain, Q_p		9.7	Ignited
First Wall Area[d]	m^2	744	744
Surface Heat Flux[e]	W/cm^2	67	44
Neutron Wall Load	MW/m^2	3.0	3.0

a) produced by Xenon injection.

b) possibly limited to several hours.

c) ICRH plus LHRF during startup only.

d) assumes divertor throat subtends 7% of the solid angle from the plasma center to the minor radius.

e) assumes divertor removes 75 of 80 parts of non-radiated plasma thermal efflux.

II.B. FUSION DRIVER SYSTEMS

II.B.1 Introduction

Fig. II.B.1 shows a schematic elevation view of the steady state, neutral beam driven tokamak breeder. There are 10 TF coils of modified dee-shape and 10 separate vacuum vessel and blanket sectors. The "hard" vacuum vessel is formed by the outer structure of the blanket sectors. Each of the 10 sectors can be removed by horizontal (i.e., radial) extraction between TF coils.

An INTOR-type single-null poloidal divertor (3) is used for particle and heat removal from the torus. A divertor was chosen over a pumped limiter because analyses carried out in the INTOR and other projects have shown that limiter impurity control physics issues have not yet been resolved and that limiter erosion issues appear to be more difficult. Divertor plasma-side erosion should be less of an issue because the divertor does not have a leading edge and because the divertor offers the possibility of a low plasma sheath potential with the prospect for low erosion of a high-Z plasma-side material such as tungsten. Nevertheless, if acceptable limiter performance can be demonstrated, there will be a cost/performance incentive for replacement of the divertor with a limiter.

The divertor is located on top to better accommodate the flow of the Be/Th fuel pebbles while providing for maximum blanket coverage. The top location also gives the ability to periodically replace the divertor plates via horizontal translation. However, the vacuum pumping ducts that lead to the basement require substantially more shielding than in the case of a divertor located at the bottom of the torus (the alternative configuration considered).

All but one set of the PF coils are superconducting and located external to the TF coils. The inside divertor coils are normal coils and are located in the TF-coil bore in order to gain better control over the diverted flux lines (see Fig. III.A.1). A few low power single-turn copper control coils are located near the plasma chamber for fine tuning of the plasma position.

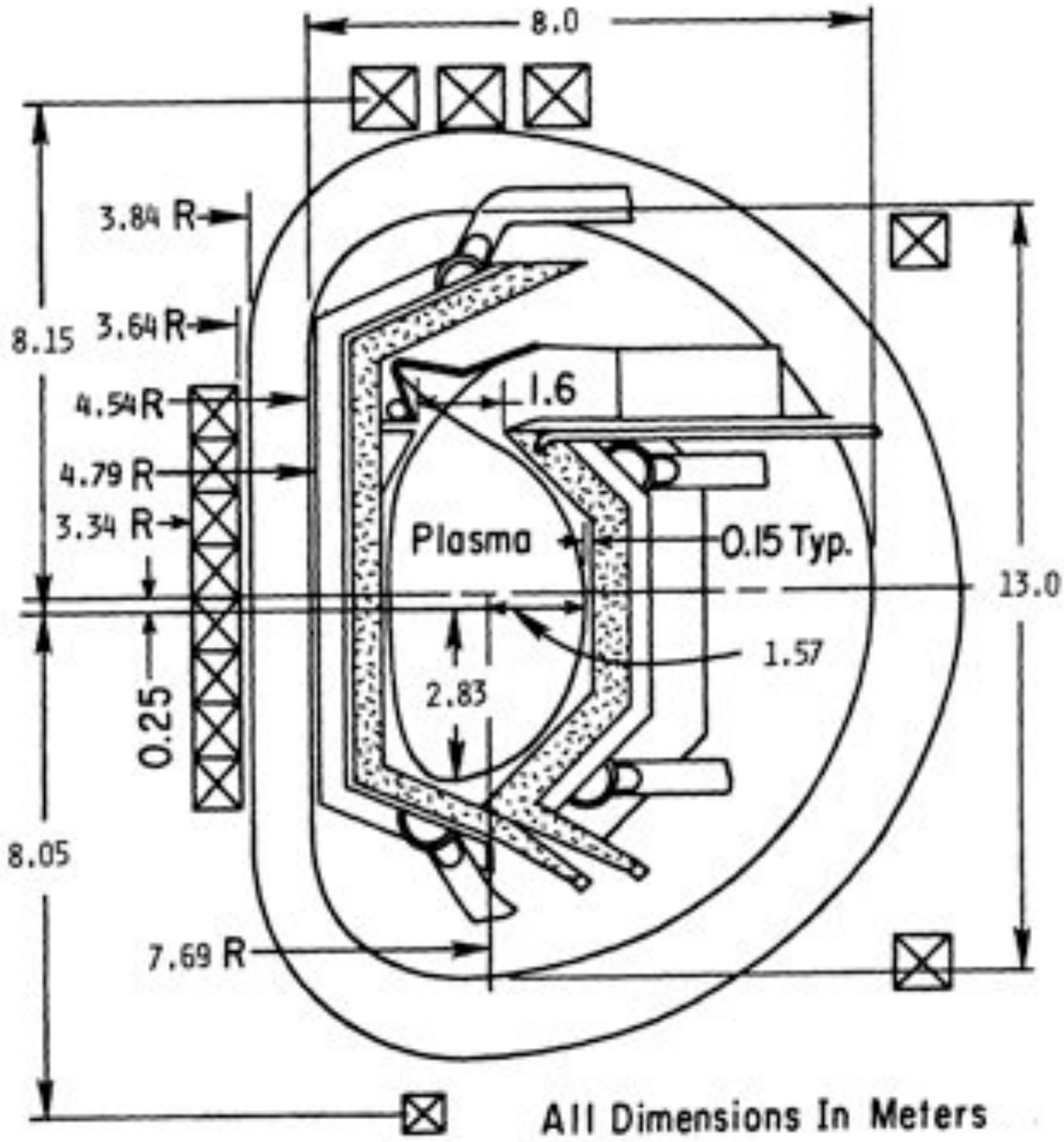

Figure II.8.1. Elevation View of the Steady State, Neutral Beam Driven Tokamak Fusion Breeder.

II.B.2 Plasma Heating and Current Drive Systems

II.B.2.a Determination of Size and Operating Parameters

The geometric parameters of the tokamak fusion breeder were determined by solving seven coupled equations that relate the required fusion power and neutron wall loading to the major radius, the maximum beta allowed in dee-shaped tokamak plasmas, the maximum plasma current that can be established when the field at the TF coil is limited to 11 T, and the inboard blanket/shield thickness. This thickness (i.e., first wall to TF coil conductor) is set at about 1.2 m to allow sufficient room for a full-scale breeding blanket, with adequate space for the cooling ducts. For P_{fusion} ~ 3000 MW, the size of the plasma is always much larger than required to attain ignition conditions (according to all scaling relations presently used for the energy confinement time, τ_E). An equilibrium τ_E is realized in part by doping the plasma with xenon to enhance radiation loss.

II.B.2.b Heating and Current Drive Options

Candidate plasma heating methods include both radiofrequency (RF) and neutral-beam techniques. Tokamak current drive by RF energy in the lower hybrid (LH) frequency has received much interest and is an experimentally proven technique at low plasma density (4). However, the dispersion relation for LH waves shows that penetration into the plasma becomes progressively more difficult with increasing beta. LH waves would not be able to penetrate the tokamak breeder plasma, where the central beta is greater than 10%. Futhermore, plasma heating by LH waves has been rather unsuccessful to date, so that heating to ignition and thermal stability control of the burning plasma by LH would be unlikely even if wave penetration were possible. Thus, an additional high power heating system would be required to permit steady-state operation. Plasma heating by ion cyclotron waves, the other main RF heating technique, has been quite successful in experimental tokamaks.

Steady State Operational Mode - To date neutral beams have proved to be the most effective plasma heating method. Neutral-beam current drive has had

only token experimental success, but the theoretical basis is strong for the high beam energies (~ 1.5 MeV) proposed here (5). Neutral-beam injection was chosen as the primary plasma heating system for the steady state operational scenario because the largest plasma temperatures and beta values to date have been obtained with neutral beams, and theoretical analyses indicate that the same beam systems can be used for bulk plasma heating and current drive. In the steady state operating mode, the operating regime is actually subignition (Q_p = 9.7) because of the continuous injection of beam power to drive the plasma current. This operational mode has the advantage that appropriate variation of the beam power provides thermal stability control, eliminating the need to identify and demonstrate another control mechanism that would be required for truly ignited operation.

The beams would be formed from D^- ions accelerated to 1.5 MeV by the techniques currently under development at LBL and elsewhere (6). In this method, the ion beams are obtained from self-extracting surface conversion D^- sources. Electrostatic quadrupole accelerators accelerate the beams to 1.5 MeV. The beams are then neutralized by photodetachment using an oxygen-iodine chemical laser. The overall injector efficiency is predicted to be at least 65%.

Between 60 and 80 MW of injected power is required to heat the plasma to ignition conditions, but about 310 MW of injected power is needed to drive the total plasma current. This circulating power loss is more tolerable for a hybrid reactor than for a "pure" fusion-electric plant because revenue from the fissile fuel product of the hybrid lessens the importance of the cost per kWe. Three beam ducts are used to inject the total current of 206 A-equivalent, with the beam orientation 35 degrees to the normal to the outer surface of the plasma in the midplane. A total of only 1-2% of the torus wall area is required for neutral-beam injection, pellet injection and plasma diagnostics. Similar access area would be required if RF heating were chosen as the principle heating method.

The only other non-ohmic heating system that is required is about 3 MW of ECRH power at 120 GHz for pre-ionization and electron heating at the beginning of the pulse. This power would be supplied by gyrotrons currently under development.

To initiate the burn, the plasma current (I_p), density (n) and temperature ($T_e = T_i$) are increased by various processes over a period of approximately 25 s.

About 3 MW of ECRH is used to preionize the filling gas and heat the electrons to $T_e > 10$ eV. The OH solenoid is then activated. The flux linkage from the solenoid and the EF coil system generates the full plasma current over a period of 15 s while T_e is raised to about 1 keV and n is increased to about 10^{14} cm^{-3}.

This density is sufficiently large to trap the 1.5 MeV neutral beams, which are activated one-by-one over the next 5 to 10 s. Together with fusion alphas, whose power density increases as T_i approaches and exceeds 10 keV, the beams heat the plasma electrons and bulk ions to their operating temperature ($\langle T_e \rangle = \langle T_i \rangle = 15$ keV).

The rate of flux change in the OH solenoid is gradually reduced to zero as the beam ions carry an increasing portion of the plasma current. The 310 MW of beam power is chosen so that the entire plasma current can be readily sustained at the expected current drive efficiency of 0.032 A/W at the operating density. Effective current drive by the beams requires that Z_{eff} be greated than 1.4. Even without xenon doping of the plasma, this level of impurity content will exist because of fusion alpha buildup and wall sputtering.

The plasma is fueled by continuous injection of frozen deuterium and tritium pellets. During the burn, the beam power and pellet injection rates are varied to keep I_p, n, and $T_e = T_i$ at levels required for a constant fusion power output. The magetic divertor plays a vital role in controlling the plasma density and ensuring stable profiles of n and T_e by removing particles and heat from the edge of the plasma. The divertor is also responsible for fusion ash removal.

Long Pulse Operational Scenario - In the long pulse operating mode, RF radiation (lower hybrid) is used to start the plasma current at low plasma density (with the assistance of the flux swing in the EF coils) and the flux swing in the OH solenoid is reserved for driving the current during the burn. The central solenoid can maintain this current for 3000 seconds at a

Z_{eff} of 2.7. With a downtime between pulses of 100 s, the duty factor is 97%. This long pulse mode has the major advantage of eliminating the 475 MWe power drain accounted for by the neutral beams in the steady state mode, and a second advantage of reducing the thermal output from the plasma from 910 MW to 600 MW. However, the pulsed mode has the disadvantage of introducing mechanical and thermal cycling of the reactor components. This latter problem is aggravated at large Z_{eff} which shortens the pulse time (see Section II.C) to increase the plasma radiation loss.

A 33% increase in pulse length could be realized by raising the maximum field in the solenoid above the presently specified value of 9 T to 12 T. Further extension of the pulse length would require an increase in the diameter of the central throat and, therefore, in reactor size and cost.

The long pulse scenario requires about 25 MW of lower hybrid radiation for current startup, and an additional 60 to 80 MW of ICRF (or NBI) for bulk plasma heating because lower hybrid RF is relatively ineffective for bulk heating. Thus, the total installed heating and current drive power is about 35% of that required in the steady state mode.

II.B.3 Vacuum Vessel and Divertor Components

The "first wall" consists of the front faces of the lobe-type blanket submodules (see Sections III.A and III.D). This approach minimizes neutron attenuation in front of the blanket relative to the use of a separate first wall. The vacuum welds are made at the outside of each sector, thus providing reactor modularity with a minimum number of welds near the plasma. The vacuum vessel resistance in the toroidal direction is specified to be adequate to permit full startup of the plasma current in 15 s or less. This resistance would be sufficiently high to prevent significant damage to the vessel in the event of a major plasma disruption (in which case the current drops to zero in a fraction of a second).

The divertor is comprised of 10 segmented modules, each with its own vacuum pumping system. All pumping of the torus is carried out via these ducts. Replacement of the divertor internal components is required periodically because of severe erosion. Each divertor module can be removed by horizontal translation between adjacent TF coils.

To maximize neutron economy, it is essential to minimize parasitic material between the mouth of the divertor and the blanket, as well as the divertor size. Futhermore, wherever possible, all in-torus components, such as the baffle defining the throat of the divertor chamber and the collector plates within the divertor chamber, should be fabricated of neutronically favorable materials. Extensive evaluations of candidate materials were carried out in the INTOR program in 1981-82. It was concluded in that program that Be and BeO are the preferred materials to serve as coverings for the first wall, baffles and divertor collector plates, with a Be thickness of up to 2 cm allowed, depending on the heat flux. In the tokamak breeder design, neutron multiplication in Be might partially compensate for neutron losses in the divertor hardware. Protective Be coating of the first wall is not required except in the region of the divertor where the particle flux is high. For this study, the entrance baffle and the neutralizer plates inside the divertor chamber were assumed to be constructed of 2-cm thick Be tiles attached to 2-cm thick (ave.) copper tubes and plates. A detailed divertor design has not been performed.

II.B.4 Magnetic Systems

II.B.4.a TF (Toroidal-Field) Coils

Table II.B.1 gives the principle parameters of the TF coils and other magnet systems of the steady state, neutral beam driven, tokamak suppressed-fission breeder. Superconducting TF coils were selected for the reasons discussed in a FY 1982 report (1). The superconductor is Nb_3Sn, which at 4.2 K will readily support the required maximum field of 11 T.

II.B.4.b Central Solenoid

As discussed in previous sections, the flux swing that can be delivered by the OH solenoid is more than adequate to provide startup of the full plasma current (steady state mode) or to drive a moderately long pulse (long pulse mode). The total field swing of +9 T to -9 T is achievable with Nb_3Sn superconductor. The maximum rate of change of field in the solenoid during startup is about 1 T/s, which is within the present state-of-the-art for a superconducting solenoid. In the steady state operating mode, the solenoid

TABLE II.B.1. NEUTRAL BEAM DRIVEN TOKAMAK DRIVER MAGNET SYSTEMS

TOROIDAL-FIELD COILS	
Conductor	Nb_3Sn
Coolant	Liquid Helium, 4 K
Number of TF Coils	10
Maximum B at Conductor	11 T (R_m = 4.29 m)
TF Ripple at Plasma Edge	0.5% peak-to-average
TF Coil Shape	Modified Dee
Overall Height	14.8 m
Horizontal Bore	8.0 m
Vertical Bore	13.0 m
Radial Build, Inboard	.65 m
Radial Build, Outboard	.65 m
Azim. thickness, Outboard	2.8 m
Open Distance Between Outboard Legs	6.6 m
POLOIDAL-FIELD COILS	
Conductor	NbTi
Coolant	Liquid He, Pool-boiled
Number:	3 EF Coils
	3 External Divertor Coils
	Internal Divertor Coils
	Other EF Coils in Central Solenoid
CURRENT-DRIVING SOLENOID	
Type	Nb_3Sn or NbTi
Coolant	Liquid He, Pool-boiled
Solenoid Outer Rad.	3.64 m
Maximum B in Solenoid	+9 T to -9 T
Maximum Flux Swing	366 Wb

current is programmed back to -9 T during the first 500 s of the burn, with the neutral-beam-driven current compensating for the very small reverse emf during this process. In the long pulse mode, the solenoid current is programmed back during the 100 s dwell time.

II.B.4.c EF (Equilibrium-Field) and Divertor Coils

All of the PF coils, with the exception of the inside divertor coils (Fig. III.A.1) are superconducting and are located external to the TF coils for ease of maintenance and replacement in the event of failure. External placement of the PF coils also facilitates modularization of the reactor. The PF coils maintain a dee-shaped plasma with the triangularity needed to maximize beta. As indicated in Fig. II.B.1, three EF coils are used to provide most of the vertical field for positioning of the plasma column. The three external divertor PF coils also create the magnetic separatrix, outside of which magnetic field lines are "diverted" into the divertor chamber.

II.C PLASMA HEAT FLUX AND WALL EROSION

In this section, the plasma heat flux and first wall erosion for the long pulse operating mode are considered. The heat fluxes and erosion will be about 50% higher for the steady state neutral beam driven mode.

II.C.1 Power Flow and Surface Fluxes

To estimate the first wall erosion, we must first calculate the power flow and particle flux to the wall and the divertor. Starting with the fusion power, P_f, the non-neutron power, P_s, is given by

$$P_s = P_f\ (0.2 + 1/Q)$$

where Q is the plasma gain (i.e., ratio of fusion to injected power). In the long pulse case, the 1/Q term equals zero because the plasma is not heated during the pulse and the 0.2 term represents the power associated with 3.5 MeV alpha fusion products. If we further define the following quantities

f_r = radiated power fraction

η_d = divertor particle power extraction efficiency

then we can define the relevant power flow as

$$P_r = f_r\ P_s$$

$$P_{cd} = (1-f_r)\ \eta_d\ P_s$$

$$P_{cw} = (1-f_r)\ (1-\eta_d)\ P_s$$

where P_r is the radiated power, P_{cd} is the divertor (charged plus neutral) particle power, P_{cw} is the (charged plus neutral) particle power deposited on the first wall, and P_s is defined above. Experimental results on tokamaks with poloidal divertors (such as PDX and ASDEX) indicated that, under optimal conditions, η_d values of 75/80 = .94 appear reasonable.

We can next define the relevant average surface fluxes as

$$P''_{rw} = Q_w f_r P_s/A_w$$

$$P''_{rd} = Q_d f_r P_s/A_d$$

$$P''_{cw} = (1 - f_r)(1 - \eta_d) P_s/A_w$$

$$P''_{cd} = (1 - f_r) \eta_d P_s/A_d$$

where A_d is the divertor surface area, A_w is the first wall surface area, Q_d is the divertor view factor, and Q_w is the first wall view factor.

If we use the following nominal values which are representative of the selected design,

$P_f = 3000$
$P_s = 600$
$\eta_d = 0.9375$
$A_w = 744\ M^2$
$A_d = 80\ m^2$
$Q_d = 0.07$
$Q_w = 0.93$

then we may express the surface fluxes in terms of the radiated fraction

$$P''_{rw} = 75\ f_r\ w/cm^2$$

$$P''_{rd} = 53\ f_r\ w/cm^2$$

$$P''_{cw} = 5.0\ (1 - f_r)\ w/cm^2$$

$$P''_{cd} = 703\ (1 - f_r)\ w/cm^2$$

For erosion, the charged particle fluxes, P_{cw} and P_{cd} are important. For heat transfer, the total heat fluxes are important. The later quantities are given by

$$P''_w = P''_{rw} + P''_{cw} = 75\ f_r + 5.0\ (1 - f_r)\ w/cm^2$$

$$P''_d = P''_{rd} + P''_{cd} = 53\ f_r + 703\ (1 - f_r)\ w/cm^2$$

II.C.2 Enhancement of Radiation Loss

In the tokamak reactor, under typical operating conditions, $f_r < 0.20$. This results in a large fraction (>80%) of the power deposited in the plasma (i.e., alpha power plus any auxiliary heating) being transported to the divertor. Since the divertor plates surface area is limited, the local heat fluxes would be very high (>2000 w/cm^2). To reduce the divertor heat flux, a means for radiating the absorbed plasma power to the first wall can be utilized. One such means is the injection of a small, controllable amount of a high-Z material, such as Xenon, into the plasma. Xenon has a sufficiently high Z (= 54) that it will not be completely ionized except at the very center of the plasma. In this case,

$$f_r = f_b + f_z$$

where (under our conditions) the bremsstrahlung radiation fraction of the total power outflow, f_b, is given by

$$f_b = 0.049\ Z_{eff}$$

and f_z, the zenon line radiation fraction, is given by

$$f_z = 0.23\ (Z_{eff} - 1)$$

Table II.C.1 shows how the radiated power fraction varies with xenon concentration. Fig. II.C.1 shows the first-wall and divertor heat fluxes as a function of f_r, for the specific parameters of the tokamak driver.

Defining f_x = xenon density/electron density, the allowed magnitude of f_x is determined by the following considerations:

1) The fusion power density is reduced by approximately the factor $(1-Z*f_x)^2$.
2) $n\tau$ is divided by the factor $1/(1 - f_r)$.
3) The loop voltage around the torus is proportional to Z_{eff}.
4) The neutral-beam current drive power is proportional to the factor $Z_{eff}/(Z_{eff}-1)$, and thus decreases with increasing Z_{eff}.
5) In smaller tokamaks, enhanced scattering of fusion alphas may increase their loss.

In the baseline operating mode of the suppressed-fission breeder, effects #3 and #5 are irrelevant. Effect #4 is beneficial. Effect #2 is actually required to reduce $n\tau$ to the equilibrium ignition value, a technique long invoked in the design of very large tokamak reactors.

TABLE II.C.1. RADIATION LOSS CONTROL BY IMPURITY ENHANCEMENT.

f_x	Z_{eff}	BREMSSTRAHLUNG RAD PWR (MW)	IMPURITY RAD PWR (MW)	TOTAL MW	f_r
0	1.0	29	0	29	.05
0.0002	1.5	44	69	113	.19
0.0004	2.0	59	138	197	.33
0.0006	2.5	74	207	281	.47
0.0008	3.0	88	276	364	.51
0.0010	3.5	103	345	448	.75
0.0012	4.0	118	414	532	.89

The only real limitation for the present case is effect #1, which results in reduced neutron wall loading for a given machine dimension beta and magnetic field. The value selected for the tokamak breeder was f_x = 0.00067, corresponding to Z_{eff} = 2.68. Then, f_r = 0.52 (312 MW), the fusion power density and wall loading are reduced by 7%, and $n\tau$ is reduced by a factor of 2.08. The nonradiated power, associated primarily with charge exchange

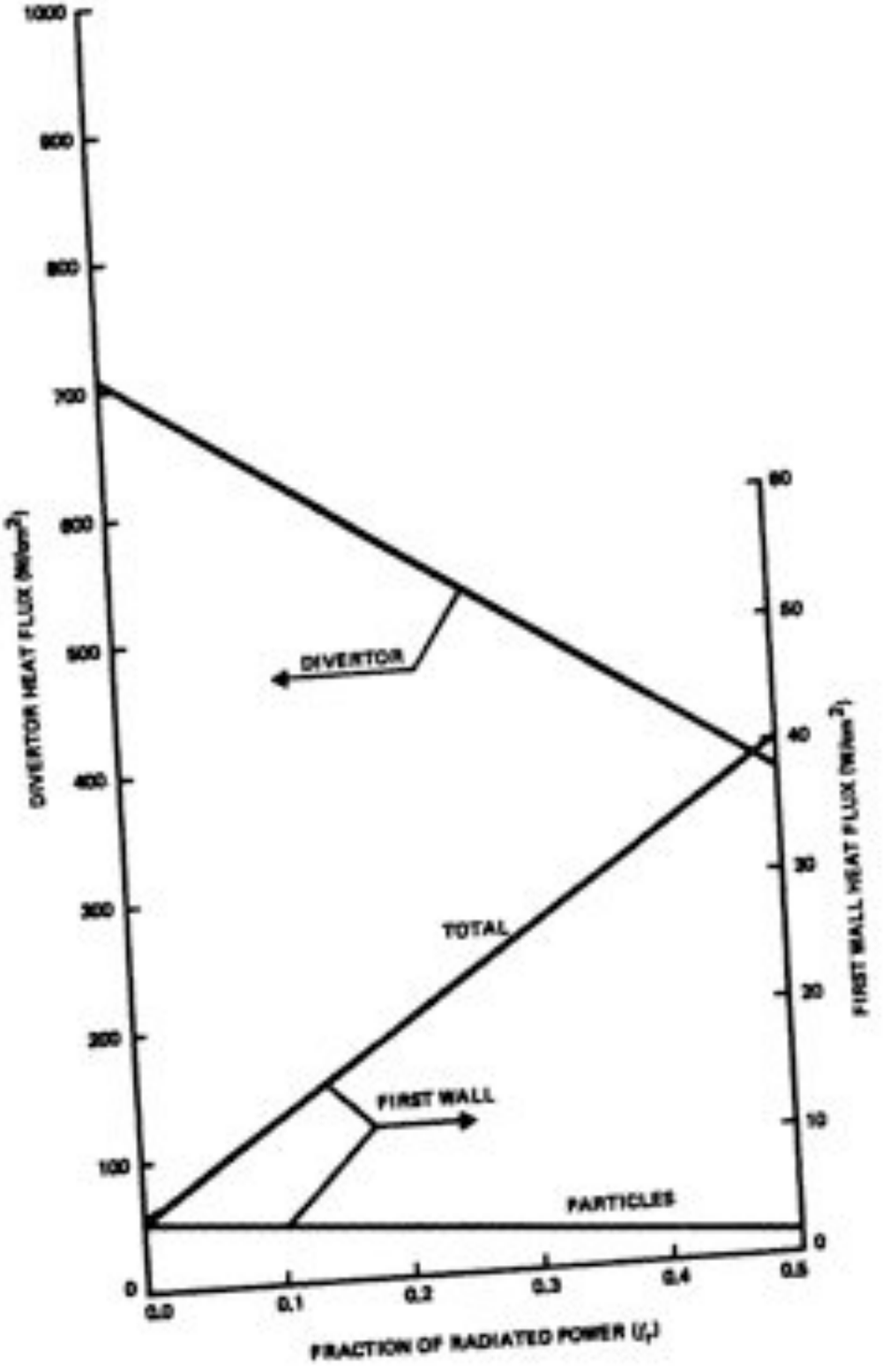

Figure II.C.1. First Wall and Divertor Heat Fluxes vs Radiated Power Fraction

neutrals, impinging on the first wall is 18 MW, which corresponds to about 3.0 W/cm^2. This value is expected to result in acceptably low erosion (see Section II.C.3).

II.C.3 Erosion of The First Wall

Physical sputtering appears to be the dominant erosion mechanism for the first wall of the reference reactor. The sputtering yield is energy dependent. It is low at low incident energies, bean peaks at intermediate energies, and decreases at higher energies. Estimating the erosion of the first wall requires knowledge of the particle composition, magnitude and energy spectrum of the particle fluxes at the first wall. For a thick scrape-off layer and efficient divertor operation, the flux of charged particles at the first wall is very small (7). Thus, the erosion will be dominated by physical sputtering caused by the charge-exchange neutrals.

There is presently large uncertainties in modeling the transport of charge exhange neutrals. Heifetz, et al., (10) developed a Monte Carlo model for characterizing neutrals in the scrape-off region. They show peaks around non-uniform regions (e.g., corners) of the first wall and near the divertor throat. Attempts to use the results from Heifetz and other published work lead to a large variation in the magnitude of the first wall erosion. Therefore, we have adoped a "representative" value of 2.25 mm/yr for first wall erosion rate. For neutrals with typical energies of 200 eV, the corresponding charge-exchange average flux is $\sim 1.4 \times 10^{15}$ $cm^{-2} \cdot s^{-1}$ (sputtering yield is 0.011 and 0.022 atoms/particle for D and T, respectively). The same erosion rate corresponds to $\sim 4 \times 10^{15}$ $cm^{-2} \cdot s^{-1}$ for neutrals with energies of $\sim$ 100 eV. Local regions with high charge-exchange neutrals flux (e.g., near the divertor throat) require special protective armors.

II.0 DESIGN ISSUES AND RECOMMENDATIONS FOR FURTHER WORK

The following is a summary of issues that should be examined in any further study of the tokamak driver.

II.0.1 Unresolved Issues

1) The ability to control the xenon concentration should be verified by one of the available plasma transport simulation codes.

2) The ability to control the plasma edge temperature to achieve a smaller erosion rate should be examined using one of the presently available divertor simulation models. However, we have used a rather conservative estimate of the first-wall sputtering rate.

3) The optimal locations and currents of the PF coils must still be determined. The need for one or more of the divertor coils to be normal coil(s) located in the bore of the TF coils should be evaluated by detailed magnetics analysis of the poloidal flux and by more detailed maintainability studies.

II.0.2 Unaddressed Issues

1) For the pulsed scenario, the effect of enhanced thermal cycling on component replacement should be further considered. The diameter of the central solenoid can be varied in order to change the length of the burn.

2) A study to minimize the cost of the TF coils should be undertaken by examining various shapes that deviate from the "standard" dee-shape while still giving the required field at the plasma and sufficient bore for the plasma vessel, divertor, and blanket/shield.

3) The possibility of substituting a pumped limiter for the poloidal divertor (with the resulting cost, maintenance, and breeding advantages) should be re-evaluated at appropriate intervals.

4) Much higher values of beta are attainable theoretically with plasmas of "bean-shaped" cross sections (8). The same fusion power could be generated at much lower toroidal field, at the expense of a more elaborate PF-coil system, including a high-current coil located at the inboard midplane. If the same magnetic field strength were used, a significantly more compact tokamak would be possible (9). Experimental tests of the effectiveness of bean-shaped plasmas will be performed in 1984 on the PBX device at PPPL (8). If these tests are successful, it will be worthwhile to carry out relative cost analysis of high-beta and low-beta options.

References, Chapter II

1) D. Grady, et al., "Preliminary Conceptual Design Study of a Suppressed-Fission Tokamak Hybrid," LLNL Report UCID-19733, January 1983.

2) R. J. Fonck, et al., "Impurity Levels and Power Loadings in the PDX Tokamak," Journal Nuclear Material, Volume 1115, 1982, pp. 343-354.

3) "INTOR, International Tokamak Reactor Phase I," IAEA, Vienna, 1982.

4) M. Porkolab, et al., "Lower Hybrid Heating and Current Drive Experiments," In Proceedings of 9th International Conference Plasma and Physics and Controlled Fusion, IAEA, Vienna, 1982, paper C-4.

5) D. R. Mikkelsen and C. E. Singer, "Optimization of Steady-State Beam-Driven Tokamak Reactors," Nuclear Technology/Fusion, Volume 4, 1983, pp. 237-252.

6) W. S. Cooper and R. V. Pyle, Eds., "The National Negative-Ion-Based Neutral Beam Development Plan," LBL Report, Pub-464, August 1983.

7) M. Abdou, et al., "Impurity Control and First-Wall Engineering," U.S. FED/INTOR Critical Issues, 1982, Volume 1, Chapter 7.

8) K. Bol, et al., "PBX: The Princeton Beta Experiment," Princeton Plasma Physics Laboratory Report, PPPL-2032, September 1983.

9) R. H. Whitley, et al., "Systems Analysis of Commercial High Beta Tokamaks," submitted for publication in American Nuclear Society Transactions of June, 1984 meeting.

10) D. Heifetz, et al., "A Monte Carlo Model of Neutral Transport in Divertor Plasma," Princeton Plasma Physics Laboratory, Rpt. PPPL-1843, (1982).

CHAPTER III

HELIUM COOLED BLANKET

III.A MECHANICAL DESIGN AND MAINTENANCE

III.A.1 Introduction

The mechanical design of a helium cooled fission suppressed blanket for the tokamak is described in this section. It is based on the driver technologies defined in Section II, but addresses a set of tokamak dimensions which are consistent with the smaller, long pulse mode driver.* A key guideline, unique to hybrid applications, was to incorporate a mobile fuel form to provide for fuel replacement/reprocessing. The remaining guidelines, as well as the design features and maintenance considerations, are discussed in subsequent sections. An alternate design concept is also presented. Finally, an assessment of the design to date is presented and several design issues are identified.

III.A.2 Design Guidelines

The reactor/blanket concept which evolved provides an arrangement consistent with the design and performance guidelines listed in Table III.A.1. Key considerations were the design of a first wall thin enough to provide attractive neutronic performance, the specification of a ferritic steel structural configuration which can be tolerant of irradiation induced swelling, and considerations relating to remote maintenance and the removal of blanket sectors. The remote maintanance guidelines, coupled with a design goal specifying that the toroidal field magnets are not to be moved, and are to last the life of the plant, require that the blanket sectors be removable within the fixed space between the toroidal magnets. Safety considerations, discussed in Section III.E, require that the reactor fuel inventory can be dumped by gravity. Definition of the poloidal field coils is presented in Chapter II.

---

* The original design guideline addressed a major radius of 6.75 m.

TABLE III.A.1 Design guidelines and parameters for the cooled fission suppressed Tokamak Fusion Breeder concept.

Design and Performance Guidelines	
Fusion Power	3000 MW
First Wall Neutron Loading	3.0 MW/m^2
First Wall Surface Heat Load	0.43 MW/m^2
Plasma Size and Radius	
Major Radius	6.75 m
Minor Radius	1.8 m
Elongation	1.8
Number of TF Coils	10
TF Coil Clear Bore (Modified "D")	
Horizontal	10.4 m
Vertical	14.4 m
Radius from Reactor Centerline to Maximum Field	3.3 m
Field on Axis	5.4 Tesla
Distance from Plasma Centerline to Divertor Coils[a]	9.6 m
Coolant	Helium
Pressure	5.1 MPa (740 psi)
Fuel Form	Composite Be/Th Pebbles (Spheres) with Rapid Dump Capability
Sphere Diameter	2 cm
Fuel Processing	Batch
Blanket Structure	Ferritic Steel[b] (2 1/4 Cr-1 Mo)
Maximum Structural Temperature	< 475°C
Blanket Lifetime	4 years

a) for other coil locations see Section II.
b) HT-9 backup.

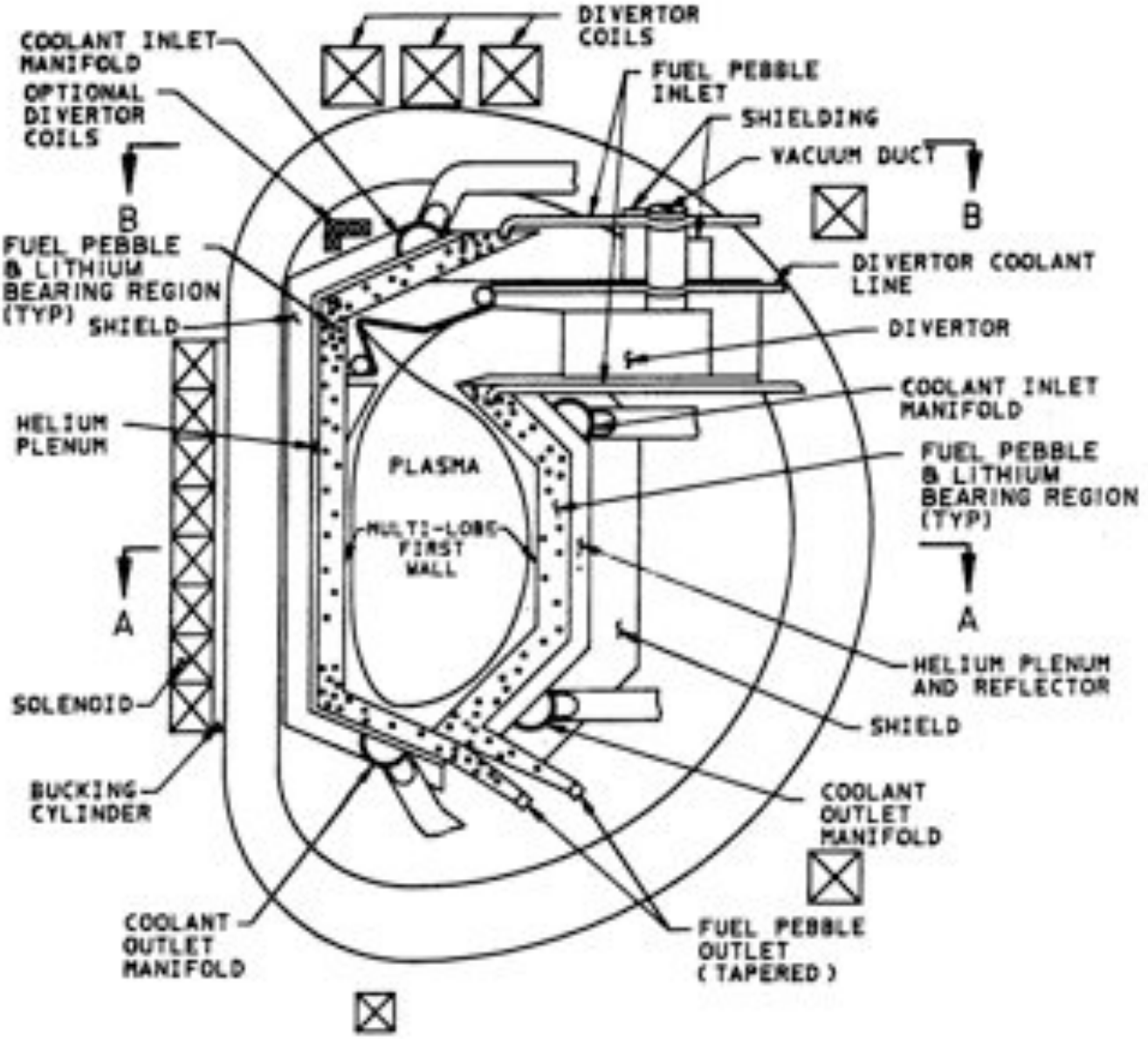

FIG. III.A.1. Cross section elevation view of the helium cooled Fusion Breeder Reactor concept with a top mounted divertor.

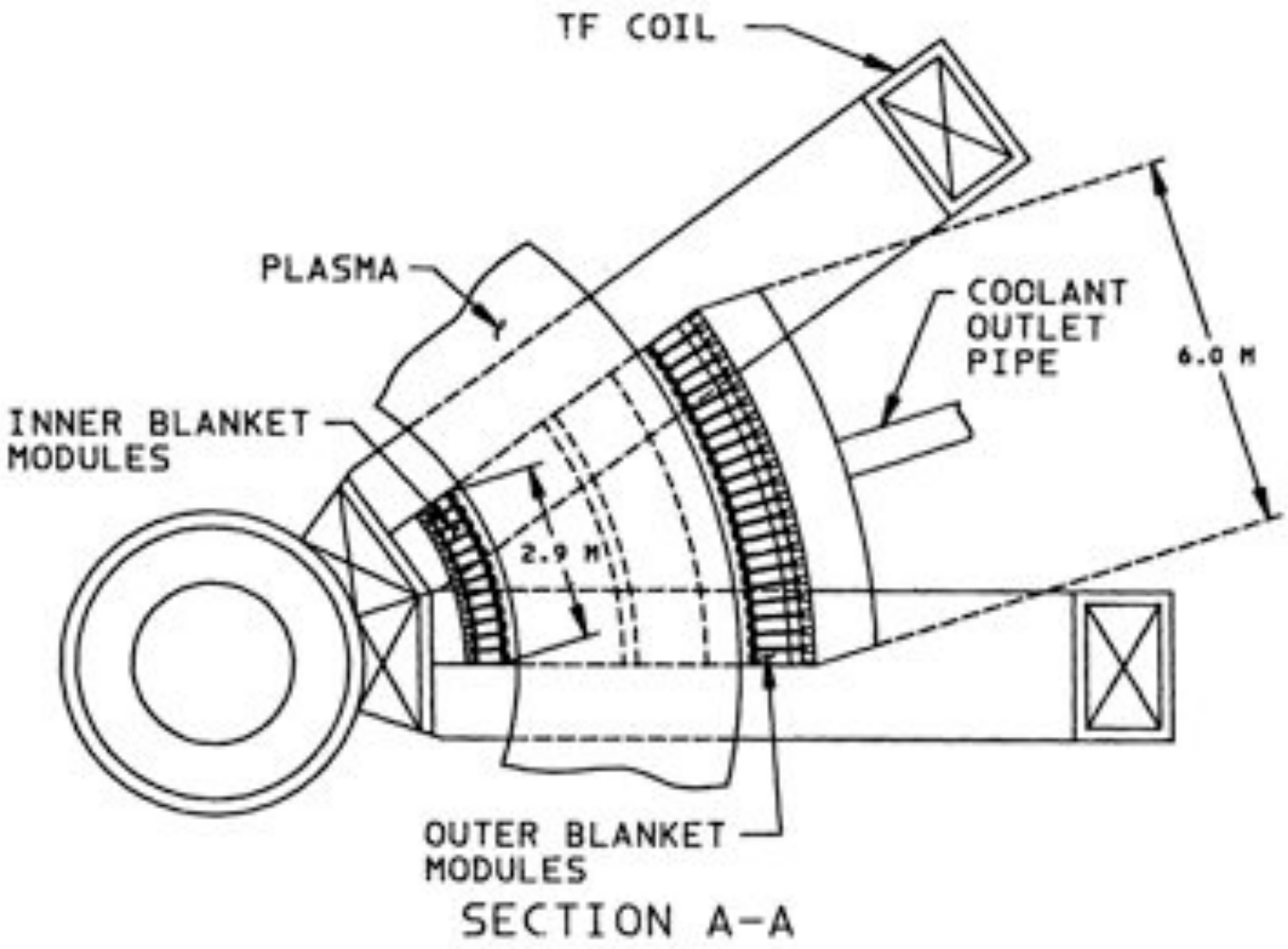

FIG. III.A.2. Top view of a Fusion Breeder Reactor sector showing section through horizontal centerline and lobe module arrangement.

III.A.3 Reactor Configuration

The helium cooled Fusion Breeder Reactor is shown in Figure III.A.1. The plasma is surrounded by poloidally oriented lobe shaped modules with circular noses which face the plasma. Figure III.A.2, which is a plan cross section through the horizontal centerline of the reactor shows the lobes and their orientation with respect to the plasma for one of the ten blanket sectors which fits within each pair of the ten superconducting toroidal field (TF) coils. The poloidal lobe arrangement allows the mobile fertile fuel in the form of spheres to be loaded at the top of the reactor, flow through the modules and be discharged at the bottom of the reactor when it is desired to dump the fuel for reshuffling/reprocessing or safety reasons. As discussed in Reference 1 and Section III.E, an independently cooled dump tank and automated fuel handling equipment are provided below the tokamak. The spheres themselves are composite Beryllium/Thorium constructed of 2 cm dia Be spheres each with a circumferential groove to accept a thorium snap ring.[1]

A different blanket internal geometry is used for the inner and outer blankets, which are located between the plasma and inner TF coil leg and between the plasma and outer leg of the TF coil, respectively. This difference results from a plasma engineering incentive to locate the plasma centerline (i.e., major radius) in the maximum possible magnetic field, or as close to the inner leg of the TF coil as possible. Specifically, if we fix the fusion power (3000 MW in this study) a thicker inboard blanket and/or shield will imply that a larger major radius will be required to provide the required power level. Consequently, a trade between maximum fissile breeding (thickest blanket and largest tokamak) and minimum cost (thinnest blanket and smallest tokamak) is implied. Lacking a more detailed optimization, a maximum inner distance of 1.6 m between the plasma edge and the inner TF coil conductor was specified. Sensitivities to the inboard shield thickness are further discussed in Section III.G. The distance between the plasma edge and TF coil conductor on the outboard side currently specified to be ~2 m, can increase with little impact on the overall design.

Each sector of the blanket (as shown in Figures III.A.1 and 2) is cooled by helium which enters coolant manifolds at the top of the blanket and exits at the bottom through main coolant pipes from the manifolds. The cooling

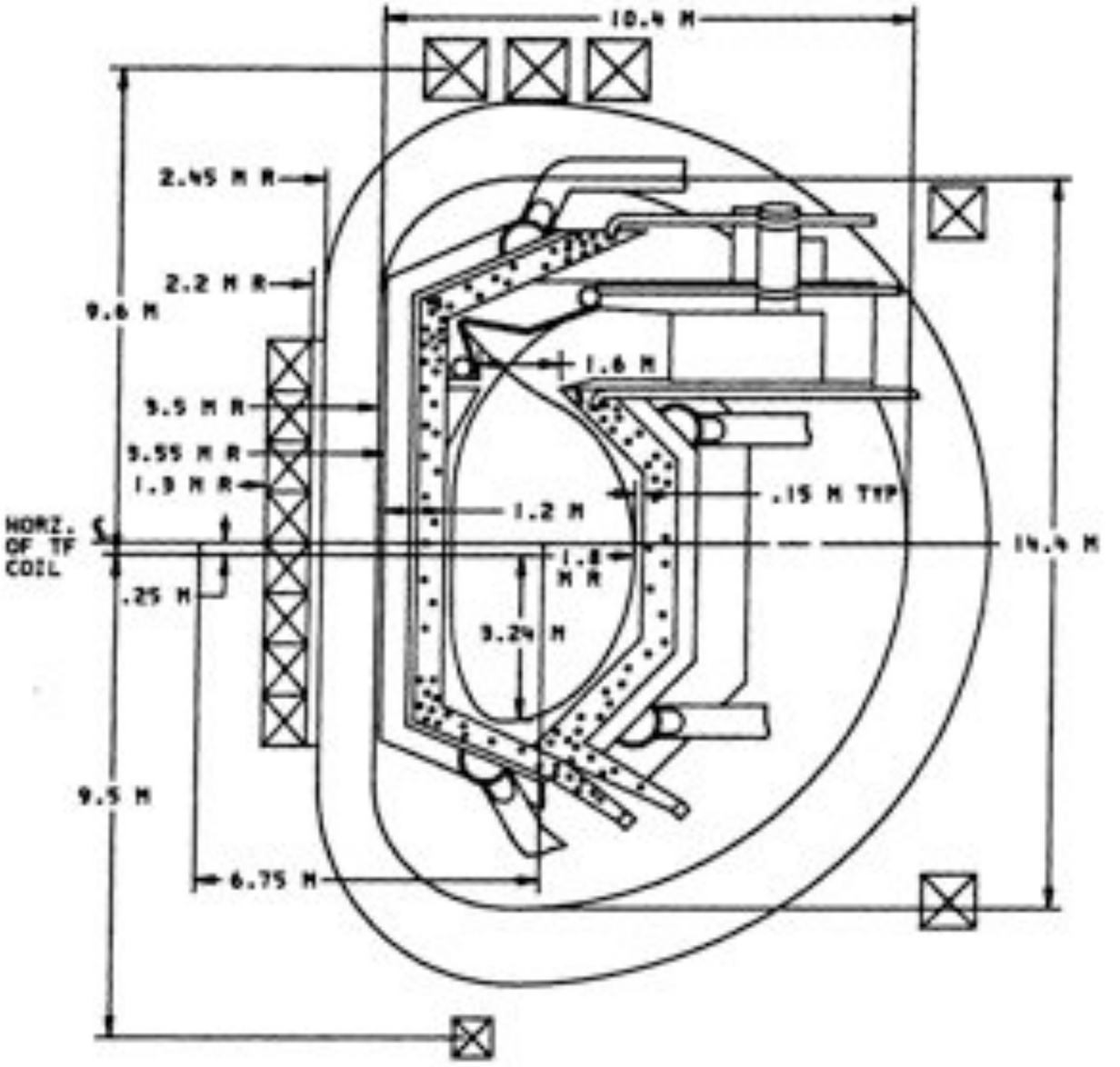

FIG. III.A.3. Reactor cross section elevation view showing typical dimensions for the helium cooled Fusion Breeder Reactor/ Blanket concept with a top mounted divertor. (Dimensions for long pulse mode of operation)

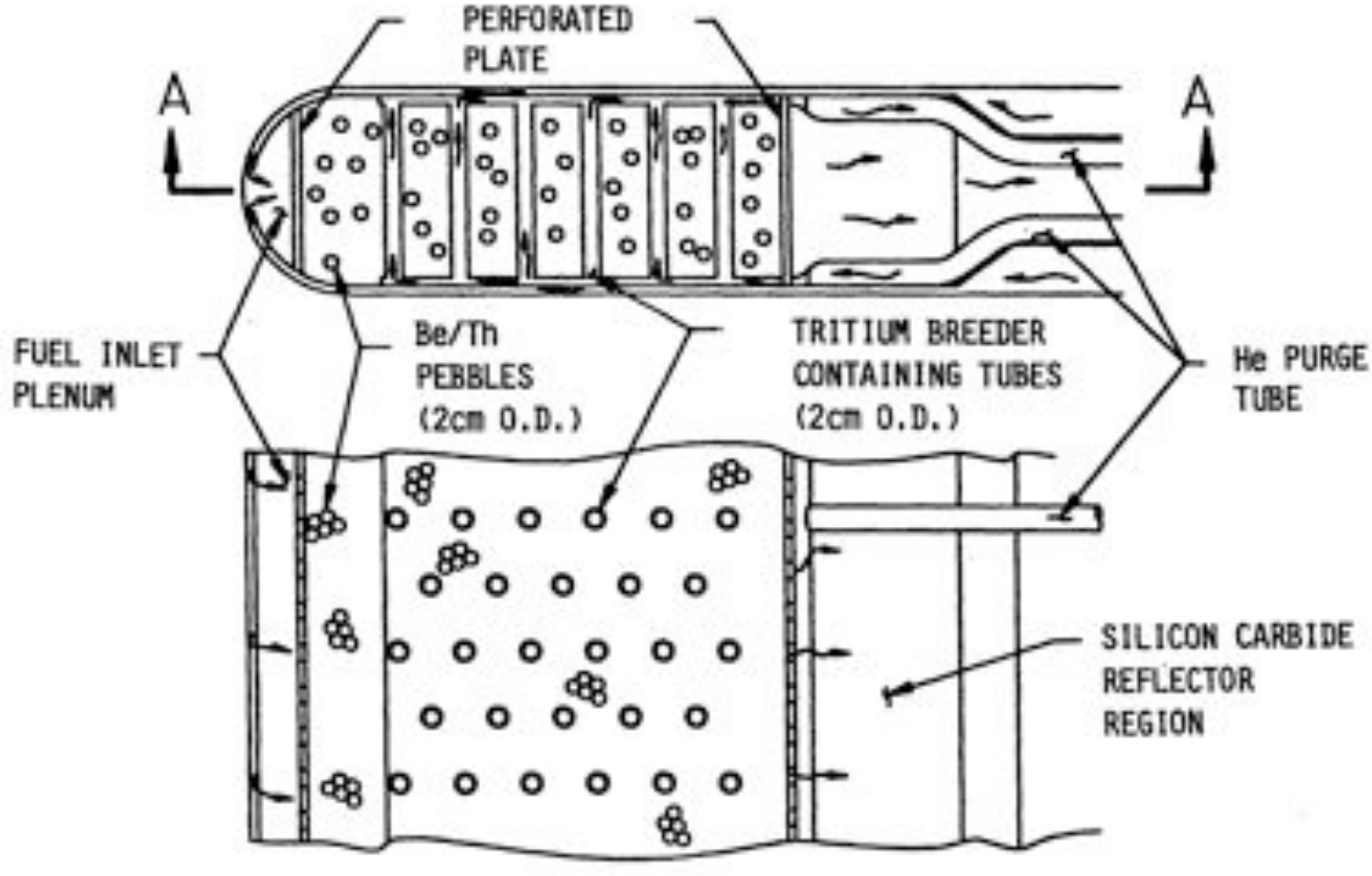

FIG. III.A.4. Enlarged cross section of the outer blanket module showing the fertile fueled and tritium breeder containing tube arrangement.

arrangement is described in more detail later. The fuel sphere inlets (top) and outlets (bottom) are also indicated in Figure III.A.1.

A water cooled poloidal divertor is located at the top of the reactor. The divertor is segmented so that there is an individual divertor segment for each sector of the reactor. The divertor is horizontally oriented so that it can be easily withdrawn and/or replaced between the TF coils without removing the sector from the reactor. This design is similar to that proposed for the INTOR reactor.[2] The divertor opening is 1.6 m wide to permit adequate room for pumping the plasma while eliminating any particle impingement on the first wall. Each divertor sector contains a cylindrical vacuum pumping duct (located at the right top of the Figure III.A.1.) which discharges into a pump located above the reactor. The six poloidal field (PF) coils, which include the three divertor coils, are shown in addition to the solenoid coil. All PF coils are located outside of the TF coils for enhanced blanket and PF coil access and maintenance. A reactor cross section elevation which provides perspective for the reactor and component sizes is shown in Figure III.A.3.

An optional preferred location for some divertor coils to be located above the inner shield, within the TF coils, is also indicated in Figure III.A.1. Such a configuration would provide a better control and definition of the magnetic field lines in the vicinity of the divertor, but would complicate maintenance should a TF coil require replacement. The location of PF coils inside the TF coil bore would, most likely, require the use of conventional copper coils with a resulting ohmic power loss.

III.A.4 Blanket Sub-Module Configuration

An enlarged view of a typical sub-module is provided in Figure III.A.4 to show details of the lobe concept. The module consists of a double wall 2 1/4 Cr-1Mo ferritic steel construction with straight side walls and a semicircular nose. The outer wall serves as the primary pressure carrying structure. The other inner portion or plenum between the double wall forms the coolant channels to provide the helium coolant which enters at the rear of the module. The coolant passes along both sides of the module to the nose. At

the center of the nose an opening is provided to permit the coolant to enter the near semicircular inlet plenum. The helium then passes through a perforated plate (shown in Figure III.A.4) into the fueled region of the modules which contains the Be/Th pebbles and rows of steel tubes containing the tritium breeder.* The tubes are 2 cm in diameter and arranged in an array with a triangular pitch of 8 cm. This geometry provides spacing of three sphere diameters between tubes to permit the spheres to flow down through the module during refueling/reprocessing. An additional set of plena are provided on each side of the module to permit a small amount of helium purge flow to be supplied to the horizontally oriented Li_2O-containing tubes to remove the generated tritium. Only a few small (~2 cm) tubes (shown in Figure III.A.4) are required to supply the purge flow to each lobe.

If the tritium breeder tubes were vertically (poloidally) oriented, fewer would be required, but some form of tube supports which would provide lateral support to the tubes would be required since the tubes (because of the additional length) would be very flexible if unsupported. However the supports would also have to provide space for the pebbles to move during loading and unloading. This arrangement should be considered for follow-on study because fewer tubes could lead to better reliability.

After passing through the fueled region and a second perforated plate at the back of the region, the main helium coolant flows through a silicon carbide reflector region and exits the module through the plenum located in the center of the back of the sub-module. Both the inner and outer blanket sub-modules are similar in design except that the inner module has a shorter fueled region and no reflector. To conserve space, the inlet and outlet plena for the coolant are also narrower in the inner blanket assembly region of the reactor. Comparison of the inner and outer blanket modules is included in Table III.A.2.

III.A.5 First Wall Design

The semicircular nose of the toroidal lobe type sub-module, Figure III.A.5, is corrugated circumferentially around the nose. The lobe type module without corrugations was considered in an earlier study for a tandem mirror.[3] The corrugations were proposed by GA and adopted for the 1983 Blanket Comparison Study[4] and this study. The issues relative to this

* Nominal tritium breeder choice is Li_2O. See Section III.B.

TABLE III.A.2 Fusion Breeder Reactor helium cooled blanket lobe concept features and comparison.

Concept Features		
Mobile Fuel Form (Composite)	Be/Th Spheres	
Sphere Dia.	2 cm	
Lobe Width	25 cm	
Inner and Outer Blanket Comparison		
	Inner	Outer
Corrugated First Wall Thickness	~1.8 cm	~1.8 cm
Corrugated First Wall Thickness (Smeared)*	~1.1 cm	1.1 cm
Structural Side Wall Thickness	0.4 cm	0.4 cm
Fuel Inlet Plenum Max Thickness	6 cm	6 cm
Fuel Zone Front and Rear Wall Thickness	2.0 cm	2.0 cm
Smeared Thickness	0.2 cm	0.2 cm
Fueled Zone (Spheres + Li_2O Compound) Thickness	49 cm	60 cm
Silicon Carbide Reflector Zone Thickness	-	20 cm
Helium Inlet/Outlet Back Plena Thickness	10 cm	18 cm
Shield Thickness	60 cm	1 m
Coolant Piping/Manifolds		
Inlet & Outlet Manifold Radius (Semicircular)	0.5 m	0.5 m
Inlet & Outlet Pipes	0.6 m Dia.	0.6 m Dia.

*Erosion Allowance Included

concept are discussed in more detail in Section III.B.3 of this report and in Reference 4. This feature permits the corrugations to deflect poloidally around the blanket sector to better accommodate radiation induced swelling and thermal expansion. The corrugated nose also deflects by flexing along the circular arc formed by its semicircular shape. The nose blends into the side walls of the modules where contact with the adjacent modules prevents any deflection. The corrugations mentioned above also blend into the uncorrugated flat side wall plates. In addition to preventing deflection of the side walls of the adjacent sub-module, each 0.4 cm thick side wall also acts as a tension tie to carry the coolant pressure load from the corrugated nose of the module to the back module support structure. The corrugation has a depth (thickness normal to the plasma) of 8.8 mm, is nominally 1.6 mm thick, and has a pitch of 6.6 mm. The space between adjacent sides of the corrugation is 2.4 mm on the outside of the lobe (facing the plasma) and 1 mm on the inside. The 1 mm groove with a baffle plate across the top serves as the flow channel for the helium which cools the first wall prior to entering the inner module to subsequently cool the fueled region of the module.

The corrugation also has a 9 mm erosion allowance to accommodate sputtering of the material from the first wall. This additional thickness, as seen in Figure III.A.5 gives a combined first wall thickness of 17.8 mm with a smeared thickness of ~11 mm when the slots in the corrugation are considered; after the erosion layer disappears the equivalent corrugation thickness is ~5 mm, so an average of ~8 mm has been used for the nuclear modeling task (Section III.C).

III.A.6 Fuel Region Design and Pebble Inlet/Outlet Piping Considerations

III.A.6.a Fuel Region. The requirement for a mobile fuel form and the selection of composite spheres in the fuel zone of the blanket imposes certain restrictions of the design of the fueled region of the blanket. Both the sphere inlet and outlet piping must be sized to prevent the spherical pebbles from binding or jamming and provide free flow of the pebbles when necessary for loading and unloading the fueled region. In addition, the blanket fuel zone must be free of unnecessary restrictions which could impede pebble motion. The spacing of the pipes or tubes containing the tritium breeder

located in the fueled region of the module, Figure II.A.4, must be adequate to allow the pebbles to move and to achieve an adequate packing fraction of 50-60%. The slot area for the pebbles to flow between pipes is ~ 6 cm x 20 cm (pipe spacing x inside module width) and is considered adequate to prevent pebble bridging or jamming under gravity flow. A trade-off between pipe spacing and pipe size can be considered if more spacing is required.

In order to minimize the thickness of the tritium breeder tubes, by minimizing the tube hoop stress and buckling loads, it would be desirable to have the helium purge flow in the tubes at approximately the same pressure* as the module coolant pressure. Conversely, it appears that only a small increase in the breeder tube thickness will suffice to provide buckling resistance at the 5.1 MPa ambient pressure. Specifically, the tubes, as currently defined, are 2 cm in diameter, 0.5 mm thick and are adequate to sustain the 5.1 MPa helium coolant pressure as a 100 MPa (14,500 psi) hoop stress. Assuming an out-of-roundness which is 10% of the tube wall thickness in amplitude, a 0.6 mm tube thickness will be required to assure buckling stability (5).

III.A.6.b Fuel Pebble Inlet/Outlet Piping. As shown in Figure III.A.1, the fuel pebble inlet piping is horizontally oriented. This orientation results in improved blanket coverage on the outboard side relative to a sloped fuel inlet below the divertor duct, but precludes the use of gravity to fill the fuel zones. Instead, each of the lobe sub-modules shown in Figure III.A.2 must be serviced by an individual pebble feed tube as shown in Figure III.A.6. Each sector requires 34 such tubes (12 inside lobes, 22 outside lobes).

The feed tubes would be operated pneumatically, transporting single pebbles from a batch tank to the blanket. Although the design of fuel handling machinery has not yet been addressed, we envision a mechanical conveyor feed machine similar to that proposed in Reference 1. To avoid cutting and welding 34 pipes per sector changeout, it appears reasonable to

* In practice, a purge system pressure of about 1 atm. less than the minimum coolant pressure would be maintained to limit tritium leadage into the main helium coolant.

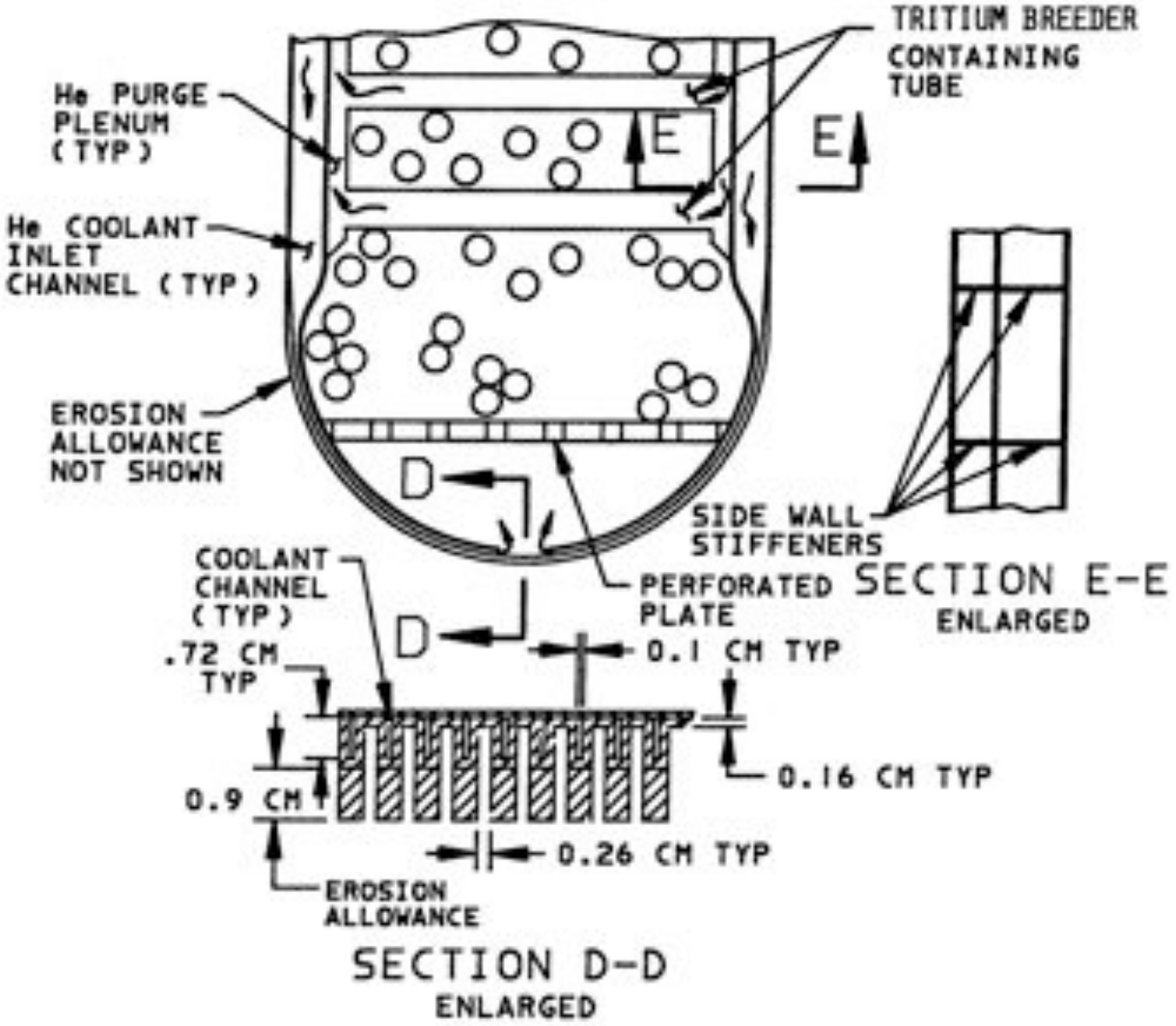

FIG. III.A.5. Enlarged view of the front of a module showing corrugated first wall, side wall stiffeners and tritium breeder containing tubes (not to scale).

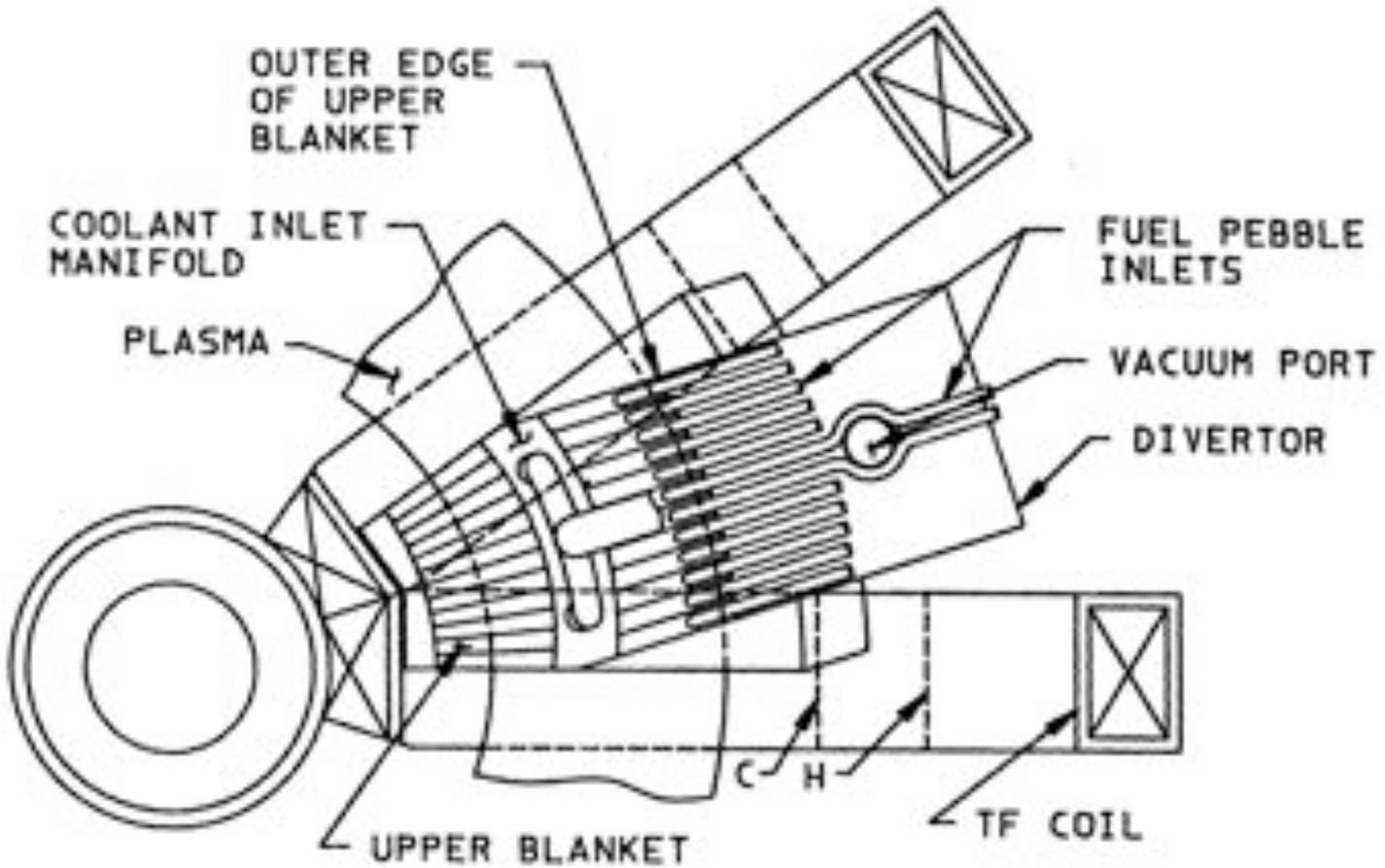

SECTION B-B
(SHIELD ABOVE UPPER BLANKET
REMOVED FOR CLARITY)

FIG. III.A.6. Top view of a sector for the Fusion Breeder Reactor illustrating upper blanket coolant inlet manifold and fuel pebble inlet pipes.

consider an arrangement such that the fuel feed system would be integral to the blanket/shield/divertor assembly (not shown). In such an arrangement, only the duct which transports bulk pebbles from storage to the fuel feed machine need be remotely cut and welded when the sector is replaced. The design of such systems should be addressed in later studies.

The fuel pebbles are discharged through the blanket by gravity since the blanket contour permits the outlets to be inclined downward as shown in Figure III.A.1. The pebbles enter a flattened funnel shaped duct which provides a single common exit from all of the 12 sub-modules in each inner blanket sector. The duct tapers to a circular pipe at the bottom of the blanket below the inner blanket. A valve (not shown) is provided below the circular cross section exit pipe to control loading and unloading. The outer blanket has a similar common outlet duct for the 22 sub-modules in the outer portion of each blanket sector. This duct discharges through a circular pipe at the bottom of the blanket near the inner blanket outlet as shown in Figure III.A.1.

In actual practice, if the blanket were divided into two equal thickness fuel zones to permit separate flow of pebbles from each zone, fuel enrichment/recycling/reprocessing would be more efficiently achieved.[1] In addition to modifications to the fuel zone, compatible outlet piping would be required. This possibility has not been addressed in the design concept and should be considered for later study.

III.A.7 Coolant Inlet/Outlet Piping Considerations

From the standpoint of simplicity (and enhancement of maintenance), the number of coolant pipes should also be minimized. As shown in Figure III.A.1, the proposed concept requires only a single inlet coolant pipe and exit coolant pipe per sector for each (inner and outer) blanket. Both the inner and outer blanket piping and manifolding are similar. The helium inlet cooling pipe enters a semicircular manifold which extends the full width of the sector (typically shown in Figure III.A.6) in order to supply coolant to each of the sub-modules in the sector. Figure III.A.7 is an enlarged composite cross section through a group of modules to which coolant is supplied and discharged. At the upper portion of the figure, the coolant enters from the semicircular inlet manifold and flows into the inlet plena at

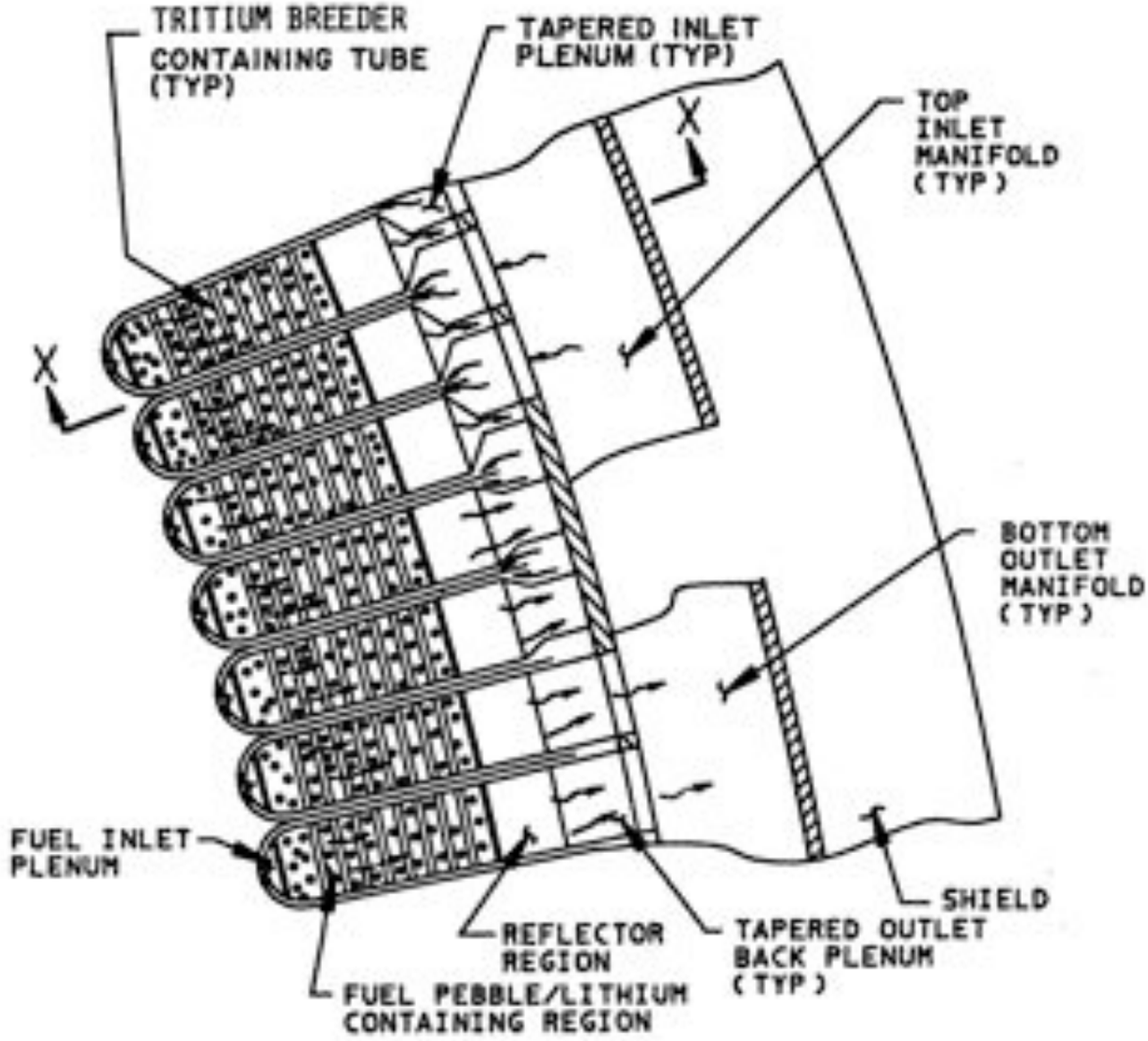

FIG. III.A.7. Enlarged view of helium cooled outer blanket module concept showing coolant manifolds and module cooling arrangement.

the back of the sub-modules. Note that the semicircular inlet/outlet manifolds do not require additional space between the blanket/shield and the TF coils. The coolant flows from the back plenum through the side walls of the modules, cools the first wall and flows through the interior of the module to cool the fuel region and the reflector region. It then enters the blanket outlet plenum. Both the inlet and outlet plena are tapered to conserve space and maintain nearly constant velocity. The inlet plenum is wide at the top and narrows towards the bottom while the outlet manifold has the opposite orientation.

The lower part of Figure III.A.7 shows the discharge from the enlarged outlet plenum into a semicircular outlet manifold at the bottom of the blanket. Typical inlet and discharge piping between manifold and main coolant pipe are shown in Figure III.A.6, which shows the inner blanket inlet manifold and coolant inlet piping. Figure III.A.8 shows a cross section perpendicular to the manifold centerline. The upper portion represents Section X-X of Figure III.A.7, which shows the inlet flow to the module first wall and fuel zone inlet plenum. The lower part of the figure represents flow through the inside of the module and subsequent discharge to the helium coolant outlet manifold. The coolant piping and manifold sizes are provided in Table III.A.2.

III.A.8 Module Edge Support Options

Several methods of supporting the side walls of the module shown in Figure III.A.7 were considered. Each has advantages and disadvantages.

One method studied was a buttress (or bookend) design which braced the thin outer wall of the last pressurized module against the strong outside wall to which all modules are attached. Figure III.A.9(a) illustrates the idea. This proposed solution provides adequate support and isolates the blanket sector from the other sectors, but the space occupied by the bracing penalizes the breeding volume of the blanket. Also, the buttresses have considerable mass and further detract from breeding by parasitic capture of neutrons.

A second method considered (Figure III.A.9(b)) is internal tie rods spanning the outermost modules. At the expense of such added structure, the end modules can self-sustain internal helium pressure. An overturning moment still will be exerted on the end modules, and their anchoring attachements to the back wall must be heavier than a "normal" module, but wasted space is avoided. This method is, perhaps, the most compatible with the current design because the end modules might replace some of their horizontal tritium breeder tubes with tie rods

The third potential solution would be to allow the end modules of one sector to support the end modules of the adjacent sector (Figure III.A.9(c)). In this case, consideration must be given to tolerance accumulation which can cause overstress of the module sidewalls. Also, unintentional "cold welding" of walls in contact could occur. This would prevent disassembly without damaging the module side-wall in contact with a neighboring sector. Both of these unpleasant effects can be overcome by a simple expedient. Aluminum oxide plates (possibly mounted on pressurized cushions) can be placed on the side walls of modules in adjacent sectors. The ceramic pads will not weld inside the cacuum, but the pad spacing and area must be controlled to minimize any local wall bending stresses in an unsupported area. The space occupied by these thin ceramic pads can be small, but there is a concern related to failure propagation between sectors. Namely, if sector A fails, sector B can expand into sector A and fail due to excessive deformation.

III.A.9 Remote Maintenance Considerations

The design guideline for 10 TF coils (modified D shape) and 10 sectors was intended to reduce the number of sectors which had to be removed while still maintaining a reasonable coil bore. The sectors should be capable of being removed horizontally without interfering with the coils. In particular, this would occur at Points D and E of the outer blanket in Figure III.9.10. The coil bore was enlarged to provide clearance for blanket removal, and various potential linterferences were checked.

A plan view of the cross sections taken in Figure III.A.10 is shown in Figure III.A.11. In the latter figure, the dotted lines identified as D through J represent Section D-D through J-J of Figure III.A.10, respectively. The figures show that the potential interferences at the locations indicated

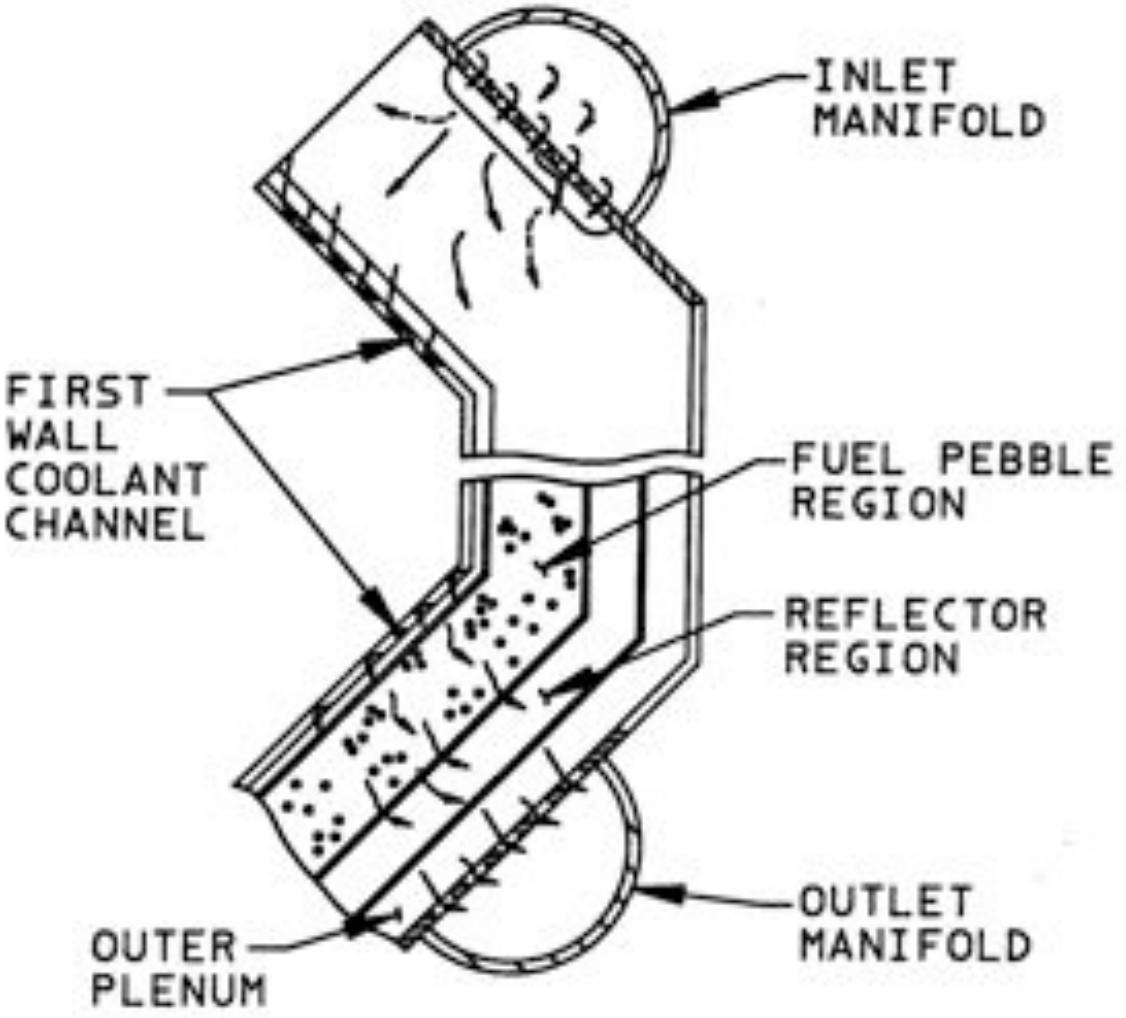

SECTION X-X

FIG. III.A.8. Cross section through Figure III.A.7 showing typical coolant flow arrangement through a lobe type module in the outer blanket.

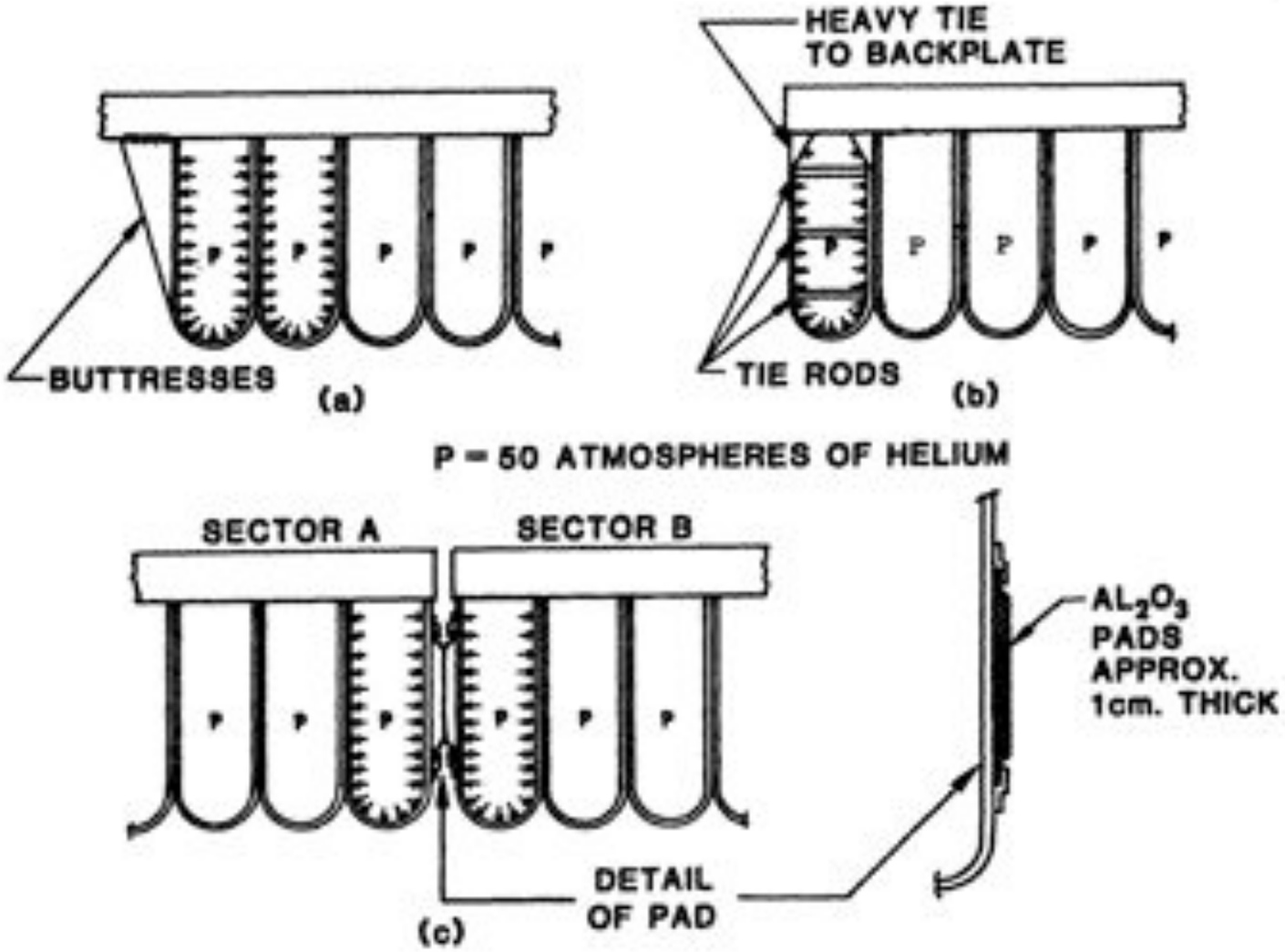

Figure III.A.9. Alternate Module End Designs.

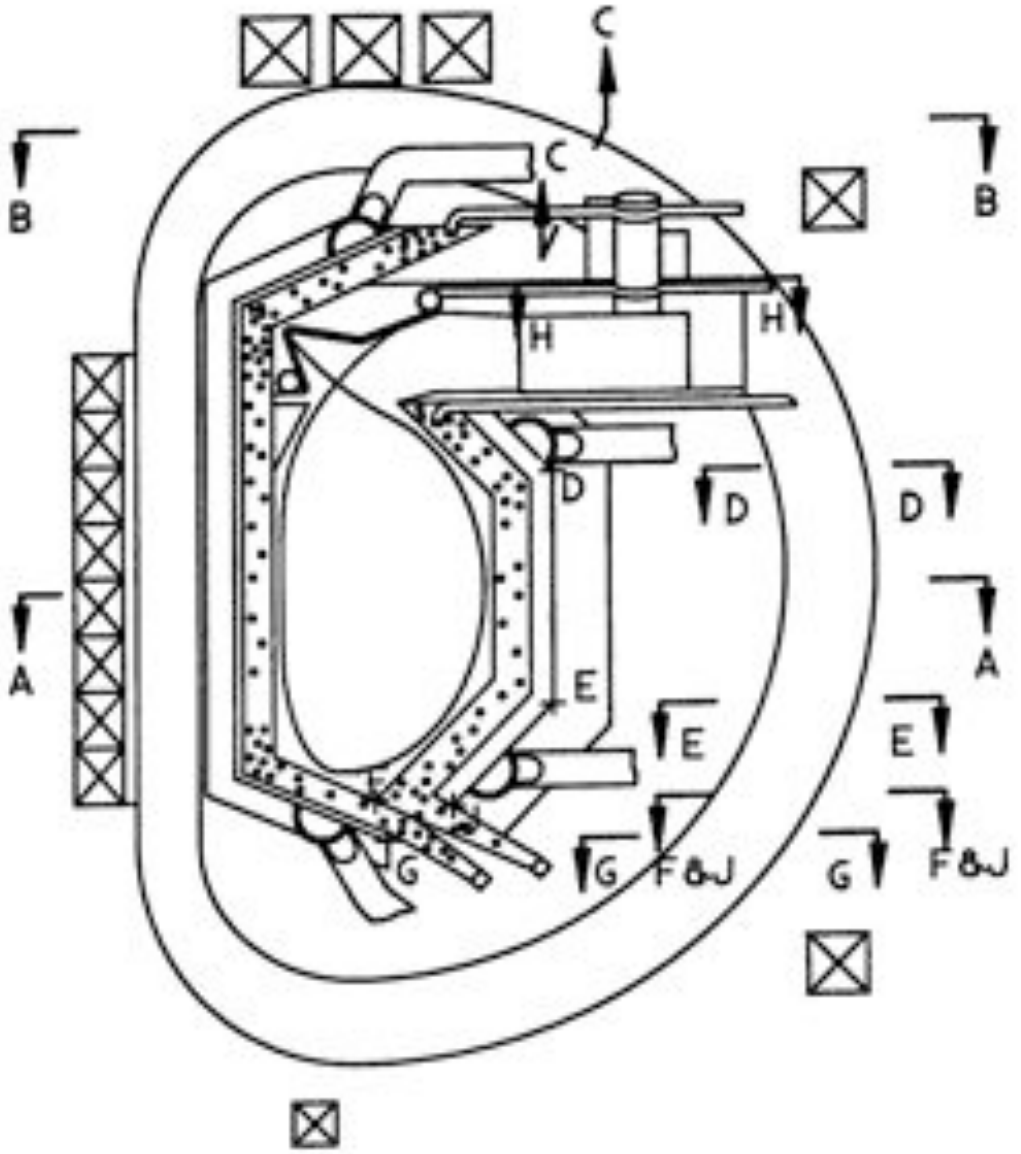

FIG. III.A.10. Cross section elevation view of helium cooled blanket concept with top mounted divertor with typical sections used to determine clearance for blanket.

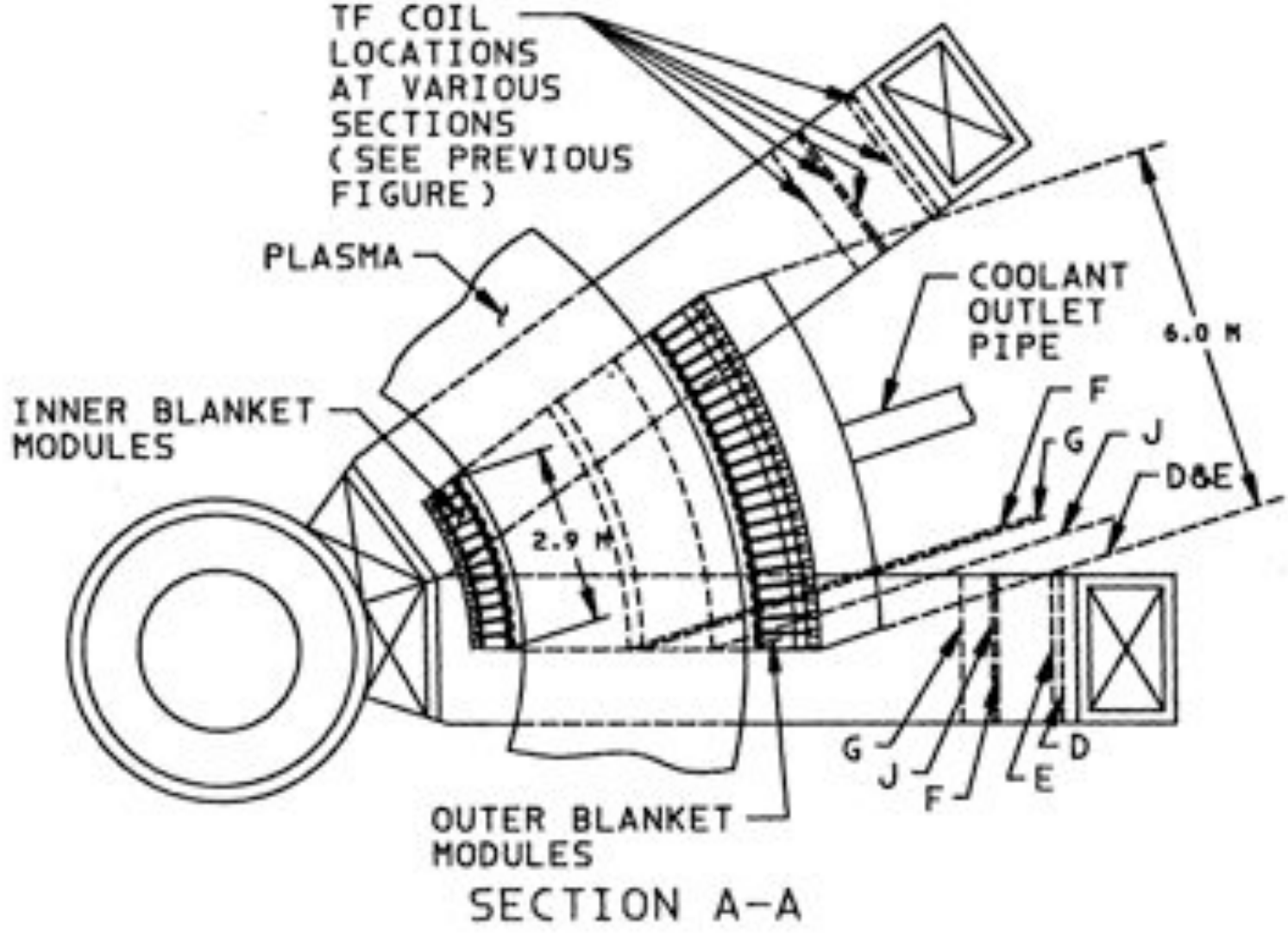

FIG. III.A.11. Reactor sector plan view showing the existing clearances between blanket sections and TF coils.

were eliminated. Similarly, the upper portions of the blanket and divertor clearances, identified by C and H on Figure III.A.6, indicate that the divertor and blanket will not interfere with the TF coils during sector removal. The blanket width at the top sector must be limited to the width which will pass between the section of the coil identified by dotted line C of Figure III.A.6 (which is the width of the divertor), but the loss of blanket coverage above the divertor due to this constraint is minimal. There is more than adequate space for the divertor since it is located at a lower elevation where the space between coils is represented by H. Based upon the above considerations, the coil size investigated with a horizontal and vertical bore of 10.4 m and 14.4 m, respectively, is fairly well optimized for removal of a sector between coils.

The piping impact on maintenance has been discussed previously in Section III.A.7. Figures III.A.1 and 6, indicate that neither piping for coolant or fuel loading/unloading will interfere since their envelopes are narrower than the other sections of the blanket.

III.A.10 Effect of Neutral Beam Penetrations*

Two neutral beam ducts penetrate the blanket. The 0.4 m wide by 0.8 m high ducts enter at an angle 35° from the normal to the plasma and require removal of portions of 6 or 7 lobe modules in this area. If the lobe is blocked at the duct, the normal flow of pebbles from the top to the bottom of the reactor cannot occur. If the fuel is channeled from the shortened lobes above the duct to the lobes below, additional design complexity would be required for the blanket. Only about 5% or less of the blanket is affected by the penetrations. The blanket design could be simplified by having modules in the regions of the penetrations restricted to tritium breeding. The effect of 5% reduction of beryllium/thorium blanket coverage should be assessed and the design simplification resulting should be considered when the concept is further developed.

Another impact of the penetration is the loss of module side wall support. As previously discussed in Section III.A.8, the pressure against the side wall of each module is compensated for or balanced by the pressure inside the adjacent module. This occurs along all modules except at the edge of the

* Subsection III.A.9 will only apply if the neutral beam driven steady state mode is selected.

sector. A balanced side load must be provided at this location when the adjacent sector is assembled. Similarly, additional side load pressure restraint or balanced load must be provided at the beam duct penetration.

III.A.11. Alternate Helium Cooled Reactor/Blanket Concept

An alternate reactor/blanket concept which in many respects is similar to the reference concept described in the previous sections was studied. Although the basic lobe shaped module was retained, the location of the divertor was at the bottom of the reactor. This had an impact on both the contour of the blanket around the plasma and divertor and of the fuel sphere inlet and outlet configuration. This difference can be noted by comparing the proposed concept (Figure III.A.1) with the alternate concept shown in Figure III.A. 12.

Because the outer blanket contour had to be inclined to permit the pebbles to be removed from the blanket by gravity, the divertor also had to be inclined downward. Consequently, the "bent" shape of the divertor was not as amenable to remote removal from the blanket assembly. If it were removed, the inclination of the divertor, would require that the lower PF coil be lowered to prevent interference with the divertor and its vacuum port. The inclined divertor concept, likewise, added additional envelope height to the sectors, would have required a larger TF coil bore to permit removal, and would increase neutron leakage. The coil bore was not resized to eliminate points of interference between the sectors and TF coils, since the top mounted divertor concept appeared more attractive. On the positive side, the alternate configuration features a less complex fueling scheme (eliminates the 34 pebble inlet pipes per sector) and reduces shielding (sky shine) concerns.

The cooling manifold concept for the alternate design is essentially the same as that described previously for the proposed concept (Figure III.A.1), except that the location of the outer blanket cooling manifolds was different. This can readily be seen in Figure III.A.11 elevation and Figure III.A.13 top view which shows the location of inlet piping and manifold for both the inner and outer blanket sectors. The figure also shows fuel sphere inlet pipes which make a transition from the circular section at the inlet to

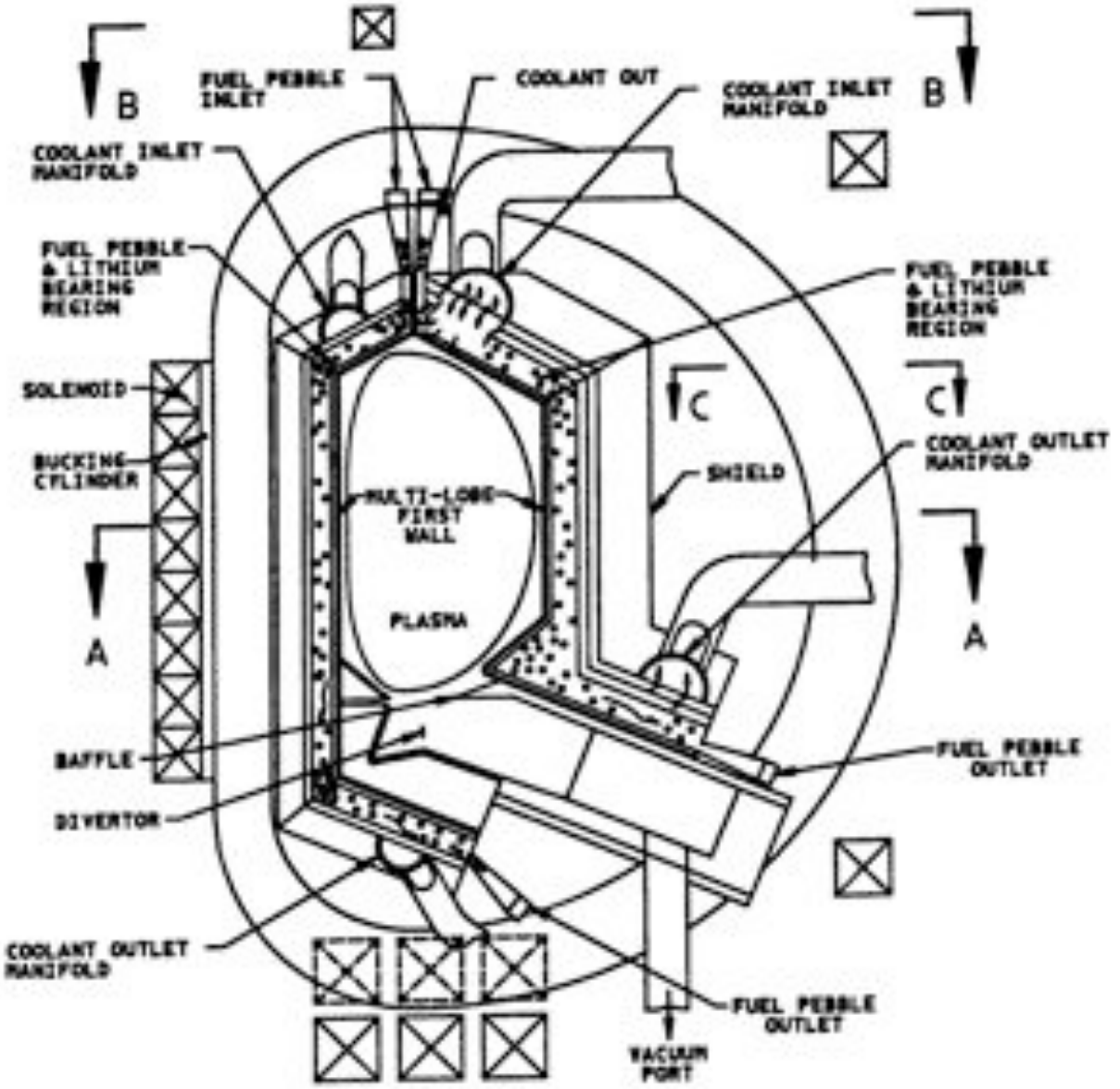

FIG. III.A.12. Reactor cross section elevation view of the helium cooled Fusion Breeder Reactor/blanket (alternate concept with bottom-mounted divertor).

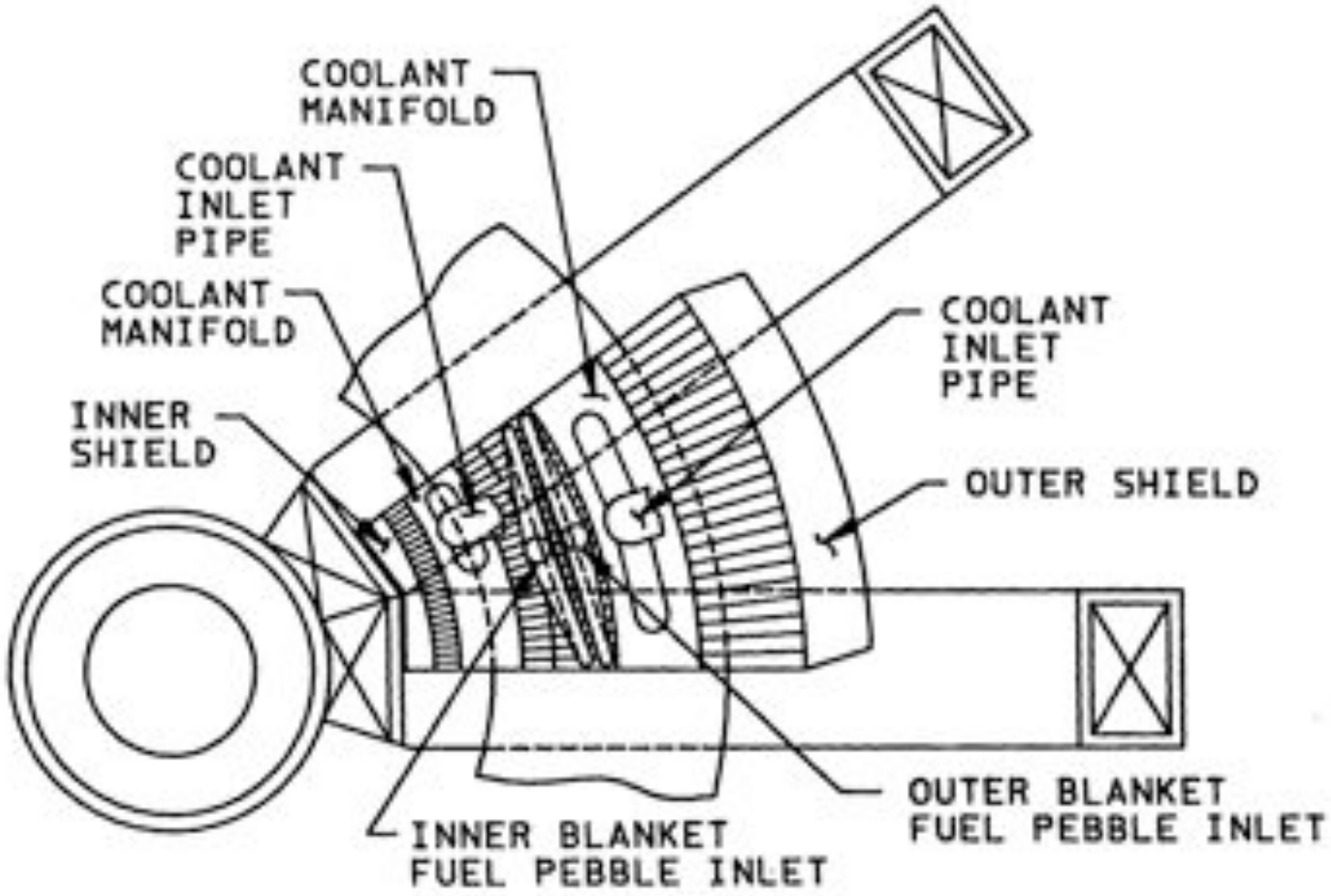

FIG. III.A.13. Top view of a sector for the Fusion Breeder Reactor illustrating upper blanket portion of coolant inlet manifolds and fueled sphere inlets (alternate concept with bottom-mounted divertor).

the flattened funnel contour at the top of the blanket to distribute fuel to all of the blanket modules. The arrangement provides a gravity feed to the spheres for loading the blanket fueled region near the top center of the reactor.

The reactor elevation, with typical dimensions for the concept, is illustrated in Figure III.A.14 and can be compared with Figure III.A.3 for the selected design concept. The three dotted divertor coils in the region of the lower part of the TF coils represent the location originally specified. The actual coil location shown (10.1 m) is about 0.5 m further from the plasma than the selected configuration specified in Table III.A.1.

III.A.12 Summary and Design Issues

The helium cooled reactor/blanket concept with a mobile fuel form appears to be a viable concept based on the scoping design and analysis effort to date. The first wall and module material thicknesses are structurally efficient and are reasonable from a neutronics standpoint. The single coolant path for the first wall and the interior of the blanket leads to a relatively simple concept. Incorporation of the mobile fuel form adds additional complexity to the design, but the advantage of in situ refueling/reshuffling should by far outweigh the alternative of removing blanket modules which could lead to excessively long reactor down-time and low availability. The use of 2 1/4 Cr-1 Mo represents a state of the art material selection, precluding the development of more exotic materials. The first wall concept is unique in that design concepts in the past have not been directed to accommodating the effect of irradiation induced swelling. The design is further enhanced by the lower swelling characteristics of ferritic steel (as opposed to austenitic) and the higher thermal conductivity which leads to lower thermal stresses. This corrugated first wall concept should be studied in greater depth because it is, in a sense, generic in that it could be adapted to other blanket designs.

However, because of the limited effort in the study to date, design issues remain which will require further study. Some of these items/issues are the following:

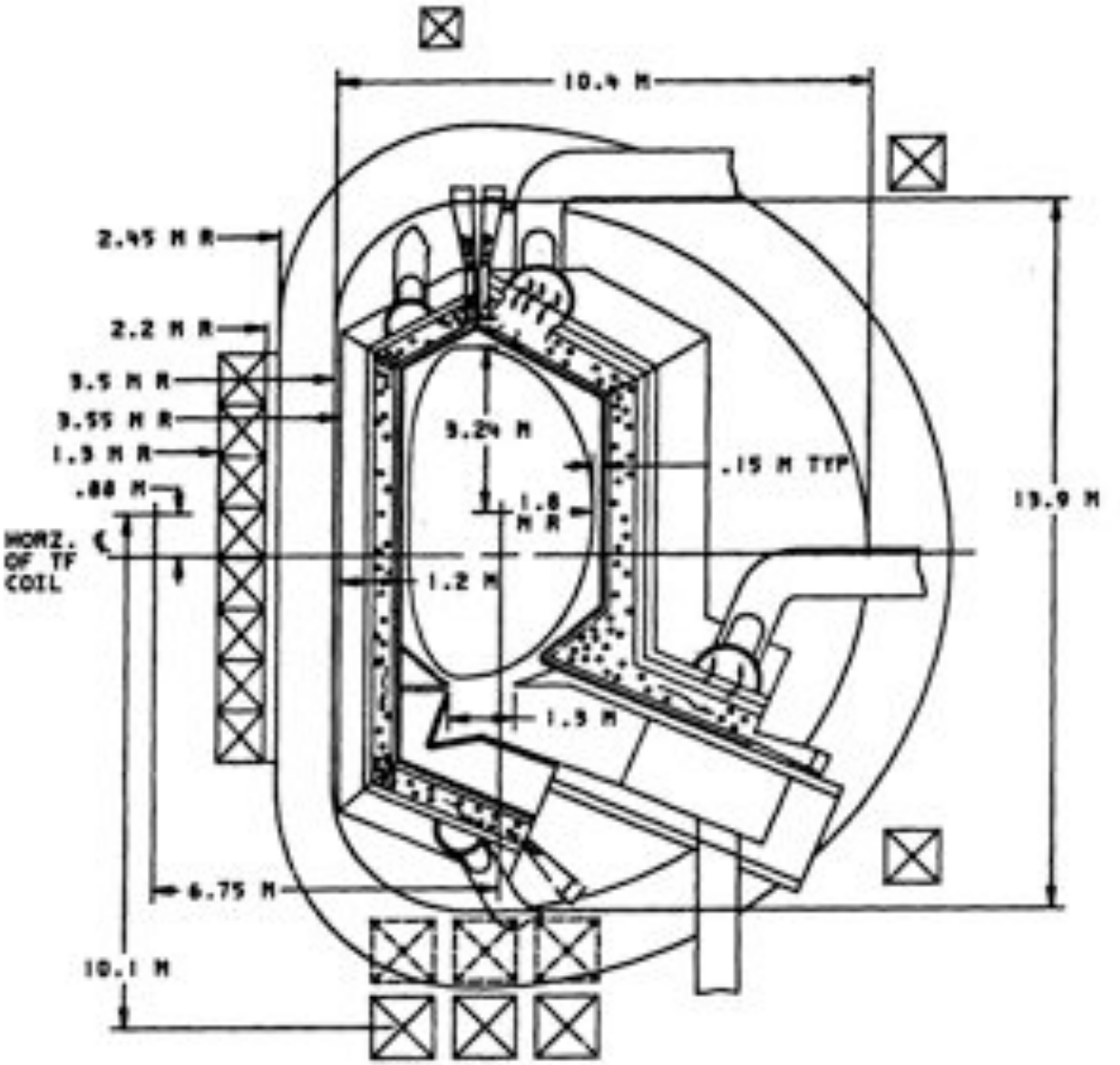

FIG. III.A.14 Reactor cross section elevation view showing typical dimensions for the helium cooled Fusion Breeder Reactor/ blanket (alternate concept with bottom-mounted divertor).

- Concepts are needed for accommodating the lobe side wall loading at the interface between blanket sectors.

- The relative merits and disadvantages of the selected horizontally (toroidally) aligned tritium breeder containing tubes in comparison with an alternative vertical (poloidal) arrangement should be investigated more completely and the most effective arrangement selected.

- The shield design should be pursued further to understand the shield/blanket interfacing and provide a concept for an integrated shield and blanket design.

- The proposed loading of the beryllium/thorium pebbles into the top of the blanket through small individual tubes should be investigated via the design of a fueling machine. The time to refuel and the achievable fuel distribution should be estimated.

- The narrow flow channels (1 mm) on the inner side of the corrugation may be sensitive to dimensional variances and may impact cooling effectiveness. The tolerance to which this channel width can be manufactured needs to be assessed.

- The relative merits of having the vacuum pumps and additional shielding above the reactor for the selected design with the top mounted divertor, versus the more conventional placement of the divertor below the reactor needs further investigation.

- A detailed consideration of the PF coil types, requirements, and locations has not been performed. Specifically, the location of one or more normal divertor coils inside the TF coil bore should be studied with respect to cost, maintainability, plasma control, and power consumption. Also, the required magnetic characteristics of the OH coil and its space requirements need further study.

- Procedures and equipment to replace the sector modules (including the divertor) require further study.

- Configuration and mechanical support arrangement for the silicon carbide reflector needs further study.

In further developing the design, efforts should include the shield, additional system interfacing components (i.e., heat exchangers, vacuum pumps, helium pumps, etc.) and interconnecting piping. The vacuum sealing boundary should be better defined and seal concepts pursued. In addition, it may be possible to further optimize the TF coil size by trade off between the size of the horizontal versus vertical bore to minimize magnet size and cost.

Finally, since the first wall is a key to blanket design, a representative section of the first wall with provisions for cooling should be tested in a high heat flux test facility.

References, Section III.A

1) D. H. Berwald, et al., "Fission-Suppressed Hybrid Reactor - The Fusion Breeder," UCID-19638, Lawrence Livermore National Laboratory, December 1982.

2) "INTOR, International Tokamak Reactor Phase One," Report of the International Tokamak Reactor Workshop, held in seven sessions in Vienna, 1980-81 International Atomic Energy Agency, Vienna, 1982.

3) J. D. Lee, et al., "Tandem Mirror Hybrid Reactor Design Study Final Report," UCID-18808, Lawrence Livermore National Laboratory, September 1980.

4) A. Blake, Practical Stress Analysis In Engineering Design, Marcil Dekker, Inc. (1982).

III.B CHOICE OF A TRITIUM BREEDER

III.B.1 Introduction

A principal goal of fusion breeder blanket design is to maximize fissile fuel production via the use of an efficient neutron multiplier (see Section III.C). A consequence of the use of a separate neutron multiplier (in this case beryllium) is that the tritium breeding material is not required to provide a capability for neutron multiplication as well. Rather, the preferred tritium breeder is required to result in a practical engineering design which minimizes both the tritium breeder volume fraction and any parasitic absorption of neutrons. As a result of this design orientation, a number of tritium breeding materials which cannot provide adequate tritium breeding in the absence of an effective neutron multiplier for fusion-electric blanket (e.g., lithium aluminate, FLIBE) can be considered for use in the fusion breeder.

Engineering considerations leading to the choice of a tritium breeder are presented in this section. This choice was made by reviewing the properties of suitable breeders and their respective design implications in the areas of breeding performance, tritium handling, and safety. A more detailed comparison between solid and liquid breeders is presented prior to the discussion of conclusions and recommendations.

III.B.2 Breeder Material Properties

Figure III.B.1 shows the mechanical configuration of the helium-cooled fission-suppressed blanket design. The tritium breeder can be contained in tubes (shown) or plates which are surrounded by the composite pebbles of beryllium and thorium. The helium coolant is passed through the packed bed of pebbles and fuel elements at high speed to provide adequate heat transfer.

The key properties of several candidate tritium breeders are summarized in Table III.B.1. These candidates were selected because they represent distinct classes of breeders: liquid versus solid, insitu neutron multiplication versus none, and tritium release as T_2 versus T_2O.

CROSS SECTION OF OUTER
BLANKET MODULE SHOWING
TRITIUM BREEDER CONTAINING TUBE ARRANGEMENT
IN FUELED REGION OF BLANKET

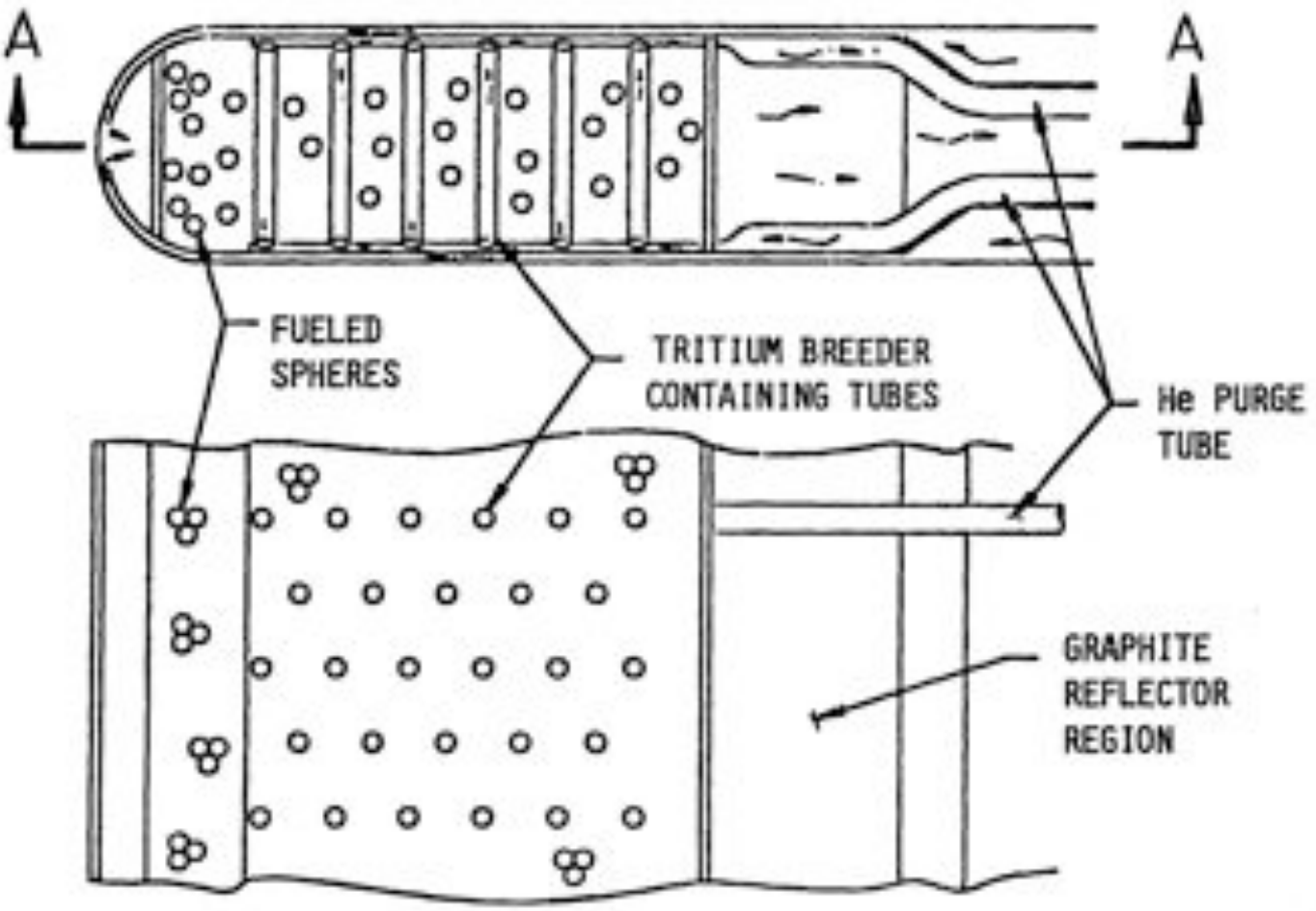

Figure III.B.1. Cross Section of Outer Blanket Module Showing Tritium Breeder Containing Tube Arrangement in Fueled Region of Blanket.

Table III.B.1. Tritium Breeder Properties and Thermal/Mechanical Aspects.

	Li_2O	$LiAlO_2$	Li_7Li_8Pb	Li	FLIBE (66-34)	FLIBE (47-53)
k(W/m-K)	3	1.73	16	56	1	0.8
ρ (kg/m^3)	2010	2520	9400	450	2000	2000
C_p (J/kg-K)	2600	1464	1600	4200	2380	2350
MP (°C)	1430	1610	235	180	460	363
Preferred Fuel Form	Plate	Plate	Tube	Tube	Tube	Tube
h (W/m^2-K)	3000	3000	2000	2000	2000	2000
Interface T_{max}, (°C) PCA/HT-9	550/550	550/550	430/475	495/550	550/550	550/550
Breeder Temperature Window (°C), min/max	420/800	420/1200	235/1370[b]	180/1370	460/1370	363/1370
Breeder ΔT (°C)	$q'''x^2/2k$	$q'''x^2/2k$	$q'''r^2/4k$	$q'''r^2/4k$	$q'''r^2/4k$	$q'''r^2/4k$
Characteristic x or r (cm), (9 W/cc)/ (18 W/cc)[c]	1.4/1.0[c]	1.6/1.13[d]	3.6/1.8[e]	5.8/2.9[e]	2.4/1.7[d]	1.9/1.4[d]
Clad/breeder fraction (%)[f]	1.8/2.5	1.6/2.2	1.4/2.8	0.8/1.7	2.1/2.9	2.6/3.6

[a]Max. temp.less than 550°C (structural stress limit) defined by max. corrosion rate of 20 μm/yr.

[b]Boiling point of Li = 1370°C at one atms.

[c]x-plate 1/2 width, r-tube radius. Helium coolant characteristics: P = 50 atm, T_{in} = 275°C: T_{out} = 500°C, $T_{coolant}$ = 420°C; q''' = 9 W/cc at Γ = 1.5 MW/m^2.

[d]Breeder element dimension limited by T_{window} and interface T_{max}.

[e]Breeder element dimension limited by interface T_{max}.

[f]Clad thickness = 0.25 mm.

Li_2O has the highest lithium atomic density among all tritium breeders and is the only solid breeder that has the potential of breeding adequate tritium without the need of a neutron multiplier. The bred tritium is expected to be released as T_2O, a chemical form which is markedly less apt to leak through the steel tube into the helium coolant than the atomic form, T_2. Thus, a purge flow tritium extraction design is usually adopted. However, recent $LiAlO_2$ insitu tritium extraction experiments (1) indicated that a large fraction of the tritium may be released in noncondensable form. Similar behavior could be expected for Li_2O. Since the results of this experiment are not fully understood, further investigations are needed. Li_2O has the disadvantage of being very hygroscopic, which implies the need for special attention during manufacturing and fabrication. Temperature control and irradiation damage effects (e.g., reductions in thermal conductivity) which influence the steady-state tritium inventory in Li_2O and irradiation growth (i.e. swelling) are key issues for this breeder (2). A final issue involves the activation of impurities the solid breeder and the radiological consequence associated with recycle of the breeder material and personnel exposure during the refabrication process.

$LiAlO_2$ is the solid breeder that has the most available and most favorable material property data. It is very stable and has a large temperature window, but requires the use of a neutron multiplier in order to obtain adequate tritium breeding. The activation of $LiAlO_2$ is an issue.

Among the Li-Pb eutectics, 17Li83Pb is favored because a low chemical reactivity results due to its high content of lead (which is also a good neutron multiplier). Is has a low melting point of 235°C and a very low solubility for tritium. Thus, the tritium inventory will be low, but the problem of handling T_2 in the blanket without excessive leakage appears to be very difficult. As shown in Table III.B.1, the weight and corrosiveness of 17Li83Pb are additional concerns (2).

Liquid lithium is known to be an excellent tritium breeder. However, its high chemical reactivity leads to potential safety concerns - especially if water cooled components are located near the blanket. Bred tritium is held in lithium in the form of LiT and normal releases will be minimized, but lithium will need to be circulated for tritium extraction outside of the blanket.

Table III.8.2. Summary of Tritium Control and Recovery Issues for Candidate Tritium Breeders.

	Li_2O	$LiAlO_2$	17L183Pb	Li	FLIBE
Tritium Form	T_2O	T_2O	T_2	LiT	T_2[a]
T Extraction:					
Helium Coolant			X		X
Breeder Circulation				X	
Purge Flow	X	X			
Stainless Steel Liner[b]				X	

[a]A design option for tritium as TF is also possible, but not selected due to corrosion issues.

[b]For safety, a stainless steel liner would be needed for the T_2 extraction system piping outside of the blanket.

Because of its low lithium density, FLIBE, a lithium-beryllium fluoride molten salt, also requires a neutron multiplier as well as isotopic enrichment in ^6Li for adequate breeding. It is known to have the advantages of excellent irradiation stability, low pressure operation, and chemical compatibility. These features imply safety advantages when compared to lithium and operational advantages when compared to the solid breeders and Li-Pb. The potential problem of TF (hydrofluoric acid) formation can be resolved by rapidly flowing the FLIBE to maintain the TF concentration at a low value and/or by the addition of a reducing agent (e.g., excess beryllium) in the salt such that BeF_2 and T_2 are formed instead of TF. In the latter case, the issue of tritium release in the form of T_2 would be similar to that for 17L183Pb.

Table III.8.2 summarizes some tritium control issues and recovery for the different breeders.

III.B.3 Some Design Implications

One key design issue is the estimated structure volume fraction required by each option and the impact on tritium and fissile material breeding performance. The characteristic fuel element dimensions and the fractions for each of the tritium breeding materials discussed earlier are presented in Table III.B.1. The characteristic dimensions were defined either by the breeder material-cladding interface temperature, or by the maximum fuel element centerline temperature. The maximum centerline temperature for the liquid breeders was set at the boiling point of lithium.

In calculating the characteristic dimensions for FLIBE tubes, the effect of natural convection was included. This effect was estimated by assuming a magnetic-laminar flow Nusselt number of 8.23 (3). Under this assumption, convection enhances the fluid heat transfer by a factor of two over purely convective heat transfer. This interpretation was compared by calculating the modified Peclet number (4), Pe, which gives the ratio of convective to conductive heat transfer in a uniform magnetic field. At a magnetic field of 4T and a characteristic dimensions of 2 cm, Pe = 2.15 was calculated for FLIBE. This is slightly higher value agrees well with the above model.

With reference to Table III.B.1., all the fuel element characteristic dimensions look reasonable. Lithium, because of its higher thermal conductivity, can provide the largest fuel element tube diameter and thus the smallest structure volume fraction. It should be noted, however, that a characteristic breeder dimension in excess of ~ 2 cm would conflict with nuclear design requirements (see Section III.C) which specify both a low tritium breeder volume fraction and dispersal of the tritium breeder as uniformly through the blanket as possible. This neutronics constraint would increase the structure volume fraction of a lithium breeder to a similar percentage as the other breeders. Table III.B.2 also indicates some safety considerations. Since lithium has a relatively high chemical reactivity, a stainless steel liner for the tritium extraction system piping and other lithium safety systems would be required.

Another key issue for the breeder comparison is the handling of tritium. For the solid breeders, a purge flow design is required for the positive control of tritium and the containment of the solid breeder. This requirement is based on the assumption that most of the generated tritium is

in the condensable form. As indicated earlier, the species of tritium released from a solid breeder purge flow design is uncertain. If the dominating species of tritium is released in noncondensable form, a reliable permeation barrier at the fuel cladding and at the steam generator tubes will have to be identified in order to satisfy the limit of tritium release to the environment.

Limited irradiation data on solid breeders exist (2) and potentially large increases in breeder volume under irradiation were identified. The swelling effect on Li_2O was found to be more severe than $LiAlO_2$. If the breeder dimension change cannot be handled by creep and design configuration, swelling tolerance will need to be configured into the design. This would have impact on design complexity and an increase of void fraction of a few percent in order to accommodate the swelling effect could introduce heat transfer/temperature control difficulties. Not enough data are available to quantify the other potential damages of the solid breeder material due to thermal and irradiation effects. These damages can also affect heat transfer and tritium inventory.

If flowing liquid breeders like 17Li83Pb and FLiBe out of the blanket for tritium removal does not satisfactorly limit releases to the primary coolant, a simpler option would be to contain these breeders in sealed, but helium pressure relieved (i.e., vented) tubes. The bred tritium would then be allowed to permeate through the tube wall and to be extracted from the main coolant. Although the flowing purge system would be eliminated, it should be noted that allowing all of the tritium to permeate into the main helium coolant could increase design complexity in the power conversion loop in order to maintain an acceptably low level of tritium leakage from the piping and steam generator. Also, this mode of tritium recovery requires the addition of oxygen to the coolant and the reliance on oxide barriers. Key issues still remain on the oxidation kinetics of T_2O under irradiation and the adequacy of the effective permeation barrier of steam generator tubings. Other design fixes like a double wall heat exchanger and tritium barrier coatings would need to be considered.

The following observations can be made from the above comparisons of the various breeders:

- Among the solid breeders, Li_2O and $LiAlO_2$ are both credible and are similar in engineering application. Li_2O was selected over $LiAlO_2$ due to existing emphasis in the fusion-electric program. $LiAlO_2$ could ultimately be preferred for this application due to its chemical stability, resistance to irradiation damage, and larger temperature window. The higher lithium density of Li_2O is an advantage, but not a high priority issue because of the separate neutron multiplier. Tritium control may be an important issue in either case.
- Among the liquids, lithium is rejected due to safety concerns (an unnecessary burden in this case).
- FLIBE and 17Li83Pb are both credible liquid breeders and are similar in engineering application. FLIBE is non-corrosive at the design operating temperature and is favored in this respect. 17Li83Pb has a lower melting temperature and is preferred if corrosion is not limiting.

In Section III.B.5, representative solid and liquid breeders are further compared.

III.B.4. Comparison Between Li_2O and FLIBE

Recognizing the potential problem of irradiation effects on the solid breeders, a direct comparison was made between the Li_2O helium purge flow option (2) and a "pressure relieved" FLIBE option. In the latter case, no FLIBE would flow, but the accumulated helium (due to tritium production in the FLIBE) would be allowed to migrate and bubble up to a free surface in a reservoir located above the blanket, thus, the pressure which would otherwise accumulate in the individual tubes (2) could be relieved. The volume above the free surface would be controlled to maintain the desired pressure (perhaps 50 ATM) and to recover any free tritium which does not leak into the primary coolant. Given the lack of solubility of tritium in FLIBE (or 17Li83Pb), an actively flowing purge system would appear to be unjustified as a mechanism to substantially avoid processing tritium in the primary coolant.

---

* The flowing FLIBE option did not appear to be a viable candidate when this report was prepared, but more recent studies indicate that an optimal combination of permeation barriers and FLIBE circulation/processing with the tritium in the form of T_2 or TF (preference unknown) could effectively limit tritium permeation to the primary loop.

Table III.8.3. Li_2O and FLIBE Comparison (Breeder Volume Fraction ~ 5% Needed for the Fission-Suppressed Design).

Issues	Li_2O (Purged)	FLIBE (Pressure Relieved)
Design		
Mechanical design	Complex/active	Less complex/passive
Helium generation	No problem	No problem
Clad/breeder fraction	~ 3%	3.6%
Characteristic dimension	1 to 1.4 cm	1.4 cm radius
Material		
Radiation damage	Effect unknown	None
Electrolytic decomposition	None	Minor
Compatibility	Good	Good[a]
Interface T window (HT-9)[b]	360-550[c]	363-550[c]
Breeder T window	410-800	363-1370
Neutronics		
TBR	No Problem	No Problem with ^6Li enrichment
Thermal/Hydraulics		
Helium, T_{out}/T_{in}	500/275	500/275
Pumping power	Acceptable	Acceptable
Hot spot temperature	Acceptable	Acceptable
Natural convection	None	Some

Table III.B.3. Li_2O and FLIBE Comparison (Breeder Volume Fraction ~ 5% Needed for the Fission-Suppressed Design). Continued

Issues	Li_2O (Purged)	FLIBE (Pressure Relieved)
Tritium Handling		
Extraction from purge system	Primary extraction mode	Secondary processing only
Form	T_2O and T_2	T_2
Tritium inventory/GW_{th}	< 2 kg	Few hundred gm
Tritium extraction from main coolant	Secondary extraction mode	Primary extraction mode
Safety and Reliability		
Module burst	Solid in tube	Molten salt in tube
Tube leakage	Burden on extraction	Molten salt in helium stream cold trap
T_2 in main helium stream	Minor effect	Design load

[a]With beryllium added for TF control.

[b]Present materials limit estimates.

[c]Upper limit due to maximum structure temperature.

Table III.B.3 summarizes the results of the comparison. The low melting point FLIBE was selected for the comparison in order to obtain the maximum operating temperature window.

From mechanical design considerations, no feasibility problem was identified. The fuel element dimensions for both designs, as determined by heat transfer considerations, are of reasonable sizes as also shown in Table III.B.1.

Considering material properties, the radiation damage effects on Li_2O are largely unknown, although recent fusion reactor irradiation results indicate that some swelling may occur at high burnups. The problem of TF formation is resolved in the FLIBE option by adding excess beryllium into the FLIBE as a reducing agent.

From the consideration of tritium handling based on unirradiated material property data, the Li_2O design blanket inventory might be less than 2 kg/GW_{th}, due mostly to the solubility of T_2O in Li_2O. The FLIBE design would have a tritium inventory of less than 1 kg/GW_{th}, due to the necessary tritium build-up in the tube to force permeation across the cladding. When considering the design effects on blanket safety and reliability, both options have multiple boundaries and can potentially tolerate minor tube in-leakage without reactor shutdown.

With the above comparison, it can be concluded that no feasibility design issues have been identified for the options considered.

III.8.5 Conclusions

From the discussion and comparison presented above, it is somewhat arbitrarily recommended that Li_2O be considered as the breeder because the issues associated with tritium release to the environment (via the primary coolant) may be less severe and because it is currently receiving the greatest attention in the national program. If the hygroscopic, irradiation damage or activation properties for Li_2O out-shadow its favorable properties, the option of using a liquid breeder or $LiAlO_2$ should be kept open.

References, Section III.8

1) R. G. Clemmer, et. al., "The TR10-01 Experiment: Insitu Tritium Recovery Results," Third Topical Meeting on Fusion Reactor Materials, Albuquerque, September 19-22, 1983.

2) "Blanket Comparison and Selection Study," Argonne National Laboratory, ANL/FPP-83-1, October 1983.

3) M. A. Hoffman, "Magnetic Field Effects on the Heat Transfer of Potential Fusion Reactor Coolants," UCRL-73993, June 1972.

4) P. L. Gierszewski, B. Mikic, and N. E. Todreas, "Natural Circulation in Fusion Reactor Blankets," Joint ASME/AICHE National Heat Transfer Conference, Orlando, Florida, July 27-30, 1980.

III.C. NUCLEAR DESIGN ANALYSIS AND PERFORMANCE

III.C.1 Objectives

At this early stage of our investigation of the tokamak-based, fission-suppressed fusion breeder, our objective was to arrive at a plausible nuclear design concept; one with the potential to produce fissile fuel (U-233) at a competitive cost while suppressing fission to enhance both safety and support ratio.

The starting point for this design was our FY82 tandem mirror fusion breeder reference blanket design.(1,2,3) The FY82 design basically consists of a pebble bed of composite Be/Th pebbles cooled by liquid lithium. The pebble bed facilitates quick refueling without blanket disassembly while the lithium is a mobile tritium breeding medium as well as the heat transfer medium. To account for the harsher environment of the tokamak (i.e., higher surface heat flux and magnetic fields), a new design evolved in which lithium was replaced by helium for cooling and by purged tubes containing a tritium breeder within, as well as behind the mobile pebble bed, for tritium breeding. As discussed in section III.B, Li_2O was selected as the tritium breeder, but several other breeding compounds (e.g., Li-Pb, FLIBE, $LiAlO_2$) can also be attractive for this application. The mobile pebble bed was retained to facilitate fuel loading and unloading.

The objective of this nuclear analysis was to appraise the performance potential by estimating net breeding of fissile material in a system that has a tritium breeding ratio of 1.0, and to estimate heating profiles for input to the heat transfer and fluid mechanics design and analysis of section III.D.

III.C.2 Methods of Analysis

The procedure used to perform the nuclear analysis consisted of developing geometric models approximating various aspects of the blanket which were then analyzed with one or two Monte Carlo transport codes: TART, a coupled neutron-photon, 3-D Monte Carlo transport code using a 175-group nuclear data set generated from ENDL, the Livermore-evaluated nuclear data library(4,5); and ALICE, a variant of TART that treats resonance effects by using the probability table method.(6) Most cases were run with 5000 source neutrons, resulting in less than 2% standard deviation.

A cross section of the actual configuration was shown in Fig. III.A.1. The models developed for the Monte Carlo analysis are simplifications of the actual geometry that are intended to reasonably approximate its important aspects.

Four models were developed and employed for this analysis. The first is a toroidal 2-D model approximating the overall aspects of the toroidal geometry. The second, a unit cell of the pebble bed, was developed to examine heterogeneous and resonance self-shielding effects. The third, also a toroidal 2-D model, was used to estimate the effects of the poloidal divertor. Results from these first three models were then combined to estimate overall performance. A fourth model, a 1-D radially zoned cylinder, was used to estimate heating profiles. This was done early in the study to provide input to the heat transfer and fluid mechanics design and analysis.

III.C.3 Toroidal 2-D Model and Results

The toroidal 2-D model is rectangular in cross section, with both radial and axial zoning. This model approximates the overall aspects of the blanket geometry and is the basic model used to estimate nuclear performance. This model is shown in Fig. III.C.1. The dimensions shown for the first walls, inner and outer blankets, top and bottom blankets and shields are the final dimensions used and reflect the limitations imposed by plasma and coil geometries. The critical inner shield thickness of 54 cm, as used in Starfire, was used to set the inboard blanket dimensions. The thin (10 cm) shield zones used in this mode are there only to provide for appropriate reflection for the blanket.

The plasma is approximated by an isotropic 14 MeV neutron source of constant density distributed in the rectangular torus as shown. The fraction of source neutrons from this source crossing the inner, outer, and top + bottom first walls are given in Table III.C.1.

The first wall in the model consists of an erosion layer (0.9 cm initially, 0.45 cm ave.), 0.6-cm Fe structure and a 6-cm He plenum. The blanket contains the Be/Th pebbles plus Li_2O-containing tubes. The rear 5 cm of the blanket consists of a dense pack of Li_2O-containing tubes. Material compositions in these zones are given in Table III.C.2. Material atom densities are given in Table III.C.3.

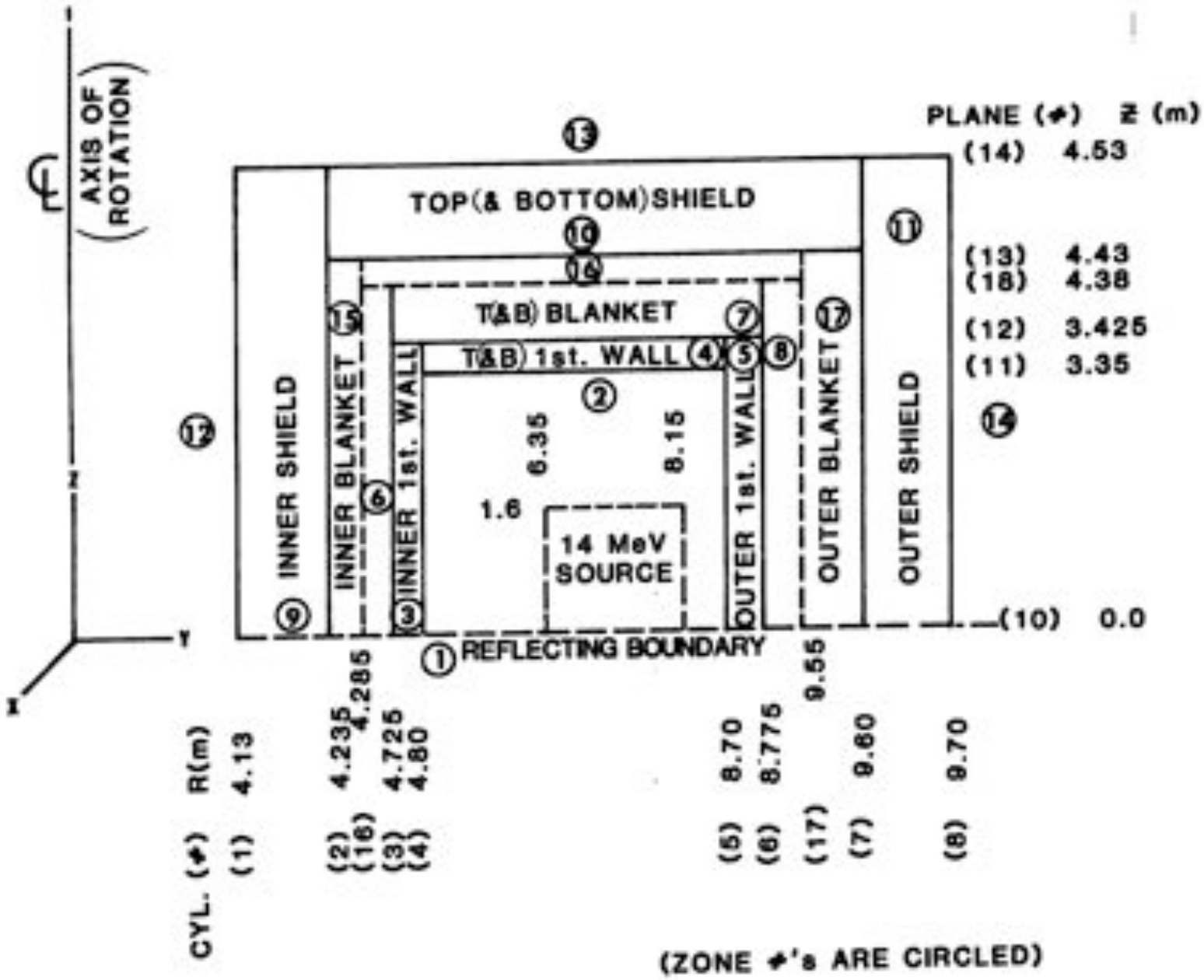

Fig. III.C.1. Toroidal 2D Model.

Table III.C.1 Source Neutron Distribution

%	To
17.3	Inner first wall
32.1	Top + bottom first wall
50.7	Outer first wall

Table III.C.2 First-Wall and Blanket Compositions

- First wall = erosion layer + structure + plena
  0.45 (ave.) cm Fe + 0.6 cm Fe + 6 cm He

- Bed with Li_2O in tubes

Material	Volume Fraction
Fe structure	.05
Fe tubes (1" OD, 20 mil wall, 7 cm pitch)	.0077
Li_2O	.0905
Be	.4510
Th	.0238
(U/Th)	(1 a/o)

- Li_2O zone

Material	Volume Fraction
Li_2O	.80
Fe	.08

Table III.C.3 Material Atom Densities
(atom/cc x 10^{-22})

First wall	Fe	1.19
(zones 3, 4, 5)		
Bed	Fe	0.49
(zones 6, 7, 8)	Li6	0.032 (4.4%)
	Li7	0.700
	O	0.367
	Be	5.60
	Th	0.0716
	U233	0.00072
Outer (Li_2O/Fe) zones	Fe	0.678
(zones 15, 16, 17)	Li6	0.389 (6 a/o)
	Li7	6.096
	O	3.24
Inner shield	W	5.06
(zone 9)	H	1.34
	O	0.67
	B10	0.07
Outer shield	Fe	6.78
(zone 10, 11)	H	1.34
	O	0.67
	B10	0.07

The toroidal 2-D blanket model was analyzed with the TART code. Breeding ratios, tritium and net U-233 ($T + F_{net}$) are listed in Table III.C.4 for four Li6/Li ratios ranging from 0.55 to 4.4. Within this range T varied between 0.70 and 1.10 while $T + F_{net}$ ranged between 1.61 and 1.83. Most of the change in $T + F_{net}$ can be attributed to (n,γ) capture in the bed's iron structure. The U-233 fission ratio (fission per 14 MeV neutrons) also varies significantly from 0.11 down to 0.042. The Th fission ratio is only 0.009, suggesting it might be worthwhile to increase the Th volume fraction as suggested by Meier(7) and by Greenspan (8).

Table III.C.4 Breeding and Other Reactions per DT Neutron vs. Li6/Li Ratio with Toroidal 2-D Model

^{6}Li/Li(%)	T	F	U(n,fiss)	T+F_{net}	Be + Fe(n,γ)
0.55	0.703	1.036	0.110	1.614	.22
1.08	0.838	0.957	0.083	1.726	.147
2.17	0.968	0.877	0.060	1.776	.093
4.4	1.096	0.786	0.042	1.834	.061

T ≡ Li(n,T)

F ≡ Th (n,γ)

F_{net} ≡ F - U(n,fiss) - U(n,γ)

A variation of this blanket, one with all of the lithium-containing breeder trubes behind, rather than in the Be/Th pebble bed, was considered first but was found to have lower T +F_{net} [1.61 (with T = 1.02) vs. 1.83 (with T = 1.10)] and also a higher n,fission reaction rate (0.096 vs. 0.051). Consequently, it was dropped in favor of having Li as well as Th in the Be zone. The factor of 2 lower fission rate with the Li and Th/U combined in the same zone shows the advantage of this configuration for suppressing fission. While the segregated configuration gives lower breeding and higher fission, it is a somewhat simpler configuration and the Be pebble bed is much thinner, ∿ 20 vs. ∿ 60 cm.

With the fusile and fissile (T and F) breeding in different zones, the maintenance of T = 1.0 is simplified. When Li and Th are in the same zone, T is set by the ^{6}Li concentration as shown in Table III.C.4. The ^{6}Li concentration decreases about 2.4%, on average, per MWY/m^2 exposure. This in turn will decrease T, but the decrease is not estimated to be significant. For example an optimistic maximum blanket exposure of 20 MWY/m^2 may decrease the ^{6}Li concentration by about 50% which, according to Table III.C.4, would decrease T by about 12%. By replacing 1/4 of the blanket modules at a time, the swing in T for the whole blanket would only be about ±1.5%. This estimate

is crude because the poloidal variation in wall loading and the radial variation in ^{6}Li "burn out" are not accounted for. These two effects should tend to counteract each other.

A breakdown of the reactions and energy deposition in the individual zones of the 2-D toroidal model (Fig. III.C.1) is given in Table III.C.5.

III.C.4 Unit Cell Model and Results

The toroidal model just described homogenizes the Be/Th pebbles, the Fe tubes and the Li_2O they contain. To determine if spatial and/or resonance self-shielding are important in the actual tube plus pebble configuration, the heterogeneous unit cell model shown in Fig. III.C.2 was developed. The unit cell models a 7 x 7-cm array of Fe tubes containing Li_2O with homogenized Be/Th pebbles between the tubes. An x-y plane source of isotropic 14 MeV neutrons is at z = 0. The sides of the unit cell are reflecting, making the model behave as an infinite array of unit cells.

This heterogeneous unit cell model was analyzed with both the TART and ALICE codes to examine both heterogeneous and resonance effects. A homogenized version of this unit cell was also analyzed with the TART and ALICE codes. Results of these four runs are given in Table III.C.6. When the heterogeneous ALICE case is compared to the homogeneous TART case, it is found that the total breeding (T +F) is nearly the same (ratio = 0.99) but the ALICE case has higher T (18%) and lower F.

The resonance effect is, thus, important insofar in determining the proper mix of Li6 and Th but apparently less important in determining total breeding. To better optimize the breeding ratios, an increase in Th is favored over decreasing Li6. Thus, captures in the structure can be prevented from becoming important, at least until U (n,fiss) reactions become significant.

Based on comparing these unit cell cases, it appears that resonance, not bed heterogeneous, effects have the major impact on performance. The ratio of the heterogeneous ALICE results to the homogeneous TART results are used to approximately correct the toroidal 2-D model results for bed heterogeneous and resonance effects.

Table III.C.5 Reactions and Energy by Zone*

Zone #		^{6}T	^{7}T	T	F	U(n,fiss)	T+F	Total Capture	Energy (MeV)
3	1st							.0125	.412
4	Walls							.0205	.688
5								.0273	1.041
6		.174	.011	.185	.138	.0074	.323	.350	4.419
7	Beds	.368	.020	.388	.281	.0152	.669	.725	9.012
8		.480	.029	.509	.367	.020	.876	.952	12.12
15	Li_2O	.010	.001	.011				.011	.085
16	Zones	.0007	-	.0007				.0007	.0048
17		.0034	.0002	.0036				.0035	.0225
9								.024	.168
10	Shields							.0003	.0042
11								.005	.023
				1.10	0.786	0.043	1.89	2.132	28.0

$T + F_{net} = 1.83$

Energy (first-wall blanket) = 27.8 MeV

(shield) = 0.2 MeV

(energy does not include decay energy)

* See Fig. III.C.1

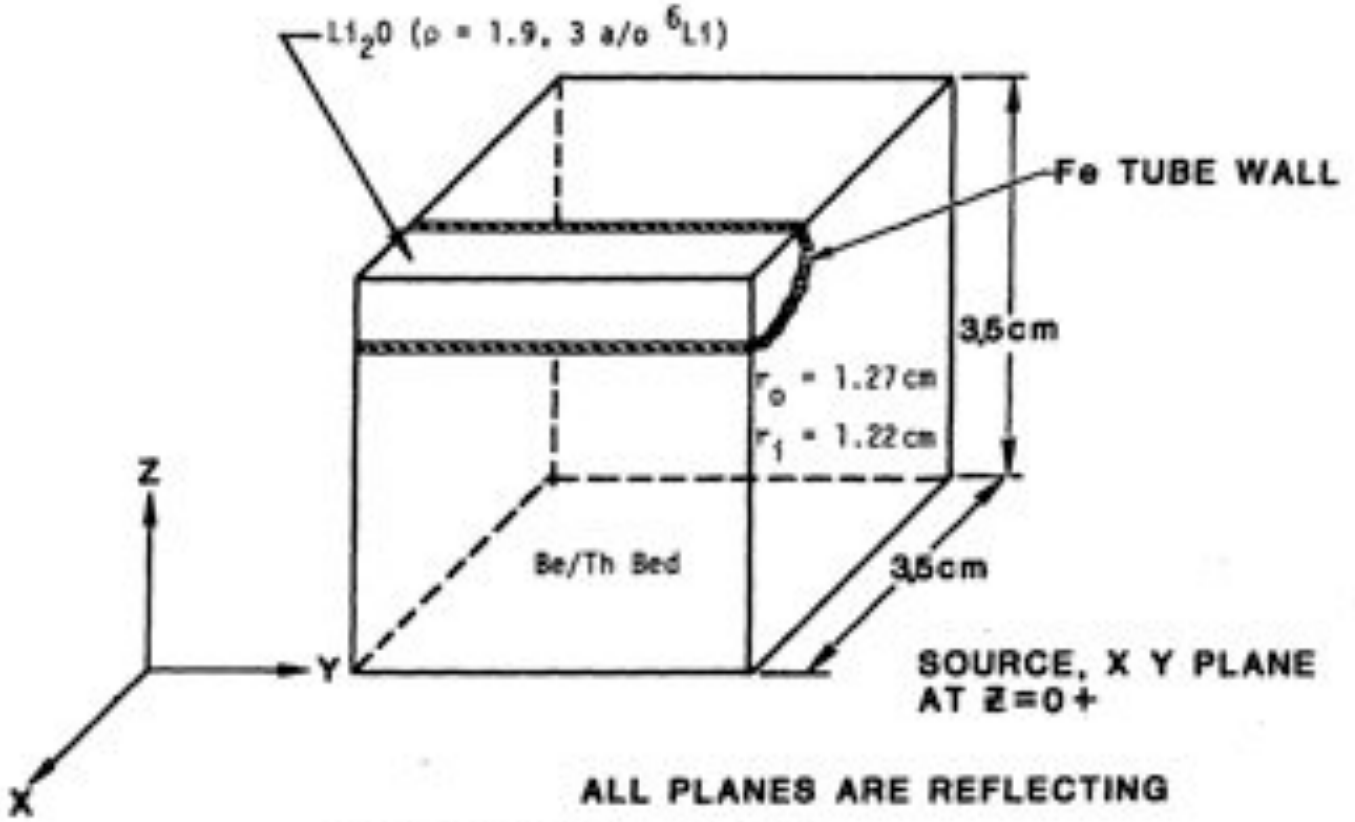

Be/ Th BED COMPOSITION

Be* = 47.5 v/o

Th** = 2.5 v/o

He = 50.0 v/o

*(Fe - 0.1 a/o in Be)

**(U - 0.5 a/o in Th)

**(Pa - 0.5 a/o in Th)

Fig. III.C.2. Unit Cell Model.

Table III.C.6 Unit Cell Model Results*

	Heterogeneous Cases		Homogeneous Cases	
	(TART)	(ALICE)	(TART)	(ALICE)
T	1.351	1.604	1.362	1.67
Th(n,γ)	1.047	.747	.999	.731
Th (n,fiss)	.011	.011	.011	.011
U (n,f)	.043	.052	.032	.039
U (n,γ)	.0063	.0053	.0051	.0043
Pa (n,γ)	.034	.028	.030	.026
Fe (n,γ)	.0203	.0213	.0154	.0126
F_{net}	.964	.662	.933	.662
$T + F_{net}$	2.32	2.27	2.29	2.33
E (MeV)	27.82	29.89	28.4	30.2
Energy partitioning (%)				
Be/Th	70	68		
Li_2O	29	31		
Fe tube	1	0.7		

* $^{6}Li/Li$ = 2.97%, U/HM = 0.5 a/o, Pa/HM = 0.5 a/o

III.C.5 Divertor Modeling and Results

The poloidal divertor requires a major penetration through the blanket as well as special materials due to its high particle and surface heat fluxes. The geometric model developed to assess the effects of the divertor on blanket performance is shown in Fig. III.C.3. Its geometry is toroidal with zone numbers circled. Zone 1 is the vacuum zone in which an isotropic, constant-density source volume is located. Zones 2-5 are standard first-wall zones as described in subsection III.C.3 and zones 6-10 and 19 are standard blanket bed zones. Zone 11 is the divertor first wall, 12.6-cm thick,

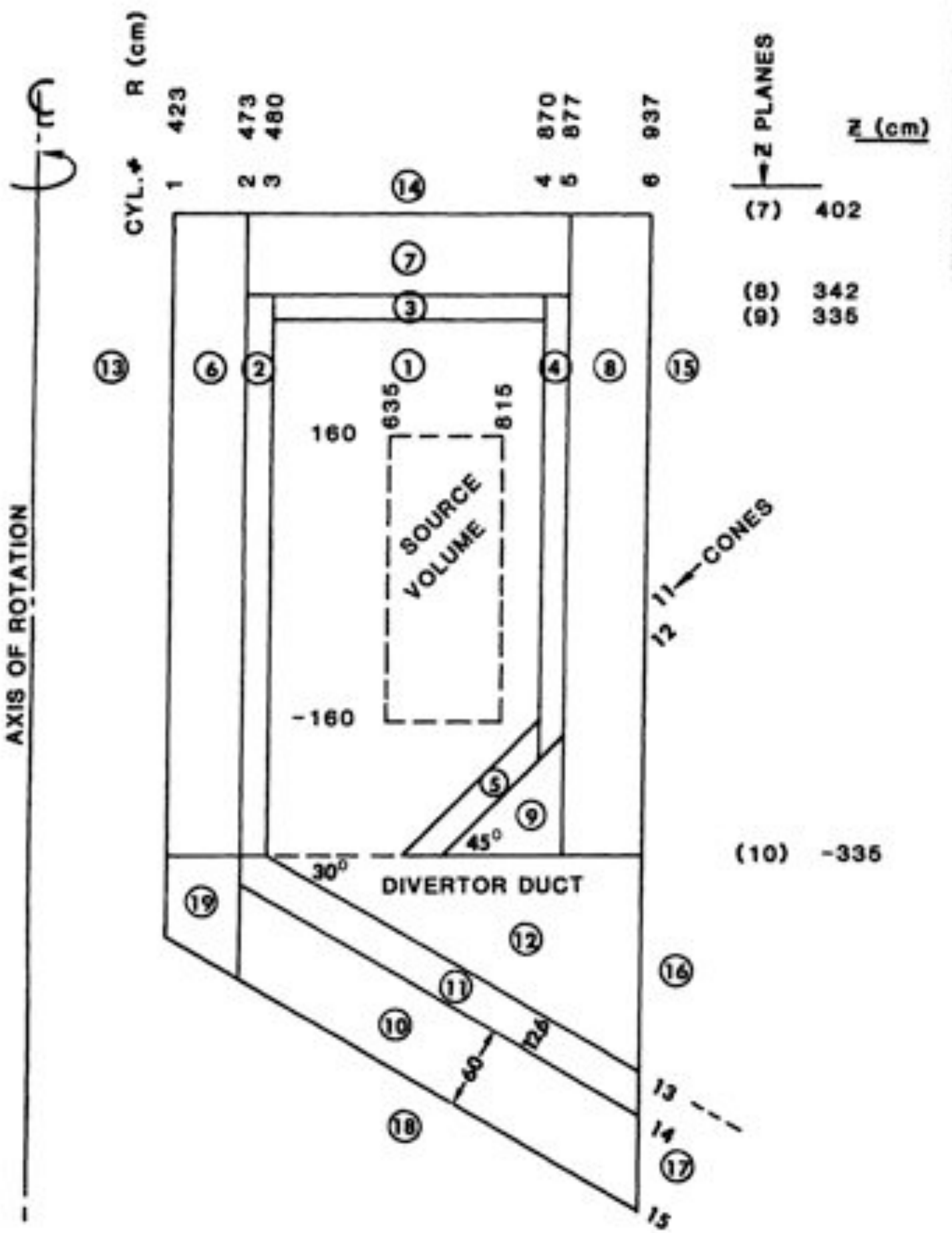

Fig. III.C.3. Divertor Model.

consisting of a homogeneous mixture of Be (1 cm), Cu (2 cm), H_2O (1 cm), Fe (2.6 cm) and He (6 cm). Zone 12 represents the divertor vacuum duct. Zones 13-18 are external leakage zones.

TART results by zone are listed in Table III.C.7. The total breeding ratio (T + F) is 1.59 and the total energy absorbed is 26.0 MeV. This problem was repeated with the divertor opening closed with a reflecting boundary. The total breeding for this second case is 1.87 and energy is 28.5 MeV. By comparing these two cases it is estimated that the divertor will cause a 15% decrease in total breeding (T + F) and a 9% decrease in blanket energy when compared to the blanket model without the divertor.

III.C.6 Estimate of Overall Performance

Results from the toroidal, unit cell and divertor models are combined to give the following estimate of overall blanket performance.

Total net breeding	1.55 (± 10%)
Tritium breeding required	1.01
U-233 net breeding	0.54 (± 30%)
Energy (@ U/HM = 1.0 a/o)	26.5 MeV (-20%, +40%)

The total net breeding value ($T + F_{net}$) is obtained by starting with toroidal model $T + F_{net}$ (1.83) and multiplying it by the ratio of the unit cell heterogeneous ALICE case to the homogeneous TART case (0.99). This product is in turn multiplied by the ratio of the with-to-without divertor model cases (0.854). The U-233 breeding ratio is then obtained by subtracting the required tritium breeding ratio, which is assumed to be 1.01. Blanket energy is calculated in a similar manner: E (@ U/HM = 1%) = 27.7 x 1.05 x 0.91 = 26.5 MeV. Decay energy is not included. The unit cell model had 1/2 the U "enrichment" used in the other model to counter the infinite nature of and lack of structure in the unit cell model. A better method of estimating U-233 fission is needed.

The above values are per DT source neutron. The uncertainties listed are crude estimates that include data and modeling-caused uncertainties in addition to the ~2% Monte Carlo statistical uncertainty. The total energy

deposited per fusion is expected to have a larger uncertainty in the upwards direction than the downwards direction due to remaining uncertainties in the details of the resonance self-shielding treatment. Not included in these estimates are effects of module end plena and n, gamma reactions in Pa-233. Heterogeneity of the composite Be/Th pebbles (not investigated) may also affect results.

Table III.C.7. Divertor Model TART Results by Zone (per DT Neutron).

Material Zones	T	F	Total Capture	Energy (MeV)
2			.011	.37
3			.010	.33
4			.020	.78
5			.008	.31
6	.176	.127	.330	4.31
7	.167	.128	.322	4.22
8	.382	.282	.726	9.93
9	.128	.095	.244	3.35
10	.060	.041	.109	1.30
11			.062	1.02
19	.004	.004	.009	0.10
Totals	.917	.677	1.85	26.0

Leakage Zones	Energy (MeV)	Leakage
13	0.07	.034
14	0.02	.019
15	0.08	.047
16	0.17	.115
17	< .01	<.001
18	< .01	.006
Totals	0.34	.221

The tritium breeding can be increased as required, but any additional bred tritium must be subtracted from the net fissile fuel production. It is important to note that even a 1% loss of tritium from a 3000 MW_t plant would represent a release of $4.5 \cdot 10^5$ curies per day! Similarly, the allowed recovery cost at 10,000 $/g would be ~ 12$M/yr per percent tritium.

III.C.7. Recommendations

Neutronically, the He-cooled composite Be/Th pebble bed blanket with tubes containing Li within the bed looks to be the best candidate considered thus far for the tokamak breeder application. In fact, it is also an attractive candidate for the tandem mirror.

It must be emphasized that this nucleonics analysis is preliminary. Future work must better quantify and reduce the uncertainties and optimize the design to maximize specific breeding. For example, significant higher specific breeding looks achievable by increasing the Th content above the ~ 2 v/o used here (7). The effects of Li tube size and pitch, composite pebble heterogeneity, module edge effects, and source geometry also need to be further investigated. And, of course, sensitivity to data uncertainties (especially beryllium) need to be quantified. In the longer run, cost optimization will require knowing the tradeoffs between breeding and bed thickness, reflector thickness and/or the effects of replacing Be in the bed with a cheaper moderator.

References, Section III.C

1. D. H. Berwald, et at., "Fission-Suppressed Hybrid Reactors - The Fusion Breeder," Lawrence Livermore National Laboratory, UCID-19638 (1983).

2. R. W. Moir, et al., "Fusion Breeder Reactor Design Studies," Proc. Fifth Topical Mtg. on the Tech. of Fusion Energy, Knoxville, TN, 1983, in Nuclear Technology/Fusion, Vol. 14, No. 2, Part 2, p. 589.

3. J. D. Lee, "Nucleonics of a Be-Li-Th Blanket For The Fusion Breeder," Proc. Fifth Topical Mtg. on the Tech. of Fusion Energy, Knoxville, TN, 1983, in Nuclear Technology/Fusion, Vol. 14, No. 2, Part 2, p. 805. Also Lawrence Livermore National Laboratory Rpt. UCRL-88237 (1983).

4. E. F. Plechaty and J. R. Kimlinger, "TARTNP: A Coupled Neutron-Photon Monte Carlo Transport Code," Lawrence Livermore National Laboratory, UCRL-50400, Vol. 14 (1975).

5. E. F. Plechaty, D. E. Cullen, R. J. Howerton and J. R. Kimlinger, "Tabular and Graphical Presentation of 175 Neutron-Group Constants Derived From The LLL-Evaluated Nuclear Data Library (ENDL)," Lawrence Livermore National Laboratory, UCRL-50400, Vol. 16, Rev. 2 (1978).

6. E. F. Plechaty and D. E. Cullen, "Resonance Self-Shielding Calculations Using The Probability Table Method," Lawrence Livermore National Laboratory, UCID-17230 (1976).

7. W. R. Meier, "A High Performance, Suppressed-Fission ICF Hybrid," 10th IEEE Sym. on Fusion Engineering, Philadelphia, PA, 1983; also Lawrence Livermore National Laboratory Rpt. UCRL-89274 (1983).

8. E. Greenspan and G. H. Miley, "Tritium Assisted Fusion Breeders," UCID-19874, Lawrence Livermore National Laboratory (1983).

III.D FLUID DYNAMICS AND HEAT TRANSFER

III.D.1 Introduction

For a tokamak reactor, the most critical heat transfer problem is the first wall design. In order to accommodate the problems of surface heat removal, surface erosion and tolerance of radiation-induced swelling, the bellows first wall design was conceived and selected for the fusion breeder blanket. Two-dimensional thermal-mechanical analyses of the bellows first wall were performed to identify the temperature and stress distributions, guide the design, and verify that it met all the design constraints.

The helium-cooled, fission-suppressed, hybrid reactor blanket has a unique fuel element configuration consisting of a packed bed of beryllium/thorium pebbles with a tritium breeder in tubes which are distributed throughout the bed.* Heat transfer calculations were performed to show that the selected ball the tube sizes can satisfy the respective material temperature limits. After the blanket, first wall and fuel element zone configurations were defined, the blanket loop pressure drops and pumping power were then calculated to assure that they are acceptable.

III.D.2 General Considerations and Design Limits

During the course of the helium-cooled, fusion breeder blanket fluid dynamics and heat transfer design, close interaction was maintained with the mechanical design, neutronics analysis, and material selection efforts. The fluid dynamics and heat transfer design of a gas-cooled reactor system should satisfy two primary requirements: high thermal efficiency and low pumping power losses. The high efficiency requirement dictates a high coolant outlet temperature, restricted only by the maximum operating temperature limits of the reactor materials. The pumping power loss requirement leads to a high system operating pressure to obtain high coolant density, a large coolant inlet-to-outlet temperature differential, and restricts the velocities of the coolant in various sections of the coolant loop. On the other hand, the restrictions on material operating temperature limits lead to high coolant velocities in the vicinity of the first wall to maintain high heat transfer coefficients.

---

* Li_2O was nominally selected as the tritium breeder and its use is assumed in this section. The general conclusions are not expected to change for other choices.

The temperature limits of key materials crucial to the design of the blanket were first established. At the same time, the pressure drop limits for different regions of the blanket were defined to establish a basis for the fluid dynamics and heat transfer design and analysis. In the blanket region, the key materials are the structural material, the neutron multiplier and the fuel material. As discussed in Section III.A, 2-1/4 Cr - 1 Mo was recommended to be the structural material. This easily manufactured ferritic steel alloy has a maximum allowable temperature of 475°C for high stress applications. Typically, the reactor first-wall will experience the highest stress and the highest flux of high energy neutrons. Thus, this temperature limit is most applicable to the heat transfer analysis of the first wall. The temperature limits for the lithium oxide (Li_2O) breeding material are T_{min} = 410°C and T_{max} = 800°C (1000°C)*(1).

As mentioned above, low coolant pressure drop in a power producing machine is important in reducing the pumping power necessary to circulate the helium coolant. The acceptable pressure drop depends upon an over-all optimization of the reactor economics. At this stage of the conceptual design, two pressure drop limits have been used. A value of approximately 5% of the thermal power was used for the pumping power for the complete coolant circuit, including the heat exchangers, the blanket, pumps, and piping. The second limit is imposed by the pressure differential capability of the helium circulator. Using a single-stage circulator, a value of $\Delta P/P < 4.3\%$ was used for the entire coolant loop.

Experience with helium-cooled nuclear power systems indicates that a helium pressure of 40 to 80 atm will be needed for an efficient primary loop design. Steam-generator design conditions dictate a minimum coolant inlet temperature of about 275°C and a minimum coolant temperature rise of above 100°C. Based on this information, a helium operating pressure of 5.1 MPa

---

*The maximum lithium oxide temperature can be increased to 1000°C for design approaches with helium purge gas flow directed only to the cold region of the breeder.

(50 atm) and an inlet temperature of 275°C were selected. For the fusion breeder blanket, an outlet temperature of 500°C was selected to give a thermal cycle efficiency of 39%. Structure temperatures above 475°C occur only toward the rear of the blanket where the stress and neutron flux are lowest.

At the present stage of the study, it is believed that heat transfer in the vicinity of the first wall will be a key design issue. In order to design for a neutron wall loading of 3 MW/m^2 and a surface heat loading in the range of 0.25 to 0.75 MW/m^2, the bellows first wall configuration, as illustrated in Figure III.A.5, was used for the analysis. In contrast to a smooth first wall, the bellows or finned design is necessary to increase the heat transfer surface area and the heat transfer coefficient. The bellows configuration is also conveniently coupled with the mechanical design requirements for the handling of static pressure and structural swelling.

III.D.3 Bellows First Wall Design

III.D.3.a Mechanical Design

The primary purpose of the first wall is to provide a boundary between the pressurized coolant and the vacuum of the plasma chamber. At the same time, it has to handle the transmission of thermal power through the wall to the high pressure helium coolant. There are two contributions to the heating of the wall. First, the volumetric power generation due to the neutron and material interaction, and the surface heat flux coming from the plasma side. In addition to these effects, the selected structural configuration has to accommodate neutron-induced swelling under high neutron fluence while being eroded away at a rate of 2.25 mm/year. (See Chapter II discussion.) A service life of four years was selected for the reference design. The above requirements are severe by conventional standards.

As shown in Section III.A, the first wall itself is a semi-cylinder forming a lobe submodule which is tied back to the structural region behind the blanket. The flat sides of the lobes are pressure balanced by adjacent lobes. Thus, the pressure is contained by pure tension in the wall. As discussed below, thermal effects can be tolerated because of the comparative

flexibility of this wall. To render the wall "soft" in the module-axis direction, so that it can tolerate distrubances in that direction, the wall is of corrugated (bellows) form. The dimensions of the bellows cross-section delineated below were decided after some iterations, but have yet to be optimized.

Manufacturing methods for such a wall are worth mentioning. The wall would not, in fact, be corrugated. Rather, it would be grooved on both sides by gang milling; this operating being carried out while the wall is a flat plate. The sides of the lobe would then be thinned and the wall finally pressed into the semi-cylindrical lobe form with the corrugations in place. Erosion capability is built in by the corrugation being 9 mm thicker than structurally needed on the plasma side. This material is expected to diminish in thickness progressively during the wall life.

III.D.3.b First Wall Thermal-Mechanical Analysis

The objective of the first wall thermal mechanical analysis was to iteratively manipulate the bellows first wall configuration in such a way as to control the associated temperatures and stresses, keeping both below specified design limits. To accomplish this objective, the two dimensional steady-state temperature distribution at the beginning and end of life was calculated for the bellows first wall using TACO2D[2], a finite element heat transfer code. The temperature profile calculated by TACO2D was then coupled along with the helium pressure boundary condition into NIKE2D[2], an implicit, finite deformation, finite element stress code. The neutron swelling effects were not included in the stress analysis. The results of TACO2D and NIKE2D were graphically displayed using the post-processors POSTACO[2] and THOR[2], respectively. Both of these codes and their accompanying post-processors are available on the magnetic fusion energy computer network.

Figure III.D.1 presents the two-dimensional bellows first wall configuration which was modeled using the above codes. This basic configuration was analyzed for two conditions: the beginning of life in which the 9 mm sacrificial layer on the plasma side of the wall has not eroded, and at the end of life in which the sacrificial layer has completely eroded. Table III.D.1

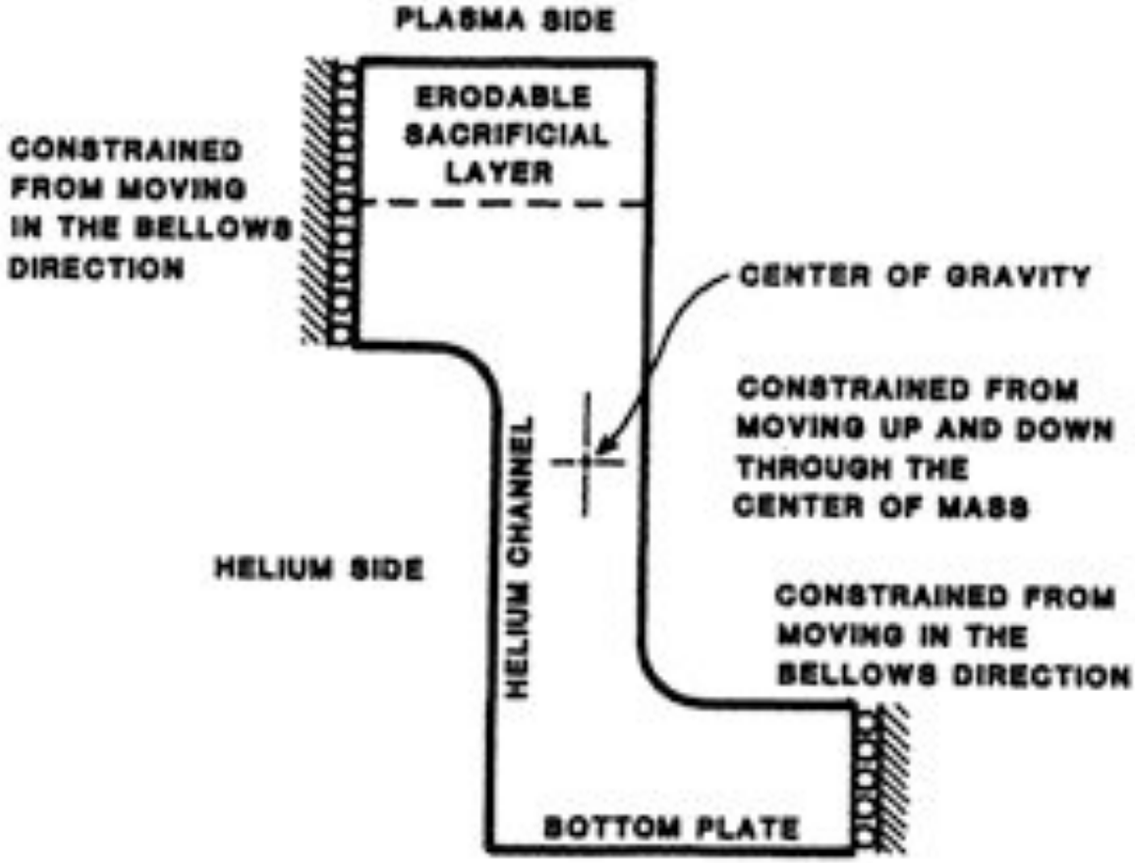

Figure III.D.1 Two-dimensional bellows first wall configurations (representation of a unit element, not to scale)

Table III.D.1 Design Guidelines for the Bellows First Wall

Material	2-1/4 Cr - 1 Mo/HT-9 (HT-9 alternate)
Neutron wall loading	3 MW/m^2
Surface wall loading	0.25 MW/m^2*
T_{max} limit, 2-1/4 Cr - 1 Mo/HT-9	475° (550°C for HT-9)
Expected ultimate tensile strength at T_{max}	435 MPa (500 MPa for HT-9)
BOL erosion layer thickness	9 mm

*A surface wall loading of 0.43 MW/m^2 was adopted late in the study. The ramifications of this increase are discussed later in this section.

lists the design guidelines used for the analysis. Table III.D.2 summarizes the thermal and structural computer inputs for the ferritic steel structural materials 2-1/4 Cr - 1 Mo and HT-9.

As shown, the principal stresses calculated by NIKE2D for the bellows first wall were computed assuming a hydrostatic pressure on the helium side of the wall coupled with the temperature profile computed by TACO2D. The wall was constrained from moving in the bellows direction along both bellows side interfaces and from moving up and down by a single point located at the wall's center of mass (see Fig. III.D.1).

Figures III.D.2 through III.D.5 graphically display the bellows first wall temperature profiles calculated by TACO2D at the beginning and end of life using both 2-1/4 Cr - 1 Mo and HT-9 structural material. Figures III.D.6 through III.D.9 present the beginning and end of life principle stresses calculated by NIKE2D. The results of these figures are summarized in Table III.D.3. This table shows that with the present bellows first wall design, the design guideline maximum temperature is slightly exceeded for both the 2-1/4 Cr - 1 Mo and HT-9 bellows first wall at the beginning of life. However, it is important to note that the hot spots are in the sacrificial layer closest to the plasma. As can be seen in Figs. III.D.6 and III.D.8, this layer is required to provide only minimal structural support. At the end of life, the design guideline maximum temperature is easily met by both the 2-1/4 Cr - 1 Mo and HT-9. The design guideline maximum stresses are met for both the 2-1/4 Cr - 1 Mo and HT-9 at the beginning of life.

These results indicate that at a surface loading of 0.25 MW/m^2, the present bellows first wall design meets the thermal and structural design guidelines using both 2-1/4 Cr - 1 Mo and HT-9 structural materials, the only exception being the beginning of life temperatures in the sacrificial layer of the wall. This layer is required to supply only minimal structural support. These temperatures are still well below the 725°C limit at which the structured material begins to be in the two phase regime. It is expected that by modifying the present configuration, the design can be optimized to lower both the temperatures and stresses even more.

Table III.D.2 Thermal and Structural Computer Inputs for the Bellows First Wall

Thermal TAC02D Inputs			
Maximum surface heat flux, (MW/m^2)[a]	0.25		
Volumetric neutron heating, (MW/m^3)	28.8		
Beginning of life helium channel convective heat transfer coefficient, (W/m^2-K)	2-1/4 Cr - 1 Mo		11940[b]
	HT-9	10950	
End of life helium channel convective heat transfer coefficient, (W/m^2-K)	2-1/4Cr	11920	
	HT-9	10920	
Bottom plate convective heat transfer coefficient, (W/m^2-K)[c]	190		
Beginning of life helium coolant temperature, (°C)	309		
End of life helium coolant temperature, (°C)	296		
Structural NIKE2D Inputs			
Helium side hydrostatic pressure, (MPa)	5.0		

[a]The surface heat flux at each nodal point (including the bellows side walls) on the plasma side is equal to the solid angle seen at that point times the maximum surface heat flux.

[b]The variation of heat transfer coefficient is due to the contribution of material volumetric power generation at the BOL and EOL, and the conductive enhancement due to the fin-like channels of the first wall.

[c]The bottom plate convective heat transfer coefficient is smaller than the helium channel convective heat transfer coefficient because heat removal at the bottom plate is from convection in the flow distribution plenum.

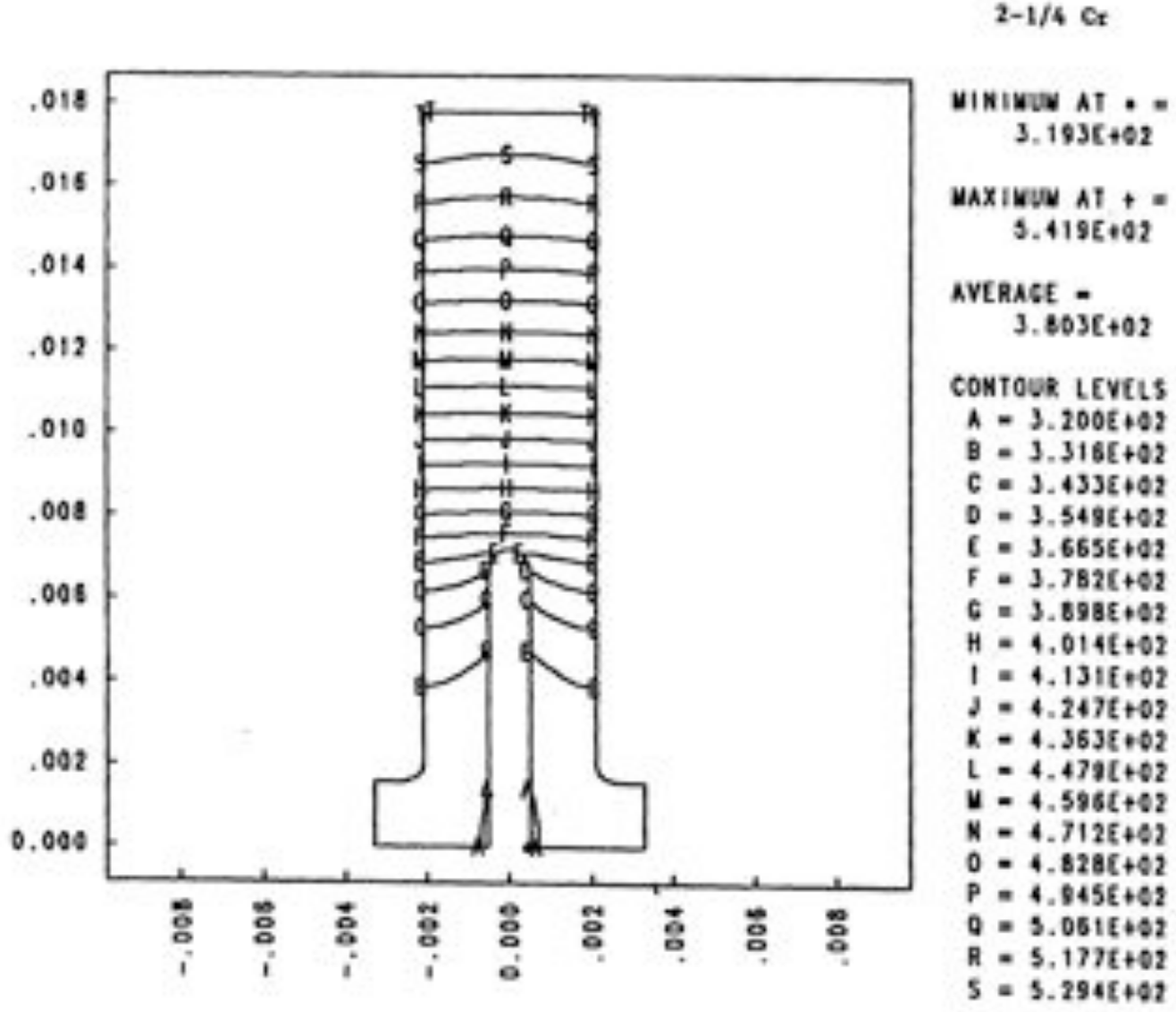

Figure III.D.2 Bellows First Wall Temperature Countours (C) at BOL for 2-1/4 Cr - 1 Mo

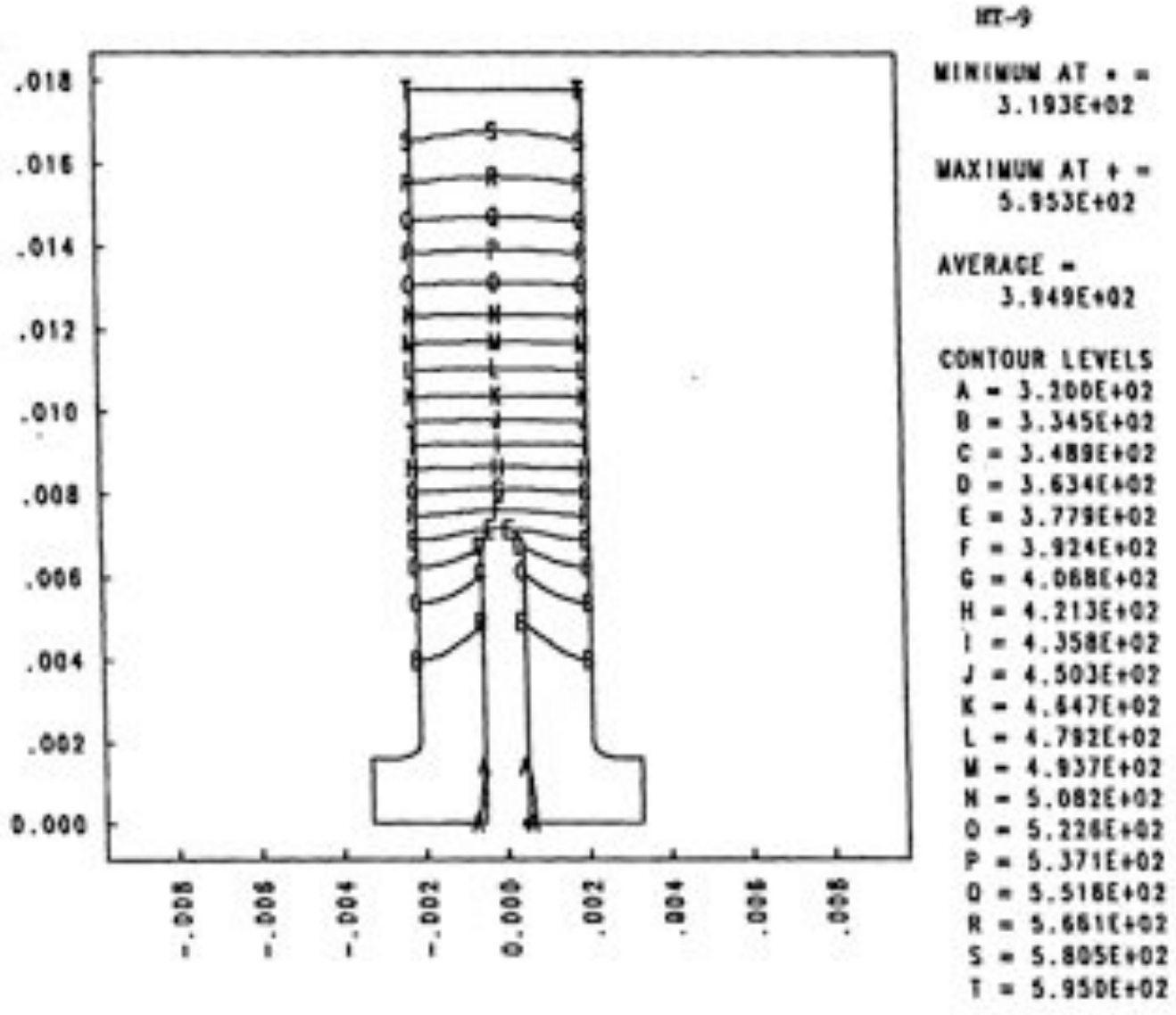

Figure III.D.3 Bellows First Wall Temperature Countours (C) at BOL for HT-9

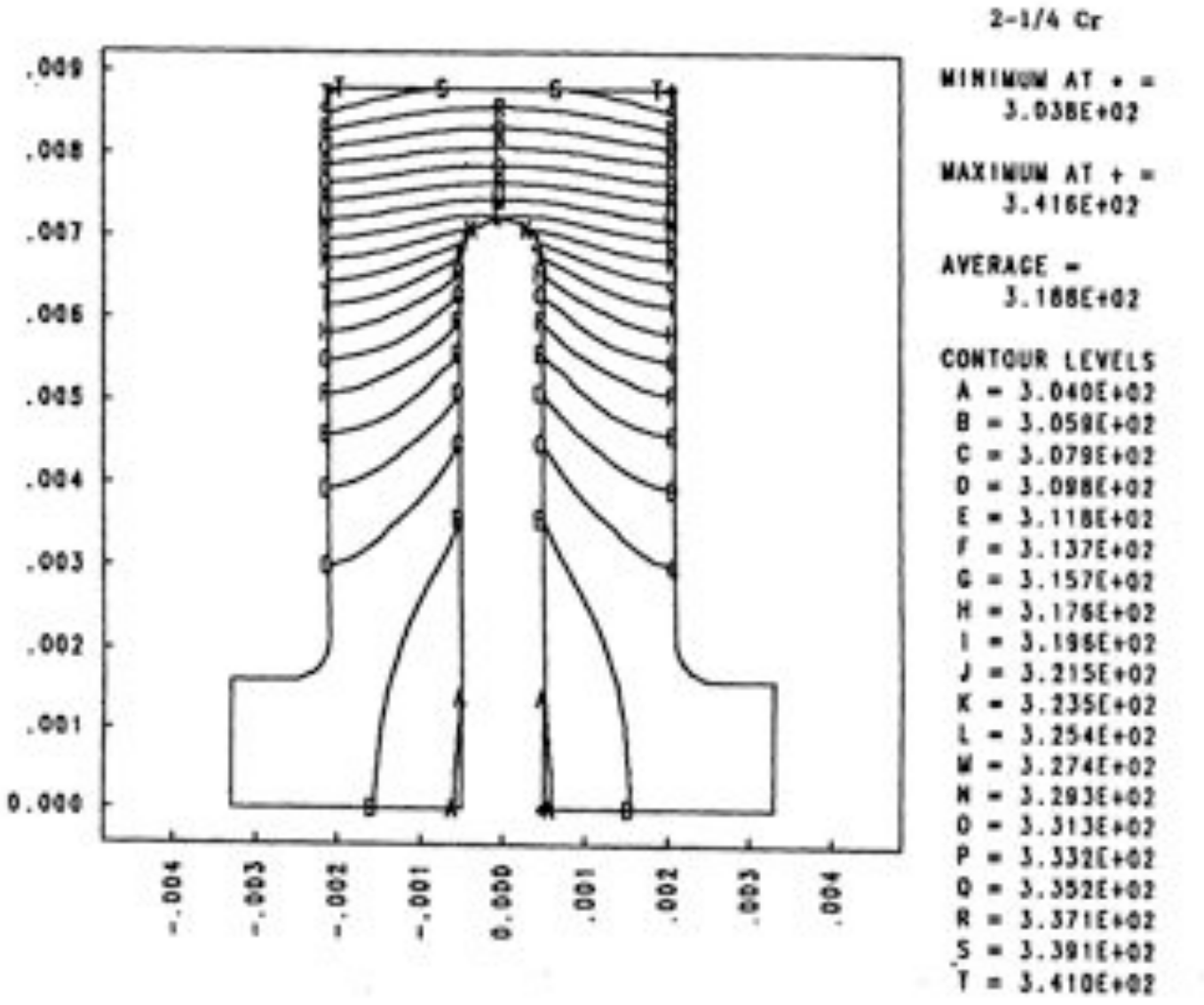

Figure III.D.4 Bellows First Wall Temperature Contours (C) at EOL for 2-1/4 Cr - 1 Mo

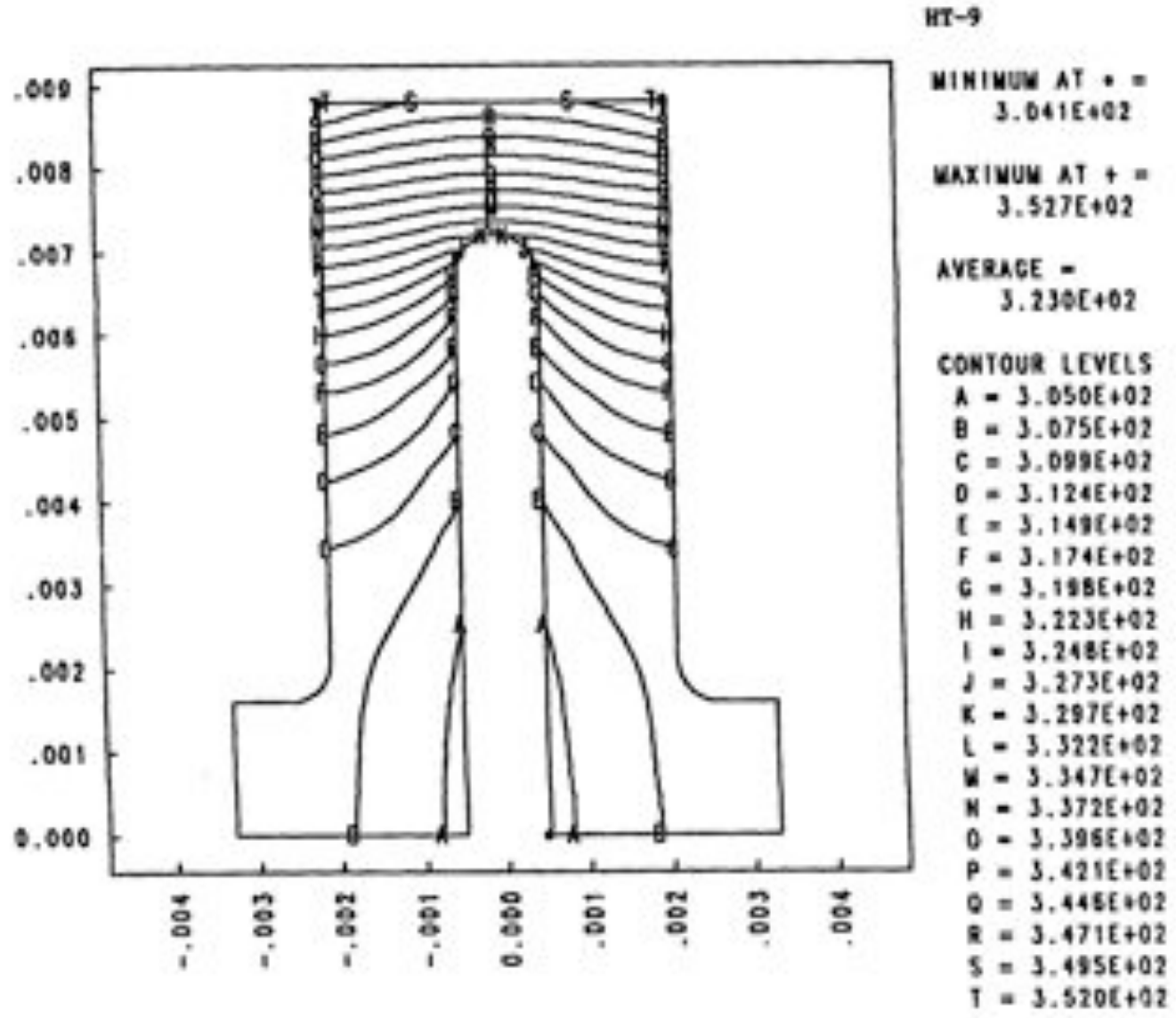

Figure III.D.5 Bellows First Wall Temperature Contours (C) at EOL for HT-9

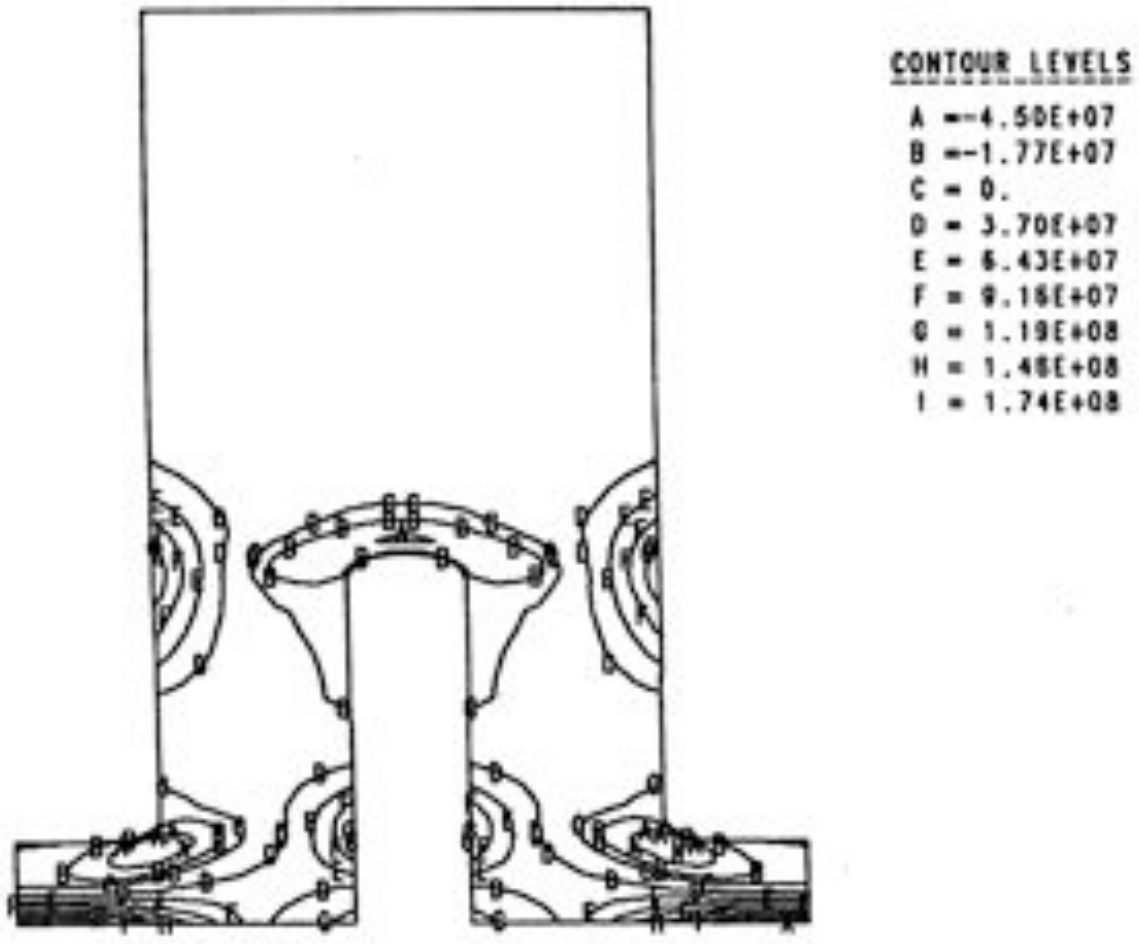

Figure III.0.6 Uneroded Bellows First Wall Thermal and Pressure Stress Contours of Maximum Principal Stress at BOL (not to scale) for 2-1/4 Cr - 1 Mo

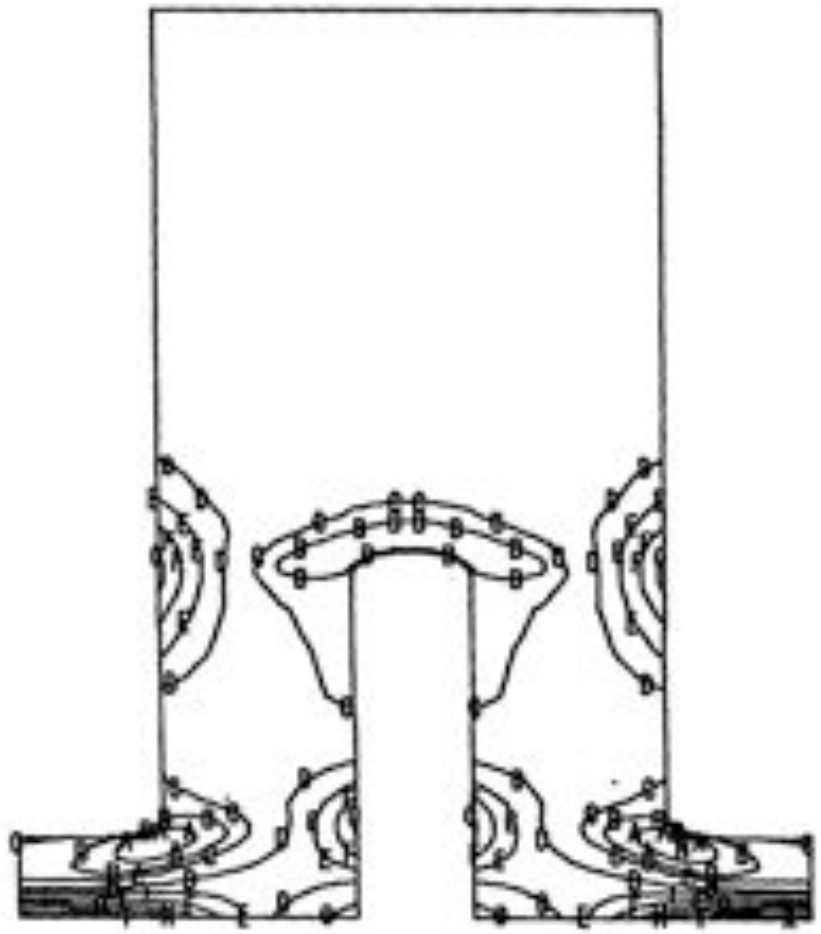

Figure III.D.7 Uneroded Bellows First Wall Thermal and Pressure Stress Contours of Maximum Principal Stress at BOL (not to scale) for HT-9

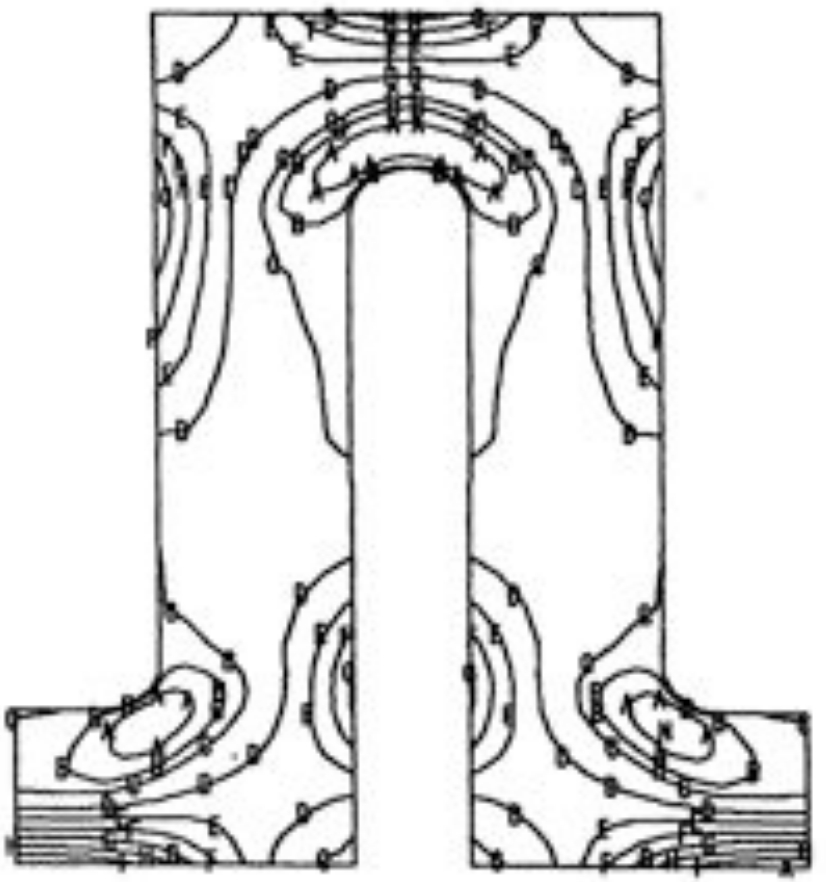

Figure III.D.8 Uneroded Bellows First Wall Thermal and Pressure Stress Contours of Maximum Principal Stress at EOL (not to scale) for 2-1/4 Cr - 1 Mo

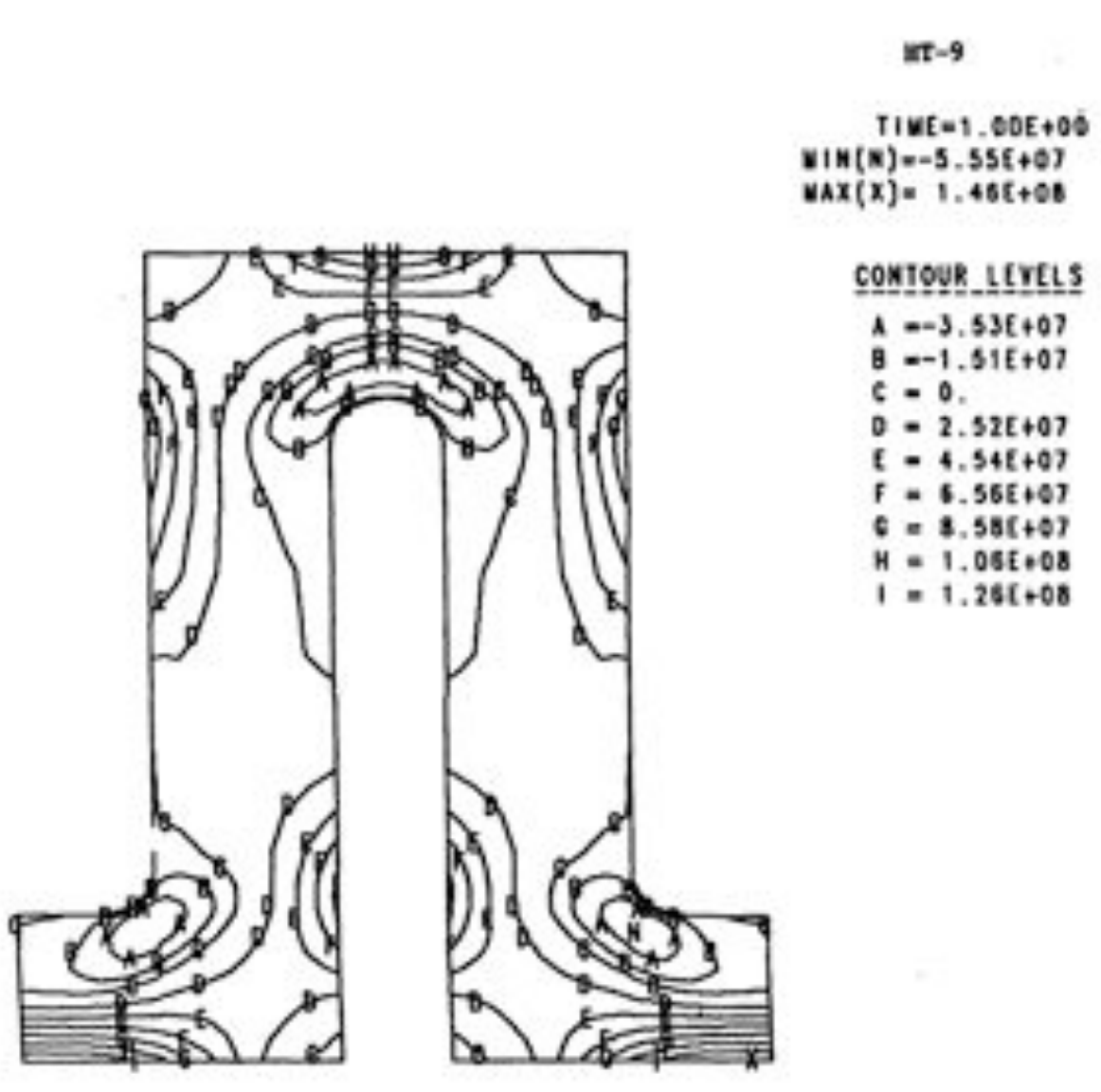

Figure III.D.9 Uneroded Bellows First Wall Thermal and Pressure Stress Contours of Maximum Principal Stress at BOL (not to scale) for HT-9

Table III.D.3 Bellows First Wall Thermal and Structural Analysis Summary

2-1/4Cr-1Mo	
Maximum temperature, (°C)	
Beginning of life	542
End of life	342
Maximum stress, (MPa)	
Beginning of life	201
End of life	176
HT-9	
Maximum temperature, (°C)	
Beginning of life	595
End of life	353
Maximum stress, (MPa)	
Beginning of life	167
End of life	146

The above calculations were performed at a neutron and surface loading of 3 and 0.25 MW/m^2, respectively. Figure III.D.10 shows the estimate T_{max} at the beginning-of-life as a function of surface loading, for 2-1/4 Cr - 1 Mo and HT-9 materials based on one-dimensional calculations and adjusted to coordinate with the two-dimensional results. It can be noted that by assuming a maximum allowable temperature of 700°C on the eroded layer where the stress capability requirement is minimum, the 2-1/4 Cr - 1 Mo and HT-9 materials can withstand surface loadings of higher than 0.6 and 0.45 MW/m^2, respectively.* Figures III.D.4 and III.D.5 illustrate that at the end-of-life, the first wall maximum temperatures for 2-1/4 Cr - 1 Mo and HT-9 materials are acceptable at a surface loading of 0.25 MW/m^2. In this comparison, the 2-1/4 Cr - 1 Mo is capable of withstanding a higher surface heat flux because of its high thermal conductivity.

III.D.3.c General First Wall Design Observations

In considering any tokamak first wall design, it should be appreciated that thermal expansion will result in large thermal stresses if the first wall is constrained. A key motivation for the proposed bellows/lobed first wall design is an ability to accommodate thermal expansion in several directions; thus greatly limiting the thermal stress. The analysis above presents a fairly mature iteration in which two-dimensional models indicate that the hottest material clearly can have very low stress levels. This feature is considered to be of major importance in this design and can probably be of use in many other blanket design concepts. The major thermal effect is to tend to cause shortening of the lobe radius, particularly at the point nearest the plasma. In the simple semi-cylindrical design this can give rise to considerable stresses. However, by changing the lobe shape from a simple radius to some other shape (for just a few millimeters at variance from a radius), it is possible to arrange moments which exactly counter those generated by the temperature effects. In this manner, it appears possible to develop a working situation where, for practical purposes, very low thermal stresses exist. This design solution can also be interpreted as preloading of the first wall. Indeed, if the simple cylindrical wall were left in this temperature/pressure

---

* A 0.43 MW/m^2 surface heat flux was selected in the final iteration. (see Section II.C)

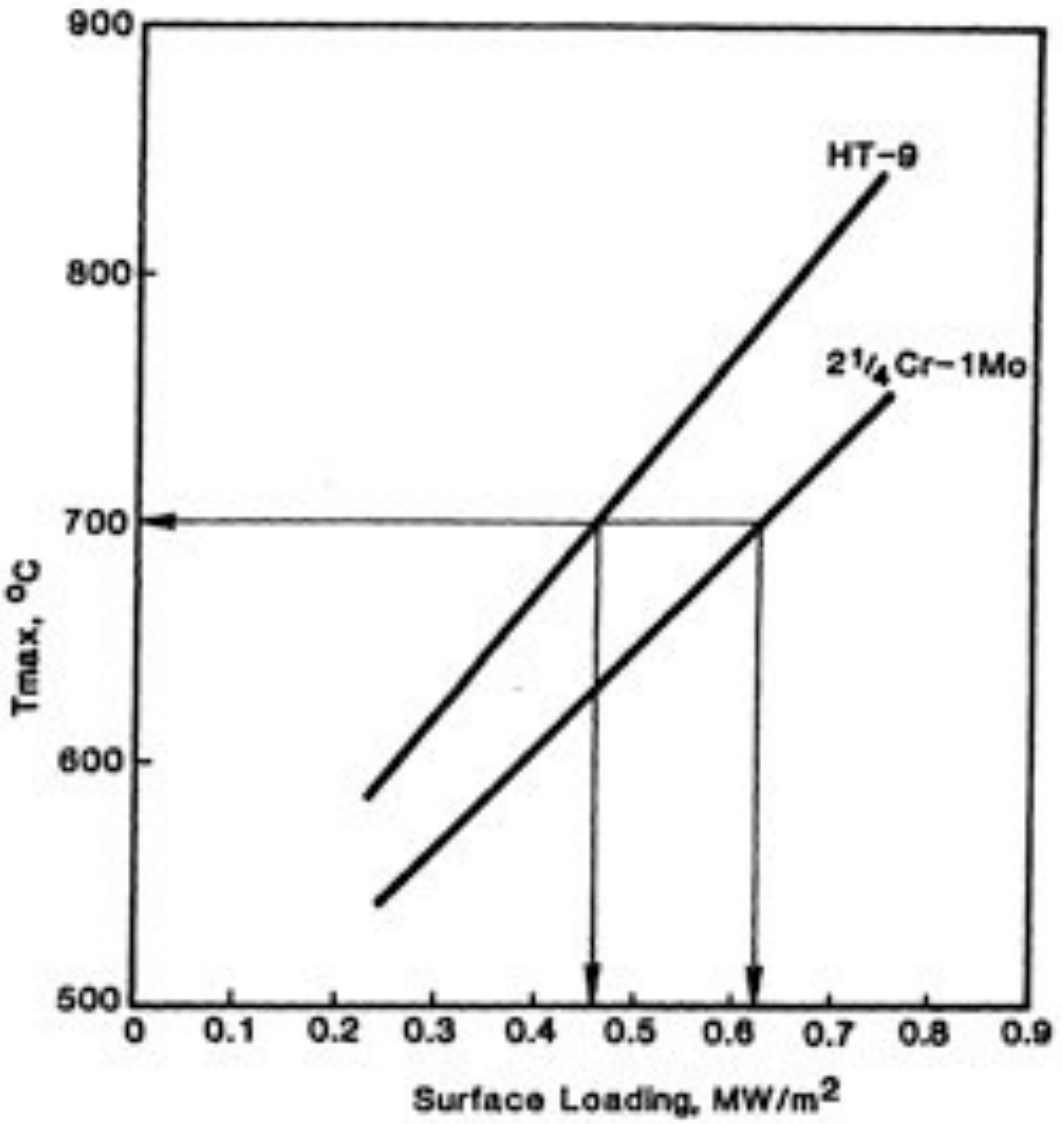

Figure III.D.10 Maximum First Wall Temperature as a Function of Surface Loading

condition long enough, it would creep to this equilibrium condition. However, in so doing, it would "use up" some of its allowed creep limit.

Irradiation swelling stress in the direction perpendicular to the corrugation can be fairly easily controlled assuming pessimistically that no creep occurs. It is considered that irradiation swelling stress should in any case be minimized so as not to deplete the creep budget (as in the thermal case). Swelling stresses in the direction parallel to the corrugation are more difficult to handle, although they can in some measure be dealt with as is the thermal stress in this direction.

Some further observations on the proposed design can be made. First, regarding the irradiation-induced dimensional changes under stress (i.e., irradiation creep), it is essential to know whether this is damaging. Present theories indicate that it may not be damaging, but that on cessation of the irradiation, the material will be hardened. It is then appropriate to ask if, in this state, do hardness and brittleness arrive together? If so, if the irradiation is stopped, restarting may require very low subsequent strains due to a low secondary creep capability. These questions need resolutions.

A final observation on the corrugated wall concerns its "fragile" form. Clearly, it is not a simple "boiler plate" specimen. Considering its design requirements, it is inevitable that it be of complex form. A similarly complex heat transfer component, the automotive radiator disperses surface heat loads of approximately 1 MW/m^2, and is constructed commonly of 0.1 mm material.

III.D.4 Blanket Fuel Element Design

Heat transfer and fluid dynamics calculations were performed for the packed bed of beryllium pebbles and Li_2O tubes. This analysis was used to determine the feasibility of the proposed configuration in satisfying materials temperature, coolant pressure drop, and mechanical design limits.

Since a heat transfer correlation for a packed bed mixture of spherical pebbles and tubes was not found, comparisons were made between the heat

transfer coefficients for a packed bed of spheres and a one-row, closely-spaced tube configuration. The one-row tube bank was used for comparison because it gives a more conservative result than a multi-row, closely-packed tube bank. Further, its heat transfer coefficient range is closer to that for a packed bed of spheres. As shown in Fig. III.D.11, the heat transfer coefficients for single row tubes and packed beds have an opposite behavior as a function of characteristic dimensions. This is because of the selected models. For the single row tube case, the distance between tubes was selected at 1 mm. To simulate the packing condition of the tube and the spheres, the 1 mm gap was selected as the reasonable minimum gap that can be maintained by wire-wrap, closed-pack tubes. As the tube size increases with a constant flow cross-section, the flow opening area reduces, thus enhancing the heat transfer. For the packed-bed configuration, the void fraction of the bed is independent of the sphere size and the heat transfer is only a function of the characteristic dimension, leading to a decrease in heat transfer coefficient as the ball diameter increases. The observation from Fig. III.D.11 is that for sphere and tube sizes in the range of 2 to 3 cm, the heat transfer coefficient is in the range of 1900 to 2600 W/m^2-K. More detailed investigation of the applicable heat transfer coefficient for the Li_2O tubes imbedded in a packed bed of balls will need to be determined by further analyses and/or experiments.

Based on the one-row tube model, the Li_2O temperature distribution as a function of radial position is given in Fig. III.D.12. The input parameters are given in Table III.D.4. It can be noted in Fig. III.D.12 that, for the selected tube size of 2 cm, the Li_2O breeder satisfies the design temperature limits. The 2-1/4 Cr - 1 Mo tube temperature is higher than the design limit of 475°C, yet this occurs only at the back of the blanket where the tube wall thickness can be increased without excessive penalty to reduce the stress. Also, the Li_2O tube does not have to have structural function, except carrying the weight of Li_2O. Consequently, a maximum steel temperature of 510°C is acceptable.

Figure III.D.13 shows the centerline temperature of the beryllium pebble and the ΔT through the pebble as a function of blanket radial position. To

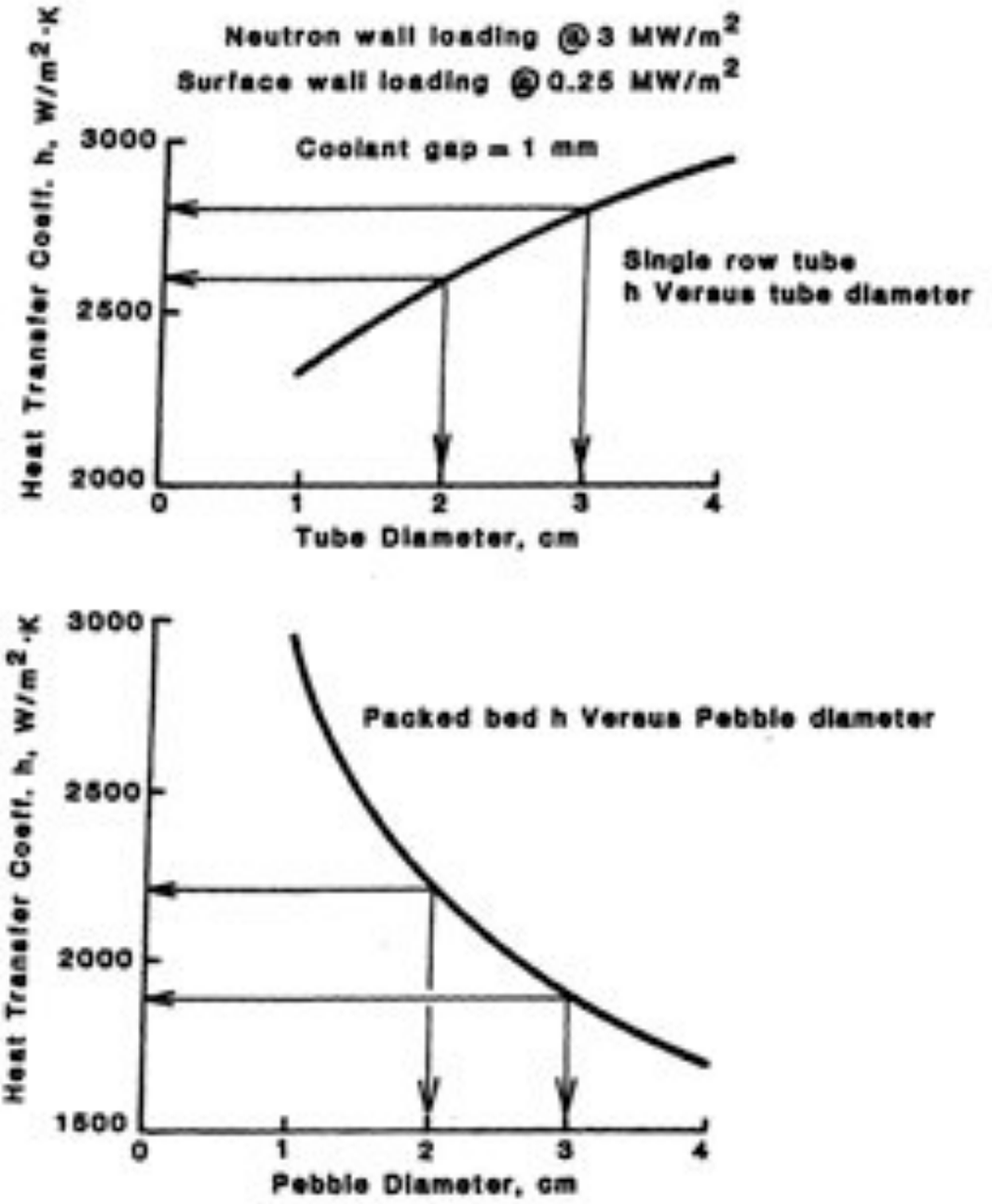

Figure III.D.11 Heat Transfer Coefficient, h, as a Function of Characteristic Dimensions.

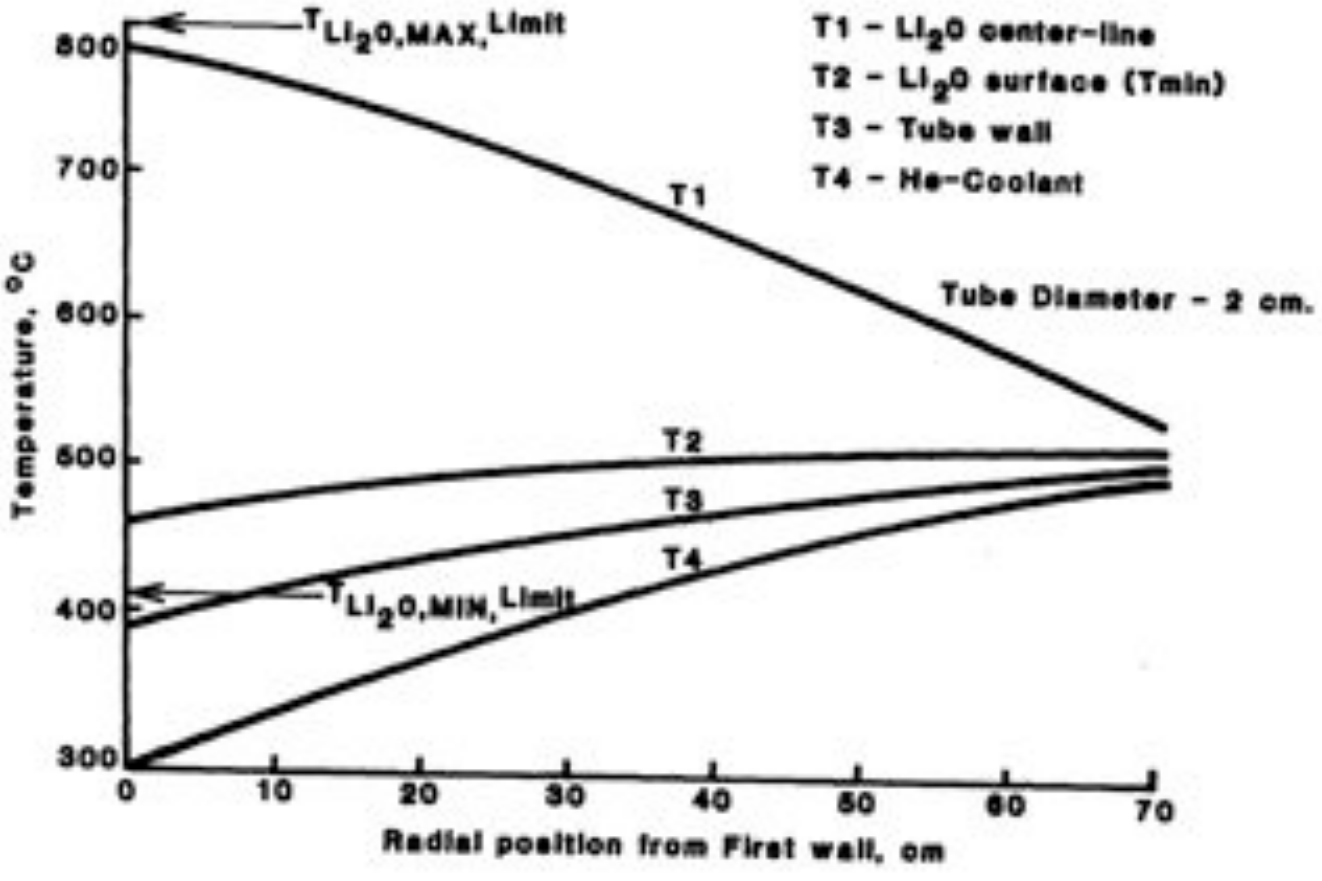

Figure III.D.12 Li_2O Tube Temperature Distribution

Table III.0.4 Fission-Suppressed Helium-Cooled Blanket Thermal-Hydraulics Input Parameters

Neutron wall loading	3 MW/m^2
Surface loading	0.25 MW/m^2
Coolant - helium at 50 atm	
T_{in}	275°C
T_{out}	500°C
$T_{coolant}$ at first wall	297°C
Blanket energy multiplication	2.175
Tube diameter	2 cm
Be/Th ball diameter	2 cm
Li_2O temperature limits, T_{max}/T_{min}	800°/410°C
Heat transfer models:	
One row closed-packed tubes	
Packed-bed ball configuration	
Neutronics inputs supplied by LLNL	

bracket the temperature range, two temperatures were calculated using a one-dimensional model by considering (1) the power density generated from the beryllium pebble only, and (2) from an averaged power density generated from the beryllium pebble and thorium metal snap-ring. The figure shows that the maximum temperature and ΔTs are acceptable as compared to those for the 3 cm beryllium pebbles for the original reference mirror design[3]. The original reference design featured thorium pins on the inside. Despite the higher power density (3 vs 1.3 MW/m^2), the newer snap-ring design is expected to provide a lower ΔT. Confirmation of the temperature and stress distribution via a two-dimensional thermal-mechanical analysis will be needed in the future.

The packed bed pumping power fraction was calculated to be 0.15% of the reactor thermal power, which is acceptable.

III.D.5 Coolant Pressure Drops and Pumping Power

Calculations were performed to estimate the total pressure drop of the whole blanket cooling circuit including the steam generators for a 5000 MW_{th} reactor with a blanket energy multiplication of two. The pressure losses due to friction, acceleration of flow from density change as a function of temperature, joints, turns, expansions, and contractions are all taken into consideration. Table III.D.5 summarizes the friction pressure drop from different blanket sections. It can be noted that the packed bed pressure drop is about 12% of the total blanket section pressure drop. Since the packed bed pressure drop is approximately proportional inversely to the square of the pebble size, care should be exercised in selecting pebbles of smaller sizes.

The total pressure drops in the blanket and in the primary coolant are given in Table III.D.6. Both $\Delta P/P$ = 3.22% and pumping power fraction of 4% are within the respective design limits of 4.3% and 6% stated in Section III.D.2. The net blanket power conversion efficiency is 36.5%.

Table III.D.5 Friction Pressure Drop for The Different Blanket Sections

Section	Flow Velocity V (m/s)	Pressure Drop ΔP (kPa)
1. Inlet manifold	57.4	2.90
2. Distribution channel	39.6	0.94
3. Side flow path	17.2	1.00
4. Grooved first wall	68.0	19.00
5. Breeder packed bed	2.0	4.40
6. Collection channel	44.4	4.32
7. Outlet manifold	65.0	3.00
Total		35.56

Table III.D.6 Total Pressure Drop in the Blanket

Pressure Drop		ΔP (kPa)	ΔP/P (%)
Friction		35.6	0.71
Turning, joining, and dividing		47.2	0.94
Expansion/contraction		13.7	0.27
Total		96.5	1.92
Total Pressure Drop in the Primary Coolant Loop			
Blanket		96.5	1.92
Sector lines,	24.4		
Ring ducts,	4.7		
Steam generator piping,	7.8		
Steam generator,	30.0		
Subtotal		66.9	1.30
Total		163.4	3.22

Total pumping power fraction
= loop pumping power/reactor thermal power × 100%
= 4%

III.D.6 Conclusions

A bellows first wall design was selected and evaluated for the FBP helium-cooled blanket design. It was designed to meet the requirements of withstanding design pressure, removing the high surface heat flux, allowing first wall erosion and handling of the potentially serious problem of neutron-induced material swelling. The structural temperature limit of 2-1/2 Cr - 1 Mo is 475°C, that of HT-9 is 550°C. With the allowable T_{max} in the non-structural erodable layer selected at 700°C and at a neutron wall loading of 3 MW/m^2, 2-1/4 Cr - 1 Mo can withstand a surface loading of 0.6 MW/m^2 as compared to 0.45 MW/m^2 for HT-9 structure.* This is due to the higher thermal conductivity of 2-1/4 Cr - 1 Mo. If the structural swelling effect were shown to be relieved by irradiation creep, then the first wall would not need to be in a bellows configuration. However, the finned geometry for high heat flux removal and the added layer for erosion allowance would still be needed in the generic design of a tokamak reactor first wall.

The blanket fuel configuration consists of cylindrical tritium breeder-filled tubes within a packed bed of beryllium balls. Each ball has a thorium snap ring around it. This configuration meets all of the thermal-hydraulic design limits. Assuming the selection of Li_2O as the breeder, the design can satisfy the difficult temperature limits throughout the blanket. The beryllium-ball centerline temperatures are acceptable and the ΔTs through the ball look reasonable. Two-dimensional thermal-mechanical calculation of the temperatures and thermally-induced radiation swelling stress is needed to confirm the design. The overall pumping power fraction of 4% for the whole coolant loop is reasonable. For the selected coolant inlet/outlet temperatures of 275°C/500°C, the power conversion gross efficiency is 39.1% and the net blanket power conversion efficiency is 36.5%.

---

* A surface heat flux of 0.43 MW/m^2 and 2-1/4 Cr-1Mo are the baseline values.

References, Section III.D

1. "Blanket Comparison and Selection Study," Argonne National Laboratory, ANL/FPP-83-1, October 1983.
2. S. Murty, "Engineering Computations at the National Magnetic Fusion Energy Computer Center," Nuclear Technology/Fusion, Vol. 4, Number 1, July 1983.
3. D. H. Berwald et al., "Fission-Suppressed Hybrid Reactor - The Fusion Breeder," Lawrence Livermore Laboratory Report, UCID-19638, December 1982.

III.E REACTOR SAFETY ISSUES

The primary safety concern of fissile-fuel producing blankets is the potential hazard associated with the release of the actinide, fission product, and activation product radioactivity. This radioactivity, produced by fissioning and parasitic captures of neutrons in the fertile and fissile materials and metallic structures, could be mobilized during postulated events which involve the large quantities of stored energy present in the system. The postulated events and sources of stored energy in the present design are briefly discussed below and are compared with those of the 1982 tandem mirror reference design[1]. The later design was subject to more detailed safety systems studies during 1983[2]. The issues of tritium safety, though requiring appropriate design attention in order to minimize routine occupational hazard, pose a relatively lower level of risk during major events and are not discussed here. Criticality is also not expected to present a safety hazard in the present design due to the low fissile concentration.

The major source of stored energy for radioactivity mobilization in the present system is the heat generated by the decay of radionuclides in the blanket. The initiating events of major consequence are those that lead to a loss of cooling capability. The major differences between the reference liquid lithium cooled tandem mirror fusion breeder[1] and the tokamak fusion breeder design are the absence of stored chemical energy from lithium reactivity, the much higher wall loading (3 versus 1.3 MW/m^2 in the reference blanket), and effects due to using a helium rather than lithium coolant (e.g., less conductive heat removal in a loss of coolant flow event, easier fuel dump, and different accident initiators). Importantly, the decay heat removal load per unit wall area will increase due to the higher wall loading, but it is expected that coolant flow can be maintained at reduced pressure in all cases with redundant helium circulators.

The maximum radionuclide hazard inventory (at time of fuel discharge) is not expected to differ substantially between the tokamak and reference tandem

mirror reactors - a result of the opposing effects of higher wall loading versus the compactness of the tokamak design. Specifically, the major contributions to the radioactive inventory per unit volume are the actinides. These reach equilibrium in roughly 60 days and their respective concentrations are proportional to the wall loading, [which is 2.4 times higher in the tokamak (3 MW/m^2)]. Despite the higher concentrations, characteristic tokamak material volumes are one-third to one-half those of the tandem mirror. Thus, the net difference in total inventory is not expected to be significant. As the enrichment is roughly proportional to the total fluence per unit volume, the irradiation time to a given enrichment is shorter at the higher wall loading tokamak. Both reactors would have comparable fissile discharge rates.

The factor of four to five lower number of modules (or sectors) in a tokamak results in a higher radioactive inventory per module. Thus, individual module failures could have correspondingly higher consequences, and heat removal systems would face higher heat loads. Other factors are the higher complexity of the tokamak and the decrease in the fuel ball adiabatic melt time and thus the shortened time for corrective action due to the higher afterheat level.

Due to the compactness of the tokamak and the absence of liquid metal MHD effects, gravity dump of the mobile fuel to a dump tank beneath the reactor is possible at a reasonable distance (~7 m) without forced flow. Heat-actuated valves in conjunction with a purely gravitational dump would provide a totally passive dump system. If a suitable nonreactive thermal contact medium within the dump tank could be identified, passive cooling may be possible in conjunction with heat pipes and convective air heat exchangers, but thermal shock to the dumped fuel could be a concern.

References, Section III.E

1. J. D. Lee et al., "Feasibility Study of a Fission-Suppressed Tandem-Mirror Hybrid Reactor," Lawrence Livermore National Laboratory Report, UCID-19327, April 1982.
2. D. H. Berwald et al., "Fission Suppressed Hybrid Reactor - The Fusion Breeder," Lawrence Livermore National Laboratory Report UCID-19638, December 1983.

III.F FUEL CYCLE AND PLANT ECONOMICS

III.F.1 Overview

In this section, the overall performance and costs of a helium cooled, beryllium blanket tokamak fusion breeder reactor are developed and combined with similar data for ^{233}U burning LWR fission reactors to obtain an estimate of the costs of electricity and bred fuel for a symbiotic electricity generation system consising of the fusion breeder, its LWR clients, and the associated fuel cycle facilities. The results are compared with economics results for LWRs of the same design which are fueled using conventionally mined and enriched uranium. All LWRs are assumed to benefit from the full recycle of all fissile uranium and plutonium isotopes (i.e., fuel reprocessing is assumed to be available and economically advantageous). The results for the tokamak fusion breeder are also compared with those for a reference case, the liquid lithium cooled tandem mirror fusion breeder design of 1982 (1).

Four tokamak cases are developed which investigate the impact of two particularly relevant issues: 1) tokamak plasma current drive and 2) breeder ownership. The current drive options are steady-state current drive by neutral beams or long pulse inductive current drive using the central solenoid coil. Both government and utility ownership are considered.

III.F.2 Discussion of Symbiotic Economics

Since the fusion breeder produces two principal products (fissile fuel and electricity), a method of economic assessment which equitably balances the cost of producing each must be established. The conceptual basis for one such method is shown in Figure III.F.1. Specifically, if an imaginary line is drawn enclosing the fusion breeder, its LWR clients (enough of them to consume all of the bred fuel), and the associated fuel cycle facilities, it is possible to construct an electricity generation system which has no net fissile fuel production or consumption and which produces only one net product--electricity. Knowing the annual capital, operating, and fuel cycle costs for both the breeder and its LWR clients, a consistent unit cost of bred fissile fuel in any given year of operation can be estimated by subtracting

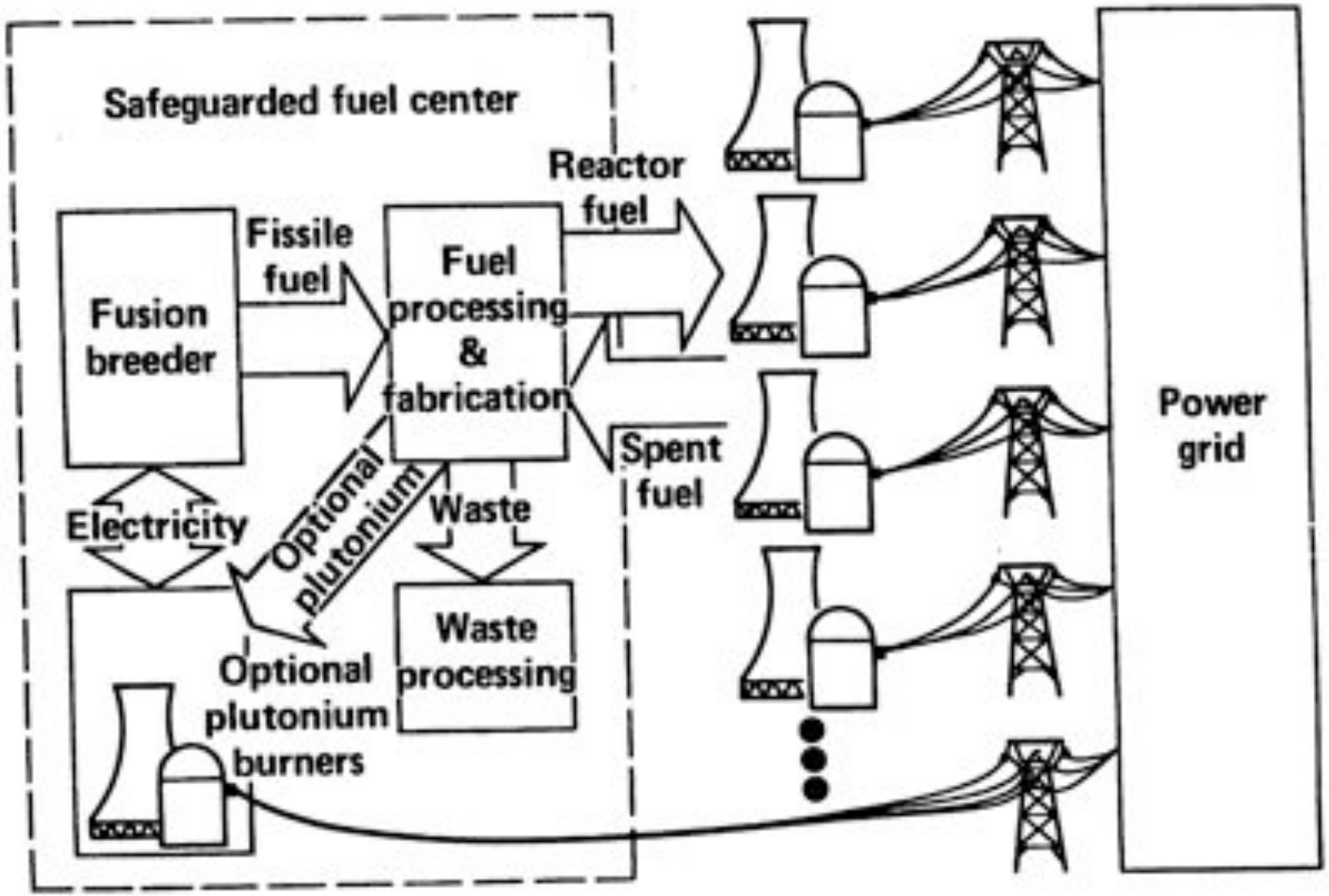

Figure III.F.1. A Fusion-Fission Electricity Generation System Would Have One Net Product - Electricity.

the electricity production revenue of the breeder (as derived above) from its overall annual operating cost (including all components) and dividing by the net fissile fuel production. It can be shown that LWRs consuming fuel at this cost will produce electricity at the same cost as the fusion breeder.

A detailed description of the methods of economic analysis used in developing the above cost estimates is beyond the scope of this section, but is provided in Reference 1. A list of the general financial input data used in this analysis is presented in Table III.F.1. Note that the economics analysis is performed over a 30-year fusion breeder plant lifetime with the appropriate consideration of inflation and escalating direct costs (both assumed to be 5%/yr over the plant lifetime).

For fusion breeder, government ownership may be the more likely option for several reasons. First, fusion breeders are, effectively, a fissile enrichment technology which (with fuel reprocessing) would eventually replace existing and advanced fissile enrichment technologies as conventional uranium resources become scarce and expensive. Enrichment facilities have historically been government owned and have been operated under government contract.

Second, to achieve economics of scale, fusion breeders will be large and expensive. Since one fusion breeder will serve 12-20 LWRs of equivalent thermal power, it is likely that most utilities would prefer to look to the federal government as a dependable provider of fissile fuel.

Third, by controlling the production and processing of fissile fuel, the government can best implement a system of technical and institutional safegards to prevent the illicit diversion of fissile materials. If the bred fuel is ^{233}U (the preferred option) a diversion resistant product can be provided to LWR operators by denaturing the ^{233}U with ^{238}U and/or spiking, etc. The small quantities of plutonium which would be produced from LWR neutron capture in the ^{238}U could be designated for consuption at an "approved" LWR site, burned in LWRs co-located within the safegarded fuel cycle center (as shown in Figure III.F.1), or disposed.

Referring to the table, note that plant construction periods of 10 years are assumed in all cases. For government financing, 100% debt financing at 3% above the inflation rate (i.e., 1.06 x 1.03 = 1.082) is assumed. In this

case, no federal, state, local taxes, insurance, or miscellaneous costs are applied.' The resulting net total fixed charge rate of 9.05%/yr is 6%/yr lower than the 15.05%/yr cost of money for a utility. Consequently, the economics for government ownership will result in a marked advantage relative to those for utility ownership of the fusion breeder. In all cases the client LWRs are assumed to be utility owned and operated.

Table III.F.1. General Financial Input Data.

	Utility Owned Breeder	Gov't Owned Breeder	Utility Owned LWR
Plant Construction Period (yrs)	10	Same	Same
Plant Lifetime (yrs)	30	Same	Same
Inflation Rate (%/yr)	5	Same	Same
General Escalation Rate (%/yr)	5	Same	Same
Debt Finance Fraction (%)	55	100	55
Return on Debt (%/yr)	8.2	Same	Same
Equity Finance Fraction (%)	45	---	45
Return on Equity (%/yr)	10.25	---	10.25
Net Discount Rate (%/yr)	9.12	8.2	9.12
Income Tax Rate on Equity (%)	50	---	50
Property Tax Rate (%)	1.45	0	1.45
Annual Depreciation (%/yr)	3.3	---	3.3
Misc. Fixed Charge and Insurance Rate (%)	0.25	0	0.25
Decommissioning Cost (% of original)	5	Same	Same
Net Total Fixed Charge Rate (%/yr)	15.05	9.05	15.05
Fixed Charge Rate on Fissile Inventory (%/yr)	7.9	3.0	7.9
Net Operation and Maintenance Cost (%/yr)	1.8	Same	Same

III.F.3 Economics for Conventionally Fueled LWR

Prior to presenting the results for symbiotic electricity generation systems, it is of interest to develop a consistent electricity cost estimate for an alternative LWR fueled by conventional uranium with full fissile

recycle and reprocessing. An understanding of the cost of electricity for the above option will provide a means to better understand the potential economic viability of a fusion breeder.

As shown in Table III.F.2, it is assumed that the LWR capital cost in 1983 dollars is 490 $/kW$_t$ (or 1.45 B/GW_e$). This value, used throughout the analysis, anticipates a stable nuclear economy and is consistent with long term planning assumptions rather than recent experience.* The fuel cycle costs shown in the table were taken from Reference 1, but were originally adapted from the results of the NASAP study (2). The U_3O_8 escalation rate of 7.1%/yr (2%/yr above general inflation) is used to reflect the expectation of an increasing mined uranium price over the 30-year life of an alternatively fueled LWR which operates during the time frame of conventional uranium depletion (e.g., beginning in the year 2020) and which is not fueled by the fusion breeder.** Specifically, the U_3O_8 price is assumed to be 55 $/kg (25 $/lb) in the first year of operation, 59 $/kg in the second, and 402 $/kg in the thirtieth year. However, accounting for the 5%/yr inflation rate, the year one worth (i.e., 1983 dollar value) of 402 dollars in year 30 is only $402/(1.05)^{29}$ = $98, indicating a 75% uranium price increase in constant 1983 dollars over 30 years. The average price of U_3O_8 during this period is 76$/kg in 1983 dollars.

The results shown in Table III.F.2 indicate that the U_3O_8 fueled LWR would produce electricity for 47.3 mil/kW$_e$H during its first year of operation. The average present value cost of electricity over the 30-year operating life, 31.0 mil/kW$_e$H, is lower than the year one value because the annual cost of electricity from the LWR increases less quickly than general inflation. The latter behavior is a well known feature of all capital intensive power production options--they are expensive to build, but are expected to payoff in later years due to low operating costs.

---

* The impact of higher LWR costs would be to increase the cost of electricity, but would also tend to make the fusion breeder more attractive as a supplier of fuel.

** Note that the price of mined uranium is assumed to be greater than or equal to the production cost with the difference attributable to profits for the mine operator.

Table III.F.2. Market Penetration Analysis - Economics Results For a U_3O_8 Fueled LMR With Reprocessing (1983 $).

LMR Capital Cost ($/kW$_t$)	490
Total Fixed Charge Rate (%/yr)	15.05
Fuel Cycle	Full Recycle
^{235}U Consumption (g/kW$_t$-yr)	0.194
Average Burnup (MWD/MTHM)	30,400
Reprocessing Cost ($/kgHM)	586
Fabrication Cost ($/kgHM)	582
Enrichment Cost ($/kgHM product)	137
Transport and Disposal Cost ($/kgHM)	102
Year One Price of Purchased U_3O_8 ($/kg)	55
Year One Cost of Electricity (mil/kW$_e$H)	49.7
U_3O_8 Escalation Rate (%/yr)	7.1
Average PV Cost of Electricity (mil/kW$_e$H)	32.6
Average PV Price of Purchased U_3O_8 ($/kg)	76

III.F.4 Tokamak Breeder Fuel Cycle

The helium cooled beryllium tokamak blanket was analyzed (see Section III.C) using the LLNL Monte Carlo transport code, TART (5), to predict fissile breeding and other nuclear reaction rates. The net fissile breeding rate per fusion neutron was 0.54 ^{232}Th (n,γ) and the fission rate was 0.06* ^{233}U (n,f) per fusion neutron at a ^{233}U concentration of 1.0 percent.

Based on material densities and volumes, reaction rates per atom can be calculated. These reaction rates, along with isotope decay constants, can be used to calculate the actinide buildup/decay in the thorium based tokamak breeder fuel cycle, shown in Figure III.F.2. To first order, the fusion breeder fuel cycle can be tracked using single first order production/destruction relationships which describe:

*Adjusted upwards for resonance self-shielding effects.

- fissions and (n,γ) breeding in ^{232}Th
- beta decays in ^{233}Pa
- fissions and (n,γ) losses in ^{233}U

The concentrations of ^{233}Pa and ^{233}U together determine the total fissile inventory. The concentration of ^{233}U determines the amount of additional fissions which add to the ^{233}Th (n,f) fissions. These additional fissions cause a linear swing in blanket power generation as the concentration of ^{233}U increases. The additional activation pathways in Figure III.F.2 are primarily of interest in determining the buildup of ^{232}U and ^{228}Th, principal activation products in the thorium fuel cycle. These have been estimated in previous studies (see reference 1) and were not estimated for the tokamak breeder.

Table III.F.3 presents the key tokamak breeder fuel cycle parameters. Figure III.F.3 shows the corresponding fuel cycle availability budget for an overall plant capacity factor of 70%. The calculation of the actinide concentrations and the development of the availability budget both assume a 90% operational availability during scheduled operation. This allows as many as 12 unscheduled and 34 scheduled outage days during the 155-day fuel cycle period. Longer unscheduled shutdown periods during scheduled operation will result in significant ^{233}Pa decay ($T_{1/2}$ = 27 days) to ^{233}U followed by higher fission rate penalties when operation is resumed. That is, the thermal systems are designed for a maximum blanket energy multiplication of 2.1 and extended shutdowns during scheduled operation can result in this power level being achieved at lower than desirable fissile discharge enrichments (i.e., < 1.43%). The consequence of discharging the fissile fuel at lower enrichment would be a small, but adverse affect upon overall economics due to a significantly larger fissile recovery (reprocessing) cost.

In comparison with more detailed fuel management schemes developed for the reference tandem mirror fusion breeder (1), and summarized in Table III.F.3, the above analysis is somewhat optimistic because it assumes that the neutron flux and fissile concentrations correspond to average values over the entire blanket. In reality, fissile fuel will be bred much faster at the front of the blanket than averaged over the blanket. Also, the probability of fissioning a ^{233}U atom will be much higher near the first wall. As a result, at an end-of-cycle condition reflecting a given average discharge enrichment, the blanket energy generation will be higher than

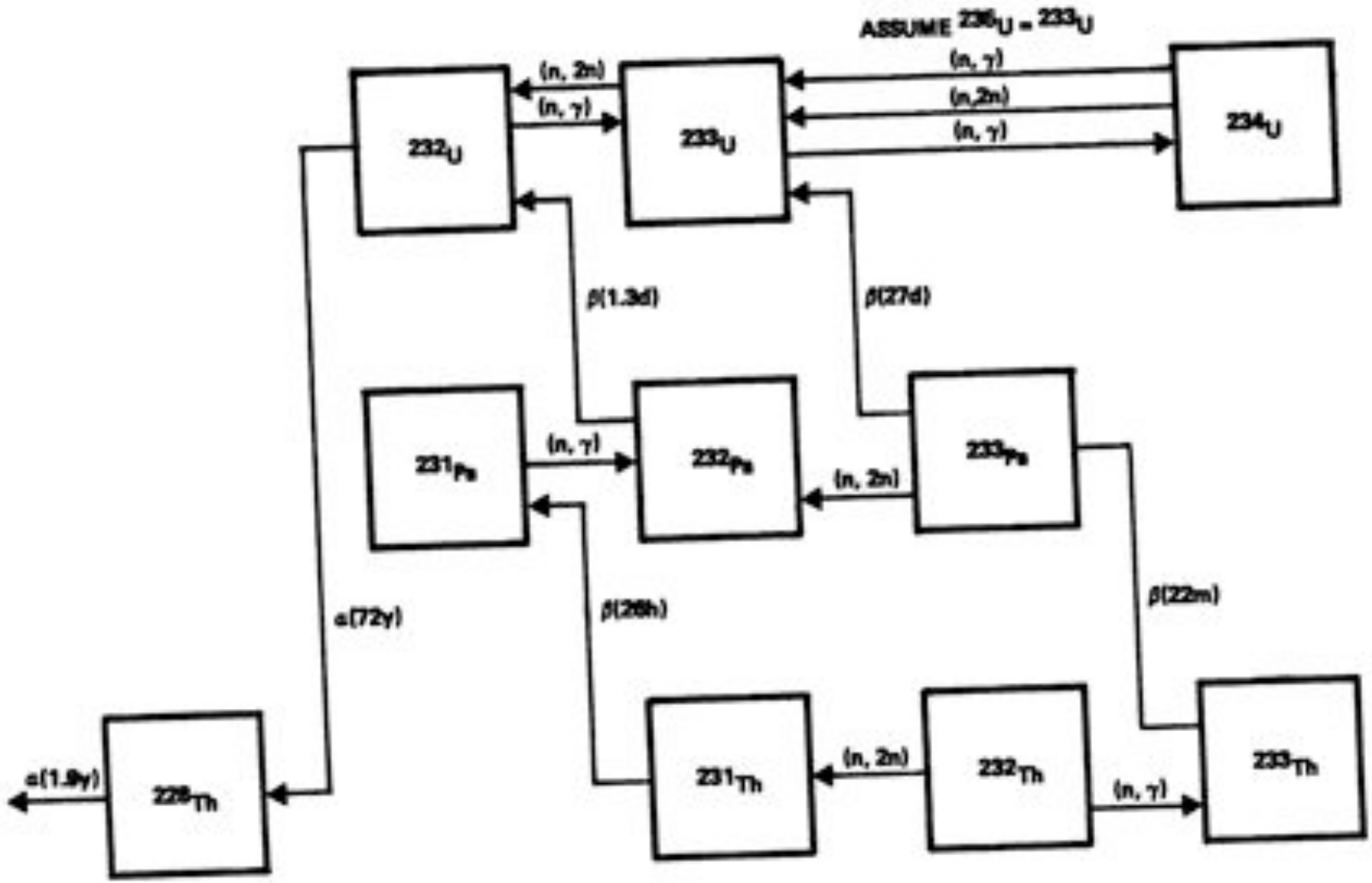

Figure III.F.2. Production and Decay Chain for Thorium Fueled Hybrid Blankets.

Table III.F.3. Summary of Breeder Fuel Cycle Characteristics.

	TOKAMAK	TANDEM MIRROR
Net Fissile Production (Kg/yr)[a]	4905	5635
Fissile Inventory (Kg)		
In-Core[a]	1535	1180
Post Discharge	2419	2815
Plant Capacity Factor (%)	70	70
Enrichment (%)[b]		
^{233}Pa	0.43	0.4
^{233}U	1.00	0.7
Total	1.43	1.1
Energy Multiplication		
BOC	1.30	1.25
EOC	2.10	2.50
AVE[a]	1.70	1.89
Full Cycle Period (days)	155	321[c]

a) average over cycle.

b) atoms per ^{232}Th atom (%).

c) 1.5 batches of fuel during this period assuming a two-zone blanket with fuel replaced twice as often in the first zone.

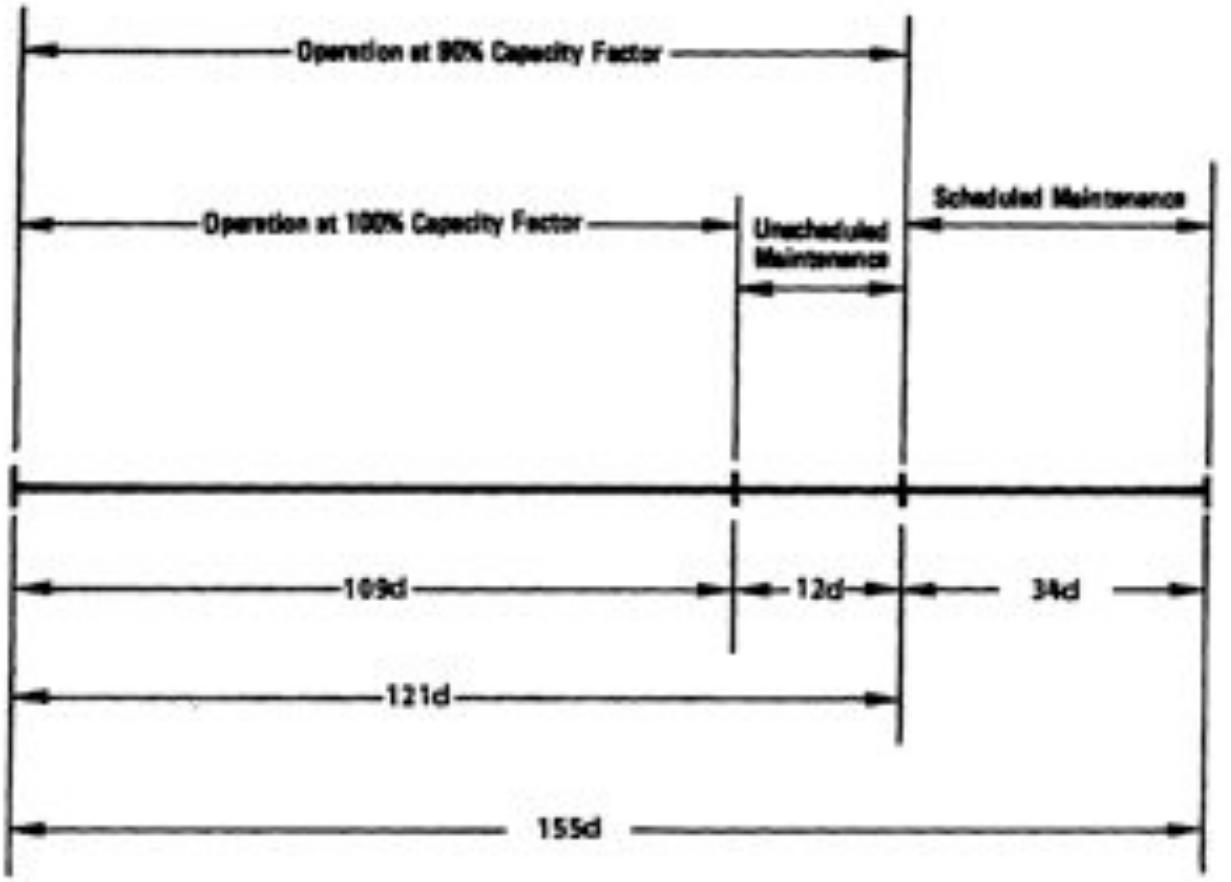

Overall Availability = 109/155 = 0.70

Figure III.F.3. Tokamak Breeder Availability Budget.

assumed in our analysis because the fissile concentration will be peaked towards the front of the blanket.

The negative impacts of this situation can be reduced, but not removed by separating the blanket into two or more radial zones (see Reference 1) and by cycling the front zone(s) more frequently than the back zone(s). This design fix will increase the average fissile discharge enrichment for a given peak blanket energy, but will result in additional mechanical complexity. More study is required in this area to determine the best compromise between fuel cycle economics and operational/mechanical complexity.

III.F.5 Fusion Breeder Performance and Cost Comparison

The performance and cost of the helium cooled, beryllium blanket tokamak breeder were modeled using TRW's Tokamak Reactor Systems Code (TRSC) (3). The results are compared with performance and cost data for the reference lithium cooled tandem mirror fusion breeder in Table III.F.4. The tokamak cases are for current drive by magnetic induction and neutral beams. The tandem mirror breeder was modeled using the Tandem Mirror Reactor Systems Code (4). Comparisons between the tandem mirror and tokamak results should be made with some reservations because 1) the two designs represent different levels of effort, and 2) the models in TRSC and TMRSC are somewhat different.

As shown in Table III.F.4, the reference tandem mirror produces the most net electricity (24% higher than the inductive current drive tokamak and 82% higher than the neutral beam driven tokamak). The inductively driven tokamak has a 47% higher (442 MW_e) net electricity production compared to the neutral beam current drive option. These results are also reflected in the net plant efficiency figures (34%, 30%, and 20%). It is clear that neutral beam driven systems will result in substantial power flow penalties.

For the inductively driven tokamak, plasma heating sytems (ECRF, ICRF, LHRF) require about 190 MW_e during plasma startup (see Chapter II). Once ignition occurs, these systems are not required since the plasma heats itself and the solenoidal coil drives the plasma current. For this particular tokamak, the plasma burntime is about 3000 seconds. The plasma and solenoidal coil reset time is assumed to be 100 seconds. As the availability can vary with solenoidal coil size, the choice of the reactor configuration was made by trading between larger reactors with higher availabilities at higher costs

Table III.F.4. Fusion Breeder Performance Comparison.

	Fusion Breeder Type		
	Reference Lithium (Tandem Mirror)	Tokamak (Inductive CD)[b]	Tokamak Neutral Beam (CD)[c]
Major radius (m)	193 (length)	6.75	7.69
Minor radius (m)	1.5 (cc radius)	1.80	1.57
Fusion power (MW)	3000	3000	3000
Pulse length (s)	ss	2700	ss
Blanket energy multiplication:			
Minimum	1.25	1.30	1.30
Maximum	2.50	2.10	2.10
Average	1.88	1.70	1.70
Gross nuclear power (MW)[a]	5100	4680	4680
Gross electric power (MW)[a]	2226	1667[f]	1850[g]
Driver recirculating power (MW)	325	6.7[f]	621
Additional recirculating power (MW)	180	275	286
Net electric power (MW)[a]	1720	1385[f]	943
Net fissile production (kg/yr)[d]	5635	4905	4905
Fissile inventory (kg)[d]	3995	3954	3954
In-core[a]	1180	1535	1535
Post discharge[e]	2815	2419	2419
Plant capacity factor (%)[a]	70.0	70.0	70.0
Plant efficiency	.34	.30[f]	.20

a) average over fuel cycle period.
b) inductive current drive.
c) neutral beam current drive.
d) includes average plant capacity factor.
e) assumed to be half-year's average production.
f) averaged over reactor operational period.
g) includes conversion of the neutral beam thermal energy deposited on the first wall.

Table III.F.5. Fusion Breeder Cost Comparison ($ Million, 1983).

	Fusion Breeder Type		
	Reference Lithium (Tandem Mirror)	Tokamak (Inductive CD)	Tokamak Neutral Beam (CD)
Land and land rights	6.3	6.3	6.3
Structures and site facilities	563	531	531
Fusion driver components[a]	863	458	1638
First wall/blanket shield[b]	499	395	423
Heat transport components[c]	502	245	258
Misc. reactor equipment	299	288	274
Turbine plant equipment	370	401	432
Electrical plant equipment	158	164	167
Misc. plant equipment	19	53	53
Fuel cycle facilities[d]	382	330	330
Direct Cost	3660	2871	4112
Contingency (20%)	732	574	822
Total Direct Cost	4392	3445	4934
Indirect cost (34%)	1485	1163	1665
Total Overnight Cost	5877	4608	6599
Cost of Interest and Escalation During Construction (17.5%)	1028	806	1155
Total Plant Cost	6905	5414	7754
Fusion Breeder Cost/LWR Cost[e]	2.76	2.36	3.38

a) includes magnets, heating systems, direct convertor.

b) includes beryllium and lithium.

c) includes circulators for helium loops.

d) includes reprocessing, beryllium fabrication, thorium fab.

e) basis: $\$/KW_t$

(reflecting increased material volumes) and smaller reactors with lower availabilities and reduced costs. The baseline inductively driven tokamak is optimized at a size slightly larger than the smallest possible machine (R_p = 6.75 m versus R_p = 6.29 m). The resulting burn cycle duty factor of 0.97 implies that the allocation for unscheduled outage must be reduced from 12 to 9 days per 121 days of operation to achieve a 70% plant capacity factor.

As shown in Table III.F.5, the cost difference between the two tokamaks is primarily caused by the high cost of the neutral beam system. The neutral beam driven tokamak is also slightly more expensive in other areas because it optimizes at a slightly larger physical size. This results because the plasma scaling relations predict a decreasing plasma current requirement as the reactor major radius increases. The optimal major radius of the 3000 MW_f neutral beam driven reactor configuration (7.69 m) represents a compromise between beam power and size. In the case of the miscellaneous reactor equipment account, the inductively driven tokamak is slightly more expensive due to various costs associated with pulsing. These include the costs of the magnet support structure, the vacuum system, and the magnet power supplies.* Overall, the direct cost of the inductively driven tokamak is estimated to be about 20% less (790 M$) than the tandem mirror and 30% less (1241 M$) than the neutral beam driven tokamak. In the latter case, the cost of the beams is the principal cost penalty.

Cost differences between the two tokamaks and the tandem mirror reflect the different nature of the two designs as well as modeling differences. A major difference arises in the fusion driver component cost category shown in more detail in Table III.F.6. Importantly, the comparatively large cost of the tandem mirror central cell magnets, first wall, blanket, and shield can be attributed to its low wall loading (1.3 MW/m^2 versus 3 MW/m^2 for the tokamak).

Heat transport system component costs are about a factor of 2 greater for the tandem mirror. This results because of the longer pipe runs and manifolding costs of the 193 m long tandem mirror. The intermediate sodium loop in the liquid metal tandem mirror heat transport system also provides a

---

* Energy storage system cost not yet included.

cost penalty. The higher electrical conversion efficiency of the liquid metal cooled tandem mirror and slightly different scaling relationships are reflected in slightly lower turbine plant equipment costs (between 8% and 14% less for the tandem mirror than the inductively driven tokamak and the neutral beam driven tokamaks, respectively). The electrical plant equipment costs are also about 5% lower for the tandem mirror due to the use of different cost factors, both proportional to the gross electric power, in the two codes. Miscellaneous plant costs also reflect different models for the tokamak and

Table III.F.6. Fusion Driver Component Costs ($ Million, 1983).

	Fusion Breeder Type		
	Reference Lithium (Tandem Mirror)	Tokamak (Inductive CD)	Tokamak Neutral Beam (CD)
Tokamak Magnets	--	355	328
TF coils	--	230	289
PF coils	--	50	37
Solenoidal coil	--	75	2
Tandem Mirror Magnets	601	--	--
Central cell	460	--	--
Barrier coil 1	40	--	--
Barrier coil 2	37	--	--
Transition coil	21	--	--
Yin-yang pair	43	--	--
RF Systems	75	103	6.3
ICRF	19	71	--
ECRF	56	6.3	6.3
LHRF	--	26	--
Neutral Beam Systems	150	--	1304
Direct Converter	36	--	--
Total Fusion Driver Components	863	458	1638

tandem mirror, whose miscellaneous costs are estimated to be small, but about 65% less than those of the tokamaks. The fuel cycle facilities for the tandem mirror are about 16% more expensive, primarily because of higher fuel throughput.

III.F.6 Economics Results For Symbiotic Electricity Generation Systems

The performance and cost results presented in the previous section were merged with similar data for LWRs and their fuel cycles to predict the symbiotic cost of electricity and the cost of bred fuel on a year-by-year and a 30-year average present value basis. The LWR fuel cycle data and economics methodology used in the analysis are described in Reference 1. The cost data has been escalated from 1982 to 1983.

Table III.F.7 shows the results of this analysis for the inductively driven tokamak breeder which supplies 19 ^{233}U burning LWRs (1 GW_e each) operating on a denatured thorium cycle (1). As shown in Table III.F.5, the breeder cost per unit thermal power is about 2.3 times the LWR cost. However, the "effective capital cost" decreases to 1.4 times the LWR cost when adjustments for government ownership of the breeder are made. As shown, this difference has only a minor impact on the cost of electricity. Because most of the electricity (~ 95%) is generated in utility owned LWRs which, dominate the symbiotic system, the symbiotic cost of electricity is always quite insensitive to perturbations in the breeder cost and/or performance.

Nevertheless, slight changes in the electricity cost represent large changes in the cost of bred fuel. This can be easily understood if one notes that at a U_3O_8 price of ~ 55$/kg, the cost of mined uranium is typically less than 10% of the life cycle cost of LWR electricity. Thus, an electricity cost increase of roughly 10% would result if the price of U_3O_8 doubled. The results shown in Table III.F.7 indicate a similar result--a 9% electricity cost differential represents a 133% ^{233}U cost differential.

In Table III.F.8, results for utility and government ownership of the neutral beam driven tokamak are presented. As expected, the cost and power flow disadvantages of the neutral beam system result in larger system electricity costs. Compared to the inductively driven tokamak, the government owned neutral beam driven tokamak produces electricity which is 14% more expensive and fissile fuel which is 200% more expensive. In the case of

Table III.F.7. Utility Versus Government Ownership Of The Inductively Driven Tokamak Breeder.

	Utility Owned	Government Owned
Total Plant Capital Cost ($M)	5414	5414
Breeder Cost/LWR Cost Ratio[a]	2.28	2.28
Total Fixed Charge Rate on Breeder Plant Capital ($/yr)	15.05	9.05
Effective Breeder Capital Cost/LWR Capital Cost Ratio	2.36	1.42
Year One Cost of Electicity (mil/kW_eH)	54.9	49.5
Average PV Cost of Electrity (mil/kW_eH)	33.4	30.6
Year One Price of ^{233}U ($/g)	96.2	36.7
Average PV Price of ^{233}U ($/g)	53.4	22.9

a) LWR cost = 490 $/$kW_t$ (1983)

Table III.F.8. Utility Versus Government Ownership Of The Neutral Beam Tokamak Breeder.

	Utility Owned	Government Owned
Total Plant Capital Cost ($M)	7754	7754
Breeder Cost/LWR Cost Ratio[a]	3.26	3.26
Total Fixed Charge Rate on Breeder Plant Capital ($/yr)	15.05	9.05
Effectjve Breeder Capital Cost/LWR Capital Cost Ratio	3.38	2.03
Year One Cost of Electicity (mil/kW_eH)	64.6	56.5
Average PV Cost of Electrity (mil/kW_eH)	38.9	34.8
Year One Cost of ^{233}U ($/g)	203	114
Average PV Cost of ^{233}U ($/g)	114	69.1

a) LWR cost = 490 $/$kW_e$ (1983).

utility ownership, the NB driven tokamak produces electricity which is 17% more expensive and fissile fuel which is 115% more expensive. Comparing government and utility ownership for the neutral beam driven tokamak, the utility owned breeder produces electricity which is 12% more expensive and fissile fuel which is 66% more expensive.

The results for the inductively driven tokamak are compared in Table III.F.9 to those for an LWR burning U_3O_8 at the current price. If the tokamak breeder is utility owned, its cost of electricity does not become equal to that of the conventionally fueled LWR until the twenty-first year of operation. The thirty year average present value of the cost of electricity is 0.77 mil/kW_eH higher than that of the U_3O_8 fueled LWR. Over a thirty year period, a cumulative loss of 4.6 $billion results. Although this case does not indicate market penetration under the very conservative conditions which were assumed (i.e., 55 $/kg U_3O_8 at the start of operation), further studies indicate a thirty-year breakeven (i.e., zero benefit) if the starting price of U_3O_8 is 91 $/kg, or about twice the current price of uranium. Higher U_3O_8 costs would lead to a net benefit for the fusion breeder.

Table III.F.9. Comparison Of a Symbiotic System Including An Inductively Driven Tokamak Fusion Breeder With a U_3O_8.

	Utility Owned	Government Owned
Delta Year One Cost of Electricity (mil/kW_eH)[a]	5.19	-0.19
Breakeven Year[b]	21	1
Delta Average PV Cost of Electricity (mil/kW_eH)[a]	0.77	-1.98
Integrated Benefit ($M)[c]	-4590	5568

a) symbiotic - conventional LWR = delta.

b) year in which delta = 0.

c) PV benefit over 30 years per fusion breeder.

In the case of government ownership, breakeven is achieved in the first year and an average 1.98 mil/kW_eH benefit accrues over the entire fusion breeder operating life. This results in an integrated benefit of 5.6 $billion over a thirty year period. If the U_3O_8 cost at the start of operation were 91 $/kg, the breakeven price for utility ownership, the integrated benefit would be dramatically increased.

A summary of results, which also provides comparisons with the conventionally fueled LWR of Section III.F.3, is shown in Table III.F.10. This table includes the inductively driven tokamaks discussed above (cases 3 and 4), two cases for the utility and government ownership of the tandem mirror lithium blanket breeder (cases 1 and 2), and two cases for the neutral beam driven tokamak breeder (cases 5 and 6). The latter machine (neutral beam driven) and its symbiotic products are expensive, whether owned by a utility or the government. Breakeven (zero net benefit over 30 years) would occur in the government ownership case at a U_3O_8 cost of 132 $/kg, which is a factor of 2.4 higher than current price of 55 $/kg.

Table III.F.10. Summary of Economic Analysis.

	Description	Average Present Value Elect. Cost (mil/KWeH)	Average Present Value ^{233}U Cost ($/g)	Breakeven Year[a]	Benefit[a] ($ B)	Breakeven U_3O_8 Price[b] ($/Kg)
1)	Mirror/Gov't	31.7	31.5	8	3.7	42
2)	Mirror/Utility	34.7	64.7	24	-8.9	116
3)	Tokamak/Gov't/Ind CD[c]	30.6	22.9	1	5.6	13
4)	Tok/Utility/Ind CD	33.4	53.4	21	-4.6	91
5)	Tok/Gov't/NB CD[d]	34.8	69.1	29	-9.5	132
6)	Tok/Utility/NB CD[d]	38.9	115	--	-24.2	250

a) nominal results assumed $55/kg ^{233}U starting price of U_3O_8 with 2%/yr escalation above inflation.

b) U_3O_8 starting price required to produce a zero net benefit over the 30 year breeder life cycle.

c) Gov't owned tokamak breeder with inductive current drive.

d) Utility owned tokamak breeder with neutral beam current drive.

The inductively driven tokamak cases are slightly improved relative to those for the tandem mirror cases, but the differences are within the modeling uncertainties. In the utility owned cases, breakeven relative to an alternatively fueled LWR (with a U_3O_8 starting price of 55 \$/kg) occurs after twenty years of operation and results in a net loss (over 30 years) of 4.6 and 8.9 \$billion, respectively. In both cases, the price of uranium must approximately double (to 91 \$/kg or 116 \$/kg) to achieve a 30 year breakeven. For government ownership of either the tokamak or the tandem mirror breeder, substantial net benefits (5.6 and 3.7 \$billion, respectively) accrue over the 30 year lifetime. The government owned tokamak breeder is predicted to break even at a U_3O_8 price as low as 13 \$/kg and the government owned tandem mirror could breakeven at U_3O_8 prices as low as 42 \$/kg.

III.F.4 Conclusions

The following conclusions result from the above modeling of the potential economic performance of the tokamak breeder:

- The tokamak breeder economics results are roughly similar to previous results for the reference tandem mirror based fusion breeder.

- Government ownership of the fusion breeders always presents substantial economic advantages and fits well into the institutional framework of a government sponsored fuel cycle center (similar to current fissile enrichment plants).

- The government owned, inductively driven, tokamak breeder could be economical at less than current U_3O_8 prices given a long term U_3O_8 price escalation rate which is 2% above inflation and a full fissile recycle nuclear economy.

- NB current drive carries a substantial economic penalty but could breakeven in a government ownership case at a market price for U_3O_8 of 132 \$/kg.

- Economic issues yet to be addressed include the potential impacts of lower LWR SWU costs, higher LWR fuel reprocessing costs, etc.

References, Section III.F

1) D. H. Berwald, et al., "Fission-Suppressed Hybrid Reactor - The Fusion Breeder," UCID-19638, Lawrence Livermore National Laboratory (1982).

2) "Non-Proliferation Alternative Systems Assessment Program," DOE/NE-0001, U.S. DOE (1980).

3) R. H. Whitley, "Tokamak Reactor Systems Code Manual," contact author at TRW, 1 Space Park, Redondo Beach, CA.

4) R. H. Whitley, "Tandem Mirror Reactor Systems Code Manual," contact author at TRW, 1 Space Park, Redondo Beach, CA.

5) J. R. Kimlinger and E. F. Plechaty, "TART Input Manual," UCID-17026 Rev. 2 (April 1, 1982).

CHAPTER IV

LITHIUM COOLED TOKAMAK HYBRID BLANKET CONCEPT

This chapter describes a lithium cooled tokamak reactor using the mobile fuel concept developed in 1982 for the reference tandem mirror fusion breeder (1) In the tokamak configuration, the magnetic fields and spatial restrictions on the inboard side lead to very high pressures when pumping a liquid metal through a packed bed, and the lack of inboard space makes gravity dumping of the fuel (required for safety) extremely difficult. These considerations have motivated the development of a design concept which eliminates the use of a neutron multiplier and fissile breeding on the inboard side. As shown in the following chapters, eliminating inboard fissile breeding has led to a relatively simple mechanical design with engineering margin in MHD pressure drops and heat transfer, but has resulted in a design with low breeding performance.

An alternative concept, discussed briefly in section IV.B, is to include a beryllium multiplier (but no thorium fuel) in the inboard blanket. This would enhance nuclear performance without requiring that the mechanical design accommodate gravity dumping, and without resulting in MHD pressure drops as high as those in a fueled inboard blanket (which would generate more heat). A more detailed feasibility assessment of this concept should be performed.

The lithium cooled tokamak concept described in this chapter is not nearly as promising as the helium cooled tokamak described in Chapter III. If a method of including thorium fuel in the inboard blanket, or another method of enhancing breeding performance is not found, this concept should probably be abandoned.

IV.A Mechanical Design Overview

Three major considerations drive the mechnical design of the lithium cooled tokamak hybrid. These are: 1) tokamak and divertor geometry, 2) gravity fuel dump, and 3) MHD induced pressures. As mentioned above, the inboard and outboard blankets have been considered separately because of the

differences in useable space and magnetic field strength. The outboard blanket, shown in Figure IV.A.1, consists of vertical Be/Th containing pods with primarily radial coolant flow. The back of the blanket consists of large poloidal flow lithium inlet and exit plenums. The pod shape provides efficient containment of the coolant pressure, and the vertical orientation allows gravity dumping of the fuel. The large inlet and exit plenums mimimize coolant velocity, and thereby pressure drop, in this region. The overall configuration of the outboard blanket is roughly similar to that of the gas cooled tokamak blanket described in Section III.A.

On the inboard side, the magnetic field is roughly a factor of two higher than on the outboard side. Consequently, if the inboard blanket were identical to the outboard blanket, an excessive blanket coolant pressure over 1000 psi would result. Although several design concepts which included thorium fuel in the inboard blanket were considered during the course of this study, no satifactory configuration was found. We therefore selected a lithium self-cooled configuration based on the UWMAK-I [Reference 2] blanket. The selected configuration assures cooling of the first wall at pressure drops comparable to those of the outboard blanket. A more rigorous design effort, new MHD flow data, or reactor physics changes may yet lead to a concept which will allow fissile breeding in a lithium cooled inboard blanket.

IV.A.1 Outboard Blanket

A horizontal cross section of the outboard breeding blanket is shown in Figure IV.A.1. The packed bed and first wall coolant loops are separated to allow better flow control. Flow in the rectangular inlet and outlet plenums is poloidal from top to bottom of the reactor, or into the page in the figure. These plenums are assumed to be lined with electrical insulation, which is protected from the lithium coolant by an additional 0.25 mm ferritic steel liner. Thus, both a poor current return path and a strong structure are provided. This sandwich insulation is located only in walls perpendicular to the magnetic field, but a substantial development effort will be required to assume the integrity of the insulator.

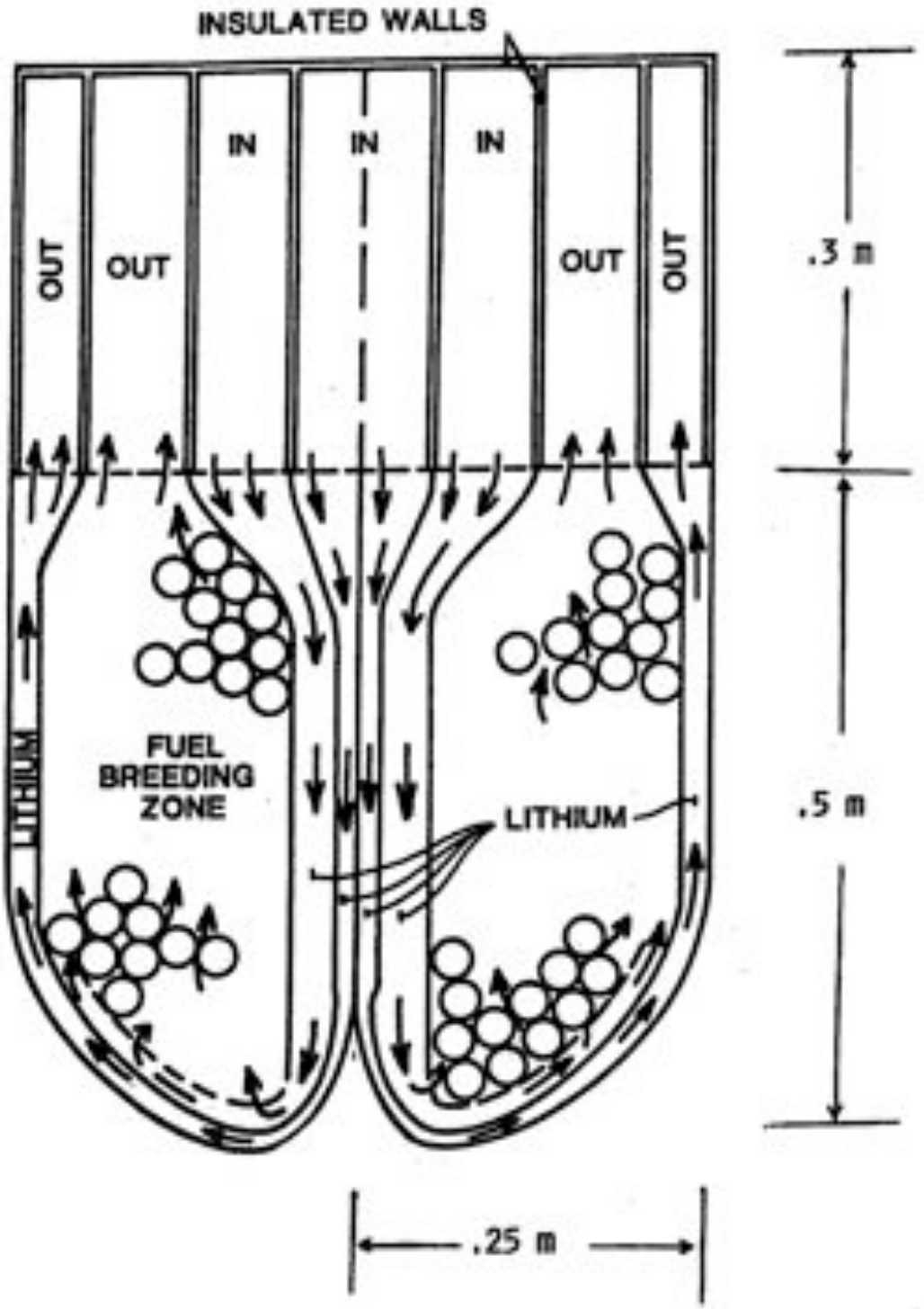

Figure IV.A.1. Outboard Blanket Module Schematic.

Flow balancing requires that the inlet and outlet plenums taper in opposite directions. Lithium will enter the inlet plenum at the top of the reactor, flow poloidally in the inlet plenum, turn 90° and enter the pod, flow around the first wall, or through the packed bed to the outlet plenum, and turn 90° again and flow toward the exit. Flow within the pods is indicated in Figure IV.A.1. Pressure drops must be equal along every flow path. Therefore, the pressure drop must be the same for lithium flowing through the pod at the top of the reactor, and thus making most of its 6.5 meter poloidal journey in the outlet plenum, as for lithium flowing through the pod at the bottom of the reactor, making most of its poloidal journey in the inlet plenum. Tapering the plenums in opposite directions is intended to keep the plenum velocities equal everywhere, and thus also keep the pod velocities equally distributed such that cooling is assured.

Since the pressure drop in the packed bed is significantly higher than that in the plenums, flow balancing in the packed bed loop in this configuration is straightforward. However, the first wall cooling loop pressure drop calculations (Section IV.C below) indicate very low pressure drops around the pod. Although low pressure drops are normally desirable, for this particular design, small imbalances in the inlet and outlet plenums can result in large velocity differences in different regions of the first wall. The flow impedance in the first wall loop may, therefore, need to be increased to ensure balanced first wall cooling.

An alternative would be to flow all the lithium around the pod nose to cool the first wall, and then back into the front of the pod to cool the packed bed. This would implement cooling of the first wall and pods, and decrease the complexity of the inlet and exit plenums. Further investigation will be required to fully understand this alternative.

The flow is opposite in adjacent pods to match pressures and temperatures across the pod walls. Although this could be accomplished in analogy to the gas cooled pods discussed in Chapter III (where coolant enters each pod along both walls, flows toward the center at the pod nose, and then back through the pebble bed), MHD velocity profiles are not well understood, and stagnation could easily occur in the lithium at the pod nose where the two opposing streams meet and turn 90°. A small stagnant core of lithium behind the first

wall would give very high first wall temperatures. We thus chose to flow the lithium around the nose to ensure cooling.

IV.A.2 Inboard Blanket

The inboard blanket configuration is shown in Figure IV.A.2. Lithium flows poloidally in the large plenums at the back of the blanket. To move from an entrance plenum to an exit plenum the flow must go through (and cool) one of the toroidally oriented mini-lobes that comprise the first wall. Flow entering a mini-lobe can move parallel to the magnetic field before moving radially toward the lobe nose, perpendicular to the field. Since the pressure drop is much lower in flow parallel to the field, the lithium will tend to spread out in this manner to minimize the velocity (and therefore the pressure) perpendicular to the field, thus guaranteeing even cooling of the mini-lobe.

Reference 3 shows that coolant/structure temperatures are move favorable for flow that transits more than one lobe in series. This is because the velocity in the lobes is increased, decreasing film drop temperatures and thus reducing the difference between the maximum bulk fluid temperature and the maximum structure temperature. However, flowing lithium in the same direction in adjacent lobes will result in large pressure and temperature differences across the walls separating the mini-lobes. This can only be tolerated by adding structural support and possibly thermal insulation, which will reduce the tritium breeding effectiveness of the blanket. We have, therefore, chosen opposing flow in adjacent lobes to equalize the temperatures and pressures across the lobe boundries. As shown in Figure IV.A.2, lithium entering every other lobe must travel a short distance back toward the blanket inlet, in the poloidal direction. This longer flow path will result in a lower volumetric flow rate in half of the lobes. However, the distance travelled, and therefore the volumetric flow in adjacent lobes, will be within 1-2% due to this effect.

As has been shown in Reference 4, the flow divider in the center of the lobe in the inboard blanket is subject to significant bending due to differential pressures on either side. This must be accommodated by adding structural support. A composite baffle filled with stagnant lithium, as shown in Figure IV.A.3, will probably be the most efficient method. This should also

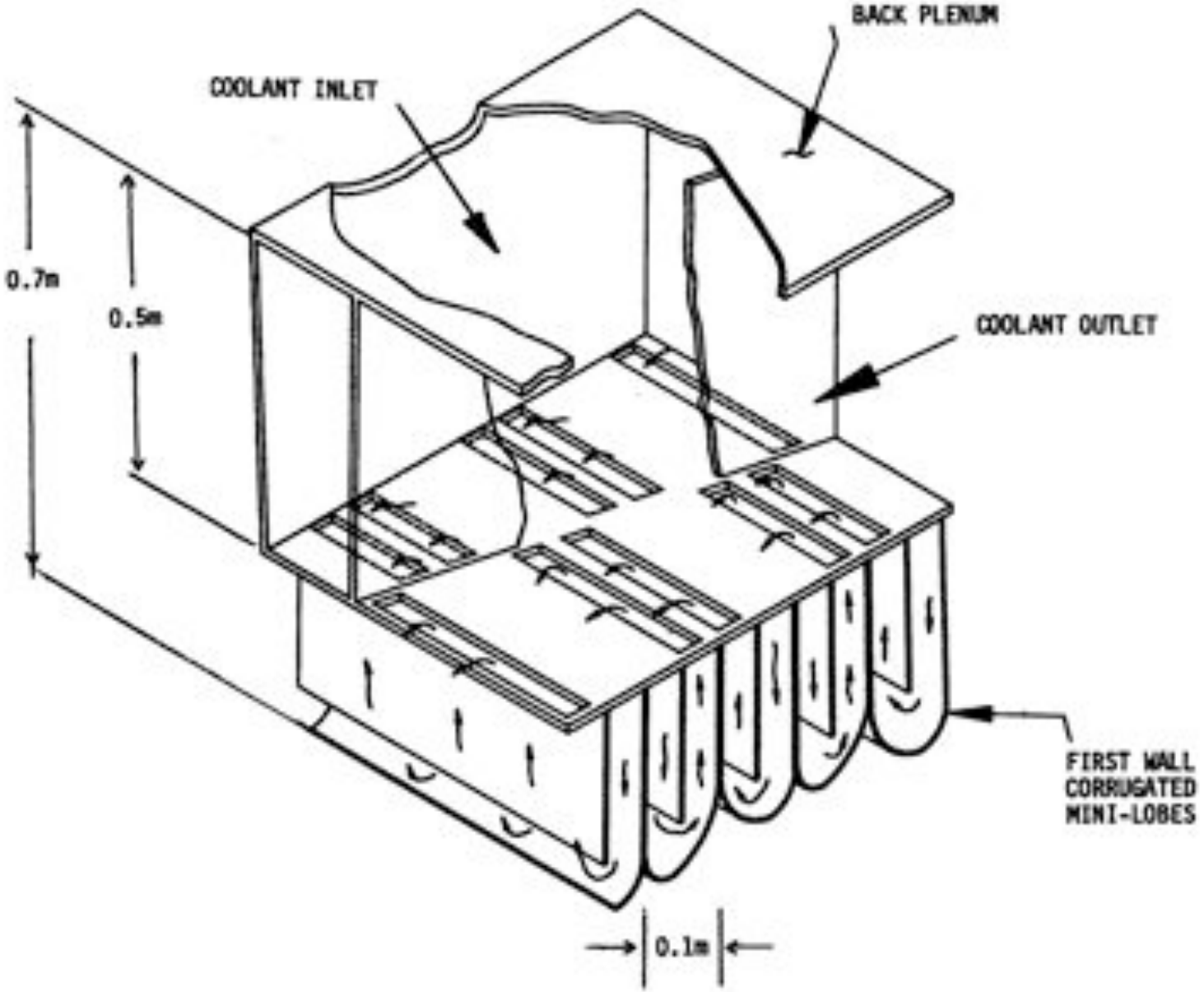

Figure IV.A.2. Inboard Blanket Module Schematic.

accommodate the temperature difference across the baffle. A thermo-mechanical analysis of this member should be performed to determine the amount of structure required.

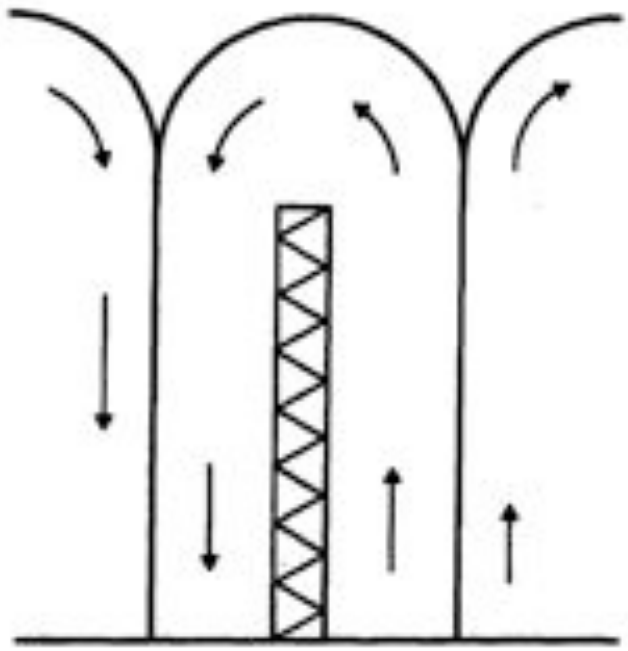

Figure IV.A.3. Composite Flow Baffle.

IV.A.3 Pod Nose Bending

The curve at the pod noses shown in Figures IV.A.1 and IV.A.2 will not be exactly semicircular because of the change in pressure around the nose. Specifically, near the outlet end of the plenums (the bottom of the blanket where the total pressure is lowest) the pressure drop in the lithium as it travels around the nose of the pod may be significant compared with the total pressure. If the pod nose cannot support bending, it will assume a constant

tension shape which deviates slightly from semicircular. The curve shown in Figure IV.A.1 is exaggerated in this respect (i.e., the pod shape should be closer to a semicircle). This principle applies to both the inboard and outboard blanket pods.

It is important to note that the first wall pods (or lobes) can be constructed to be in constant tension (no bending) under full power. However, changing the flow velocity will change the required shape, putting the walls in bending. The following analysis gives a brief derivation of the shape of the curve, and applies the result to the pressures indicated in the MHD analysis below. The analysis indicates that the deflection is small, and thus changes in operating power may not present a problem.

Force balance (see Figure IV.A.4) requires that the tensile forces in the member balance the pressure forces:

$$Pds = T_1 \sin \frac{d\phi}{2} + T_2 \sin \frac{d\phi}{2}$$

Constant tension gives:

$$T_1 = T_2 = T$$

and from the small angle:

$$Pds = Td\phi \quad \text{or} \quad d\phi = \frac{Pds}{T}$$

From analytic geometry:

$$d\vec{r} = \cos\phi ds\vec{i} + \sin\phi ds\vec{j}$$

and

$$d\vec{r} = dx\vec{i} + dy\vec{j}$$

thus:

$$x = \int \cos\phi ds \qquad y = \int \sin\phi ds$$

$$= \int \cos\left[\frac{1}{T}\int P ds'\right] ds \qquad = \int \sin\left[\frac{1}{T}\int P ds'\right] ds$$

Since the actual pressure as a function of position around the pod nose is not well characterized, we have simply taken a linear variation of pressure with arc length:

$P = P_0 + As$
P_0 = pressure at the start of the curve of the pod nose
A = a constant
s = arc length along curve C

Taking the boundary conditon as:

$$\phi = +\frac{3\pi}{2} \text{ at } x = 0,\ y = 0, \text{ and } s = 0$$

The constant tension pod nose shape is then given by:

$$x = \int_0^s \sin[s'(P_0 + As')/2/T]\, ds'$$

$$y = -\int_0^s \cos[s'(P_0 + As'/2)/T]\, ds'$$

which can be solved numerically.

In the outboard blanket, the pressure drop per unit length varies greatly as the flow turns from perpendicular to the magnetic field to parallel with it and back to perpendicular as it goes around the pod nose. A pressure drop is assumed to be associated with the turning, as discussed in section IV.C below. In the inboard blanket, flow around the pod nose remains perpendicular to the magnetic field, however, the field varies slightly and effects of this variation are not well understood.

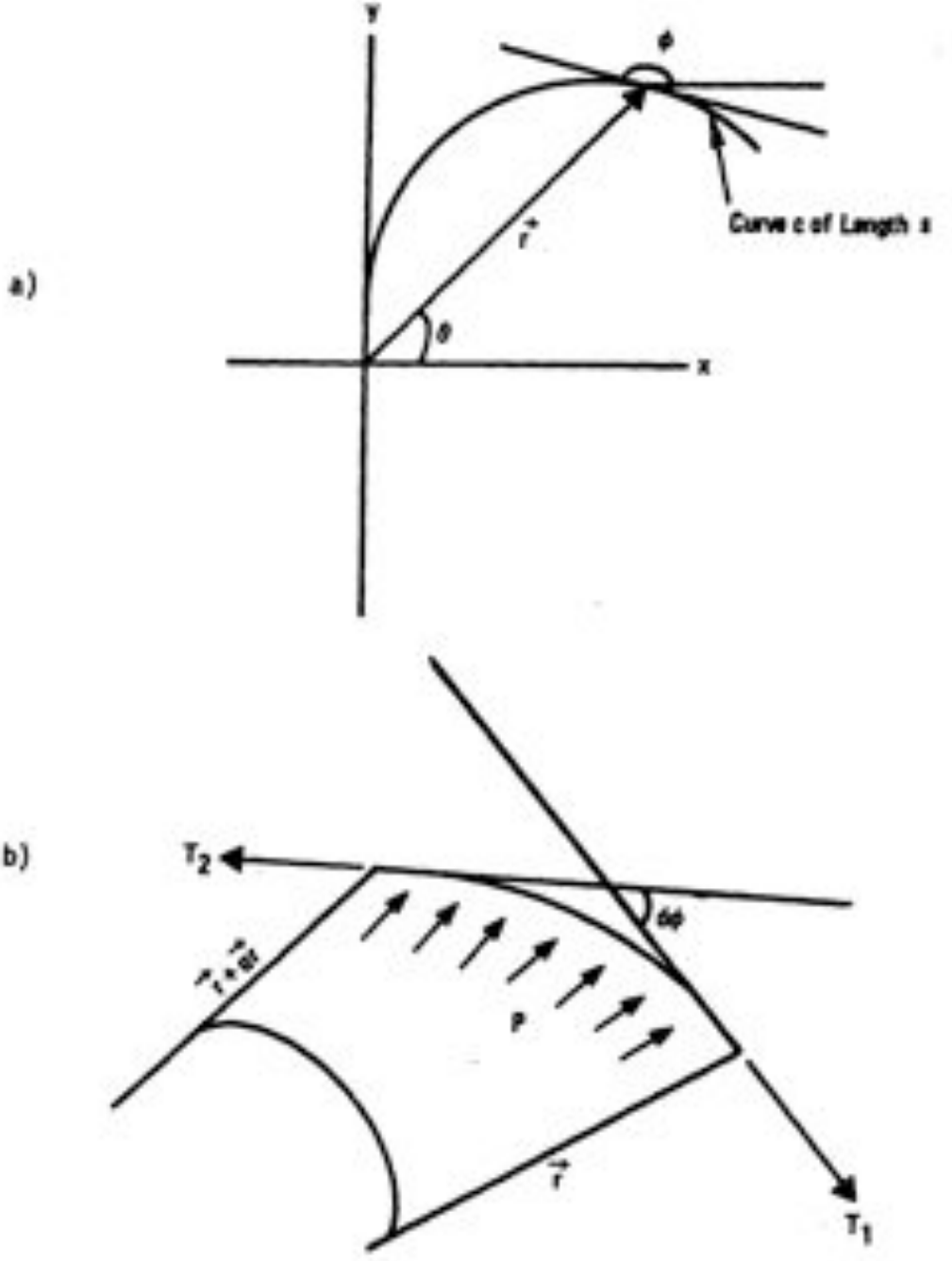

s = arc length along curve c.

ϕ = angle between the x axis and the tangent to curve c.

T = tensile force in member.

P = internal pressure.

Figure IV.A.4. Geometry of Pod Nose Bending Problem.

Results for a pressure at the inlet to the outboard blanket pod nose ten times that of the outlet and for an outlet pressure of zero are compared with a cylindrical pressure vessel in Figure IV.A.5. Table IV.A.1 gives the maximum deflection in millimeters from a cylinder of the pod nose for the inboard and outboard blankets at worst case pressures taken from section IV.C. Although stresses have not yet been calculated, this analysis indicates that differential pressures around the pod nose will not produce significant bending stresses for the inboard and outboard blanket configuration considered here. Note that bending stresses produced in this manner can be considered as secondary stresses because they are self relieving. Bending of the structure will cause the shape to approach the constant tension shape, thus reducing the bending stress.

TABLE IV.A.1 Deflection of Constant Tension Pod Noses from a Cylinder

Approx. Blanket	Pod Nose Inlet Pressure (MPa)	Pod Nose Outlet Pressure (MPa)	Inlet/Outlet Pressure Ratio	Pod Nose Radius (cm)	Maximum Deflection (mm)
Inboard	1.670	1.542	1.083	5	.006
Outboard	0.1943	0.1907	1.019	12.5	.05
——	1.5	0.15	10	12.5	6.4

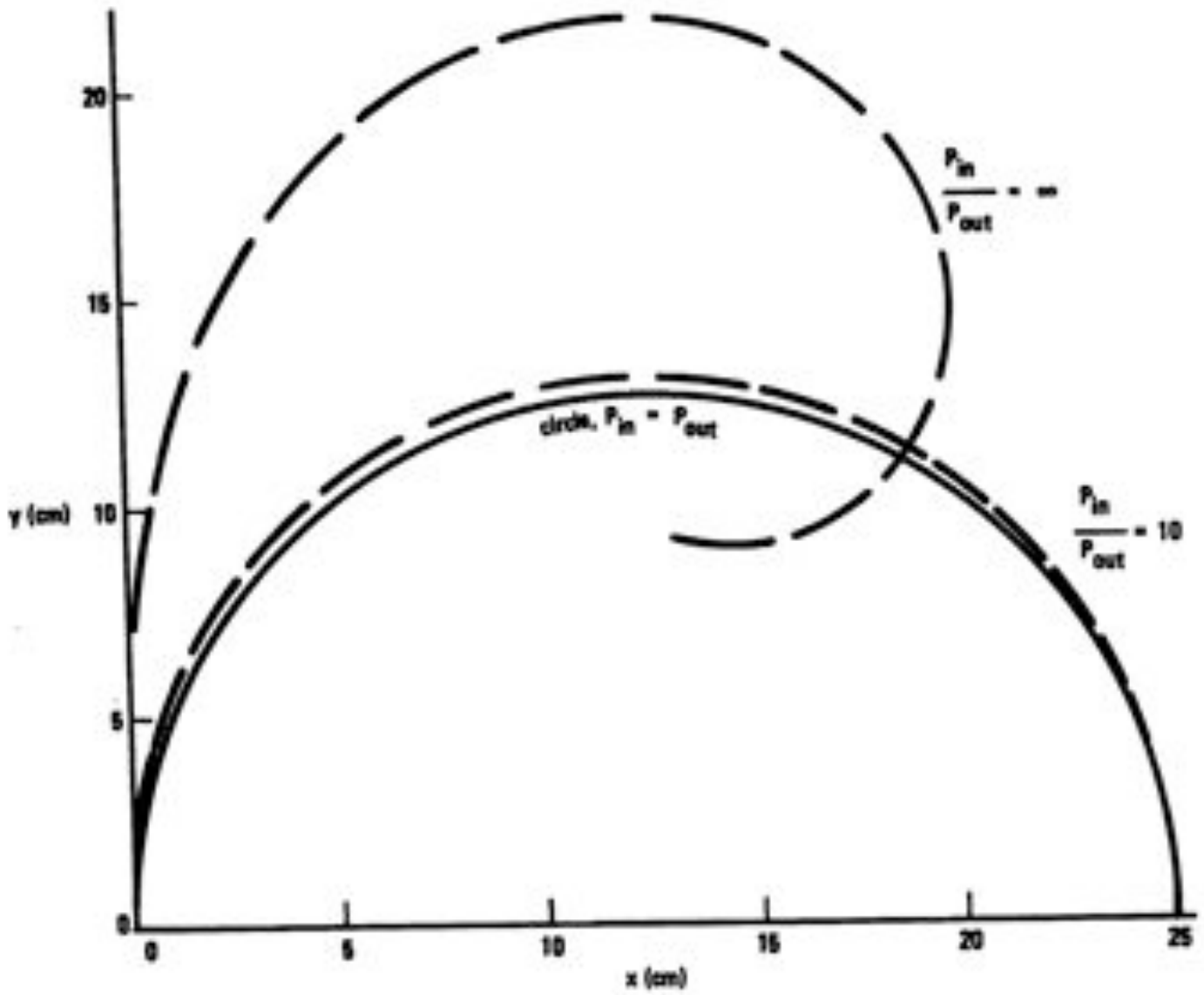

Figure IV.A.5. Constant Tension Curves for Pressures That Vary Linearly With Arc Length.

References, Section IV.A

1) D. H. Berwald, et al., "Fission-Suppressed Hybrid Reactor - The Fusion Breeder," UCID-19638, Lawrence Livermore National Laboratory (1982).

2) B. Badger, et. al., "UWMAK-I, A Conceptual Torodial Fusion Reactor Design," University of Wisconsin, UWFDM-68 (1974). (see IV.C ref. 1)

3) D. K. Sze, W. E. Stewart, "Lithium Cooling For a Low Beta Tokamak Reactor," Proc. of: Technology of Controlled Thermonuclear Fusion Experiments and Engineering Aspects of Fusion Reactors, November 1972.

4) G. Yagawa and M. Masuda, "Finite Element Analysis of Magnetohydrodynamics and Its Application to Lithium Blanket Design of a Fusion Reactor," Nuclear Engineering Design 71 (1982).

IV.B NUCLEAR DESIGN

IV.B.1 Objectives

The initial step in developing a fission-suppressed blanket for a tokamak was to try and use the reference blanket developed for the tandem mirror.(1,2,3) This blanket consists of Be/Th composite pebbles cooled by liquid lithium. Major differences between the tandem mirror and tokamak which affect blanket design are the higher first wall heat loads, higher magnetic fields and longer coolant flow paths in the tokamak blanket. These differences amplify the MHD problems associated with pumping the liquid metal coolant through the blanket, especially on the inboard side. This problem is greatly reduced if the Be/Th pebbles are removed from the blanket's inboard leg.

The objective of this nuclear analysis was to evaluate the effect on breeding of removing the Be/Th pebbles from the inner blanket, leaving only Li in the inner blanket.

IV.B.2 Method of Analysis

The procedure used to evaluate the effect of removing the Be/Th pebbles from the inner blanket consisted of developing a 2-D toroidal model and using the TART Monte Carlo code to calculate breeding with and without the Be/Th pebbles in the inner blanket. The TART runs were made with 5000 source neutrons, resulting in a less than 2% standard deviation. The resonance effects discussed in section III.C are not included in this analysis.

IV.B.3 2-D Toroidal Model and Results

The configuration of the 2-D toroidal model used to assess this question is as shown in Fig. III.C.1 except that the blanket is composed of single (not double) zones. The thicknesses and composition of the first wall and blanket zones are listed below in Table IV.B.1. The Be/Th/Li blanket is analogous to that developed for the tandem mirror breeder design. Its ^{6}Li atom fraction is artifically high to correct for pebble bed heterogeneous effects.(3)

Monte Carlo results (by zone and totals) of both the Li and Be/Th/Li inner blanket cases are listed in Table IV.B.2.

Table IV.B.1 Thicknesses and Materials Compositions of First Walls and Blankets

- Inner first wall - 1 cm Fe
- Outer and top and bottom first walls
  10 cm, 90 v/o Li (.2 a/o Li6) + 10 v/o Fe
- Li Blanket (inboard side only)
  60 cm, 95 v/o Li (.2 a/o Li6) + 5 v/o Fe
- Be/Th/Li blankets (outboard, top and bottom)
  60 cm, 5 v/o Fe + 53 v/o Be + 2.9 v/o Th (0% U-233) + 38 v/o Li (1 a/o Li6)

Table IV.B.2 Results of TART Monte Carlo Runs

	Inner Blanket Type	
	Li	Be/Th/Li
Inner blanket (zone 6)		
T^6	.102	.165
T^7	.099	.022
F	-	.163
E (MeV)*	2.26	3.23
Top + bottom blankets (zone 7)		
T^6	.239	.266
T^7	.028	.028
F	.246	.248
E*	4.53	4.69

Table IV.B.2 Results of TART Monte Carlo Runs (cont'd)

	Inner Blanket Type	
	Li	Be/Th/Li
Outer blanket (zone 8)		
T^6	.331	.334
T^7	.044	.044
F	.326	.326
E*	6.42	6.45
Top + bottom first walls (zone 4)		
T^6	.032	.041
T^7	.073	.075
E*	1.69	1.78
Outer first wall (zone 5)		
T^6	.042	.044
T^7	.124	.124
E*	2.68	2.71
Totals		
T	1.113	1.143
F	.572	.737
T + F	1.68	1.88
E* (M)	19.03 (1.35)	19.4 (1.38)

* No γ transport and no decay energy

IV.B.4 Comparison of Results and Recommendations

To estimate the actual fissile breeding ratios (F) of the two cases, one with the Be/Th/Li inner blanket, the other with the Li-only inner blanket, the following corrections are made to the results given in Table IV.B.2.

$$T + F = [(T + F)_{Beds} \cdot \text{Het. Corr.} + T_{Other}](\text{Plena Corr.})(\text{Divertor Corr.})$$
$$F = T + F - T_{Req}$$

where:

$(T + F)_{Beds}$ ≡ sum of T + F in the Be/Th/Li beds from Table IV.B.2

T_{Other} ≡ sum of T in the non-bed Li-containing zones

Het. Corr. ≡ Be/Th/Li pebble bed heterogeneous correction. Values taken from Ref. 3

Plena Corr. ≡ correction to account for module plena and end effects. Value assumed to be the same as for the rerference tandem mirror blanket (3).

Divertor Corr. ≡ correction due to having a divertor. Value taken from Subsection III.C.5.

T_{Req} ≡ assumed overall value of tritium breeding required.

<u>For case with all bed blanket:</u>

$$T + F = [(1.60) \cdot 0.943 + 0.284](.971)(.854)$$
$$= 1.79 \cdot 0.971 \cdot 0.854 = 1.49\ (\pm\ 10\%)$$
$$F = 1.49 - 1.01 = 0.48\ (\pm\ 30\%)$$

<u>For case with Li inner blanket:</u>

$$T + F = [(1.21) \cdot 0.943 + 0.472](.971)(.854)$$
$$= 1.62 \cdot 0.971 \cdot 0.854 = 1.34(\pm\ 10\%)$$
$$F = 1.34 - 1.01 = 0.33\ (\pm\ 40\%)$$

The fissile breeding ratio of 0.33 estimated above for the Li inner blanket case is 31% below the Be/Th/Li inner blanket case and is considered too low for this blanket configuration to be considered further. We are thus inspired to look for another variant of this blanket that would have a higher breeding ratio.

One such variant might be a blanket configuration with the Be/Th/Li beds on the outer, top, and bottom sides with a Be/Li blanket (no fissile breeding) on the inboard side. In this case, overall breeding (i.e., T + F) would be preserved, but if the ratio of thorium-to-^{6}Li were not increased, such a blanket would overbreed in tritium. Rather than decreasing the ^{6}Li fraction,

recent studies (4) indicate that a substantial increase in the thorium fraction (perhaps balanced by a smaller increase in the ^{6}Li fraction) would be most beneficial.

Based on the low fissile breeding ratio estimated for the case of no Be/Th pebbles on the inner blanket, it is recommended that it be dropped and the blanket modification discussed above be investigated as one alternative to the He-cooled variation of the Be/Th blanket with full coverage described in Chapter III.

References, Section IV.B

1. D. H. Berwald, et al., "Fission-Suppressed Hybrid Reactors - The Fusion Breeder," Lawrence Livermore National Laboratory, UCID-19638 (1983).

2. R. W. Moir, et al., "Fusion Breeder Reactor Design Studies," Proc. Fifth Topical Mtg. on the Tech. of Fusion Energy, Knoxville, TN, 1983, in Nuclear Technology/Fusion, Vol. 14, #2, Part 2, p. 589.

3. J. D. Lee, "Nucleonics of a Be-Li-Th Blanket for the Fusion Breeder," Proc. Fifth Topical Mtg. on the Tech. of Fusion Energy, Knoxville, Tn, 1983, in Nuclear Technology/Fusion, Vol. 14, #2, Part 2, p. 805. Also Lawrence Livermore National Laboratory Rpt. UCRL-88237 (1983).

4. W. R. Meier, "A High Performance, Suppressed-Fission ICF Hybrid," 10th IEEE Sym. on Fusion Engineering, Philadelphia, PA, 1983; also Lawrence Livermore National Laboratory Rpt. UCRL-89274 (1983).

IV.C LITHIUM FLUID DYNAMICS AND HEAT TRANSFER

IV.C.1 Introduction

A key problem in the design of lithium-cooled blankets for a tokamak reactor is the calculation of MHD pressure drops. Although the set of MHD equations for the calculation of pressure drops through B-field gradients, turns, contractions, entrance, and exit flows are still uncertain, available sets of equations were used and compared to determine feasibility of the design. The general design approach is to minimize the flow velocity by maximizing the flow cross-sectional area wherever possible. This leads to the selection of a non-fissile fuel breeding blanket for the inboard side of the reactor where the magnetic field strength is high.

A blanket configuration similar to the UWMAK-I[1] design shown in Fig. IV.C.1 was used in the inboard side. For the outboard blanket, the new design shown in Fig. IV.C.2 was adopted. In order to handle the surface heat flux of the tokamak reactor (0.25 MW/m^2 in this analysis), the design approach was to minimize the amount of coolant flowing at the first wall (to keep the pressure drop and total pumping power low) but to maximize the coolant velocity to keep the coolant temperature rise within specific material temperature limits. Results show that with the selected inboard/outboard blanket configurations, the maximum blanket pressure drops are reasonable at <2.3 MPa (330 psi) and can be reduced by further design optimization. The material temperature limits can also be met.

The following sequence summarizes the approach in the blanket MHD calculation:

- Calculate and compare the pressure drops using the equation from Hunt and Holroyd,[2,3] and from Picologlou[4] when applicable.
- Assume the pressure drop for turns is negligible when both legs are normal to the B-field.
- Assume the pressure drop through an expansion flow is negligible.

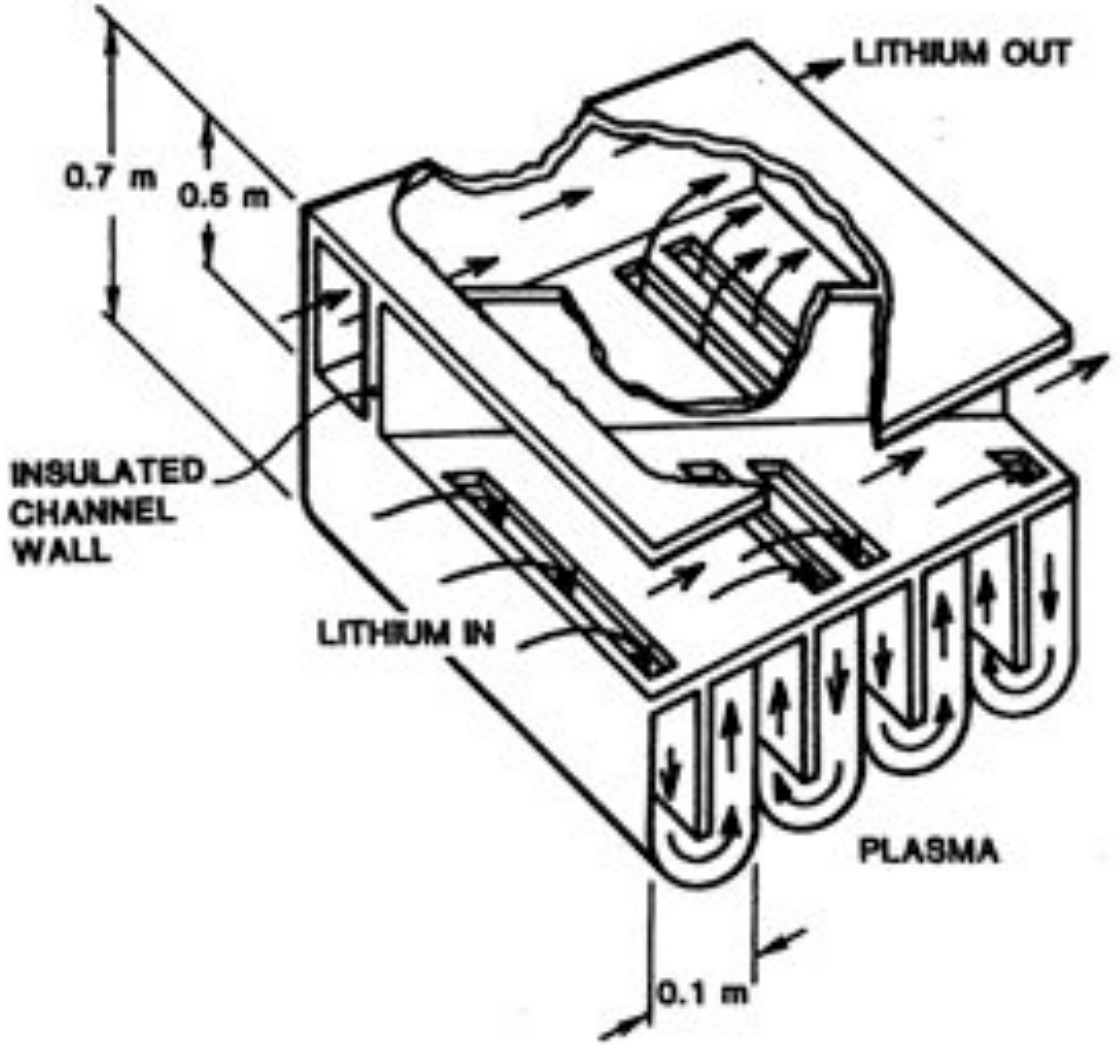

Fig. IV.C.1 Inboard Blanket Module Schematic

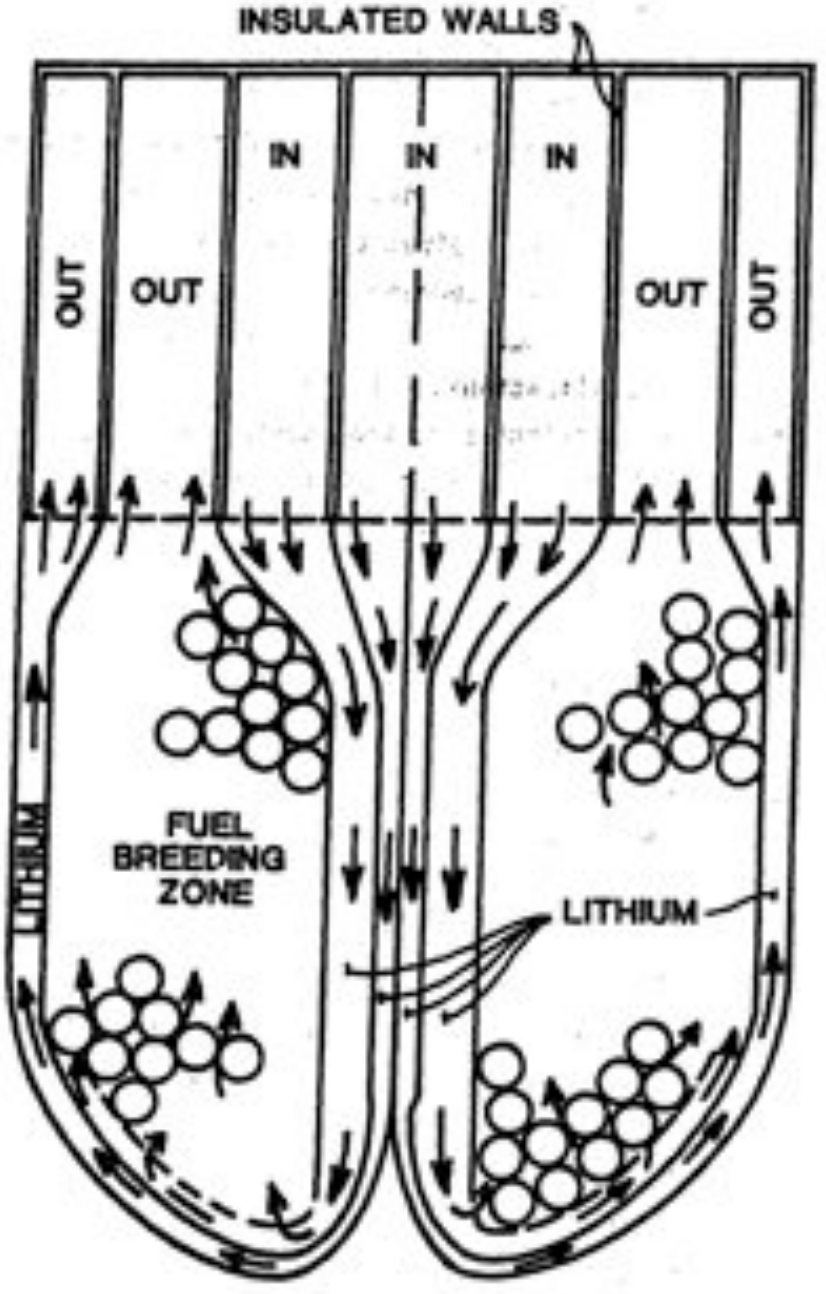

Fig. IV.C.2 Outboard Blanket Module Schematic

- Calculate the pressure drop through contractions by using the equations recommended by Hunt and Holroyd.[2,3]

IV.C.2 MHD Equations Review

Key sets of applicable MHD equations are given in Table IV.C.1. The set recommended by Hoffman and Carlson[5] was used for the 1982 Fusion Breeder Study.[6] The constant K has to be determined graphically and is supported by very limited experimental results. The set of equations supplied by Hunt and Holroyd[2,3] gives distinct recommendations for the calculations of inlet, gradient-B, turning, expansion and contraction pressure drop calculations. The latest set of equations supplied by Picologlou[4] also has detailed specifications. The only agreement between these sets of MHD equations is for straight pipe flow normal to the magnetic field. Since the sets of equations given by Hunt and Holroyd, and Picologlou are more complete, they will be the only sets compared in this study.

IV.C.3 Blanket Configurations

Figures IV.C.1 and IV.C.2 give the inboard/outboard blanket configurations for the fusion breeder study. In order to keep the module pressure and coolant pressure drop to acceptable levels in the high field inboard region of the tokamak reaction, we recommend that the packed-bed fertile material be omitted in this version. This both increases the available flow area and decreases the amount of power in the blanket. Both effects will reduce the coolant velocity, and hence the pressure drop. The UWMAK-I type[1] of blanket module was selected because the plenum region is relatively simple in geometry, thus allowing the possibility of using thin clad insulated walls. The module is designed to take different surface wall loadings by adjusting the front lobe dimension, thus adjusting the length of the liquid metal flow path and liquid metal channel depth for material temperature control.

Table IV.C.1 MHD Equations

MHD ΔP Formula	Hoffman and Carlson[5]	Hunt and Holroyd[2,3]	Picologlou (ANL)[4]
Straight pipe Transferse $\vec{B}$	$\ell\sigma uB^2 \frac{c}{1+c}$	$\ell\sigma uB^2 \frac{c}{1+c}$	$\ell\sigma uB^2 \frac{c}{1+c}$
Inlet/contraction	$K\sigma uB^2 a$	$0.2\ \sigma uB^2 \sqrt{\ell}\ a$	$0.2\ \sigma uB^2 \sqrt{\ell}\ a$
Varying B	$K\sigma uB^2 a$	$0.2\ \sigma uB^2 \sqrt{\ell}\ a$	$\sigma uB^2 \left(\frac{1}{r_2} - \frac{1}{r_1}\right) \frac{r^2 c}{1+c}$ (For B = B(r) in Tesla]
Bend			
A. One leg parallel to $\vec{B}$	$K\sigma uB^2 a$	$\sigma uB^2 \sqrt{\ell}\ a$	$\frac{1}{2}\ \sigma uB^2 a N^{-1/3}$ $= \frac{1}{2}\ u^{4/3} B^{4/3} \sigma^{2/3} \rho^{1/3} a^{2/3}$
B. Both legs normal to $\vec{B}$	0	0	0

K = pressure drop coefficient,
c = $(\sigma_w t_w)/(\sigma a)$,
B = magnetic field strength,
u = fluid velocity,
σ = fluid electrical conductivity,
N = $\sigma B^2 a/\rho u$ - magnetic interaction parameter.
ρ = fluid density,
σ_w = wall electrical conductivity,
a = 1/2 channel width in the direction of B,
t_w = wall thickness,.
ℓ = flow path length,.

For the outboard region, the configuration shown in Fig. IV.C.2 was selected. Separation of the first wall and fertile zone coolant routing allows for adjustment of the first wall flow speed by changing the coolant gap dimension. Thus, various surface loadings can be addressed. A potential design simplification can be obtained by combining the two outlet streams into one.

Figure IV.C.3 is a schematic of the inboard/outboard coolant routings. It illustrates the key dimensions and magnetic field strengths (numbers in brackets) at different reactor radial positions.

IV.C.4 Inputs and Results

Table IV.C.2 summarizes the input parameters for the blanket MHD calculations.

Table IV.C.2 Thermal-Hydraulic Calculation Input Parameters

Reactor thermal power	5000 MW
Neutron wall loading	3 MW/m^2
Surface wall loading	0.25 MW/m^2
Coolant - lithium	
T_{in}/T_{out}	340°/430°C
Outboard blanket energy multiplication	2
Inboard power fraction	0.325
Magnetic field strength	$B(r) = \frac{33}{r}$ Tesla

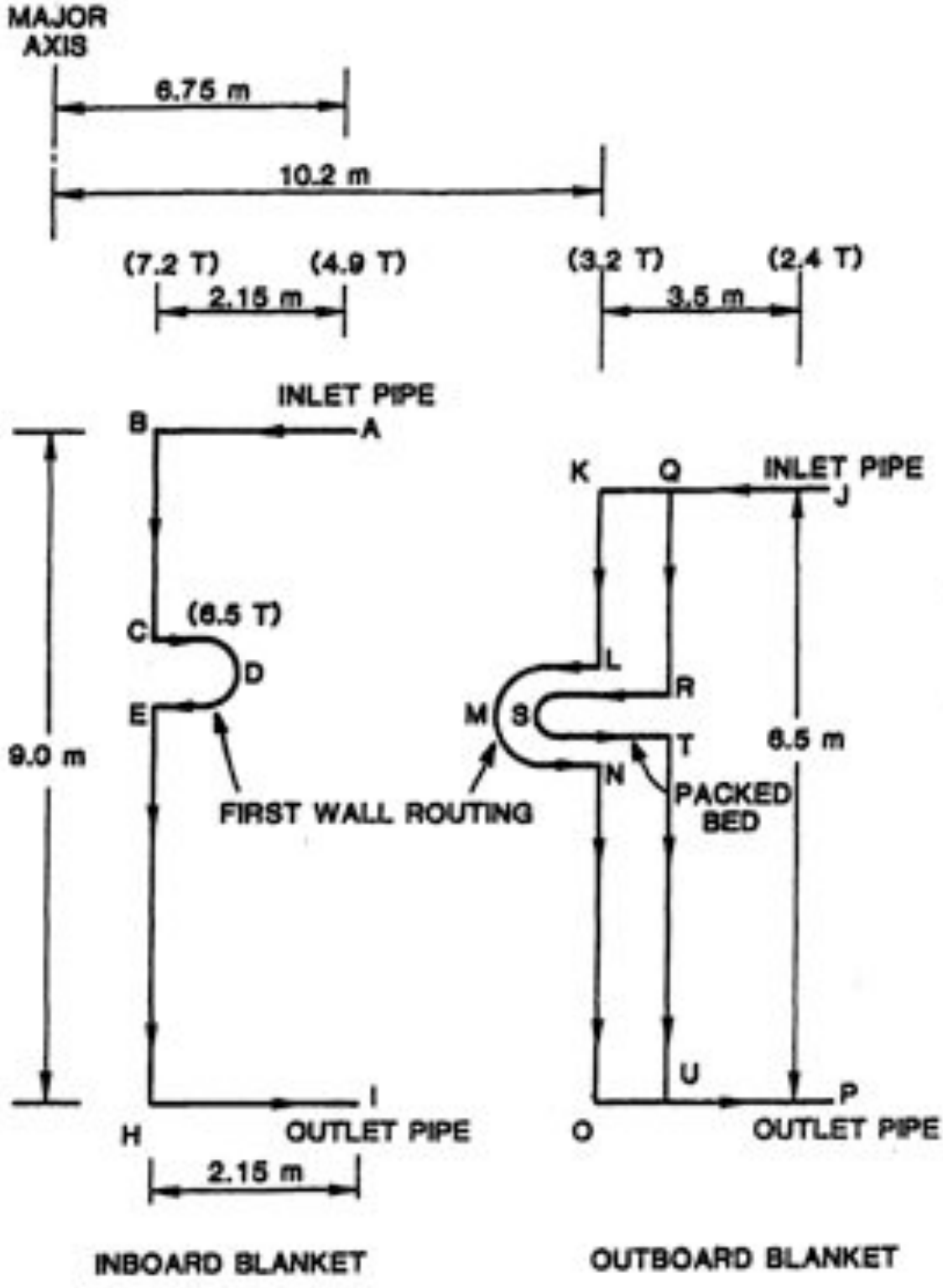

Fig. IV.C.3 Inboard and Outboard Blankets Coolant Routing Schematics

The channel characteristic dimensions and the pressure drops for respective channels and turns are given in Tables IV.C.3 to IV.C.5.

The pressure drops for the inboard blanket, outboard first wall, and outboard blanket sections are also given in Tables IV.C.3 to IV.C.5, respectively. The results calculated by using the Hunt and Holroyd,[2,3] and Picologlou[4] sets of equations are presented as is a worst case estimate consisting of the highest values in each category. Comparing the two sets of results, for the inboard blanket case, different results were obtained for the gradient B-field and turning calculations, yet the total pressure drops for the whole loop are similar, since they are dominated by the pressure drop due to straight channel flow across field lines, which is the only calculation that is agreed upon by the different authors.

The magnitudes of the inboard/outboard blanket pressure drops are approximately equal. For the outboard blanket, the pressure drop is dominated by the packed bed pressure drop. A similar design of using packed bed design would not be acceptable because the high magnetic field strength at the inboard region would result in a pressure drop in excess of 5 MPa (800 psi).

Considering the first wall heat flux and the volumetric power generation in the first wall and the lithium, the maximum first wall temperature was calculated conservatively from the conduction of heat through the first wall to lithium at the maximum coolant temperature at the outlet of the first wall. For these calculations, the first wall coolant bulk temperature was taken to be the same as the blanket coolant outlet temperature at 430°C. The inboard and outboard blankets first wall maximum temperatures were calculated to be 551°C and 470°C, respectively. From design feasibility considerations, these temperatures are acceptable, since they are located at the outlet end of the first wall where the structural loading requirement is much reduced. To provide improved heat transfer, if necessary, the first wall channel dimensions can be varied to adjust the coolant temperature increase in the channel, thus maintaining the structural material temperature below the specified limit.

Table IV.C.3 Inboard Blanket Parameters and Pressure Drops

	Characteristic Dimension (m)	Magnetic Field Strength (T)	Wall Thickness (m)	Channel Length (m)	Fluid Velocity (m/s)	Conductance Ratio (C)	Hunt and Holroyd (kPa)	Picologlou (kPa)	Worst Case
A - Inlet[a]	0.5	6.9	2.5×10^{-4}	0	1.05	2.5×10^{-4}	124.0	124.0	124.0
AB - B gradient[a]	0.5	6.9 - 7.2	2.5×10^{-4}	2.15	1.05	2.5×10^{-4}	267.0	61.4	267.0
B - Turn	(Both legs are normal to B-field)						0	0	0
B - Expansion	(Assumed to be zero)						0	0	0
BH - Channel[a]	0.25	7.2	2.5×10^{-4}	9	0.57	5.2×10^{-4}	429.0	429.0	429.0
C - Turn	(Both legs are normal to B-field)						0	0	0
C - Expansion	(Assumed to be zero)						0	0	0
CD - B gradient	0.025	6.7 - 6.5	3×10^{-3}	0.2	0.16	0.06	27.3	240.0	240.0
D - Turn (↓ to ↑)	0.025	6.5	3×10^{-3}		0.16	0.06	128.0	8.0	128.0
DE - B gradient	0.025	6.5 - 6.7	3×10^{-3}	0.2	0.16	0.06	27.3	240.0	240.0
E - Turn	(Both legs are normal to B-field)						0	0	0
E - Contraction	0.025	6.7	3×10^{-3}		0.16 - 0.57	0.06	349.0	349.0	349.0
H - Turn	(Both legs are normal to B-field)						0	0	0
H - Contraction[a]	0.35	7.2	2.5×10^{-4}		0.57 - 1.05	0.38×10^{-3}	899.0	899.0	899.0
HI - B gradient[a]	0.5	7.2 - 6.9	2.5×10^{-4}	2.15	1.05	2.5×10^{-4}	267.0	61.4	267.0
I - Exit	(Assumed to be zero)						0	0	0
						Total	2517	2411	2543
					Blanket Maximum Pressure @ B (Inboard blanket inlet)		2126 (308 psi)	2226 (323 psi)	2552 (3709 psi)

[a] The design assumes the use of a 0.25 mm thick stainless steel clad lining the inside of the channel.

Table IV.C.4 Outboard First Wall Parameters and Pressure Drops

	Characteristic Dimension (m)	Magnetic Field Strength (T)	Wall Thickness (m)	Channel Length (m)	Fluid Velocity (m/s)	Conductance Ratio (C)	Hunt and Holroyd (kPa)	Picologlou (kPa)	Worst Case
J - Inlet[a]	0.75	2.4	2.5×10^{-4}		0.98	1.7×10^{-4}	34.2	34.2	34.2
JK - B gradient[a]	0.75	2.4 - 3.2	2.5×10^{-4}	3.5	0.98	1.7×10^{-4}	61.0	14.1	61.0
K - Turn	(Both legs are normal to B-field)						0	0	0
K - Expansion	(Assumed to be zero)						0	0	0
KQ - Channel	0.15	3.2	3×10^{-3}	6.5	0.11	0.01	225.0	225.0	225.0
L - Turn	(Both legs are normal to B-field)						0	0	0
L - Expansion	(Assumed to be zero)						0	0	0
LM - B gradient	0.005	3.2 - 3.4	3×10^{-3}	0.5	0.02	0.3	0.4	78.7	78.7
M - Turn	0.005	3.4	3×10^{-3}		0.02	0.3	3.6	0.7	3.6
MN - B gradient	0.005	3.4 - 3.2	3×10^{-3}	0.5	0.02	0.3	0.4	78.7	78.7
N - Expansion	(Assumed to be zero)						0	0	0
N - Turn	(Both legs are normal to B-field)						0	0	0
O - Turn	(Both legs are normal to B-field)						0	0	0
O - Contraction[a]	0.15	3.2	2.5×10^{-4}		0.11 - 0.98	0.84×10^{-3}	120.1	120.1	120.1
OP - B gradient[a]	0.75	3.2 - 2.4	2.5×10^{-4}	3.5	0.98	1.7×10^{-4}	61.0	14.1	61.0
P - Exit	(Assumed to be zero)								
						Total	686	566	663
						Blanket Maximum Pressure @ X	422 (61 psi)	530 (76 psi)	580 (84 psi)

[a] The design assumes the use of a 0.25 mm thick stainless steel clad lining the inside of the channel.

Table IV.C.5 Outboard Fertile Zone Blanket Parameters and Pressure Drops

	Characteristic Dimension (m)	Magnetic Field Strength (T)	Wall Thickness (m)	Channel Length (m)	Fluid Velocity (m/s)	Conductance Ratio (C)	Hunt and Shimoyd (kPa)	Picologlou (kPa)	Worst Case
J - Inlet	0.75	2.4	2.5×10^{-4}		0.98	1.7×10^{-4}	34.2	34.2	34.2
JQ - B gradient[a]	0.75	2.4 + 3.2	2.5×10^{-4}	3.5	0.98	1.7×10^{-4}	61.0	14.1	61.0
Q - Turn	(Both legs are normal to B-field)						0	0	0
Q - Contraction[a]	0.75	3.2	2.5×10^{-4}		0.98 + 1.26	1.7×10^{-4}	87.0	87.0	87.0
QU - Channel[a]	0.15	3.2	2.5×10^{-4}	6.5	1.26	0.84×10^{-3}	218.0	218.0	218.0
R - Turn	(Both legs are normal to B-field)						0	0	0
R - Expansion	(Assumed to be zero)						0	0	0
RS - B gradient	0.15	3.2 + 3.4	3×10^{-3}	0.5	0.24	0.1	8.2	337.4	337.4
S - Turn	0.15	3.4	3×10^{-3}		0.24	0.1	40.8	4.0	40.8
ST - Packed Bed[b]	0.09	3.4 + 3.2	3×10^{-3}	0.5	0.055	0.02	906.0	906.0	906.0
T - Turn	(Both legs are normal to B-field)						0	0	0
T - Contraction	0.09	3.2	3×10^{-3}		0.055 + 1.26	0.02	487.0	487.0	487.0
U - Turn	(Both legs are normal to B-field)						0	0	0
U - Expansion	(Assumed to be zero)						0	0	0
UP - B gradient[a]	0.75	3.2 + 2.4	2.5×10^{-4}	3.5	0.98	1.7×10^{-4}	61.0	14.1	14.1
P - Exit	(Assumed to be zero)								
						Total	1903	2101	2185
					Blanket Maximum Pressure @ Q		1808	2053	2090
							(262 psi)	(298 psi)	(303 psi)

[a] The design assumes the use of a 0.25 mm thick stainless steel clad lining the inside of the channel.

[b] A radial outward flow model across the toroidal magnetic field was used in the calculation. The average fluid flow velocity was used in the packed bed pressure drop calculation. (Reference 6.)

IV.C.5 Conclusions and Recommendations

Considering the MHD pressure drops and the estimated maximum temperatures for the inboard and outboard blankets, the following conclusions and recommendations can be made:

1. The present blanket design approach of breeding fissile material only in the outboard blanket is acceptable both from pressure drop and temperature considerations.

2. As indicated in Tables IV.C.3 and IV.C.4, the key differences in the two sets of MHD equations are on gradient B-field and turning calculations. Although the total pressure drops predicted by the two sets of equations are similar, the individual terms differ significantly and experiments will be needed to understand the differences.

3. Nevertheless, some confidence in the result is provided because the worst case pressure drop is only slightly higher than that predicted in either set of models.

4. It should be noted that if the blanket flow plena are not assumed to be insulated by the use of an 0.25 mm thick stainless steel liner, the increase in pressure drop would be proportional to the channel wall thickness. At a wall thickness of 3 mm, just the channel pressure drop for the inboard/outboard blankets would be 2574 kPa (373 psi)/1308 kPa (190 psi), respectively. These high pressure drops would be unacceptable when other pressure drops are considered. This indicates the importance of developing the insulated metallic liner or other wall electrical insulation, as a way of reducing the Hartmann flow pressure drops.(7)

5. The packed bed MHD pressure drop calculation was developed in 1982 under the Fusion Breeder Program.(6) As indicated in Table IV.C.5, the packed-bed pressure drop contributes significantly to

the total outboard blanket pressure drop. Experimental verification of the MHD packed-bed pressure drop will be needed.

6. To further optimize the design, experimental determination of the MHD effect on liquid metal heat transfer will be needed in order to determine flow channel sizes and routings such that the impact of MHD pressure drop can be minimized.

References, Section IV.C

1. B. Badger et al., "Wisconsin Tokamak Reactor Design," UWFDM-68, November 1973.
2. J. C. R. Hunt and J. R. Holroyd, "Applications of Laboratory and Theoretical MHD Duct Flow Studies in Fusion Reactor Technology," CLM-R169, Culham Laboratory, 1977.
3. R. J. Holroyd, J. T. D. Mitchell, "Liquid Lithium as a Coolant for Tokamak Fusion Reactors," Culham Laboratory Report CLM-R231, UKAEA, 1982.
4. "Blanket Comparison and Selection Study," Argonne National Laboaratory Report, ANL/FPP-83-1, October 1983.
5. M. A. Hoffman, G. A. Carlson, "Calculation Techniques for Estimating the Pressure Losses for Conducting Fluid Flows in Magnetic Fields," UCRL-51010, 1971.
6. Special topics report on MHD pressure drops. See Section I.B of this report for complete reference.
7. G. W. Sutton, A. Sherman, Engineering Magnetohydrodynamics, McGraw-Hill Series in Mechanical Engineering, 1965.

U. S. Government Printing Office: 1988/2-587-002/24048